Natural Disaster Science and Mitigation Engineering:
DPRI Reports

Hiroshi Kawase *Editor*

Studies on the 2011 Off the Pacific Coast of Tohoku Earthquake

Natural Disaster Science and Mitigation Engineering: DPRI Reports

NATURAL DISASTER SCIENCE AND MITIGATION ENGINEERING: DPRI REPORTS

Series Description:

Because of the high concentration of population in urban habitats and the strong linkage to infrastructures that support a modern urban lifestyle, natural disasters such as floods, typhoons, earthquakes, tsunamis, landslides, and volcanoes always create new areas of severe damage whenever they occur. Japan is a "disaster country" of sorts: the Japanese have had to survive many different kinds of natural disasters and consequently they have accumulated a substantial body of knowledge in the phenomenology and mitigation of natural disasters. This series of books presents recent advances in all aspects of natural disasters and related mitigation technologies developed in Japan to be shared with the international community.

The areas covered in this series include

1. Earthquake risk
2. Strong motions and damage prediction for urban structures
3. Volcanic eruptions
4. Ground failures
5. Climate and water disasters
6. Fire and environmental disasters
7. Disaster management and mitigation

For further volumes:
http://www.springer.com/series/11773

Hiroshi Kawase
Editor

Studies on the 2011 Off the Pacific Coast of Tohoku Earthquake

Springer

Editor
Hiroshi Kawase
Disaster Prevention Research Institute (DPRI)
Kyoto University
Kyoto, Japan

ISSN 2196-4394 ISSN 2196-4408 (electronic)
ISBN 978-4-431-54417-3 ISBN 978-4-431-54418-0 (eBook)
DOI 10.1007/978-4-431-54418-0
Springer Tokyo Heidelberg New York Dordrecht London

Library of Congress Control Number: 2013949612

Printed on acid-free paper

Springer is part of Springer Science+Business Media (www.springer.com)

Foreword

On the afternoon of March 11, 2011, a huge earthquake and accompanying tsunamis caused horrifying damage in the northern part of Japan, taking the lives of more than 18,900 people in the Tohoku region. This event evolved into the most widespread and complicated disaster in the modern history of disasters in Japan. On behalf of the Disaster Prevention Research Institute (DPRI) of Kyoto University, I hereby express my sincere condolences for those who lost their families and friends, to those who lost their homes and workplaces, and to those who were forced to leave their hometowns.

DPRI was founded in 1951 in response to serious damage caused by a huge typhoon that struck Japan in that year. DPRI researches nearly all natural hazards, including earthquakes and volcanic explosions, floods, tsunamis, tidal waves, typhoons and other atmospheric phenomena, and landslides and associated geohazards. The researchers who work in DPRI have specialties extending from natural science, engineering, and informatics, to social sciences. With such coverage, we conduct comprehensive research ranging from the prediction of hazards and investigation into their mechanisms, development of technologies to prevent and reduce associated disasters, analysis and measures of response and recovery immediately after disasters, to methodologies for disaster risk management. DPRI also serves as a national research center in which researchers working for Japanese universities on natural disasters and their prevention and/or mitigation use the experimental and observatory facilities owned by DPRI and work jointly with the DPRI researchers.

The six decades since the inception of DPRI have been marked by a notable increase in the degree and intensity of natural disasters. Various factors, both natural and social, are responsible for the changes. The severity of extreme weather phenomena (such as flood and drought) has escalated due primarily to recent climate variations. Rapid urbanization and densification also have contributed to the increased impact of disasters. The 1995 Hanshin-Awaji Disaster killed more than 6,000 people. The disaster was caused by an inland fault rupture, and numerous houses and buildings located in the city of Kobe and its neighboring towns collapsed because of very intense near-fault ground motions. In the 2011 Tohoku Disaster, the huge tsunamis caused by an ocean-ridge earthquake of magnitude 9.0 were the

primary cause of the death toll. This most recent disaster was also characterized by the vastness of the affected regions and by the complexity in which one disaster triggered another, as the overall catastrophe evolved into a perfect storm of disaster. The unprecedented risks disclosed by this calamity pose many challenges for us to overcome.

In response to the numerous lessons learned from this disaster, DPRI has initiated a comprehensive research effort on the establishment of a more resilient society, in which both safety and security are ensured against huge natural disasters such as the 2011 Tohoku Disaster. Along the lines of this effort, DPRI hereby wants to offer a series of volumes titled Natural Disaster Science and Mitigation Engineering, published by Springer, with the intention of sharing with international communities that have been engaged in natural disasters and mitigation our experiences and knowledge accumulated in these decades. The volumes include the surveys and findings acquired from a number of research projects led by DPRI researchers, post-disaster investigations into the causes and effects of the disaster, and a series of recommendations for the advancement of various measures to prevent and/or reduce disasters that could hit our globe in the coming years.

Masayoshi Nakashima
Director
Disaster Prevention Research Institute (DPRI)
Kyoto University

Preface

This is the first volume of the Disaster Prevention Research Institute (DPRI) series of reports titled Natural Disaster Science and Mitigation Engineering, published by Springer Japan. This volume is devoted to the surveys and findings from a number of projects led by DPRI researchers on the earthquake that occurred off the Pacific Coast of Tohoku on March 11, 2011, and the subsequent disaster, referred to here as the Great East Japan Disaster. The earthquake is considered to have caused complex, widespread, and long-lasting disaster sequences all over Japan as well as in other parts of the world.

The impact of the earthquake and disaster can be seen in almost all aspects of social activities in Japan. It is totally beyond my expertise to summarize its impact; however, I would like to note here one major issue raised in the seismic and earthquake engineering community as a direct consequence of the disaster and one major issue that has not been raised yet but should be.

Before the earthquake, the national Headquarters for Earthquake Research Promotion (HERP) provided National Seismic Hazard Maps for Japan to the public. On those maps, all the major sources of the probabilistic occurrence of earthquakes supposedly had been evaluated quantitatively, reflecting all of the current best knowledge of seismology, geology, geomorphology and tectonics. Despite about eight years of serious efforts, the HERP failed to predict the occurrence of the Tohoku disaster. Precisely speaking, they failed to include a scenario with such a large magnitude as that of the earthquake off the Tohoku coast.

There are many reasons for not including that possible scenario in their calculation of the seismic hazard in Tohoku, and technically it is relatively easy to fix the problem after the occurrence (actually, the basic hazard level of ground motions would not be much different even if we consider that scenario because of its low recurrence rate). However, the fundamental issue raised is not just models to be used but the credibility of the hazard map itself, which is quite a political and/or sociological issue. If we think that it is a safe bet for predictors to raise the probability in response to such an extraordinary scenario, we can always include an extreme case, such as one scenario beyond the rational expectation based on previous data. The M9 scenario of the Central Disaster Management Council, Cabinet Office,

Government of Japan seems a good example of that kind of extreme scenario, to which we cannot assign any rational value of probability because it has never happened before in the long history of earthquake occurrence along the Nankai Trough subduction zone. We can call this kind of psychological/political tendency of public skepticism regarding hazard estimates "A burnt child dreads the fire" syndrome. This is not a scientific issue but rather a sociological one regarding the experts' responsibility to the public on the subject of hazard estimates. I believe that a rational person would prefer to be told the actual truth rather than exaggerations even when there was the good motivation of preventing unexpected disaster.

Another issue that has not been raised yet but should be brought up is the adequacy of the current seismic code in Japan. Despite the high peak accelerations widely observed in the eastern part of Tohoku as well as in the northern part of the Kanto region, structural damages to buildings were minimal, probably less than 10% of the total structural damage, and probably fewer than 100 people were killed as a direct consequence of building collapses, including falling furniture and debris, together with objects falling due to other, non-structural damage. We can call it a victory of Japanese seismic design and practice. However, if no damage from any earthquakes is what we require, we just need to make buildings safer no matter what the ground motions at a site will be. Apparently the 2011 earthquake shows that buildings are actually much stronger than required by the seismic design code so that there is a large gap between the reality and the theory. If no structural experts considered any modification of the current seismic code and no building owners in Japan complained because of the "unexpectedly good" performance of the current (probably expensive) buildings, the reality–theory gap means nothing to anyone. However, as soon as we consider a modification of the code in one way or another, we must face the mystery of our stock of buildings for their "unexpectedly good" performance.

As readers will see, this volume is not intended to resolve these specific issues, but several chapters may have a stronger relation to these issues than others have. I hope that readers will find the content of this volume interesting and will use the information herein to consider these issues and other issues that the Tohoku earthquake and the subsequent disaster raised, both in Japan and in the rest of the world, in order to build a safer and more secure society.

Hiroshi Kawase
Editor
Disaster Prevention Research Institute (DPRI)
Kyoto University

Contents

1 Introduction 1
Hiroshi Kawase

2 Coseismic Deformations of the 2011 Tohoku, Japan, Earthquake and Triggered Events Derived from ALOS/PALSAR 3
Manabu Hashimoto, Yo Fukushima, and Youichiro Takada

3 Source Process of the 2011 Off the Pacific Coast of Tohoku Earthquake 17
Kimiyuki Asano, Haruko Sekiguchi, Tomotaka Iwata, Wataru Suzuki, Shin Aoi, and Takashi Kunugi

4 Field Survey of the Damage Caused by the 2011 Off the Pacific Coast of Tohoku Earthquake Tsunami 37
Tetsuya Hiraishi, N. Yoneyama, Y. Baba, and R. Azuma

5 Revisiting the Concept of Tsunami *Tendenko*: Tsunami Evacuation Behavior in the Great East Japan Earthquake 49
Katsuya Yamori

6 Soil-Slide Avalanches of Pyroclastic Fall Deposits Induced by the 2011 Off the Pacific Coast of Tohoku Earthquake 65
Masahiro Chigira, Akito Nakasuji, Shinya Fujiwara, and Masayuki Sakagami

7 Estimation of Strong Motion During the 2011 Northern Nagano Earthquake and an Associated Building Damage Survey 87
Masumi Yamada, Masayuki Yamada, Christine Smyth, Yui Fukuda, Yoshinori Fujino, and Koji Hada

8 Landslides in Urban Residential Slopes Induced by the 2011 Off the Pacific Coast of Tohoku Earthquake 103
Toshitaka Kamai, Hidemasa Ohta, Yasunori Ban, and Hidehiko Murao

9 Soil Amplification and Nonlinearity Studies at K-Net Sites in Miyagi Prefecture, Tohoku, Japan Based on H/V Spectral Ratios for Earthquake Ground Motions 123
Fumiaki Nagashima, Hiroshi Kawase, Shinichi Matsushima, Francisco J. Sánchez-Sesma, Takashi Hayakawa, Toshimi Satoh, and Mitsutaka Oshima

10 Soil Liquefaction Along the Tokyo Bay Coast Induced by the 2011 Off the Pacific Coast of Tohoku Earthquake 137
Shuji Tamura

11 Sediment-Related Disasters Caused by the Nagano-ken Hokubu Earthquake in the Heavy Snow Season 157
Sumio Matsuura, Masahiro Chigira, Yuki Matsushi, and Takashi Okamoto

12 High-Resolution Local-Scale Simulations of Meteorological Conditions and Wind Fields over the Fukushima Region in March 2011 177
Tetsuya Takemi and Hirohiko Ishikawa

13 Uncertainty in Simulation of Global Transport of Radioactive Tracer Emitted from Fukushima Daiichi Nuclear Power Plant 187
Takao Iguchi, Hitoshi Mukougawa, and Takeshi Enomoto

Contributors

Shin Aoi National Research Institute for Earth Science and Disaster Prevention (NIED), Tsukuba, Japan (Chapter 3)

Kimiyuki Asano Disaster Prevention Research Institute (DPRI), Kyoto University, Kyoto, Japan (Chapter 3)

Ryokei Azuma Disaster Prevention Research Institute (DPRI) of Kyoto University, Kyoto, Japan (Chapter 4)

Yasuyuki Baba Disaster Prevention Research Institute (DPRI) of Kyoto University, Kyoto, Japan (Chapter 4)

Yasunori Ban Disaster Prevention Research Institute (DPRI), Kyoto University, Kyoto, Japan (Chapter 8)

Masahiro Chigira Disaster Prevention Research Institute (DPRI), Kyoto University, Kyoto, Japan (Chapters 6, 11)

Takeshi Enomoto Disaster Prevention Research Institute (DPRI), Kyoto University, Kyoto, Japan (Chapter 13)

Yoshinori Fujino NEWJEC Inc., Osaka, Japan (Chapter 7)

Shinya Fujiwara Kokusai Kogyo Co. Ltd., Tokyo, Japan (Chapter 6)

Yui Fukuda NEWJEC Inc., Osaka, Japan (Chapter 7)

Yo Fukushima Disaster Prevention Research Institute (DPRI), Kyoto University, Kyoto, Japan (Chapter 2)

Koji Hada NEWJEC Inc., Osaka, Japan (Chapter 7)

Manabu Hashimoto Disaster Prevention Research Institute (DPRI), Kyoto University, Kyoto, Japan (Chapter 2)

Takashi Hayakawa Institute of Technology, Shimizu Corporation, Tokyo, Japan (Chapter 9)

Takao Iguchi Disaster Prevention Research Institute (DPRI), Kyoto University, Kyoto, Japan (Chapter 13)

Hirohiko Ishikawa Disaster Prevention Research Institute (DPRI), Kyoto University, Kyoto, Japan (Chapter 12)

Tomotaka Iwata Disaster Prevention Research Institute (DPRI), Kyoto University, Kyoto, Japan (Chapter 3)

Toshitaka Kamai Disaster Prevention Research Institute (DPRI) of Kyoto University, Kyoto, Japan (Chapter 8)

Hiroshi Kawase Disaster Prevention Research Institute (DPRI), Kyoto University, Kyoto, Japan (Chapters 1, 9)

Takashi Kunugi National Research Institute for Earth Science and Disaster Prevention (NIED), Tsukuba, Japan (Chapter 3)

Shinichi Matsushima Disaster Prevention Research Institute (DPRI), Kyoto University, Kyoto, Japan (Chapter 9)

Yuki Matsushi Disaster Prevention Research Institute (DPRI), Kyoto University, Kyoto, Japan (Chapter 11)

Sumio Matsuura Disaster Prevention Research Institute (DPRI), Kyoto University, Kyoto, Japan (Chapter 11)

Hitoshi Mukougawa Disaster Prevention Research Institute (DPRI), Kyoto University, Kyoto, Japan (Chapter 13)

Hidehiko Murao Murao Chiken Co., Ltd., Toyama, Japan (Chapter 8)

Fumiaki Nagashima Disaster Prevention Research Institute (DPRI), Kyoto University, Kyoto, Japan (Chapter 9)

Akito Nakasuji Kokusai Kogyo Co. Ltd., Tokyo, Japan (Chapter 6)

Hidemasa Ohta Ohta Geo-Research Co., Ltd., Nishinomiya, Japan (Chapter 8)

Takashi Okamoto Forestry and Forest Products Research Institute (FFPRI), Tsukuba, Japan (Chapter 11)

Mitsutaka Oshima Institute of Technology, Shimizu Corporation, Tokyo, Japan (Chapter 9)

Masayuki Sakagami Kokusai Kogyo Co. Ltd., Tokyo, Japan (Chapter 6)

Francisco J. Sánchez-Sesma Institute of Engineering, UNAM, Mexico City, Mexico (Chapter 9)

Toshimi Satoh Institute of Technology, Shimizu Corporation, Tokyo, Japan (Chapter 9)

Haruko Sekiguchi Disaster Prevention Research Institute (DPRI), Kyoto University, Kyoto, Japan (Chapter 3)

Christine Smyth Disaster Prevention Research Institute (DPRI), Kyoto University, Kyoto, Japan (Chapter 7)

Wataru Suzuki National Research Institute for Earth Science and Disaster Prevention (NIED), Tsukuba, Japan (Chapter 3)

Youichiro Takada Disaster Prevention Research Institute (DPRI), Kyoto University, Kyoto, Japan (Chapter 2)

Tetsuya Takemi Disaster Prevention Research Institute (DPRI), Kyoto University, Kyoto, Japan (Chapter 12)

Shuji Tamura Disaster Prevention Research Institute (DPRI), Kyoto University, Kyoto, Japan (Chapter 10)

Tetsuya Hiraishi Disaster Prevention Research Institute (DPRI), Kyoto University, Kyoto, Japan (Chapter 4)

Masumi Yamada Disaster Prevention Research Institute (DPRI), Kyoto University, Kyoto, Japan (Chapter 7)

Masayuki Yamada NEWJEC Inc., Osaka, Japan (Chapter 7)

Katsuya Yamori Disaster Prevention Research Institute (DPRI), Kyoto University, Kyoto, Japan (Chapter 5)

Nozomi Yoneyama Disaster Prevention Research Institute (DPRI), of Kyoto University, Kyoto, Japan (Chapter 4)

Chapter 1
Introduction

Hiroshi Kawase

Abstract The Tohoku earthquake on March 11, 2011, officially named as "Off the Pacific Coast of Tohoku, Japan Earthquake" by JMA, caused an unprecedentedly severe disaster on the northeastern part of Honshu (Tohoku), Japan. In this first volume of the series of books, namely, Natural Disaster Science and Mitigation Engineering: DPRI reports, we covered various aspects of investigations on scientific findings as well as issues related to the disaster and the subsequent evacuation due to the earthquake. The series of books presents recent advances in natural disaster sciences and mitigation technologies developed in Japan, which would be valuable for the mitigation of disasters due to similar kind of future events around the world.

The Mw9.0 Tohoku, Japan, earthquake on March 11, 2011, which is officially named as the 2011 Off the Pacific Coast of Tohoku, Japan Earthquake by Japan Meteorological Agency (JMA), could be the largest event in Japanese history. The earthquake is the so-called mega-thrust event at the plate interface between the North American Plate and the Pacific Plate, which generated a huge tsunami that devastated towns on the coast and brought over 18,000 fatalities and missing. About 100,000 houses were totally lost mainly due to tsunamis, and the total estimated direct loss would be over 200 billion US dollars. The level VI accident at the Fukushima Daiichi nuclear power plant of Tokyo Electric Power Co. was also due to the unexpected level of the tsunami height at the plant.

It is essential to investigate various aspects of the disaster in order to prevent this kind of tragic event happen again. To that end DPRI initiated emergency investigation collaboration projects to perform the field surveys and data analyses in close collaboration with other researchers at different universities and institutions

H. Kawase (✉)
Disaster Prevention Research Institute (DPRI), Kyoto University, Kyoto, Japan
e-mail: kawase@zeisei.dpri.kyoto-u.ac.jp

H. Kawase (ed.), *Studies on the 2011 Off the Pacific Coast of Tohoku Earthquake*,
Natural Disaster Science and Mitigation Engineering: DPRI reports,
DOI 10.1007/978-4-431-54418-0_1,

immediately after the earthquake. This volume includes findings acquired from a number of reconnaissance teams lead by DPRI researchers and post-earthquake investigations into the causes and effects of the disaster.

In Chaps. 2 and 3, we collect reports on the source characterization of the main shock based on the geophysical data in the two extreme period ranges, one for infinitely long period and the other for short period up to several tens of seconds.

In Chaps. 4 and 5, we report the field survey results of the tsunami damage in the Tohoku district and the problems associated with the evacuation process from tsunami in the Tohoku district. We also collect the reports for the induced soil slide observed widely in the Tohoku district in Chap. 6 as natural phenomenon caused by the earthquake. Then from Chaps. 7 to 9, we collect investigation focused on man-made structures such as buildings and man-made slopes.

In Chaps. 10 and 11 we collect reports on the damage on ground due to liquefaction and landslide with the heavy snow coverage. Finally, we have two chapters, Chaps. 12 and 13, on meteorological surveys to trace the diffusion process of radioactive release by the Fukushima NPP accident.

As you can notice, we have collected variety of investigation reports on various aspects of the Tohoku disaster, which may provide invaluable information to initiate further detailed studies to prevent/mitigate similar disasters in future anywhere in the world.

Chapter 2
Coseismic Deformations of the 2011 Tohoku, Japan, Earthquake and Triggered Events Derived from ALOS/PALSAR

Manabu Hashimoto, Yo Fukushima, and Youichiro Takada

Abstract The Tohoku earthquake on March 11, 2011, caused a remarkably large deformation on the island of Honshu, Japan. By analyzing ALOS/PALSAR data, a range increase of up to 3.6 m at the tip of the Oshika Peninsula, the closest point to the epicenter, was detected from ascending orbits. Combining ascending and descending interferograms, this peninsula was confirmed to have subsided and shifted eastward. This deformation may have been caused by a huge reverse slip on the plate interface near the trench axis.

This large deformation induced local earthquakes with magnitudes of 6 or larger and volcanic unrests. Among them, the April 11 M7.0 event in southern Fukushima Prefecture occurred on previously unrecognized active faults. More than nine fringes showing range increases were found in the vicinity of the epicenter of the Fukushima event. This observation is consistent with normal faulting on faults whose motion was previously not recognized. We also found slight range increases in volcanic regions in Northeast Japan. These observations imply that the March 11 shock induced large extensional stress in the crust of eastern Japan.

Keywords ALOS/PALSAR • Crustal deformation • Synthetic aperture radar • Triggered events

2.1 Introduction

The Mw9.0 Tohoku, Japan, earthquake on March 11, 2011, is the largest event in Japanese history. The Global CMT solution implies large thrust faulting on the plate interface (Fig. 2.1), which generated a huge tsunami that devastated towns on the coast and brought 18,812 fatalities and missing as of June 20, 2012.

M. Hashimoto (✉) • Y. Fukushima • Y. Takada
Disaster Prevention Research Institute (DPRI), Kyoto University, Kyoto, Japan
e-mail: hashimoto.manabu.7e@kyoto-u.ac.jp

H. Kawase (ed.), *Studies on the 2011 Off the Pacific Coast of Tohoku Earthquake*,
Natural Disaster Science and Mitigation Engineering: DPRI reports,
DOI 10.1007/978-4-431-54418-0_2,

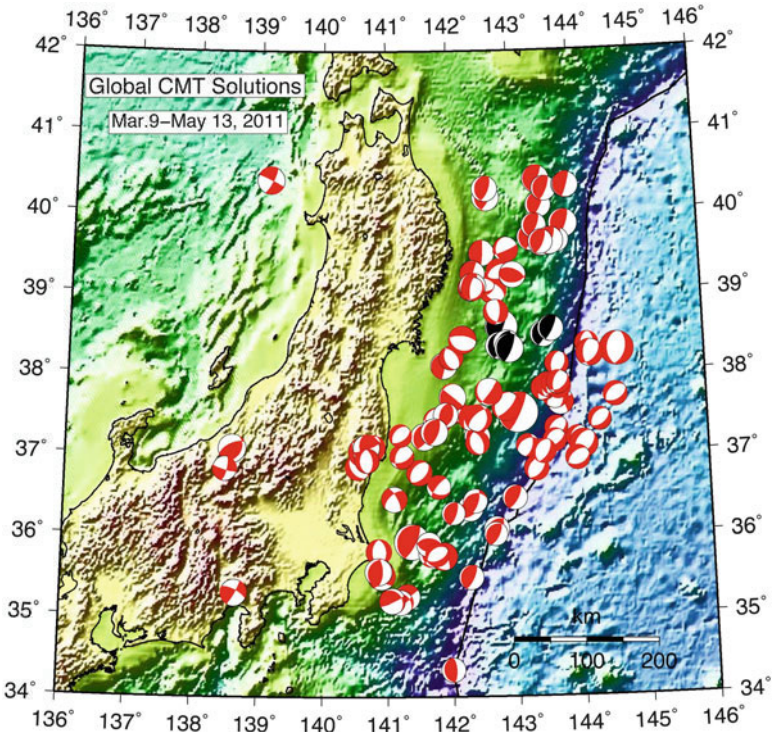

Fig. 2.1 Distribution of CMT solutions of events (Mw>6.0) during March 9 to May 13, 2011 (Harvard University Global CMT 2011). *Black symbols* are those for foreshocks. The biggest one is for the mainshock

It is essential to reveal deformations on the Japanese islands in order to understand the mechanism of this extreme event and to improve long-term forecasting. A dense continuous GPS observation network (GSI's Earth Observation Network; GEONET) has been deployed by the Geospatial Information Authority, Japan (e.g., Sagiya 2004), and the coseismic deformation was immediately reported based on its data (Ozawa et al. 2011; Simons et al. 2011). Synthetic Aperture Radar Interferometry (InSAR) is another suitable technique for the detection of crustal deformation. InSAR has an advantage in its spatial resolution over GPS. After the main shock of the Tohoku earthquake a lot of earthquakes and volcanic unrest were induced all over eastern Japan. InSAR is the best method to detect coseismic deformation associated with these induced events, because the size of these events is comparable to or smaller than the spacing of the network of GEONET.

Since its launch in 2006, the Advanced Land Observation Satellite (ALOS) has been making observations of the Earth. ALOS has a SAR sensor, the Phased Array-type L-band SAR (PALSAR). PALSAR gives us excellent data which reveal coseismic deformations such as the 2008 Wenchuan and the 2010 Haiti earthquakes (e.g., Hashimoto et al. 2010; Hashimoto et al. 2011). We have been working for the

Earthquake Working Group, a special project for the Evaluation of ALOS for the Disaster Mitigation, under the coordination of GSI and the Japan Aerospace Exploration Agency (JAXA), since 2007. When a large earthquake occurs, the working group requests urgent observations and analyses acquired images. Unfortunately, ALOS terminated its operation due to a sudden power failure on April 22. It is regrettable that the PALSAR images of the Tohoku earthquake are the last message from ALOS. In this report, we show results of analyses of PALSAR images acquired before and after the 2011 Tohoku earthquake.

2.2 Acquisition of ALOS/PALSAR

PALSAR has two modes of observation useful for InSAR: strip-map and ScanSAR mode. Strip-map mode images are ~70 km wide and have a high spatial resolution. On the other hand, ScanSAR mode images are ~350 km wide, but the spatial resolution is low. Furthermore a synchronization of bursts between two ScanSAR images is required to obtain high coherence. Therefore we requested JAXA to acquire both modes of images depending on the conditions such as the availability of archived images or conflict with other observations.

Unfortunately, ALOS experienced a power failure on April 22, and JAXA announced the completion of operation in May. Therefore we could not obtain full coverage of eastern Japan, but the ALOS/PALSAR data gave us invaluable information on the biggest earthquake in the history of Japan.

2.3 Image Processing

Strip-map mode images are acquired from ascending orbits, while ScanSAR mode images are obtained from descending orbits. Two strip-map mode pairs are also acquired from descending orbits. Precise orbits are used in processing. Unfortunately the perpendicular baselines for the ScanSAR–ScanSAR pairs are longer than 2,000 m, which resulted in only partially coherent interferograms. Therefore, we only show strip-map interferograms here.

We processed images with Gamma®. A hole-filed SRTM digital elevation model (Jarvis et al. 2008) was used for the 2-pass differential interferometry.

2.4 The March 11 Mainshock

First, we discuss the deformation field observed by PALSAR. Figures 2.2 and 2.3 show the ascending and descending interferograms, respectively. We obtained high coherence in the plain area, but coherence is relatively low in the mountains. This low coherence may be attributed mainly to snow coverage.

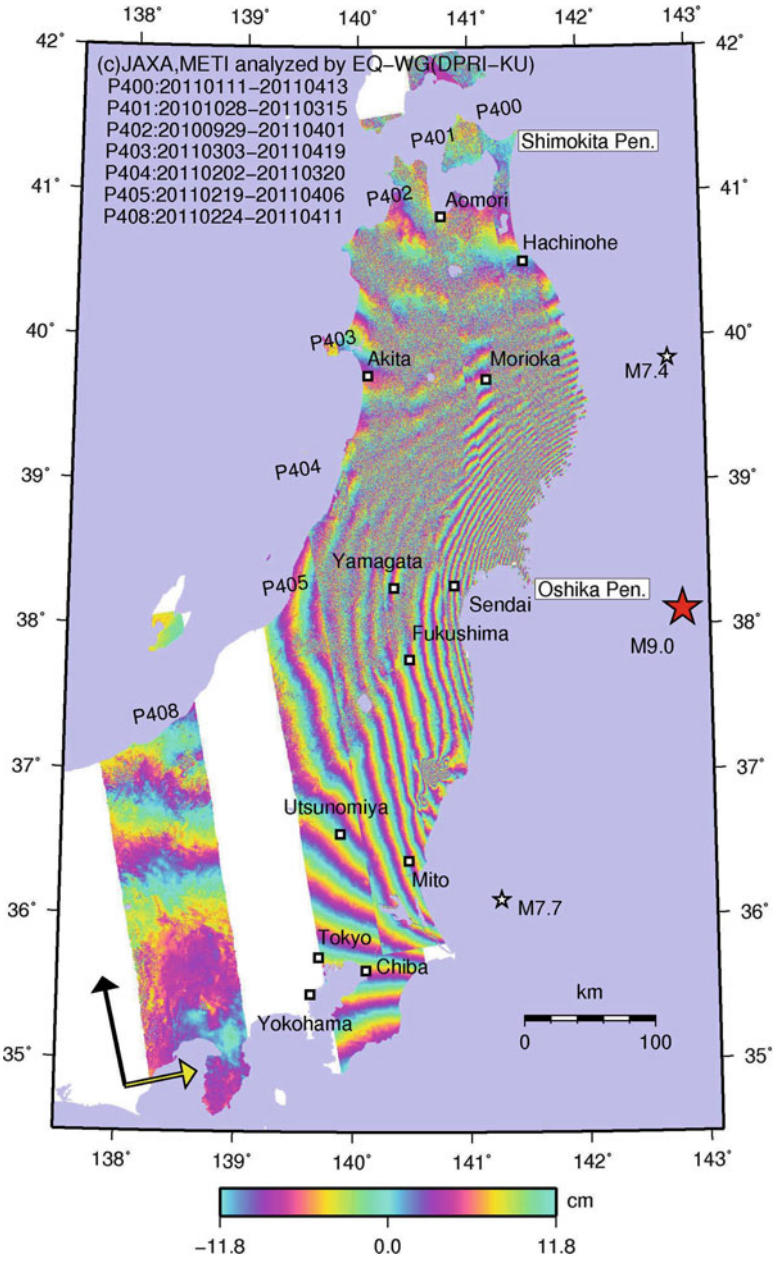

Fig. 2.2 Asecnding interferograms. 1 cycle of color scale indicates 11.8 cm changes in line of sight distance. Black and yellow arrows show the direction of flight of satellite and line of sight, respectively. Red and white stars denotes the epicenter of the mainshock and aftershocks, respectively

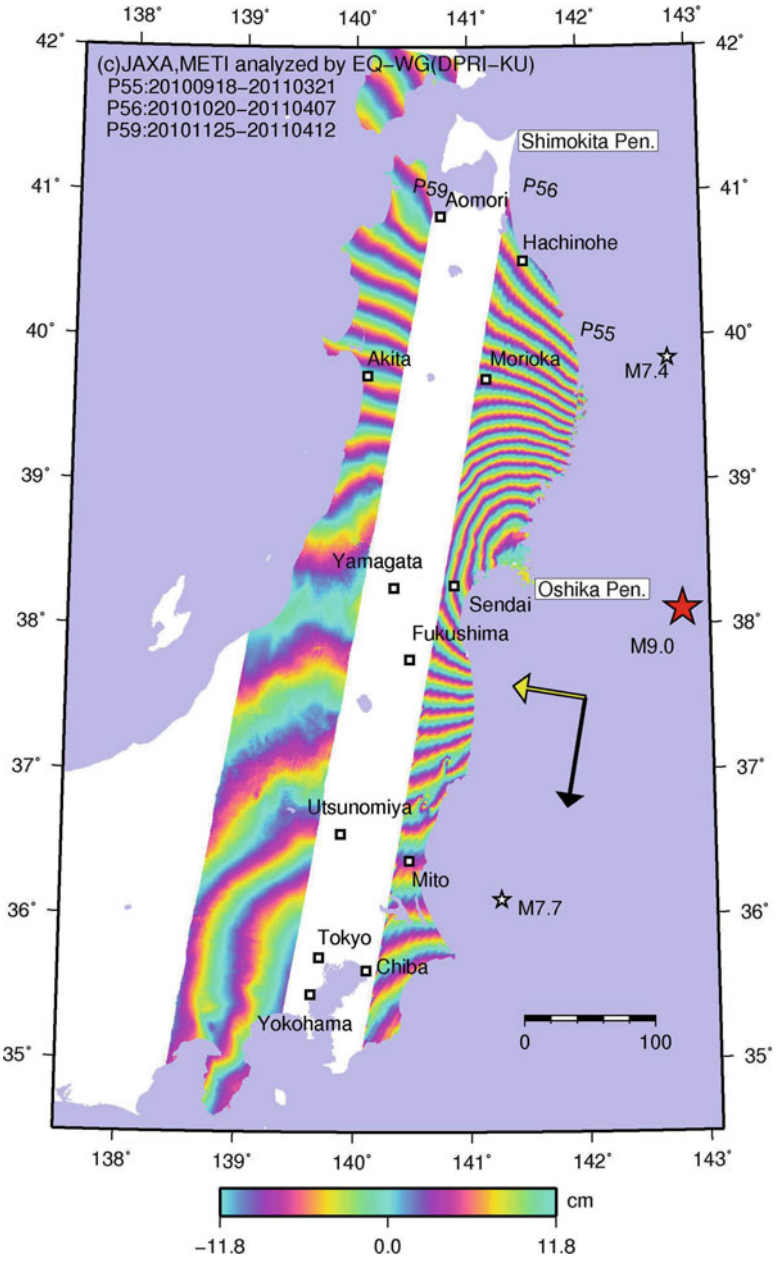

Fig. 2.3 Desecending interferograms. See also Legend of the Fig. 2.2.

2.4.1 Coseismic Interferograms

In Fig. 2.2, we notice 30–31 cycles of fringes from the northern tip of the Shimokita Peninsula (northernmost point of Honshu) to the southern tip of the Oshika Peninsula for the path 401 (eastern strip). This measurement and pattern of change in color indicate a range increase of about 3.5–3.6 m between these two points. Broad concentric fringes suggest that the eastern half of the Japanese islands deformed largely.

Figure 2.3 shows the descending interferograms. We also recognize concentric fringes whose center is located at the Oshika Peninsula. The pattern of changes of color indicates range decrease. We can count 18–19 cycles (2.1–2.2 m) from Hachinohe to the Oshika Peninsula. It is noteworthy that the fringes widened near the tip of the peninsula, which suggests that eastward displacement and subsidence compensate for each other.

Fortunately, PALSAR observed the same area from two directions. Therefore we can deduce two components of displacements. However, interferograms sometimes suffer from systematic errors possibly due to orbital inaccuracy or ionospheric disturbances. We corrected them with GPS displacements (Ozawa et al. 2011). After the correction, we combined ascending and descending interferograms to obtain east–west and quasi-vertical components (Fig. 2.4). We found ~5 m eastward shift of the Oshika Peninsula and ~1 m subsidence along the Pacific coast for all of eastern Japan.

2.4.2 Slip Distribution

In order to understand the mechanism of this gigantic earthquake, we performed an inversion of slip distribution using the algorithm proposed by Fukahata and Wright (2008). We assumed a single fault plane dipping toward the west from the trench axis with a 600 km length. In this inversion, we simultaneously estimated dip angle of the fault plane. We also assumed that the depth of the fault ranges from surface to 100 km. Only dip-slip components of slip were estimated. Since we have data only on the west side of the source, a preliminary inversion found that it is very hard to estimate the strike-slip component simultaneously with the dip-slip component.

So far we searched an optimal dip angle in a range from 10 to 20° and found 20° gives the minimum ABIC (Akaike's Bayesian Information Criterion). Though there is a possibility that more steep dip angles give better results, we adopted this value since the nodal plane of the CMT solution has a shallow dip angle. Furthermore, a model with higher variable slip distribution can explain the data better because there are no data above the source area and data on land have no resolving power of slip; however, we prefer a relatively smoother solution. We selected solutions with a seismic moment consistent with GCMT (Figs. 2.5 and 2.6).

The peak slip of ~50 m is located between the epicenter and trench axis. This model is roughly consistent with that of Simons et al. (2011) obtained from GPS, tsunami, and seismic data. Synthetic interferograms are consistent with the observed ones.

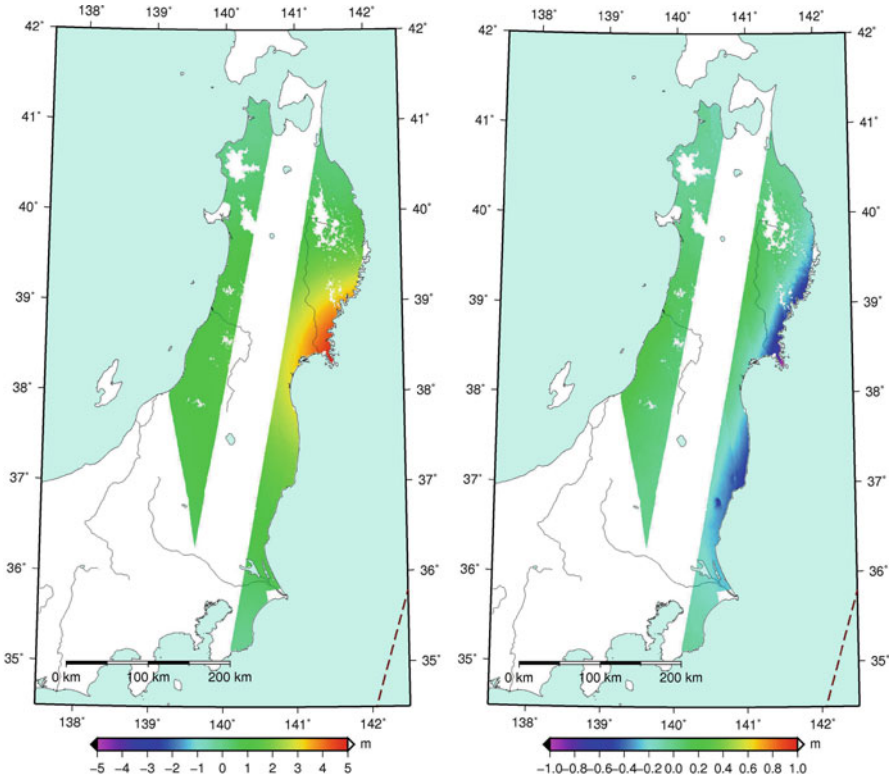

Fig. 2.4 Result of 2.5D analysis. (*Left*) E-W component, (*right*) quasi-vertical component

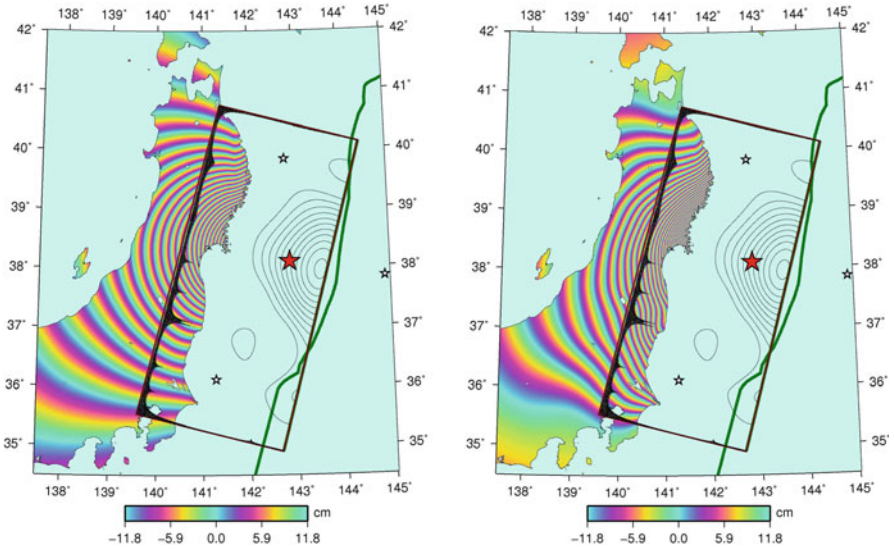

Fig. 2.5 Synthetic interferograms. (*Left*) Descending, (*right*) ascending. *Rectangle* indicates surface projection of modeled fault plane. Slip contours of 5 m are also shown. *Star* is the epicenter of the mainshock

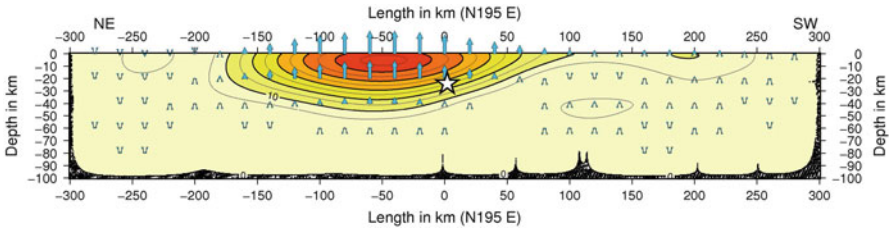

Fig. 2.6 Slip distribution projected onto the vertical cross section along the strike of a modeled fault. Contours show the estimated slip. Interval of the thick contours is 10 m. Thin contours indicate 5 m interval of slip. The maximum slip of about 50 m in the shallow part of the fault (red zone)

2.5 Triggered Events

In Figs. 2.2 and 2.3, we notice several local disturbances. These are deformations due to induced earthquakes, volcanic unrests, and possible landslides. Figure 2.7 shows the residual interferograms of the previous inversion. Local disturbances are more clearly recognized.

2.5.1 The April 11 Fukushima Earthquake

The most prominent signal of induced activities is found north of Mito. Since March 19, a seismic swarm including a couple of M>6 events occurred in southern Fukushima and northern Ibaraki prefectures. On April 11, the largest event with Mw6.6 occurred and its aftershock activity still continues. Since the hypocenters of these induced earthquakes are shallow, InSAR detected coseismic deformation (Fukushima et al. 2013). Figure 2.8 shows a close-up of its source area in an ascending interferogram (Path 403). We can count more than 18 fringes (>2.1 m) there. Discontinuities of fringes correspond well to the surface ruptures (Ishiyama et al. 2011). The pattern of change in color implies range increase and its peak is located on the west side of the faults. Since a normal faulting mechanism was observed, the western blocks are on the hanging wall side. Interestingly, the peak is located in mountain ranges, while the central part between reverse V-shaped faults is a valley. These observations are inconsistent with local topography. This area has experienced no large earthquake in its history. Therefore, we think old faults were reactivated by large extensional stress change due to the March 11 mainshock.

2.5.2 Local Disturbances in Interferograms

We recognized other local disturbances due to earthquakes larger than Mw6 (Mw6.3 Northern Nagano earthquake of March 12 and other events in southern Fukushima and northern Ibaraki areas). However, there are several local disturbances that may

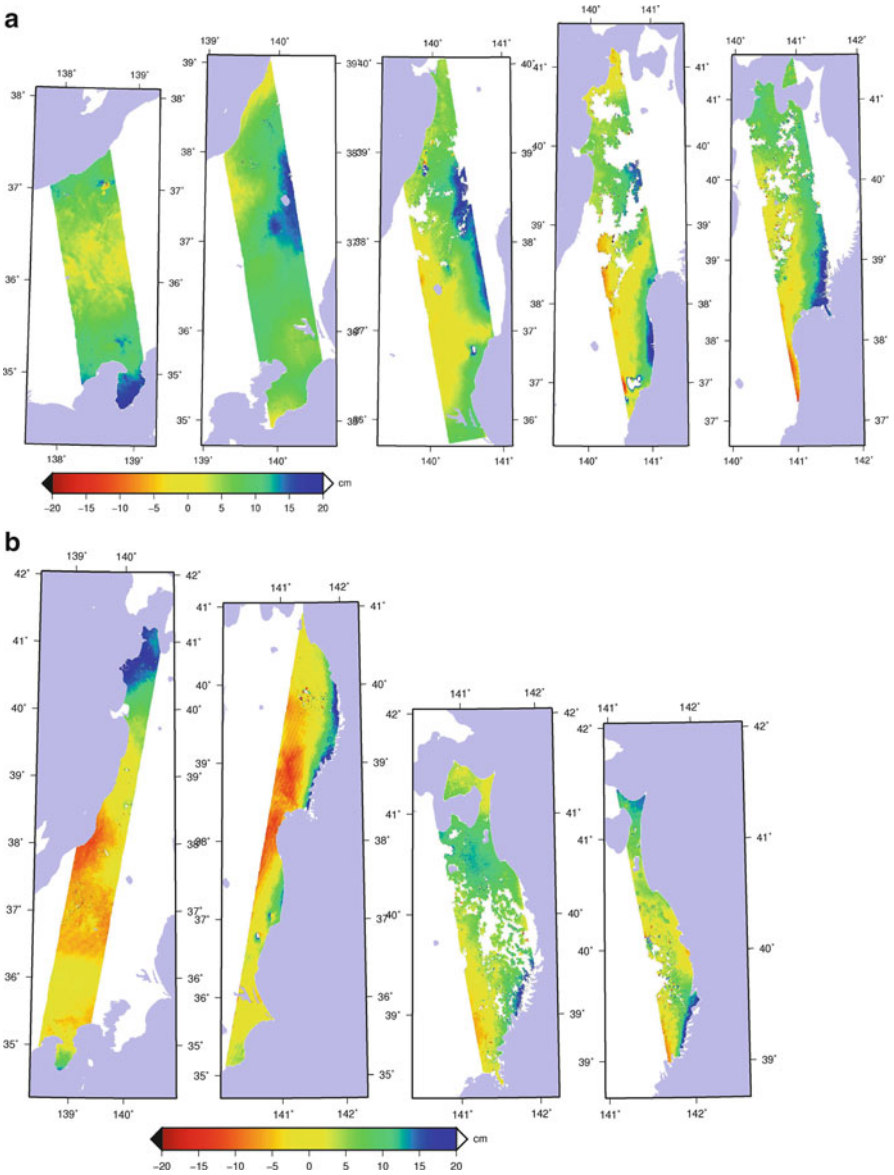

Fig. 2.7 (**a**) Residuals of the inversion in ascending interferograms from path 408 (*left*) to 402 (*right*). (**b**) Residuals of the inversion in descending (*left*: path 59 and 56) and ascending interferograms (*right*: path 401 and 400)

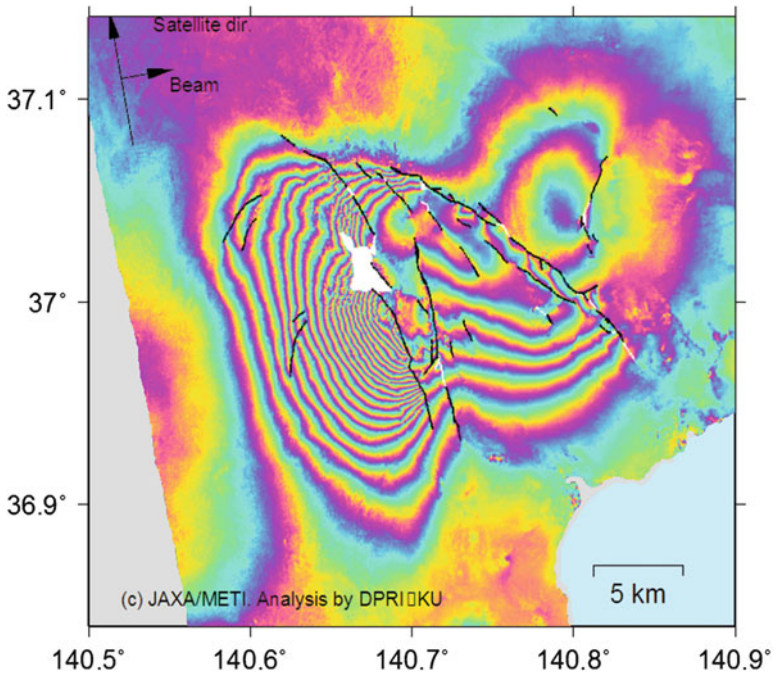

Fig. 2.8 Close-up of interferogram in the epicentral area of the April 11 southern Fukushima earthquake (Mw6.6). *Solid lines* are recognized traces of faults

not be accompanied by significant earthquakes. In the residual interferograms of paths 402 and 403, tiny green spots can be seen north of Sendai (Fig. 2.7a). Figure 2.9 is a close-up of the original interferogram for path 402. We have elliptical fringes of one cycle west of Hanayama Lake and near Mt. Kurikoma. The former might be related to the activity of a landslide, while the latter might be related to volcanic activity (Fig. 2.9).

2.6 Comparison of Intensity Images

SAR is a powerful tool used to detect areas of tsunami inundation. Since no reflected signals are detected in areas covered with water, we can detect the area of tsunami inundation by comparing intensity images of pairs spanning a tsunami. We painted the pre- and post-images with cyan and red, respectively, in proportion to the observed intensity and combined them. Cyan colors indicate that little signals were detected in the post-earthquake image, implying the existence of water. Figure 2.10 shows the intensity difference image of ScanSAR images of the

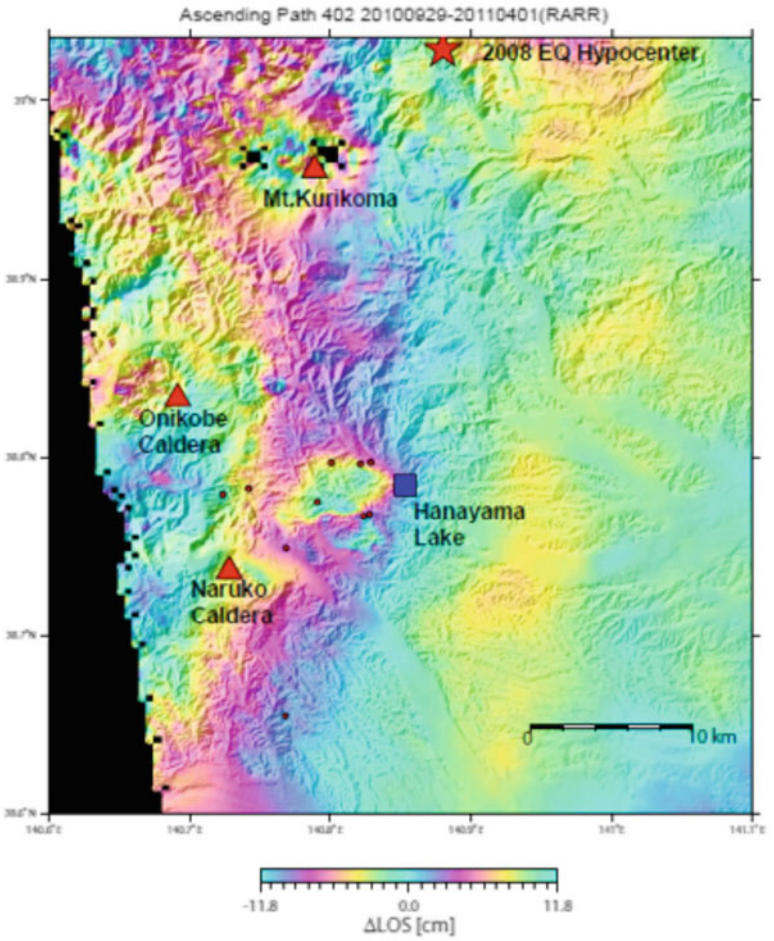

Fig. 2.9 Close-up of detrended interferogram of path 402. Two elliptical fringes are recognized near Hanayama Lake and Mt. Kurikoma

southern Sendai area. The post-earthquake image was acquired on March 31, 20 days after the earthquake, but we notice cyan colors nearly 5 km from the ocean. It is obvious that this area was still flooded 3 weeks after the tsunami.

It is a great loss that the ALOS terminated operation, although it left invaluable data. We observed coseismic deformation from the 2011 Tohoku earthquake that covered the eastern half of the Japanese islands. Furthermore, localized deformations associated with induced seismic activities were also detected. We are going to analyze images to reveal deformations associated with this epoch-making event as well as induced activities.

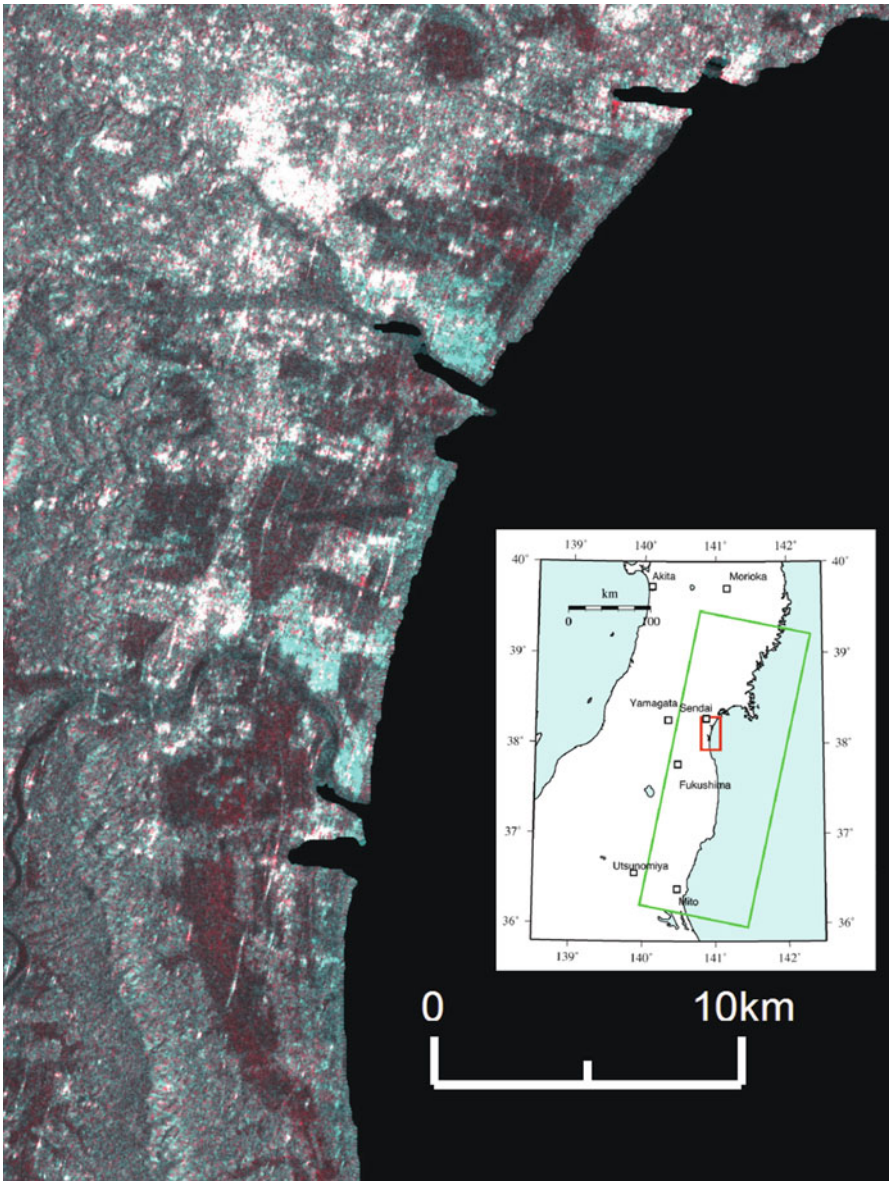

Fig. 2.10 Comparison of intensity images south of Sendai. Pre- and post-earthquake images were acquired on June 28, 2010, and March 31, 2011, respectively, in the ScanSAR mode. *Inset* shows the location of the image. *Red* and *green rectangles* depict areas of this image and the original image (Path 61, Frame 2850, Beam 1), respectively

2.7 Summary

We found very large deformation due to the March 11 mainshock and local deformations due to induced earthquakes using ALOS/PALSAR images. PALSAR images suggest a huge slip on the interface between plates near the trench axis. We also found other local deformations near volcanoes or possible landslides. Especially, the April 11 southern Fukushima earthquake caused deformation that is inconsistent with local topography. We are going to deduce characteristics of these deformations and understand its mechanism.

Unfortunately, ALOS/PALSAR completed its operation in May. JAXA is preparing the next L-band SAR mission. We believe the next mission, ALOS-2, will definitely contribute to the earthquake science.

Acknowledgements PALSAR level 1.0 data are shared among PIXEL (PALSAR Interferometry Consortium to Study our Evolving Land Surface) and provided from JAXA under a cooperative research contract with ERI, Univ. Tokyo, and the Earthquake Working Group (Geospatial Information Authority) under the JAXA's project "Utilization of ALOS for Disaster Mitigation." The ownership of PALSAR data belongs to METI (Ministry of Economy, Trade and Industry) and JAXA.

References

Fukahata Y, Wright T (2008) A non-linear geodetic data inversion using ABIC for slip distribution on a fault with an unknown dip angle. Geophys J Int 173:353–364

Fukushima Y, Takada Y, Hashimoto M (2013) Complex ruptures of the 11 April Iwaki earthquake (Mw6.6) triggered by the 2011 Mw9.0 Tohoku, Japan, earthquake. BSSA 103:1572–1583. doi:10.1785/0120120140

Harvard University Global CMT Project (2011) http://www.globalcmt.org/

Hashimoto M, Enomoto M, Fukushima Y (2010) Coseismic deformation from the 2008 Wenchuan, China, earthquake derived from ALOS/PALSAR images. Tectonophysics 491:59–71

Hashimoto M, Fukushima Y, Fukahata Y (2011) Fan delta uplift and mountain subsidence during the 2010 Haiti earthquake. Nat Geosci 4:255–259. doi:10.1038/ngeo1115

Ishiyama T, Sato H, Ito T, Sugito N, Echigo T, Kato N, Imaizumi T (2011) The surface earthquake fault of the 11th April 2011 earthquake in Hamadoori Fukushima pref. http://outreach.eri.u--tokyo.ac.jp/eqvolc/201103_tohoku/eng/hamadoori/

Jarvis A, Reuter HI, Nelson A Guevara E (2008) Hole-filled SRTM data V4. International Centre for Tropical Agriculture (CIAT). http://www.srtm.csi.cgiar.org

Ozawa S, Nishimura T, Suito H, Kobayashi T, Tobita M, Imakiire T (2011) Coseismic and postseismic slip of the 2011 magnitude-9 Tohoku-Oki earthquake. Nature. doi:10.1038/nature10227

Sagiya T (2004) A decade of GEONET: 1994–2003 – the continuous GPS observation in Japan and its impact on earthquake studies. Earth Planets Space 56:xxix–xli

Simons M et al (2011) The 2011 magnitude 9.0 Tohoku-Oki earthquake: mosaicking the megathrust from seconds to century. Science 332:1421. doi:10.1126/science.1206731

Chapter 3
Source Process of the 2011 Off the Pacific Coast of Tohoku Earthquake

Kimiyuki Asano, Haruko Sekiguchi, Tomotaka Iwata, Wataru Suzuki, Shin Aoi, and Takashi Kunugi

Abstract The kinematic source process of the 2011 Off the Pacific Coast of Tohoku earthquake is studied using strong motion data both in low- and high-frequency ranges. The slip distribution is estimated by the waveform inversion analysis using velocity waveforms in the frequency range from 0.01 to 0.125 Hz at strong motion stations along the Pacific coast. The strong motion generation area (SMGA) is estimated by the strong ground motion simulation in 0.1–10 Hz using the empirical Green's function method. The slip distribution is characterized by a large asperity with peak slip of 48 m which is imaged in the shallower portion of the source fault near the Japan Trench. Four SMGAs are identified in the deeper portion of the source fault. Unlike the past M7–8 subduction-zone plate-boundary events, the SMGAs and the asperity seem to be complementary in space. But the rupture time of each SMGA matches the timing of slip in each area. The total size of SMGAs is much smaller than the asperity area. This event coincides with empirical scaling relationships between total rupture area, asperity area, SMGA, and its seismic moment proposed for subduction-zone plate-boundary earthquakes by previous papers although the asperity abstracted for this event may have different nature from those of past smaller earthquakes.

Keywords Relationship between slip distribution and strong motion generation area • Scaling relationship • Source process of the 2011 Tohoku earthquake • Strong motion data • Strong motion generation area

K. Asano (✉) • H. Sekiguchi • T. Iwata
Disaster Prevention Research Institute (DPRI), Kyoto University, Uji, Japan
e-mail: k-asano@egmdpri01.dpri.kyoto-u.ac.jp

W. Suzuki • S. Aoi • T. Kunugi
National Research Institute for Earth Science and Disaster Prevention (NIED), Tsukuba, Japan

H. Kawase (ed.), *Studies on the 2011 Off the Pacific Coast of Tohoku Earthquake*,
Natural Disaster Science and Mitigation Engineering: DPRI reports,
DOI 10.1007/978-4-431-54418-0_3,

3.1 Introduction

The 2011 Off the Pacific Coast of Tohoku earthquake (Mw9.0, hereafter the 2011 Tohoku earthquake) which occurred at 14:46 on 11 March 2011 (JST = UT + 9) is the best observed megathrust earthquake, thanks to the present dense observation network in Japan. For example, nationwide dense strong motion observation networks K-NET and KiK-net operated by the National Research Institute for Earth Science and Disaster Prevention (NIED) (Aoi et al. 2004, 2011) succeeded in recording the acceleration waveforms during the mainshock at 1,223 stations as of December 2011 (Kunugi et al. 2012). The seismic intensity of 7 in the intensity scale of the Japan Meteorological Agency (JMA) was observed at Tsukidate, Kurihara city 175 km west of the epicentre, and the seismic intensity of 6+ was observed at many sites in Tohoku and Kanto districts (see, e.g. Hoshiba et al. 2011).

Figure 3.1 shows the spatial distribution of the observed peak ground acceleration (PGA) and the peak ground velocity (PGV) at strong motion stations in east and central Japan. These strong motion stations include the K-NET and KiK-net stations and the seismic intensity observation sites of JMA. Among these stations twenty stations in Tohoku and Kanto districts recorded ground accelerations larger than the gravitational acceleration.

Figure 3.2 shows the record sections of the north–south components of observed original acceleration waveforms and filtered velocity waveforms along the Pacific

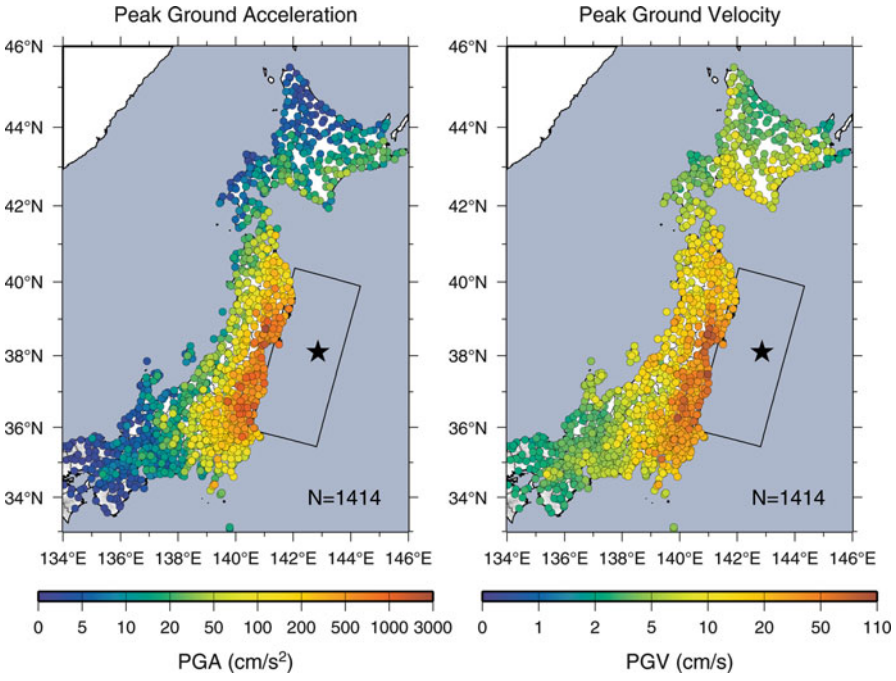

Fig. 3.1 Observed peak ground acceleration (*left*) and peak ground velocities (*right*) during the 2011 Tohoku earthquake at K-NET, KiK-net, and JMA strong motion stations

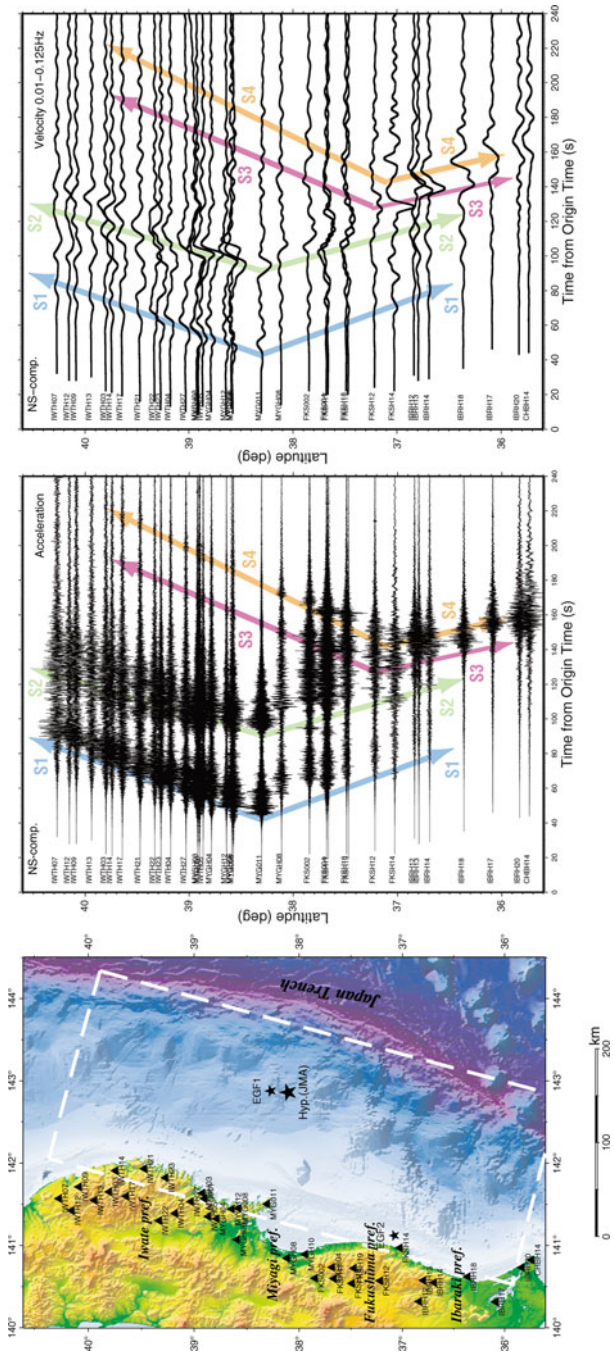

Fig. 3.2 Record sections of north–south components of observed original ground acceleration waveforms and filtered ground velocity waveforms in 0.01–0.125 Hz ordered by the latitude

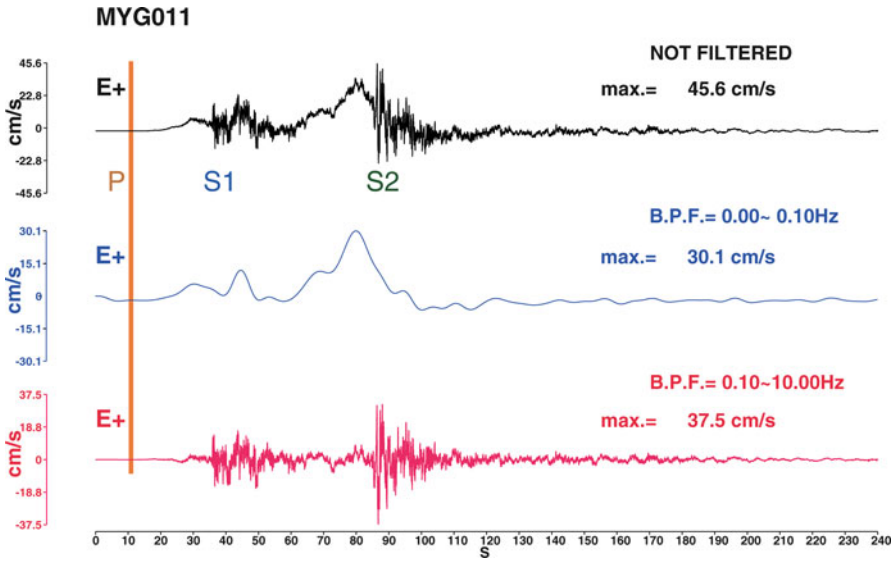

Fig. 3.3 Observed ground velocity waveforms of the east–west component at MYG011 without band-pass filter (*top*), low-pass filtered at 0.1 Hz (*middle*), and band-pass filtered between 0.1 and 10 Hz (*bottom*)

coast ordered by the latitude of stations. Four distinctive wave packets propagating northward and southward are recognized from the record section of the observed acceleration. Both the first (S1) and second wave packets (S2) are originated from off Miyagi prefecture, but S1 and S2 are separated by approximately 40 s. The third wave packet (S3) propagates from off Fukushima prefecture, and the fourth wave packet (S4) propagates from off the border between Fukushima and Ibaraki prefectures. Those observed characteristics of strong ground motions give us a brief image of the source process related to the strong ground motion generation during the 2011 Tohoku earthquake. However, these acceleration wave groups do not exactly correspond to the distinctive phases observed in the low-frequency (0.01–0.125 Hz) velocity waveforms, which means that spatiotemporal distributions of rupture contributing to high- and low-frequency wave radiation are different (Fig. 3.3).

In this chapter, we introduce the kinematic source process inverted from strong motion data in low-frequency band of 0.01–0.125 Hz by Suzuki et al. (2011) and the source model composed of strong motion generation areas (SMGAs) estimated by the forward modelling of broadband strong ground motion in 0.1–10 Hz by Asano and Iwata (2012). We will discuss the spatial relationship between large slip and SMGA to understand strong motion generation process during the 2011 Tohoku earthquake by comparing past subduction-zone plate-boundary earthquakes in northeast Japan.

3.2 Source Process by Waveform Inversion in Low-Frequency Band

3.2.1 Method

Suzuki et al. (2011) employed the multi-time-window linear waveform inversion method (Olson and Aspel 1982; Hartzell and Heaton 1983) to derive the rupture process. They assumed a rectangular fault model (Fig. 3.2), constructed to follow the geometry of the Pacific plate (Hasegawa et al. 1994). The strike and dip angles of the fault plane were set to 195° and 13°, respectively. The fault plane had a length of 510 km and a width of 210 km and was divided into 30×30 km^2 subfaults. The slip history of each subfault was represented by 25 6-s time windows, each of which was separated by 3 s, allowing slip for 78 s. The rupture starting point was set to 38.10°N, 142.85°E, 24 km deep, referring to the hypocentre determined by the NIED and JMA.

Strong motion data used for the inversion analysis was the S wave portion of the 0.01–0.125 Hz velocity waveforms of 10 K-NET stations and of 26 KiK-net borehole stations within 120–400 km epicentral distances. The observed and synthetic waveforms are aligned on the S wave arrivals. Green's functions were calculated using the discrete wave number method (Bouchon 1981) and the reflection/transmission matrix method (Kennett and Kerry 1979). The rupture propagation effect inside the subfault, expected from the first time window triggering velocity, was considered by convolving the moving dislocation (Sekiguchi et al. 2002). A one-dimensional underground structure model for the calculation of the Green's function was constructed for each station considering the three-dimensional crustal structure model (Fujiwara et al. 2009). The rupture process was inverted using the least squares method with an inequality constraint (Lawson and Hanson 1974), to limit the variation of the rake angle to within 90° centred at 90°, i.e. the pure dip slip angle. The smoothing constraint on slips was applied following the procedure proposed by Sekiguchi et al. (2000).

3.2.2 Result

Figure 3.4a, b shows the slip distribution estimated from their inversion analysis. The contour interval is 5 m. A large slip area, in which the slip is larger than 20 m, extends from the area around the hypocentre to the shallower part of the fault plane. A maximum slip of 48 m is estimated to the east of the hypocentre near the trench axis, far off Miyagi prefecture. The slips near the coastline are relatively small, except off Miyagi prefecture, where the slip is greater than 5 m from the coastline to the trench. The total seismic moment of the derived model is 4.42×10^{22} Nm (Mw9.0). The first time window triggering velocity of 3.2 km/s was selected because

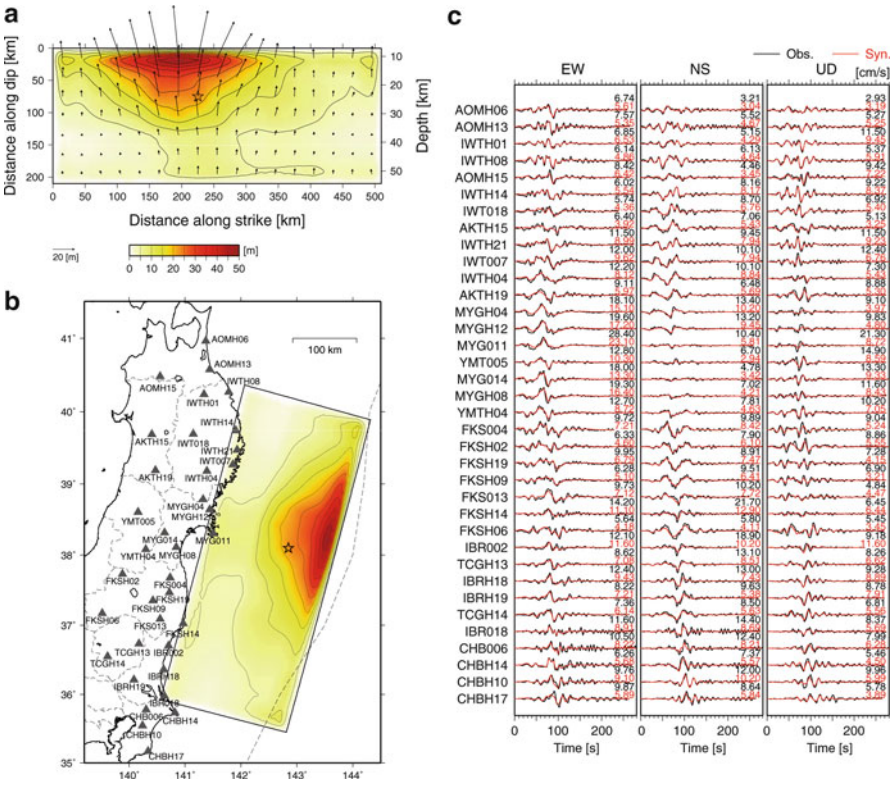

Fig. 3.4 **(a)** Slip distribution of the source fault plane, **(b)** slip distribution projected on the map, and **(c)** comparison between the observed (*black*) and synthetic (*red*) velocity waveforms between 0.01 and 0.125 Hz (Suzuki et al. 2011)

this velocity gives the smallest residual value (Fig. S1 in Suzuki et al. 2011). The observed and synthetic waveforms are compared in Fig. 3.4c. In order to observe the temporal characteristics, we show the slip distribution every 10 s with a contour interval of 1 m in Fig. 3.5. The first remarkable moment release started 20 s after the initial break, when the rupture occurred around the hypocentre. Then, at approximately 40 s, the rupture proceeded northward along the trench axis and toward the down-dip direction. Somewhat later, the rupture also extends southward along the trench axis. The largest slip event occurred from 60 to 100 s, with the rupture expanding toward the down-dip direction from the area along the trench axis. In this stage, large slip occurred continuously far offshore of southern Iwate, Miyagi, and northern Fukushima prefectures. The slip amount of the largest slip event was considerably decreased when raising the low-frequency limit of the data for the inversion to 0.02 Hz. This means that the largest slip event radiated seismic waves high in lower-frequency components (<0.02 Hz).

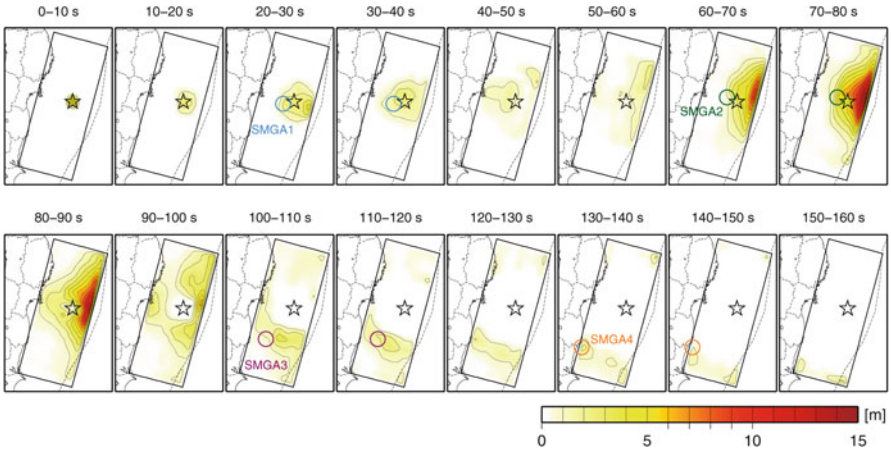

Fig. 3.5 Snapshot of slip amount at every 10 s from the initial break (Suzuki et al. 2011) with locations of SMGAs (Asano and Iwata 2012)

The last stage starts at around 100 s, where the rupture propagated southward in the area off Fukushima and Ibaraki prefectures. The entire rupture almost ceased within 150 s. The slip-velocity time function (Fig. 3 in Suzuki et al. 2011) shows that the subfaults around the hypocentre and the shallow part of the fault experienced two slip events.

3.3 SMGA Source Model for Strong Motion Simulation in 0.1–10 Hz

3.3.1 Location and Rupture Time of SMGAs

Asano and Iwata (2012) assumed that each wave packet S1–S4 seen in the record section of the observed acceleration waveforms (Fig. 3.2) is generated from corresponding strong motion generation area, SMGA1–SMGA4. SMGA is defined as the area characterized by a large uniform slip velocity within the total rupture area, which reproduce near-source strong ground motions up to about 10 Hz (Miyake et al. 2003). Asano and Iwata (2012) modelled those SMGAs to fit the simulated ground motions to the observed ones. They fixed the hypocentre at the location determined routinely by JMA (red star in Fig. 3.6) and assumed that each SMGA is on the surface of the subducting Pacific slab, whose depth was determined by Nakajima and Hasegawa (2006) and Nakajima et al. (2009).

Asano and Iwata (2012) read the onset of S1–S4 in the observed waveforms at K-NET and KiK-net stations along the coast to determine the location of rupture

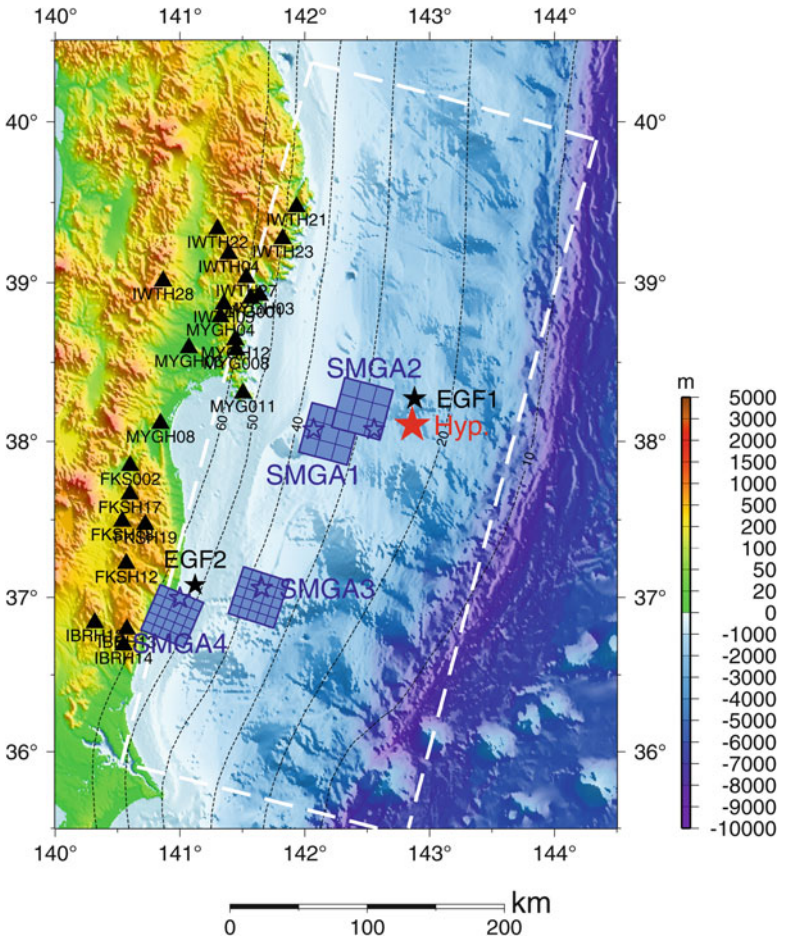

Fig. 3.6 Source model for broadband strong motion simulation between 0.1 and 10 Hz composed of four SMGAs projected on the map (Asano and Iwata 2012)

starting point and rupture time for each SMGA objectively. The optimum set of parameters was determined to minimize the root mean square of difference between the observed and theoretical travel times by grid search. The one-dimensional velocity structure model was assumed, and the difference between the observed and theoretical travel times was corrected by using an Mw6.0 foreshock (EGF1 in Fig. 3.6) occurring at 03:16 on 10 March 2011 (JST) as a reference event, whose location was fixed at the hypocentre determined by JMA. The search intervals in the grid search were 0.005° for latitude and longitude and 0.1 s for rupture time.

The estimated locations of the rupture starting points of the four SMGAs are indicated by the open stars in Fig. 3.6. The rupture delay times from the origin time are estimated to be 24.1, 65.4, 106.5, and 133.0 s, respectively. The spatial

uncertainty in the dip direction is relatively larger than that in the strike direction due to the nonuniform distribution of observed stations surrounding the source region (see Asano and Iwata 2012).

3.3.2 SMGA Source Modelling for Broadband Strong Ground Motion Simulation

Asano and Iwata (2012) constructed the source model composed of four SMGAs based on broadband strong motion simulation from 0.1 to 10 Hz using the empirical Green's function method by Irikura (1986). In this method, the ground motion for a target event is synthesized by summing up the records of small events with a filtering function which corrects the difference in the slip-velocity time function between the large and small events following the source scaling law and the ω^{-2} source spectral model (Irikura 1986; Miyake et al. 2003). These scaling relationships are controlled by two parameters N, which corresponds to the ratio of spatial dimension and slip amount between the large and small events, and C, which corrects the difference in the stress drop between the large and small events.

The scaling parameters N and C were determined for each SMGA by a source spectral fitting method (Miyake et al. 1999, 2003). This method derives these parameters by fitting the observed source spectral ratio between the large and small events to the theoretical source spectral ratio following the ω^{-2} source spectral model. The moment ratio and the corner frequency of the target and small events were estimated by the grid search algorithm. The propagation path effects were corrected for geometrical spreading for the body waves and an attenuation factor. The frequency-dependent quality factor, $Q(f) = 110f^{0.69}$ obtained by Satoh et al. (1997) in this region and the S wave velocity of 4.46 km/s were used to correct the attenuation factor. The records of an Mw6.0 event, which occurred at 03:16 on 10 March 2011 (JST), were used as EGF for SMGA1 and SMGA2 (EGF1), and those of an Mw5.5 event, which occurred at 22:12 on 22 October 2005 (JST), were used as EGF for SMGA3 and SMGA4 (EGF2). The epicentres of two EGF events are shown in Fig. 3.6. N values are 3, 3, 5, and 5 for SMGA1, SMGA2, SMGA3, and SMGA4, respectively. C values were estimated to be 10.6 and 4.0 for SMGA3 and SMGA4, respectively. C values for SMGA1 and SMGA2 were searched together with other unknown parameters in the following strong motion simulations because these C values were not constrained well by the source spectral fitting method due to the small number of N.

Then, the source parameters of the four SMGAs were estimated based on the broadband strong motion simulations using the empirical Green's function method. The best set of parameters was searched by minimizing the residuals of acceleration envelopes and displacement waveforms through a grid search (Miyake et al. 1999, 2003). The parameters to be estimated by the grid search are the spatial dimensions, rise times of the EGF events, the stress drops (i.e. C values) and rupture starting subfaults of each SMGA, and the rupture propagation velocities within the SMGAs. The length L, width W, and rise time T of the SMGA are given by Nl, Nw, $N\tau$ from

Table 3.1 Source parameters of SMGAs

	SMGA1	SMGA2	SMGA3	SMGA4
Latitude (°N)	38.075	38.075	37.060	36.995
Longitude (°E)	142.070	142.555	141.655	141.000
Depth (km)	36.8	28.0	37.1	53.8
Rupture time (s)	24.1	65.4	106.5	133.0
Strike (°)	195	195	198	203
Dip (°)	13	13	17	20
N	3	3	5	5
C	12.0	14.0	10.6	4.0
Length (km)	36	36	35	35
Width (km)	36	36	35	35
Area (km^2)	1,296	1,296	1,225	1,225
Rise time (s)	6.90	6.90	1.70	1.70
Seismic moment (Nm)	4.57×10^{20}	5.33×10^{20}	3.07×10^{20}	1.16×10^{20}
Stress drop (MPa)	23.9	27.8	17.5	6.6
Slip amount (m)	5.2	6.1	3.7	1.4

Latitude, longitude, and depth are defined at the rupture starting point of individual SMGA

the length l, width w, and rise time τ of the EGF event. The search range and its grid interval of the model parameters in the grid search are referred to Asano and Iwata (2012). The stress drops of the EGF events were calculated assuming the circular crack source model (Eshelby 1957). The strike and dip angles of each SMGA were determined based on the local geometry of the plate interface (Nakajima and Hasegawa 2006; Nakajima et al. 2009). The deeper SMGA has slightly steeper dip angle because of the bending of the subducting Pacific slab. The strong motion stations used in this modelling are indicated by the solid triangles in Fig. 3.6.

3.3.3 Result

Figure 3.6 shows a map view of the estimated source model. The source parameters of each SMGA are listed in Table 3.1. The rupture within SMGA1 propagates towards the up-dip direction, whereas that within SMGA2 propagates towards the down-dip directions. The ruptures of SMGA3 and SMGA4 located southwest of the hypocentre mainly propagate in southwest direction. The rupture propagation velocity within each SMGA is 4.0 km/s. The stress drops of four SMGAs range from 6.6 to 27.8 MPa.

Figure 3.7 shows the comparison between the observed and synthetic acceleration, velocity, and displacement waveforms in the frequency range from 0.1 to 10 Hz at 23 strong motion stations. The synthetic ground motions explain well the characteristics of observed ground motion in the broadband frequency range.

Asano and Iwata (2012) pointed out that SMGA1, SMGA2, and SMGA3 spatially overlap the source area of past M7 class earthquakes in 1936, 1933, and 1938, respectively.

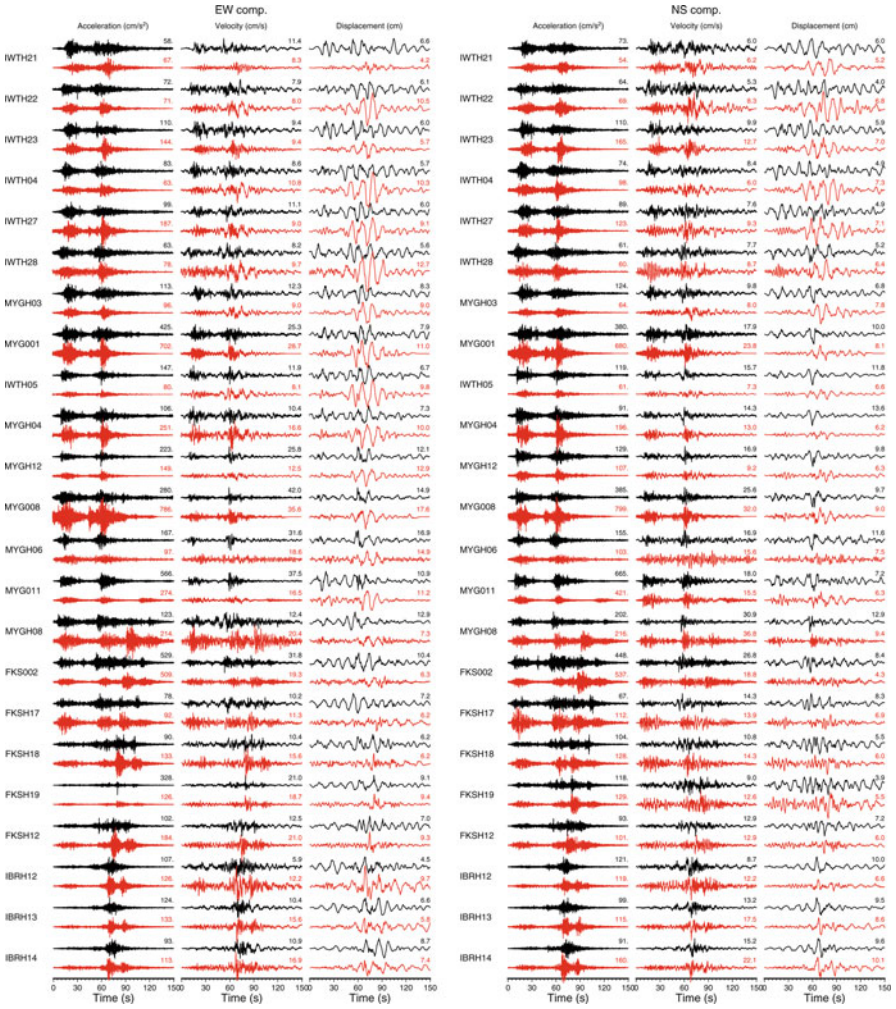

Fig. 3.7 Comparison between the observed and synthetic horizontal acceleration, velocity, and displacement waveforms in 0.1–10 Hz (Asano and Iwata 2012)

3.4 Relationship Between Heterogeneous Rupture Process and Strong Motion Generation Areas

3.4.1 Spatial Relationship Between Slip Distribution and SMGAs

The spatial relationship between large slip area and SMGA has been argued for past earthquakes. As for inland crustal earthquakes, Miyake et al. (2003) concluded that the location and size of SMGA correspond to the asperity, or large slip area on the

source fault. Suzuki and Iwata (2007) analysed the 2005 off Miyagi earthquake (M_{JMA} 7.2), which was a subduction-zone plate-boundary event occurring west of the epicentre of the 2011 Tohoku earthquake. They confirmed that two SMGAs of the 2005 off Miyagi earthquake existed inside the asperity area estimated by the kinematic waveform inversions but size of that area was significantly smaller than asperity area. The source model of the 2003 off Tokachi earthquake (M_{JMA} 8.0) also shows the same features (Kamae and Kawabe 2004). That is, most cases of past subduction-zone plate-boundary earthquakes show the overlap of asperity and SMGA areas. It should be noted that the kinematic waveform inversion studies for the 2003 off Tokachi and 2005 off Miyagi earthquakes use finer spatial grid than current studies for the 2011 Tohoku earthquake and the analysed frequency range is partly overlapped with those used for SMGA modelling. Suzuki (2008) proposed a hierarchical broadband source model for plate-boundary earthquake in which SMGA is a localized area inside the asperity area having particularly high slip velocity.

The SMGAs of the 2011 Tohoku earthquake by Asano and Iwata (2012) and the final slip distribution obtained by Suzuki et al. (2011) are compared in Fig. 3.8. SMGA2 is located near the edge of the asperity and the others are outside the asperity. That is, the large slip area and SMGAs are apparently not overlapped in space for the 2011 Tohoku earthquake. It is a significant characteristic of this event that is different from past M7–8 subduction-zone plate-boundary events in this region. The frequency dependence of rupture process is one answer for the question why SMGA and asperity is apparently complementary in space. Recently, Lay et al. (2012) proposed depth-varying seismic characteristics with four distinct failure domains (domain A to D) extending along the megathrust from the trench to the down-dip edge of the seismogenic zone based on the analyses for three megathrust earthquakes in the world. The domain B from 15 to 35 km deep, which is defined as a portion generating large displacements over large-scale region with only modest coherent high-frequency radiation, corresponds to the asperity of this event. The domain C from 35 to 55 km deep defined as rupture of smaller isolated patches producing bursts of coherent high-frequency energy corresponds to four SMGAs.

In order to see temporal relationship between slip progression and SMGA rupture, the locations of the four SMGA estimated by Asano and Iwata (2012) are compared with the temporal slip history in low-frequency range estimated by Suzuki et al. (2011) in Fig. 3.5. The rupture time of the four SMGAs matches the timing of slip occurrence in each area on the fault plane. This figure implies the possibility that smaller scale local slip peaks in the inverted source process match the SMGAs and such local slip peaks are masked by the dominating large slip near the trench in the final slip distribution.

For solving this problem, the more detailed slip inversion analysis using higher-frequency waveforms, finer spatial grids, and reliable Green's functions is required to see whether the localized small asperity or high slip-velocity area corresponding to SMGAs can be resolved or not.

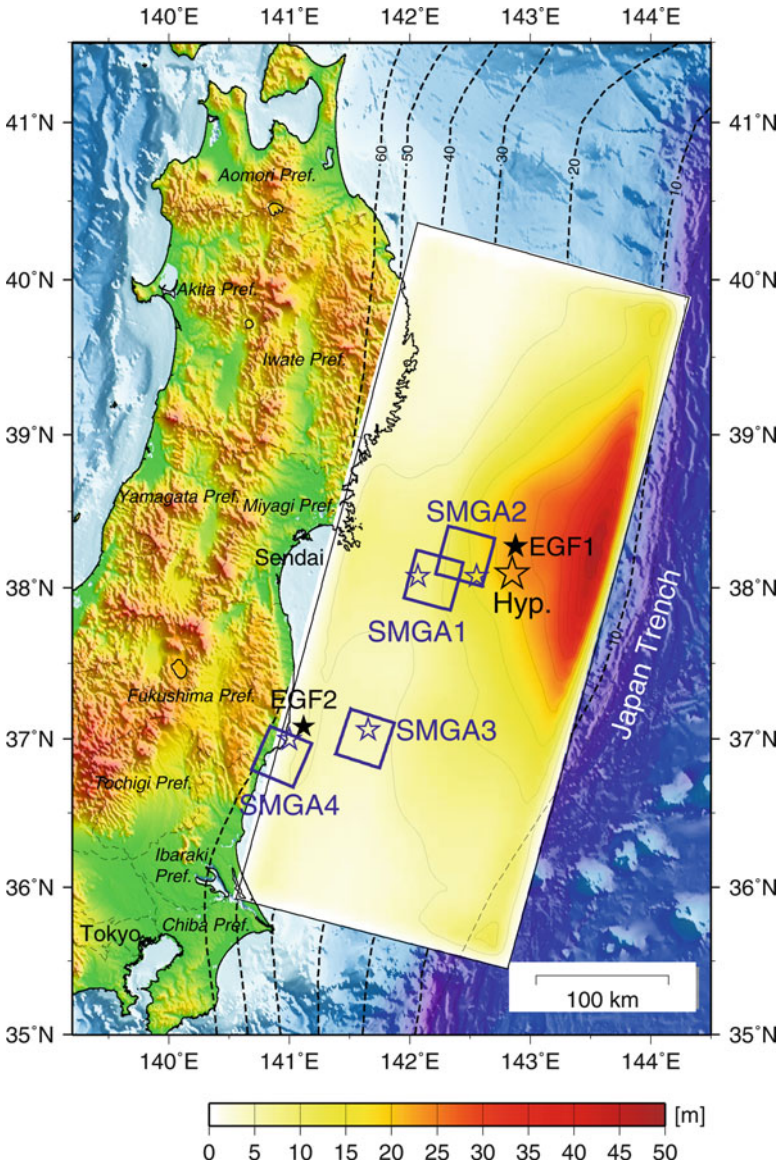

Fig. 3.8 Spatial comparison between SMGAs by Asano and Iwata (2012) and final slip distribution by Suzuki et al. (2011)

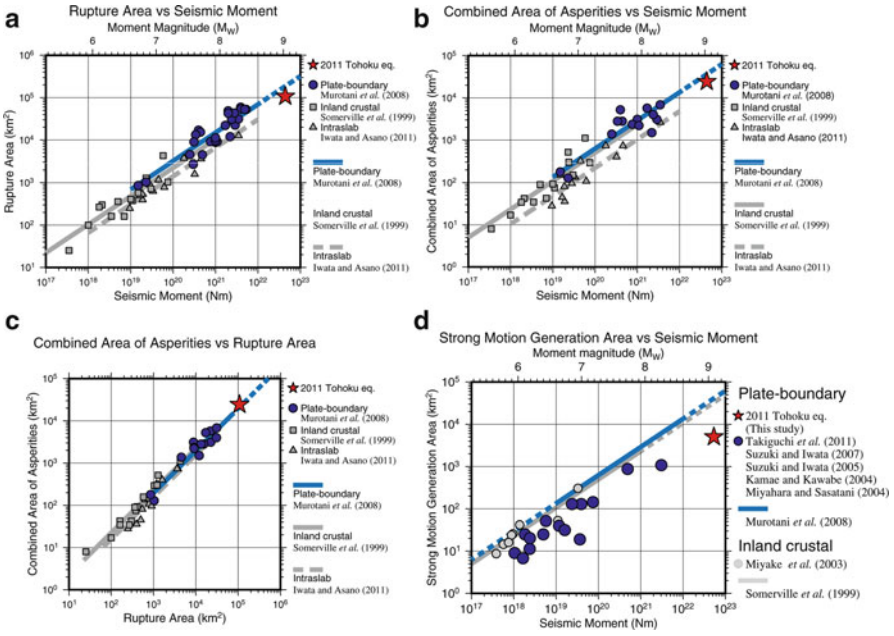

Fig. 3.9 Scaling relationships between **(a)** total rupture area and seismic moment, **(b)** combined area of asperities and seismic moment, **(c)** combined area of asperities and total rupture area, and **(d)** strong motion generation area and seismic moment

3.4.2 Scaling Relationships

In this section, we compare the source features of this earthquake obtained by Asano and Iwata (2012) and Suzuki et al. (2011) with the empirical scaling relationships between the size of SMGA and seismic moment and between rupture area and asperity area.

The empirical scaling relationships between rupture area, total asperity area, and seismic moment for plate-boundary earthquakes are studied by Murotani et al. (2008). Murotani et al. (2008) compiled the heterogeneous slip models of 26 plate-boundary earthquakes in Japan and characterized the total rupture area and asperities following the procedure proposed by Somerville et al. (1999). We extracted the total rupture area and asperities of the 2011 Tohoku earthquake following the same procedure and found them as 107,100 and 24,300 km^2, respectively. Those values are plotted in Fig. 3.9a–c together with other events studied in the previous studies. The rupture area and asperity of the 2011 Tohoku earthquake follow the empirical scaling relationship by Murotani et al. (2008). The rupture area and asperity of plate-boundary earthquakes have relatively larger dimensions than those of inland crustal (Somerville et al. 1999) and intraslab earthquakes (Iwata and Asano 2011) of the same seismic moment. But we have to be careful in treating the asperity area abstracted for this earthquake by the conventional method. As discussed in the

Subsection 3.4.1, the asperity of this event radiated low-frequency dominantly and does not include SMGAs. Its nature may be different from those abstracted for the past M7–8 plate-boundary earthquakes.

Combined area of SMGAs of the 2011 Tohoku earthquake obtained by Asano and Iwata (2012) is 5,042 km^2. The total size of SMGA is about 1/5 of the asperity area. This value against the seismic moment is plotted in Fig. 3.9d together with the SMGA areas for the other earthquakes. SMGA source models have been constructed for past plate-boundary earthquakes in northeast Japan: the 1994 far off Sanriku earthquake (Mw7.7) by Miyahara and Sasatani (2004), the 2003 off Tokachi earthquake (Mw8.3) by Kamae and Kawabe (2004), the 2005 off Miyagi earthquake (Mw7.2) by Suzuki and Iwata (2007), and the 1982 and 2008 off Ibaraki earthquakes (Mw7.0 and 6.8) by Takiguchi et al. (2011). Suzuki and Iwata (2005) analysed other Mw6.0–7.0 plate-boundary earthquakes in northeast Japan. Miyake et al. (2003) analysed SMGA for inland crustal events in Japan and concluded that the size of SMGA corresponds to the size of asperity for inland crustal earthquakes. That is, SMGA for inland crustal earthquakes follows the empirical scaling relationship for asperity and seismic moment proposed by Somerville et al. (1999). On the other hand, the size of SMGA of plate-boundary earthquakes in northeast Japan is smaller than those of inland crustal earthquakes of the same seismic moment. This fact indicates that the stress drop of SMGA for subduction-zone plate-boundary earthquakes is larger than that of inland crustal earthquakes (Suzuki and Iwata 2007). The 2011 Tohoku earthquake also shows similar tendency with previous subduction-zone plate-boundary earthquakes.

3.5 Source Models by Other Research Groups

For the 2011 Tohoku earthquake, many research groups in seismology and geodesy are extensively working on analysing the heterogeneous source process using various kinds of data (strong motion, teleseismic body and surface waves, static and high-rate GPS, InSAR, tsunami waveform, etc.). In Table 3.2, we summarize the spatiotemporal heterogeneous slip models derived using seismological data (e.g. strong motion, teleseismic, and high-rate GPS data) from published papers. Most of papers use multiple time windows for each subfault in their source inversion analysis (Ide et al. 2011; Koketsu et al. 2011; Lay et al. 2011; Lee et al. 2011; Suzuki et al. 2011; Yagi and Fukahata 2011a; Yokota et al 2011; Yoshida et al. 2011a, b; Yue and Lay 2011), whereas the others use single time window with variable slip duration (Ammon et al. 2011; Hayes 2011; Shao et al. 2011). Peak slip amount in these source models varies from 28 to 63 m. The rupture dimension differs by a factor of two.

SMGA source model is also published by Kurahashi and Irikura (2011). Back-projection analyses using teleseismic and regional array dataset are studied to infer frequency-dependent seismic wave radiation process on the fault (Honda et al. 2011; Ishii 2011; Kiser and Ishii 2012; Koper et al. 2011; Meng et al. 2011; Roten et al. 2012; Wang and Mori 2011; Zhang et al. 2011).

Table 3.2 Summary of source models using seismological data

Reference	Data	Hypocentre information	Strike/dip	Fault size (km^2)	Subfault size (km^2)	Vr (km/s)	Seismic moment (Nm)	Peak slip (m)	Inversion method
Ammon et al. (2011)	Teleseismic P and Rayleigh High-rate GPS	USGS	202/12	600×210	15×15	1.5 ($r<100$ km), 2.5	3.64×10^{22}	41	Ammon et al. (2005)
Hayes (2011)	Teleseismic P&SH (0.005–1 Hz) Rayleigh and Love (0.002–0.005 Hz)	USGS	194/10	625×260	25×20	Variable	4.90×10^{22}	33	Ji et al. (2002)
Ide et al. (2011)	Teleseismic P (0.005–1 Hz)	–	–	440×240	20×20	Infinity	4.5×10^{22}	30	Ide (2001)
Koketsu et al. (2011)	Teleseismic P (0.002–0.25 Hz) Strong motion (0.01–0.1 Hz) GPS static disp	JMA + dep. 17 km	200/12	480×150	30×30	2.5	3.8×10^{22}	36	Yoshida et al. (1996)
Lay et al. (2011)	Teleseismic P	Zhao et al. (2011)	202/10	380×200	20×20	1.5 ($r<100$ km), 2.5	4.0×10^{22}	63	Kikuchi and Kanamori (2003)
Lee et al. (2011)	Teleseismic P (0.005–0.2 Hz) Strong motion (0.01–0.2 Hz) GPS static disp.	JMA	193/14	660×240	20×20	3.5	3.67×10^{22}	50	Lee et al. (2006)
Shao et al. (2011)	Teleseismic P&SH (0.003–0.5 Hz) Rayleigh and Love (0.003–0.006 Hz)	JMA	198/10	475×200	25×20	Variable	5.75×10^{22}	59	Ji et al. (2002)
Suzuki et al. (2011)	Strong motion (0.01–0.125 Hz)	NIED and JMA	195/13	510×210	30×30	3.2	4.42×10^{22}	48	Hartzell and Heaton (1983)
Yagi and Fukahata (2011a)	Teleseismic P (0.001–0.38 Hz)	JMA + dep. 22 km	200/12	500×200	20×20	2.8	5.7×10^{22}	51	Yagi and Fukahata (2011b)
Yokota et al. (2011)	Teleseismic P (0.002–0.25 Hz) Strong motion (0.01–0.1 Hz) GPS static disp. tsunami	JMA + dep. 17 km	200/5, 12, 20	480×180	30×30	2.5	4.2×10^{22}	35	Yoshida et al. (1996)
Yoshida et al. (2011a)	Strong motion (0.005–0.05 Hz)	JMA	193/10	468×228	12×12	2.5	4.3×10^{22}	47	Hartzell and Heaton (1983)
Yoshida et al. (2011b)	Teleseismic P (0.002–1 Hz)	JMA	201/9	510×240	30×30	1.8	4.3×10^{22}	28	Kikuchi and Kanamori (2003)
Yoshida et al. (2011b)	Strong motion (0.01–0.15 Hz)	JMA	201/9	475×175	25×25	2.5	3.4×10^{22}	38	Ide et al. (1996)
Yue and Lay (2011)	High-rate GPS (DC-0.04 Hz)	Zhao et al. (2011)	202/10, 22	475×175	20×20	1.5 ($r<100$ km), 2.5	4.8×10^{22}	60	Hartzell and Heaton (1983)

3.6 Summary

We compared the source process of the 2011 Tohoku earthquake seen in lower- and higher-frequency bands and discussed their relation based on the kinematic source model inverted from strong motion data in 0.01–0.125 Hz by Suzuki et al. (2011) and the SMGA model estimated by the forward modelling of strong ground motion in 0.1–10 Hz by Asano and Iwata (2012). The slip distribution is characterized by a large asperity with peak slip of 48 m which is imaged in the shallower portion of the source fault near the Japan Trench east of the epicentre rupturing from 60 to 100 s after the initial break. The entire rupture lasted about 150 s. Four SMGAs are identified in the deeper portion of the source fault. The rupture area and asperity of the 2011 Tohoku earthquake coincide with the empirical scaling relationship for plate-boundary earthquake derived by Murotani et al. (2008). Although the asperity of this event abstracted based on slip amount may have different nature from those of past earthquakes compiled in Murotani et al. (2008), the SMGA area is significantly smaller than asperity area, which is similar to past plate-boundary events in north-east Japan. Unlike past events, the SMGAs and the asperity apparently do not overlap for this earthquake, whereas the rupture time of each SMGA matches the timing of slip in each area. This is a significant difference between the 2011 Tohoku earthquake and past M7–8 subduction-zone plate-boundary events in this region. The frequency-dependent characteristics of spatiotemporal slip history of this event might cause this difference because the target frequency ranges of current two studies almost do not overlap. The source modelling for strong motion prediction of future subduction-zone plate-boundary mega earthquakes should be advanced based on the knowledge obtained from this event.

Acknowledgments The strong motion data of K-NET, KiK-net, and JMA are used in this study. The digital data of the geometry of the Pacific plate is compiled and provided via the Internet by Dr. Fuyuki Hirose at the Meteorological Research Institute of JMA. Most of figures were produced by using the Generic Mapping Tools (Wessel and Smith 1998).

References

Ammon CJ, Ji C, Thio H-K, Robinson D, Ni S, Hjorleifsdottir V, Kanamori H, Lay T, Das S, Helmberger DV, Ichinose G, Polet J, Wald D (2005) Rupture process of the great 2004 Sumatra-Andaman earthquake. Science 308(5725):1133–1139

Ammon CJ, Lay T, Kanamori H, Cleveland M (2011) A rupture model of the 2011 off the Pacific coast of Tohoku earthquake. Earth Planets Space 63(7):693–696

Aoi S, Kunugi T, Fujiwara H (2004) Strong-motion seismograph network operated by NIED: K-NET and KiK-net. J Jpn Assoc Earthq Eng 4(3):65–74

Aoi S, Kunugi T, Nakamura H, Fujiwara H (2011) Deployment of new strong motion seismographs of K-NET and KiK-net. In: Akkar S et al (eds) Earthquake data in engineering seismology. Geotechnical, Geological and Earthquake Engineering 14. Springer, Dordrecht, pp 167–186

Asano K, Iwata T (2012) Source model for strong ground motion in 0.1–10 Hz during the 2011 Tohoku earthquake. Earth Planets Space 64(12):1111–1123

Bouchon M (1981) A simple method to calculate Green's function for elastic layered media. Bull Seismol Soc Am 71(4):959–971
Eshelby JD (1957) The determination of the elastic field of an ellipsoidal inclusion, and related problems. Proc Roy Soc A 241(1226):376–396
Fujiwara H, Kawai S, Aoi S, Morikawa N, Senna S, Kudo N, Ooi M, Hao K, Hayakawa Y, Toyama N, Matsuyama H, Iwamoto K, Suzuki H, Liu Y (2009) A study on subsurface structure model for deep sedimentary layers of Japan for strong-motion evaluation. Technical Note of the NIED 337, DVD-ROM (in Japanese)
Hartzell SH, Heaton TH (1983) Inversion of strong ground motion and teleseismic waveform data for the fault rupture history of the 1979 Imperial Valley, California, earthquake. Bull Seismol Soc Am 73(6A):1553–1583
Hasegawa A, Horiuchi S, Umino N (1994) Seismic structure of the northeastern Japan convergent margin: a synthesis. J Geophys Res 99(11):22,295–22,311
Hayes GP (2011) Rapid source characterization of the 2011 Mw9.0 off the Pacific coast of Tohoku earthquake. Earth Planets Space 63(7):529–534
Honda R, Yukutake Y, Ito H, Harada M, Aketagawa T, Yoshida A, Sakai S, Nakagawa S, Hirata N, Obara K, Kimura H (2011) A complex rupture image of the 2011 off the Pacific coast of Tohoku Earthquake revealed by the MeSO-net. Earth Planets Space 63(7):583–588
Hoshiba M, Iwakiri K, Hayashimoto N, Shimoyama T, Hirano K, Yamaya Y, Ishigaki Y, Kikuta H (2011) Outline of the 2011 off the Pacific coast of Tohoku Earthquake. Earth Planets Space 63(7):547–551
Ide S (2001) Complex source processes and the interaction of moderate earthquakes during the earthquake swarm in the Hida-Mountains, Japan, 1998. Tectonophysics 334(1):35–54
Ide S, Takeo M, Yoshida Y (1996) Source process of the 1995 Kobe earthquake: determination of spatio-temporal slip distribution by Bayesian modeling. Bull Seismol Soc Am 86(3):547–566
Ide S, Baltay A, Beroza GC (2011) Shallow dynamic overshoot and energetic deep rupture in the 2011 Mw9.0 Tohoku-Oki earthquake. Science 332(6036):1426–1429
Irikura K (1986) Prediction of strong acceleration motions using empirical Green's function. In: Proceedings of the 7th Japan earthquake engineering symposium, Tokyo, pp 151–156
Ishii M (2011) High-frequency rupture properties of the Mw9.0 off the Pacific coast of Tohoku earthquake. Earth Planets Space 63(7):609–614
Iwata T, Asano K (2011) Characterization of the heterogeneous source model of intraslab earthquakes toward strong ground motion prediction. Pure Appl Geophys 168(1–2):117–124
Ji C, Wald D, Helmberger DV (2002) Source description of the 1999 Hector Mine, California, earthquake, part I: Wavelet domain inversion theory and resolution analysis. Bull Seismol Soc Am 92(4):1192–1207
Kamae K, Kawabe H (2004) Source model composed of asperities for the 2003 Tokachi-oki, Japan, earthquake (M_{JMA}=8.0) estimated by the empirical Green's function method. Earth Planets Space 56(3):323–327
Kennett BLN, Kerry NJ (1979) Seismic waves in a stratified half space. Geophys J Roy Astr Soc 57(3):557–583
Kikuchi M, Kanamori H (2003) Note on teleseismic body-wave inversion program. http://www.eri.u-tokyo.ac.jp/ETAL/KIKUCHI/
Kiser E, Ishii M (2012) The March 11, 2011 Tohoku-oki earthquake and cascading failure of the plate interface. Geophys Res Lett 39:L00G25. doi:10.1029/2012GL051170
Koketsu K, Yokota Y, Nishimura N, Yagi Y, Miyazaki S, Satake K, Fujii Y, Miyake H, Sakai S, Yamanaka Y, Okada T (2011) A unified source model for the 2011 Tohoku earthquake. Earth Planet Sci Lett 310(3–4):480–487
Koper KD, Hutko AR, Lay T, Ammon CJ, Kanamori H (2011) Frequency-dependent rupture process of the 2011 Mw9.0 Tohoku earthquake: comparison of short-period P wave backprojection images and broadband seismic rupture models. Earth Planets Space 63(7):599–602
Kunugi T, Aoi S, Suzuki W, Nakamura H, Morikawa N, Fujiwara H (2012) Strong motions of the 2011 Tohoku-Oki earthquake. Natural Disaster Research Report, NIED 48:63–72 (in Japanese with English abstract)

Kurahashi S, Irikura K (2011) Source model for generating strong ground motions during the 2011 off Pacific coast of Tohoku earthquake. Earth Planets Space 63(7):571–576

Lawson CL, Hanson RJ (1974) Solving least squares problems. Prentice-Hall, New Jersey, 340 pp

Lay T, Ammon CJ, Kanamori H, Xue L, Kim MJ (2011) Possible large near-trench slip during the 2011 Mw9.0 off the Pacific coast of Tohoku earthquake. Earth Planets Space 63(7): 687–692

Lay T, Kanamori H, Ammon CJ, Koper KD, Hutko AR, Ye L, Yue H, Rushing TM (2012) Depth-varying rupture properties of subduction zone megathrust earthquakes. J Geophys Res 117(B4):B04311. doi:10.1029/2011JB009133

Lee S-J, Ma K-F, Chen H-W (2006) Three-dimensional dense strong motion waveform inversion for the rupture process of the 1999 Chi-Chi, Taiwan, earthquake. J Geophys Res 111(B11):B11308. doi:10.1029/2005JB004097

Lee S-J, Huang B-S, Ando M, Chiu H-C, Wang J-H (2011) Evidence of large scale repeating slip during the 2011 Tohoku-Oki earthquake. Geophys Res Lett 38(19):L19306. doi:10.1029/2011GL049580

Meng L, Inbal A, Ampuero J-P (2011) A window into the complexity of the dynamic rupture of the 2011 Mw9 Tohoku-Oki earthquake. Geophys Res Lett 38:L00G07. doi:10.1029/2011GL048118

Miyahara S, Sasatani T (2004) Estimation of source process of the 1994 Sanriku Haruka-oki earthquake using empirical Green's function method. Geophys Bull Hokkaido Univ 67:197–212 (in Japanese with English abstract)

Miyake H, Iwata T, Irikura K (1999) Strong ground motion simulation and source modeling of the Kagoshima-ken Hokuseibu earthquakes of March 26 (M_{JMA} 6.5) and May 13 (M_{JMA} 6.3), 1997, using empirical Green's function method. Zisin 2 (J Seism Soc Jpn) 51(4):431–442 (in Japanese with English abstract)

Miyake H, Iwata T, Irikura K (2003) Source characterization for broadband ground-motion simulation: kinematic heterogeneous source model and strong motion generation area. Bull Seismol Soc Am 93(6):2531–2545

Murotani S, Miyake H, Koketsu K (2008) Scaling of characterized slip models for plate-boundary earthquakes. Earth Planets Space 60(9):987–991

Nakajima J, Hasegawa A (2006) Anomalous low-velocity zone and linear alignment of seismicity along it in the subducted Pacific slab beneath Kanto, Japan: reactivation of subducted fracture zone? Geophys Res Lett 33(16):L16309. doi:10.1029/2006GL026773

Nakajima J, Hirose F, Hasegawa A (2009) Seismotectonics beneath the Tokyo metropolitan area, Japan: effect of slab-slab contact and overlap on seismicity. J Geophys Res 114(B8):B08309. doi:10.1029/2008JB006101

Olson AH, Aspel RJ (1982) Finite faults and inverse theory with applications to the 1979 Imperial Valley earthquake. Bull Seismol Soc Am 72(6A):1969–2001

Roten D, Miyake H, Koketsu K (2012) A Rayleigh wave back-projection method applied to the 2011 Tohoku earthquake. Geophys Res Lett 39(2):L02302. doi:10.1029/2011GL050183

Satoh T, Kawase H, Sato T (1997) Statistical spectral model of earthquakes in the eastern Tohoku district, Japan, based on the surface and borehole records observed in Sendai. Bull Seismol Soc Am 87(2):446–462

Sekiguchi H, Irikura K, Iwata T (2000) Fault geometry at the rupture termination of the 1995 Hyogo-ken Nanbu earthquake. Bull Seismol Soc Am 90(1):117–133

Sekiguchi H, Irikura K, Iwata T (2002) Source inversion for estimating the continuous slip distribution on a fault—introduction of Green's functions convolved with a correction function to give moving dislocation effects in subfaults. Geophys J Int 150(2):377–391

Shao G, Xi L, Ji C, Maeda T (2011) Focal mechanism and slip history of 2011 Mw9.1 off the Pacific coast of Tohoku earthquake, constrained with teleseismic body and surface waves. Earth Planets Space 63(7):559–564

Somerville PG, Irikura K, Graves R, Sawada S, Wald D, Abrahamson N, Iwasaki Y, Kagawa T, Smith N, Kowada A (1999) Characterizing crustal earthquake slip models for the prediction of strong ground motion. Seismol Res Lett 70(1):59–80

Suzuki W (2008) Estimation of broadband source process based on strong motion modeling. Ph.D Thesis, Kyoto University, 130 pp

Suzuki W, Iwata T (2005) Source characteristics of interplate earthquakes in northeast Japan inferred from the analysis of broadband strong-motion records. Eos Trans AGU 86(52), Fall Meet. Suppl., Abstract S43A-1040

Suzuki W, Iwata T (2007) Source model of the 2005 Miyagi-oki, Japan, earthquake estimated from broadband strong motions. Earth Planets Space 59(11):1155–1171

Suzuki W, Aoi S, Sekiguchi H, Kunugi T (2011) Rupture process of the 2011 Tohoku-Oki mega-thrust earthquake (M9.0) inverted from strong-motion data. Geophys Res Lett 38:L00G16. doi:10.1029/2011GL049136

Takiguchi M, Asano K, Iwata T (2011) The comparison of source models of repeating subduction-zone earthquakes estimated using broadband strong motion records –1982 and 2008 Ibaraki-ken-oki M7 earthquakes–. Zisin 2 (J Seismol Soc Japan) 63(4):223–242 (in Japanese with English abstract)

Wang D, Mori J (2011) Rupture process of the 2011 off the Pacific coast of Tohoku earthquake (Mw9.0) as imaged with back-projection of teleseismic P-waves. Earth Planets Space 63(7):603–607

Wessel P, Smith WHF (1998) New, improved version of generic mapping tools released. Eos Trans AGU 79(47):579

Yagi Y, Fukahata Y (2011a) Rupture process of the 2011 Tohoku-oki earthquake and absolute elastic strain release. Geophys Res Lett 38(19):L19307. doi:10.1029/2011GL048701

Yagi Y, Fukahata Y (2011b) Introduction of uncertainty of Green's function into waveform inversion for seismic source process. Geophys J Int 186(2):711–720

Yokota Y, Koketsu K, Fujii Y, Satake K, Sakai S, Shinohara M, Kanazawa T (2011) Joint inversion of strong motion, teleseismic, geodetic, and tsunami datasets for the rupture process of the 2011 Tohoku earthquake. Geophys Res Lett 38:L00G21. doi:10.1029/2011GL050098

Yoshida S, Koketsu K, Shibazaki B, Sagiya T, Kato T, Yoshida Y (1996) Joint inversion of the near- and far-field waveforms and geodetic data for the rupture process of the 1995 Kobe earthquake. J Phys Earth 44(5):437–454

Yoshida K, Miyakoshi K, Irikura K (2011a) Source process of the 2011 off the Pacific coast of Tohoku earthquake inferred from waveform inversion with long-period strong-motion records. Earth Planets Space 63(7):577–582

Yoshida Y, Ueno H, Muto D, Aoki S (2011b) Source process of the 2011 Off the Pacific coast of Tohoku earthquake with the combination of teleseismic and strong motion data. Earth Planets Space 63(7):565–569

Yue H, Lay T (2011) Inversion of high-rate (1 sps) GPS data for rupture process of the 11 March 2011 Tohoku earthquake (Mw9.1). Geophys Res Lett 38:L00G09. doi:10.1029/2011GL048700

Zhang H, Ge Z, Ding L (2011) Three sub-events composing the 2011 off the Pacific coast of Tohoku earthquake (Mw9.0) inferred from rupture imaging by back-projecting teleseismic P waves. Earth Planets Space 63(7):595–598

Zhao D, Hunag Z, Umino N, Hasegawa A, Kanamori H (2011) Structural heterogeneity in the megathrust zone and mechanism of the 2011 Tohoku-oki Earthquake (Mw9.0). Geophys Res Lett 38(17):L17308. doi:10.1029/2011GL048408

Chapter 4
Field Survey of the Damage Caused by the 2011 Off the Pacific Coast of Tohoku Earthquake Tsunami

Tetsuya Hiraishi, N. Yoneyama, Y. Baba, and R. Azuma

Abstract The 2011 Off the Pacific Coast of Tohoku Earthquake occurred at 14:46 on March 11, 2011. The earthquake's epicenter was off the Pacific Coast of the Tohoku region in Japan. The intensity of this earthquake was huge, and the gigantic tsunami that it generated affected not only Tohoku Coast but also most of Japan's Pacific coast. This paper describes a part of the results of the field survey done by the DPRI team along the Sendai Coast.

Keywords Inundation height • Run-up height • The 2011 Off the Pacific coast of Tohoku Earthquake • Tsunami survey

4.1 Introduction

The 2011 Off the Pacific Coast of Tohoku Earthquake (2011) occurred at 14:46 on March 11, 2011. The earthquake's epicenter was off the Pacific coast of the Tohoku region in Japan. The intensity of this earthquake was huge, and the gigantic tsunami that it generated affected not only Tohoku Coast but also most of Japan's Pacific coast. Although the DPRI's maritime observatory was 1,000 km away from the tsunami's origin, it was still able to obtain a clear tsunami profile, shown in Fig. 4.1. Shortly after the event, the DPRI sent a team to the Miyagi Prefecture to investigate the tsunami's impact along the coast. This chapter describes the initial survey results along with some observations made from the interviews of the affected residents of the region.

T. Hiraishi (✉) • N. Yoneyama • Y. Baba • R. Azuma
Disaster Prevention Research Institute (DPRI) of Kyoto University, Kyoto, Japan
e-mail: hiraishi.tetsuya.2c@kyoto-u.ac.jp

H. Kawase (ed.), *Studies on the 2011 Off the Pacific Coast of Tohoku Earthquake*,
Natural Disaster Science and Mitigation Engineering: DPRI reports,
DOI 10.1007/978-4-431-54418-0_4,

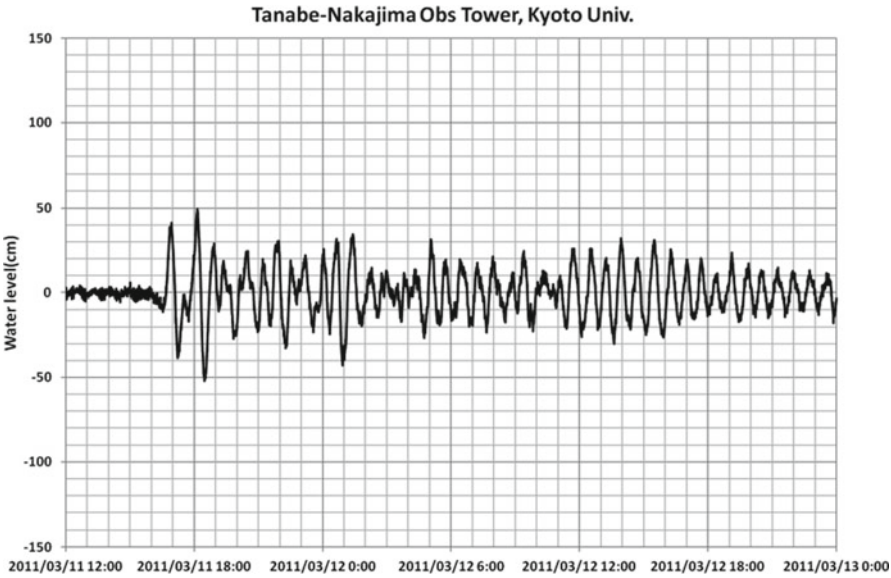

Fig. 4.1 The tsunami profile obtained at the DPRI Shirahama Observatory

4.2 Tsunami Heights

Japan has been hit by many earthquakes in the past. Figure 4.2 shows the moment magnitude of some of the largest earthquakes recorded in historical documents. The 2011 Tohoku Earthquake, however, is the largest and most severe that modern Japan has experienced. The tsunami it generated is the first one to affect a densely populated coastal urban area.

Tsunami heights in coastal areas are described using two measures: one is inundation height measured in traces on remained houses and another run-up heights measured in hilly slopes. Figure 4.3 depicts both measures of tsunami height as they are applied in coastal areas.

Figure 4.4 shows the 2011 Tohoku tsunami height distribution recorded by survey groups from several universities and research institutions. Figure 4.5 shows a comparison of the 1863, 1933, and 2011 tsunami run-up heights.

The group dispatched from DPRI mainly covered the flat farming areas in Miyagi Prefecture. The team of DPRI reached Miyagi area through Niigata area.

Figure 4.6 shows the first survey's data for the 2011 tsunami height distribution in Matsushima Bay. Tsunami height was defined as the height reached above the tide level at each target area. In the figures, the latest tsunami arrival time is assumed to be 15:30, as reported by residents during interviews. A more accurate arrival time could not be defined because of breakdowns at coastal tide stations and power failures that occurred after the earthquake. Figure 4.7 shows the tsunami height distribution data obtained in a second survey that was conducted for Kamaishi Harbor, which has one of the largest breakwaters in the world.

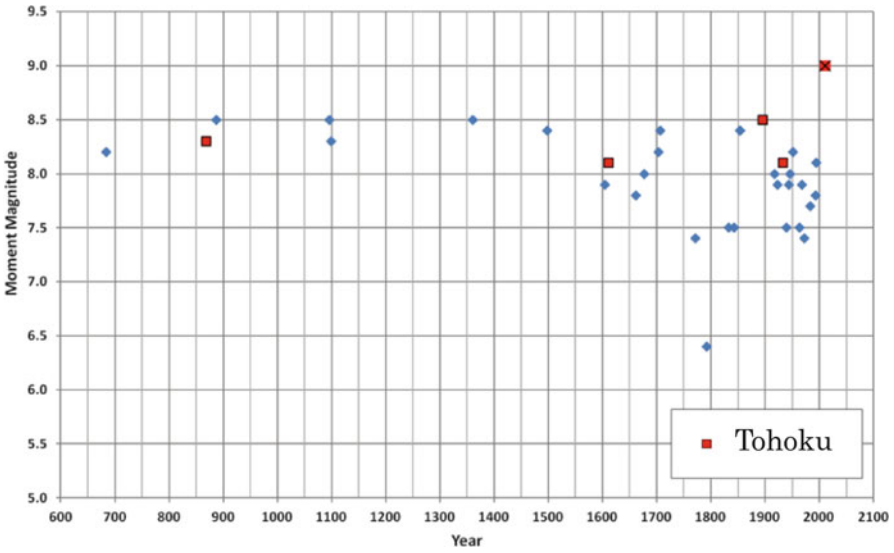

Fig. 4.2 Moment magnitude of historic tsunami earthquakes in Japan

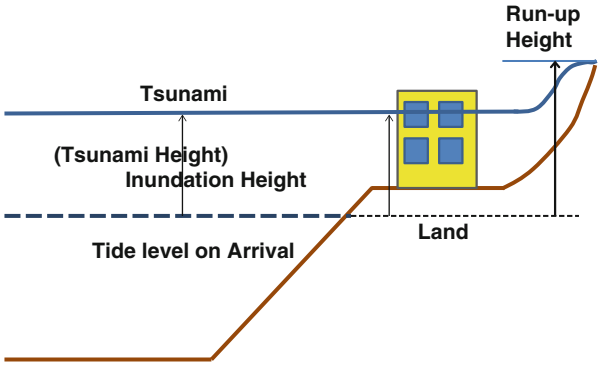

Fig. 4.3 Measurements of tsunami heights in coastal areas

Tsunami heights in the northern part of the Tohoku Coast in 2011 were comparable to those recorded for the 1863 Meiji-Sanriku and 1923 Showa-Sanriku Earthquake Tsunamis. However, tsunami heights in the southern part of the Tohoku Coast were much higher than would have been expected in comparison with these two earlier events. The tsunami joint survey group compared the Meiji-Sanriku and Showa-Sanriku tsunami run-up heights with the 2011 Tohoku Earthquake Tsunami run-up heights (Fig. 4.5). The run-up height in the Meiji-Sanriku tsunami was higher in several places than in the 2011 Tohoku tsunami. A notable characteristic of the 2011 Tohoku tsunami is that the run-up height was generally larger in the southern part of the Tohoku area. No experience in the recent years in the southern area cause delay of evacuation and relatively lower coastal tide walls and sea walls

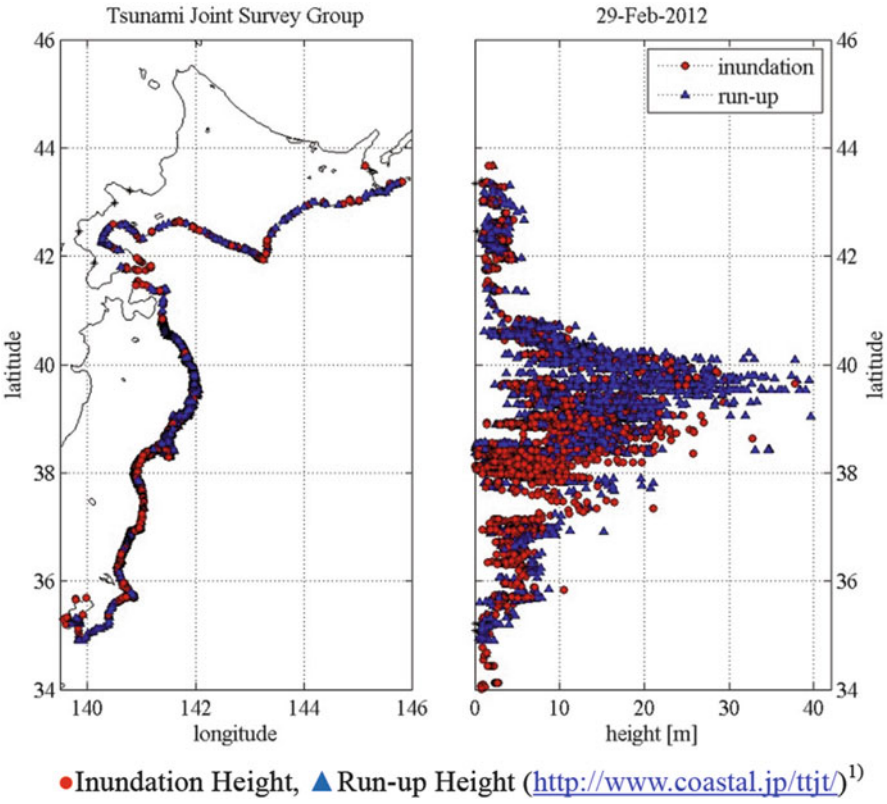

Fig. 4.4 The 2011 Off the Pacific Coast of Tohoku earthquake Tsunami

existence. Also unfortunately, the population was not prepared because no tsunamis had occurred in the recent year. Evacuation was delayed and damage was worse that it might have been because coastal tide walls low and no breakwaters had been built.

In the Tohoku region, the maximum run-up height was about 39 m, and inundation height was 10–40 m. The inundation height in Matsushima Bay was about 10–15 m, except where Matsushima Harbor was protected by small offshore islands. The small offshore islands had an apparent mitigation effect, as the inundation height behind the islands was about 3 m. In the second field survey, tsunami height distribution was obtained for Kamaishi Harbor, where the largest tsunami breakwater had been constructed to prevent tsunami and stormy waves. In assessing the scope of the Tohoku Earthquake Tsunami it is important to note that the tidal stations were unable to obtain any tsunami wave profiles in shallow waters. Neither could the offshore observation buoy network catch any real-time tsunami profiles, mainly because of electrical power outages just after the earthquake. The Ministry of Land, Infrastructure, Transport and Tourism (MLIT) has an offshore GPS buoy for wave observation (illustrated in Fig. 4.8). Though the real-time tsunami warning was not broadcast because of the electricity outage at the land station, the offshore tsunami

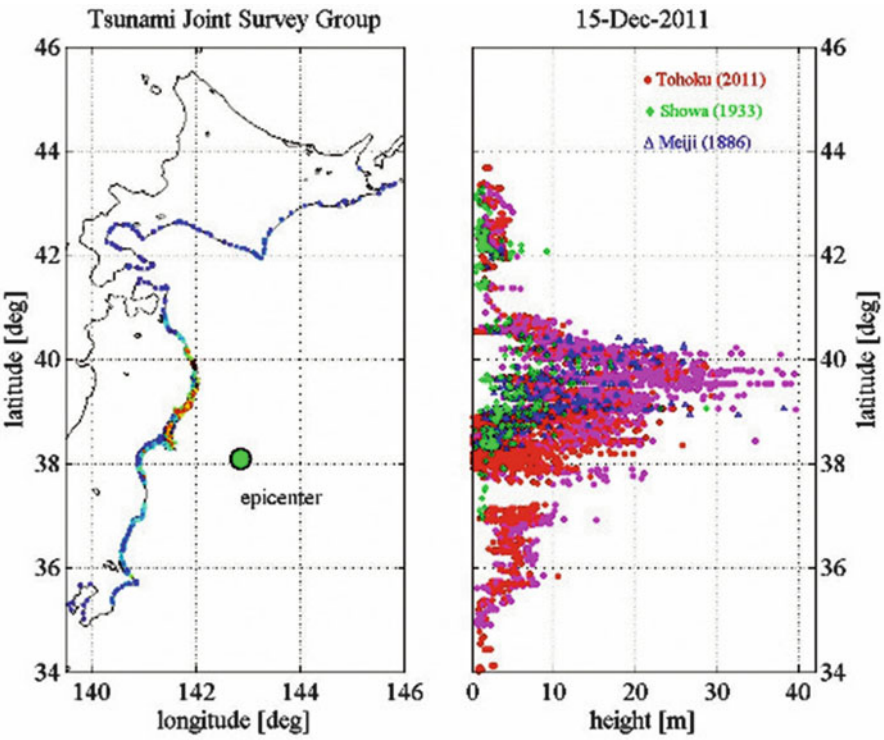

Fig. 4.5 Comparison of run-up heights from the 1886, 1933, and 2011 tsunamis (*pink triangle* shows the 2011 Off the Pacific Coast of Tohoku earthquake Tsunami)

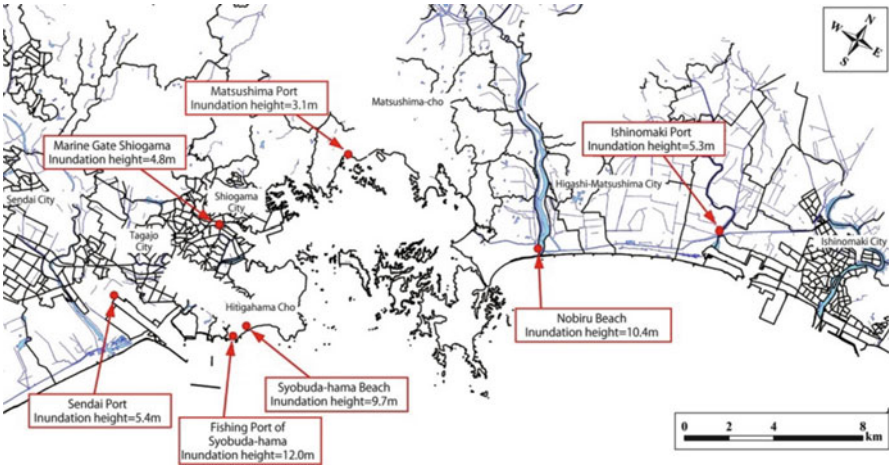

Fig. 4.6 Tsunami heights at various locations around Matsushima Bay

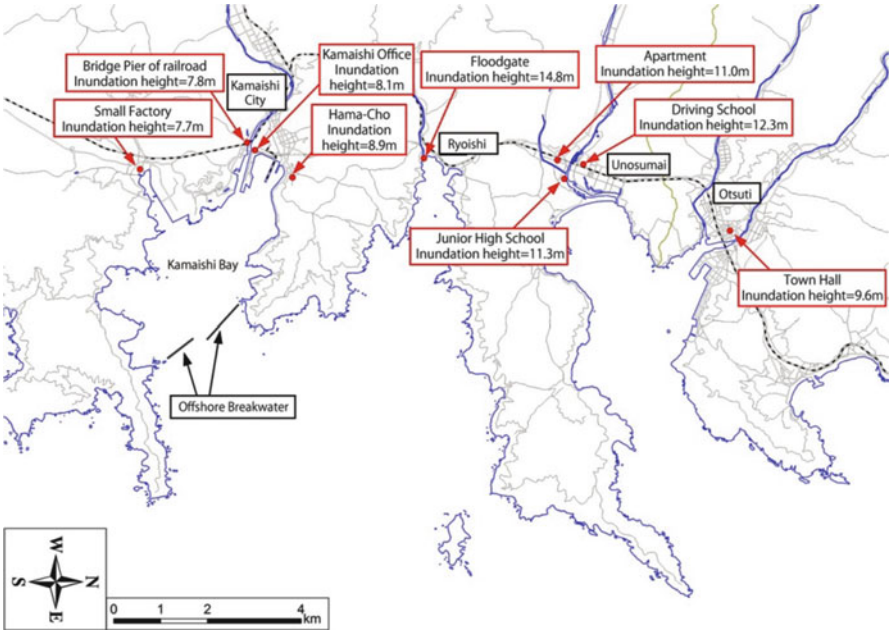

Fig. 4.7 Tsunami height at Kamaishi Harbor and its vicinity

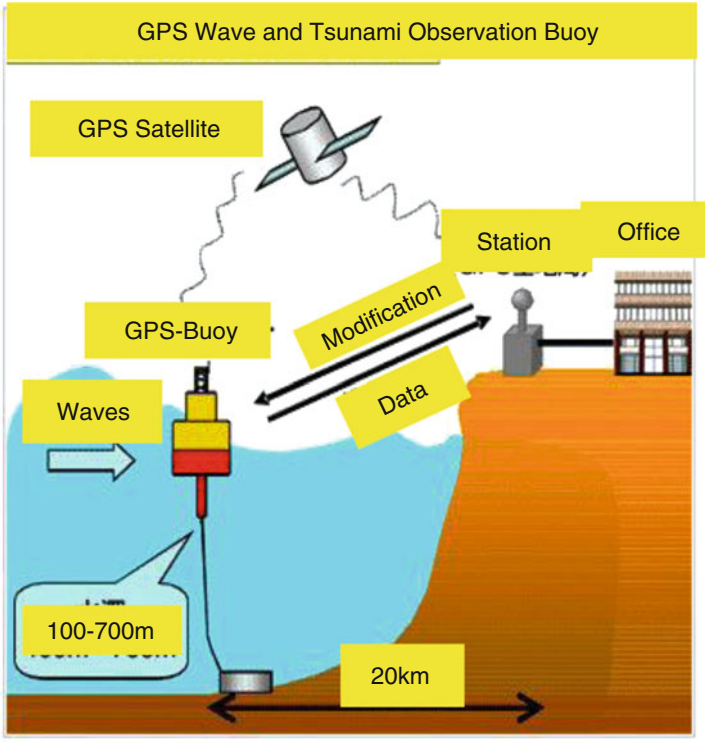

Fig. 4.8 GPS tsunami and offshore wave observation system (MLIT)

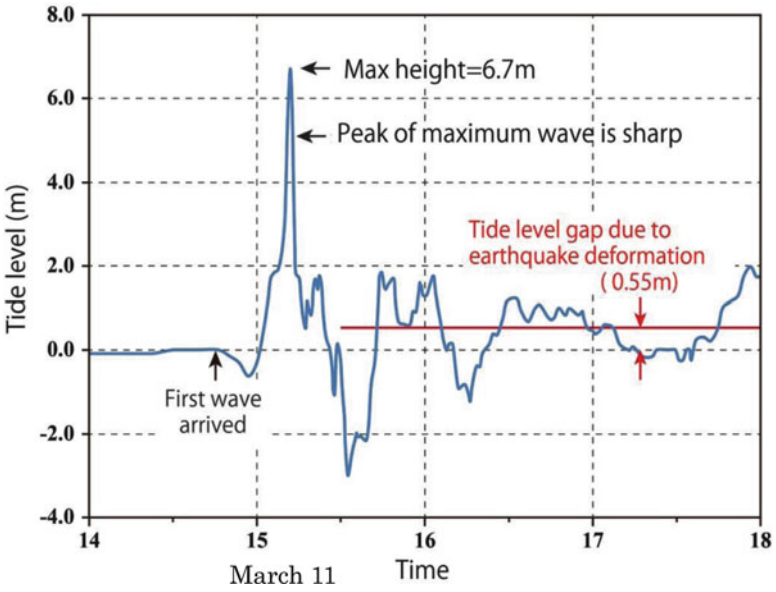

Fig. 4.9 Tsunami profile obtained from GPS buoy off Kamaishi in the south Iwate Prefecture

profiles were obtained in an analysis of the data from MLIT's buoy. Figure 4.9 shows a tsunami profile recorded 20 km from the Kamaishi Harbor. The tsunami profile has one sharp peak of about 6 m, followed by a low, flat peak. These peaks relate to the initial displacements caused by the earthquake at the fault plane on the seafloor. Right now analytical studies are carried out to clear the earthquake faults.

4.3 Tsunami Hazard

Several types of tsunami damage were observed in our field survey. The total scope of tsunami damage along the Tohoku Pacific Coast is still under investigation. The survey areas are the Miyagi Prefecture (around Matsushima Bay, as shown in Fig. 4.6) and the Kamaishi Bay (shown in Fig. 4.7). The coast of the Miyagi prefecture is flat, with urbanized areas mixed with cultivated areas. Inundation was recorded to be 3 km from the shoreline in most parts of the prefecture. The inundation height of the tsunami was 10–15 m at its maximum. The Kamaishi Harbor, located on the left side of Fig. 4.7, is protected by a breakwater, as shown in the figure. The breakwater was partially damaged, mainly because of overtopping tsunami waves. The Kamaishi Harbor has tidal barriers built following the 1933 Sanriku tsunami. As seen in Fig. 4.5, these barriers were mostly destroyed by force of the tsunami and scouring at the base of the barriers.

Figure 4.10 shows evidence of tsunami height at a shopping center in Shiogama Marin gate (Fig. 4.6). The inundation height marked in the photograph by the arrow is 6.3 m. Figures 4.11 and 4.12 show damage to wooden houses and a

Fig. 4.10 Evidence of tsunami height left at a shopping center

Fig. 4.11 Damaged wooden houses on the Shobutahama coast

concrete-reinforced apartment on the Shobutahama Coast. The wooden house was completely destroyed by the tsunami, while in the apartment building, only the windows on the side facing the shore were washed out. This indicates that concrete-reinforced buildings taller than four stories might be suitable for use as tsunami evacuation centers in coastal regions.

Fig. 4.12 Survived concrete-reinforced apartment building at the coast

Fig. 4.13 Shipping containers left on the beach

Figure 4.13 shows shipping containers that were carried from Sendai Port (shown in Fig. 4.6); 324 containers washed away from the port, and they proved to be serious obstacles for the emergency sea transport at the initial stages of response to the disaster. The photograph was taken along the Shobutahama Coast. The containers remain on the beach. No effort is being made to clean them up. In harbor area, the

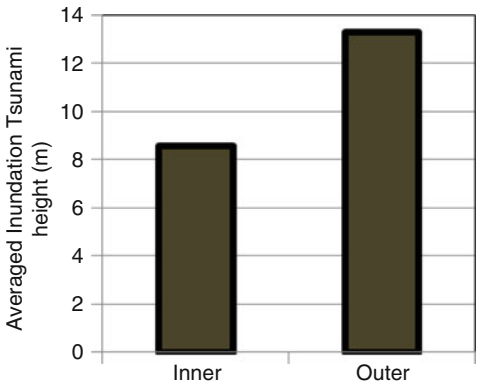

Fig. 4.14 Effect of tsunami breakwater

debris of wrecked vessels and shipping containers drifting into the ocean has to be resolved to keep navigation routes safe.

A 3D image of the scoured mound of the Kamaishi breakwater was obtained using data from MLIT's field survey (http://www.mlit.go.jp/common/000140273.pdf). The original water depth at the breakwater mouth was 60 m, and the height of mound was 30 m. Therefore breakwater crown height was higher than normal tidal level. During the tsunami event, overtopping waves and heavy scouring caused widespread damage to the breakwaters themselves. Almost half of trapezoid-type caissons moved out of place and rotated. However, it is likely that the bore-wave pressures of the tsunami front were greatly reduced in the areas that had breakwaters. Figure 4.14 shows the comparison of tsunami inundation height measured at the inner and outer breakwaters (shown in Fig. 4.7). The average tsunami inundation height in the urban area behind the breakwater was about two thirds that in areas where the tsunami energy was uniform along the coastline. Figure 4.15 shows the northern part of the damaged breakwater.

4.4 Tsunami Deposits

A survey of the types and amounts of deposits left by historical tsunamis provides important data in order to predict future tsunami risks for a given area. We conducted a tsunami deposit survey 3 months after the 2011 Tohoku Earthquake. We took samples from the target area, namely, Agawanuma Pond, which is a small agricultural pond near the Shobutahama coast (Fig. 4.6). Figure 4.16 shows the debris that flowed into the pond from surrounding townships. The mud layer on the surface of pond is surely the deposit brought in by the tsunami flows. Figure 4.17 shows the core samples taken from the center of pond and the beach. The deviation of diameter at the surface is smaller than in the deeper part, and the averaged

Fig. 4.15 Kamaishi breakwater after tsunami event

Fig. 4.16 An example of tsunami debris in Agawanuma Pond

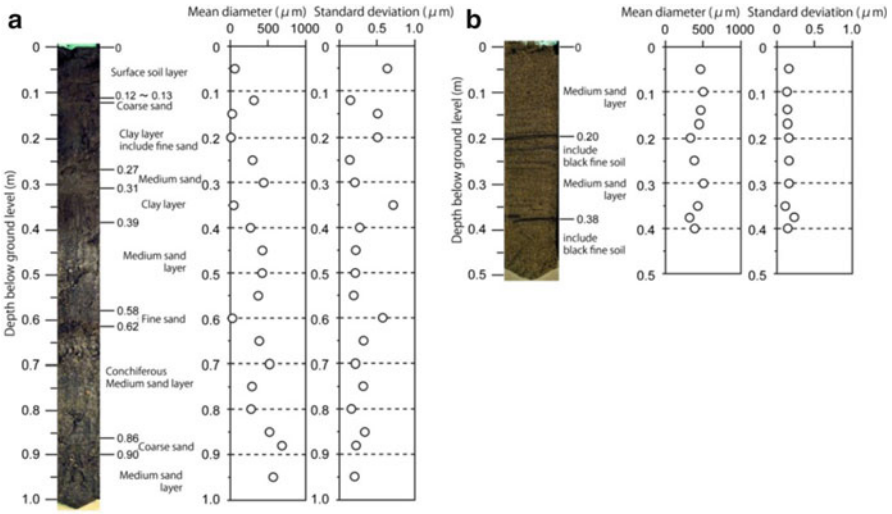

Fig. 4.17 Core samples from (**a**) Agawanuma Pond and (**b**) Shobutahama Beach

diameter is finer than the other in the pond bowling core. Meanwhile, the beach core sample shows no evidence of tsunami deposits. The layer of fine mud is about 10-cm thick. A more detailed chemical analysis is being conducted.

4.5 Conclusions

We found several characteristics of tsunami damages from the fieldworks. The results are as follows:

1. The 2011 Off the Pacific Coast of Tohoku Earthquake caused the greatest tsunami in Japanese history and endangered densely populated urban areas.
2. Tsunami inundation heights reached 10–15 m at the maximum. The only clear tsunami profile was obtained from the GPS wave observation buoy operated by MLIT.
3. Concrete-reinforced apartments were relatively lightly damaged, even where inundation heights reached 11 m.
4. The offshore breakwater had the effect of reducing the tsunami's impact, though the breakwater itself was heavily damaged mainly due to scouring at the base.
5. A core sample of tsunami deposits in a pond in a coastal area shows a mud layer of 10-cm thick.

Reference

The 2011 Off the Pacific Coast of Tohoku Earthquake (2011) Tsunami Survey Team. http://www.coastal.jp/ttjt/. Accessed 12 April 2012

Chapter 5
Revisiting the Concept of Tsunami *Tendenko*: Tsunami Evacuation Behavior in the Great East Japan Earthquake

Katsuya Yamori

Abstract This paper discusses the concept of "tsunami *tendenko*," which has become widely known, particularly after the massive tsunami triggered by the 2011 Off the Pacific Coast of Tohoku earthquake (hereafter referred to as "Great East Japan Earthquake") on March 11, 2011. In Japanese, *tendenko* refers to an "everyone for him/herself" mindset, which calls for a quick tsunami evacuation without waiting for others, not even one's parents or children. The word *tendenko* has been handed down in the Tohoku region as an important code of action to be observed in local communities at risk of tsunami, because a quick evacuation to higher ground without taking care of anyone has been considered the only way to escape from the complete destruction of a devastating wave. This paper reexamines the notion and implications of *tendenko* from a sociopsychological perspective. Specifically, this work aims to demonstrate that, in addition to its commonly used definition, *tendenko* is a multilayered term integrating at least four meanings and functions: (1) emphasizing the principle of self-reliance, (2) encouraging others to seek refuge, (3) fostering mutual trust in advance, and (4) reducing feelings of self-reproach among survivors. *Tendenko* is examined by drawing on its etymology, social survey data from the Great East Japan Earthquake and other tsunami evacuations, and the findings of studies in the field of social psychology. This paper will also show how this concept symbolizes the complexity of tsunami evacuation and offers a path toward a solution.

Keywords Conflict • Crossroad • Evacuation • Tsunami *tendenko*

K. Yamori (✉)
Disaster Prevention Research Institute (DPRI), Kyoto University, Kyoto, Japan
e-mail: yamori@drs.dpri.kyoto-u.ac.jp

H. Kawase (ed.), *Studies on the 2011 Off the Pacific Coast of Tohoku Earthquake*,
Natural Disaster Science and Mitigation Engineering: DPRI reports,
DOI 10.1007/978-4-431-54418-0_5, © Springer Japan 2014

5.1 The Great East Japan Earthquake and Tsunami *Tendenko*

It is plain for all to see that, in addition to ensuring the safety of nuclear power plants, averting damage from the ensuing tsunami was the greatest challenge to disaster prevention posed by the Great East Japan Earthquake. This is because more than 90 % of the estimated 20,000 victims (including missing persons) lost their lives in the tsunami. The "Expert Panel Report on Earthquake and Tsunami Countermeasures in Light of the Lessons Learned from the 2011 Tohoku-Pacific Ocean Earthquake" published by the Central Disaster Prevention Council (2011a) (CDPC Report) delivered the following frank assessment: "A review of coastal protection infrastructure shows that although it proved effective up to the tsunami height for which it was designed, the recent massive tsunami and subsequent devastation underscored the shortcomings of disaster prevention measures that were overly dependent on this infrastructure." Much of this infrastructure (such as tsunami seawalls) did not function properly and failed to prevent the destructive tsunami from reaching people's homes. In fact, according to the Reference Figures and Tables section of the CDPC Report (2011b), the total area inundated by the tsunami exceeded 560 km^2, which is comparable to the total area occupied by Metropolitan Tokyo's 23 special wards (621 km^2).

A substantial amount of published data from large-scale surveys and individual case studies has shown that the manner in which people evacuated from these perilous conditions made the difference between life and death. Examples of large-scale survey data can be seen in a document by the CDPC Expert Panel (2011c), the results of surveys by the Ministry of Land, Infrastructure, Transport and Tourism (2011) and Weathernews Inc. (2011), and a survey report by the Survey Research Center Co., Ltd. (2011). Conversely, examples of individual case studies can be seen in books by publishers Sanriku Shimposha K.K. (2011) and Bungeishunju Ltd. (2011) and author Shunji Murai (2011). In order for the Great East Japan Earthquake's devastation not to have been in vain and in order to prepare for the potential damage of massive tsunamis expected to follow the next major earthquakes in the *Tokai* (literally East Sea), *Tonankai* (literally Southeast Sea), and *Nankai* (literally South Sea) areas of Japan, tsunami evacuation is one of the greatest disaster prevention challenges currently facing Japanese society.

Within this context, the phrase "*tsunami tendenko*" (also referred to as "*inochi tendenko*" or "life *tendenko*"), believed to have been handed down by ancestral inhabitants of the tsunami-prone Sanriku region, has recently garnered renewed attention as a term that epitomizes the essence of tsunami evacuation, that is, quickly escaping to higher ground. The evacuation of elementary school children in Kamaishi City (described below as the "miracle of Kamaishi") has also served to reiterate the importance of *tendenko.* This is because Prof. Toshitaka Katada of Gunma University, who for many years taught emergency evacuation techniques to the region's elementary and junior high school children, based the three evacuation principles that form the core of tsunami disaster prevention education on a reconsideration of the meaning of *tendenko* (Research Center for Disaster Prevention in the Extended Tokyo Metropolitan Area 2011). Incidentally, Prof. Katada asserts that the Kamaishi event was not a miracle but rather the result of prior education and preparation.

In the next section I will briefly examine the etymology of *tendenko*.

5.2 Etymology of *Tendenko*

As mentioned above, the term *tendenko* is known to have been passed down over many years by the ancestral inhabitants of the Sanriku region located on the north-eastern part of the main island of Honshu. However, the precise period in which the term originated is uncertain. According to renowned tsunami researcher Fumio Yamashita (born 1924), who is credited with bringing about the term's widespread use (Yamashita 1997, 2005, 2008), *tendenko* has its origins in the actions of Yamashita's father (who also survived the giant tsunami generated by the 1896 Meiji-Sanriku earthquake) during the tsunami triggered by the 1933 Showa-Sanriku earthquake (see Sect. 5.6 for details). However, Yamashita's father also claims to have heard the word from his grandfather. Moreover, Yoshi Tabata (born 1925), who has been active in passing on her experiences of the tsunami damage caused by 1933 Showa-Sanriku earthquake, also claims to have heard the term used by her grandfather who lived through the 1896 Meiji-Sanriku earthquake. These accounts demonstrate that the word *tendenko* dates back more than a century before the 1896 Meiji-Sanriku earthquake.

At a tsunami symposium held in 1990 in Taro Town (currently Miyako City), Iwate Prefecture, which was also heavily damaged by the recent tsunami, Yamashita recounted one of his father's episodes that caught the attention of several disaster prevention researchers. Then, in the 1993 Hokkaido Earthquake off the southwest coast of the island of Hokkaido, a number of events served to reaffirm the importance of *tendenko*. This in turn led to increased interest in the concept, and in 2003 it was covered in an editorial piece appearing in the national newspaper *The Asahi Shimbun* (Yamashita 2008).

However, despite the subsequent occurrence of globally significant tsunami damage from the 2004 Indian Ocean Tsunami as well as tsunamis generated by the 2003 Miyagi-oki earthquake, the 2004 earthquake off the southeast coast of Kii Peninsula, and the 2010 Chile Earthquake, the tsunami evacuations performed within Japan were consistently low-key affairs (Katada et al. 2005; Katada 2006; Kondo et al. 2011). With the teachings of *tendenko* yet to fully permeate the Japanese consciousness, the nation then experienced the events of March 11, 2011.

5.3 Meaning 1: Emphasizing the Principle of Self-Reliance (Protecting One's Own Life)

Yamashita describes tsunami evacuation as follows:

Basically, to escape with your life from the awesome speed and wall of destruction that is the tsunami, you must flee quickly and urgently on your own as though in a race against the seconds and minutes, disregarding all others including your parents and siblings even though doing so may seem heartless. Doing so is the way to minimize casualties and protect as many lives as possible from a tsunami (Yamashita 2008, pp 52–53).

Tendenko thus primarily describes a cardinal rule for emergency tsunami evacuation, which appears to hinge on the importance of protecting one's own life or, in other words, on the principle of what is today referred to in Japan as *jijo* which literally means "helping one's self" or "self-reliance."

In fact, this meaning is often used when describing *tendenko* ("Inochi wo mamoru chie" Production Committee 2007; The Asahi Shimbun Company 2011). Apart from evaluation of specific issues such as whether to evacuate by car or to head to the evacuation area designated by the local government, the majority of tsunami evacuation surveys from the Great East Japan Earthquake mentioned in Sect. 5.2 all stressed the importance of this interpretation of *tendenko*, that is, the need to evacuate quickly.

However, as Yamashita repeatedly reminds readers in his book, the word is actually a "lamentable teaching" that the people of the Sanriku region were compelled to develop after recurrent tragedies in which families and relatives all "perished together" (*tomodaore*) in massive tsunamis (Yamashita 2008, pp 52–53). It is therefore crucial to note that, although the original meaning of *tendenko* agrees with meaning 1, it does not simply emphasize the importance of "self-reliance" or the principle of self-responsibility during tsunami evacuation.

This point has already been expressed in a variety of ways in Yamashita's works. For instance, "*tendenko* contains the nuance of acting separately and individually based on a mutual understanding and recognition as implied by Japanese expressions such as…'*yoshi, koko wa tenden ni yaro*' [literally 'ok, let's do this separately']" (Yamashita 2008, p 231). This point is crucial because it suggests that in order for *tendenko* to be effective, the basic prerequisite of mutual understanding and trust within families and local communities must be met. This aspect will be separately discussed in further detail under meaning 3 of *tendenko* in Sect. 5.5.

Yamashita also makes the following statement: "I have described 'tsunami *tendenko*' as a lamentable teaching because it leaves the emotionally irreconcilable issue of what to do about those who are vulnerable to natural disasters and need assistance to evacuate such as children, physically impaired elderly persons, and the physically disabled" (Yamashita 1997, p 175). It has already been pointed out that *tendenko* is not an all-encompassing solution in that it does not address issues concerning people who would have difficulty evacuating.

In fact, this emerged as a major issue in the Great East Japan Earthquake. For example, *The Mainichi Shimbun* (The Mainichi Newspapers Co., Ltd. 2011) carried an article entitled "Jury still out on *tendenko*: conflict with voluntary disaster prevention organizations." The article described how members of these organizations and voluntary firefighters died (i.e., *tomodaore*) trying to save those who were incapable of *tendenko*. This article also captured the poignant words of one surviving resident: "If someone asks for your help you have to go. This tsunami made me realize that I couldn't do *tendenko*." *The Kahoku Shimpo* (2011), a daily newspaper based in Sendai, also featured an article on a discussion of the pros and cons of *tendenko* at a special committee of the Kamaishi City Council in which a councilor questioned the wisdom of promoting it as an all-encompassing solution, to which members of the governing council responded that *tendenko* is not simply a principle of self-reliance and is by no means solely a matter of "as long as I survive."

As such, the fact that *tendenko* is not restricted to the plain and simple self-reliance principle of "protecting one's own life" as described in meaning 1 but also contains a deeper meaning is also suggested to some extent in the works of Yamashita, who could be described as the father of *tendenko* in modern usage. With this in mind, the next section will take a closer look at the complex elements contained in the teaching of *tendenko*.

5.4 Meaning 2: Encouraging Others to Seek Refuge (Not Simply for One's Self)

The prevailing theme here is that *tendenko* fulfills a function that goes beyond the simple principle of self-reliance. Specifically, it encourages the evacuation behavior not only of the individual who is already seeking refuge but also of others who are yet to do so. The key to this function lies in the individual who has started seeking refuge acting as an evacuation trigger (i.e., providing effective evacuation information) to many others in the vicinity who witness and recognize the individual's behavior. Observing the behavior of people who are already escaping is a powerful source of disaster information that can encourage others to evacuate (Yamori 2009; Kawata 2010), and the teaching of *tendenko* cleverly leverages this mentality. In other words, the wisdom of *tendenko* lies not only in escape but also in encouraging escape or escaping together.

This meaning can be illustrated by several pieces of actual corroborative evidence. For example, one of the three principles that facilitated the above-mentioned "miracle of Kamaishi" was "*Sossen hinansha tare*" (literally "take the initiative in evacuating"). That this principle is the modern-day equivalent of *tendenko* can be seen in the following journal article on Kamaishi by Prof. Katada:

I tell the students "You should be the first to evacuate." The children appear hesitant, so I tell them "By protecting your own life you help to protect the lives of those around you. If someone evacuates then others are more likely to follow suit. If you evacuate then everyone else will too. You should take the initiative in evacuating to help save others." In the recent tsunami, members of the junior high school's soccer team took the evacuation initiative by warning the elementary school students of the oncoming tsunami (Katada 2011).

A photograph capturing the moment in which Kamaishi residents escaped to higher ground actually shows not only the junior high school students who took the evacuation initiative but also the elementary school students being guided by the hand by their elder student counterparts and the residents of Kamaishi following behind.

There are even quantitative data indicating that the initial *tendenko* evacuees (i.e., the evacuation leaders) not only protect their own lives but also serve to provide disaster information that saves the lives of others. A field survey conducted by Prof. Katada on the evacuation of Owase City in Mie Prefecture where a tsunami evacuation warning was issued following the above-mentioned 2004 earthquake off the southeast coast of Kii Peninsula (in which two quakes occurred on September 5, 2004, between evening and midnight) revealed some intriguing facts on the

evacuation rates of each area. Evacuation rates for both quakes were highest in the port town of Minato-machi located on Owase's coast, but this is an obvious outcome given its geographical location.

Rather, the data of interest pertain to the town of Nakai-machi which had the next highest evacuation rates in both quakes despite not being directly adjacent to the coast. This was because the route to Minato-machi's designated evacuation site passed through Nakai-machi whose residents therefore observed the evacuation and followed suit. Thus, the *tendenko* behavior of Minato-machi's residents would have helped to save the lives of Nakai-machi residents, although in this case a large-scale tsunami fortunately did not eventuate. This result is consistent with data obtained from another survey by Katada et al. (2005) on hypothetical evacuation scenarios (i.e., what type of event would cause you to evacuate?). Specifically, 40.6 % of respondents claimed that they would evacuate "upon seeing/hearing the Japan Meteorological Agency's tsunami warning on TV/radio" and 50.5 % would evacuate if they "perceived a change in the ocean after an earthquake." Meanwhile, rather than changes in the external environment or broadcast disaster information, 64.1 % of respondents claimed that they would seek shelter if they "saw the neighbors evacuating" and 73.1 % would do so if "instructed to evacuate by the head of their neighborhood association or neighbors," demonstrating that the presence or appeals of other evacuees evoke a stronger response (percentages were calculated based on the total number of respondents who indicated that they would evacuate in the event of each situation).

The same trends have also been shown to have occurred during the Great East Japan Earthquake. For instance, a document from the 7th Meeting of the CDPC Expert Panel (CDPC 2011c) contained the results of a field survey on evacuation behavior in which residents were asked "What initially caused you to evacuate?" Of the 763 valid survey responses, the most common response was, naturally, "I thought there would be a tsunami because of the big quake" at 48 %. The next most common answer was "Because my family members or neighbors suggested that we evacuate" at 20 %, followed by "Because I heard or saw a tsunami warning" at 16 % and "Because my neighbors were evacuating" at 15 %. These data also suggest that evacuation behavior begets similar behavior or, in other words, that *tendenko* is a potential catalyst for encouraging others to evacuate.

I will now look at one more piece of evidence to suggest that the teaching of *tendenko* leverages the cumulative effect that evacuees have on creating even more like-minded people, specifically the results of an experimental study on collective behavior conducted by Sugiman et al. (1988). Based on a field experiment performed in an actual underground shopping arcade, this study undertook a comparative validation of the effects of two different evacuation guidance methods in a simulated fire within a confined space. In the first, the "follow-directions method," leaders indicated the direction of the exit by speaking in a loud voice and gesturing with their arms, which is the conventional method used in an evacuation. In the second, the "follow-me method," each leader instructed a small group of evacuees consisting of one or two people in their immediate vicinity to follow them and subsequently escorted the evacuees to the exit. In this second method, the leaders did not tell the evacuees where the exit was located or address multiple evacuees in a loud voice.

As a result, a higher evacuation rate was achieved by using the follow-me method despite some constraints. This outcome was attributed to the fact that, in the follow-me method, the core of the evacuation group, which initially consisted of the leader and one or two evacuees, rapidly absorbed people in the vicinity who had not been directly addressed by the leader, triggering a ripple effect that in turn generated a stream of evacuees toward the exit in a faster and more effective manner than those who adhered to the follow-directions method. The existence of this collective behavior mechanism was subsequently demonstrated in greater detail in a follow-up study by Okada and Takeuchi (2011) based on computer simulations.

It is apparent that the leader and the first few evacuees in the follow-me method were the first to practice *tendenko* or, to put it another way, were the "lead evacuees" (although the lead evacuee typically guides the evacuation while speaking in a loud voice to followers, so strictly speaking, this role combines the traits of both the follow-me and follow-directions methods). *Tendenko* therefore also possesses the wisdom of *kyoujo* (which literally means "mutual help" in contrast to the above-mentioned *jijo* or self-reliance) to help everyone by quickly and effectively forming a stream of evacuees based on the ripple effect. This experiment thus establishes that *tendenko* is "not simply for one's self" and is by no means solely a matter of "as long as I survive" as touched upon in Sect. 5.3.

5.5 Meaning 3: Fostering Mutual Trust in Advance

The previous section pointed out that *tendenko* also has the function of *kyoujo* or mutual help, but if we were to establish chronological phases, we would see that both meaning 1 (i.e., the standard meaning) and meaning 2 relate to functions of *tendenko* that occur during emergency evacuation. This section, on the other hand, will show that the teachings of *tendenko* encompass not only the emergency phase but also the preparatory or routine phase.

The implication here is that in order for *tendenko* to function effectively, a certain important precondition must be met, namely, the person intending to practice *tendenko* must trust that loved ones—the people that he or she wants most to survive—will definitely do the same. For example, parents at home who perceived the threat of a tsunami would likely be unable to practice *tendenko* unless they could expect their child facing the same situation at school to do the same. It is therefore vital to the principles of *tendenko* that each individual who practices it trusts that their loved ones are just as capable of doing the same.

Furthermore, this trust must be complementary so, using the previous analogy, children at school would not be able to perform *tendenko* unless they could trust that their parents were doing the same. In essence, this trust must be mutual. Of course, I do not intend to assert that the absence of this trust would definitely prevent one party from practicing *tendenko*. In fact, many people in the Great East Japan Earthquake had no choice but to practice *tendenko* without knowing the fate of their loved ones. It is certain, however, that the effectiveness of *tendenko* improves dramatically if this mutual trust has been fostered.

To summarize, the following conditions should ideally be met for *tendenko* to function effectively. (1) I trust that you will practice *tendenko;* otherwise I will be unable to do so. (2) You trust that I will practice *tendenko*; otherwise you will be unable to do so. This mutual trust then moves to a higher level and takes on a more detailed aspect like that of a Russian nesting doll, specifically. (3) You trust that I trust you to practice *tendenko* so we can both do so with peace of mind; and (4) I trust that you trust me to practice *tendenko* so we can both do so with peace of mind. Thus, the formation of this mutual trust on multiple levels and in multiple directions among family members, neighbors, and the local community is a prerequisite for the effective realization of *tendenko*.

I will now examine a specific case and survey data that serve to demonstrate the importance of such mutual trust. First, the survival of the schoolchildren in Kamaishi can again be cited as an example of effective mutual trust. Prof. Katada, who led the "miracle of Kamaishi," provided the following guidance during disaster prevention education prior to the tsunami:

Could you really evacuate on your own without regard for your family members if you thought a tsunami was approaching? In most cases, you probably couldn't. … But unless you do, your entire family could perish just as our ancestors feared. *Tendenko* means establishing a relationship of trust within your family by regularly discussing your tsunami evacuation method and agreeing that you will all evacuate even if the tsunami strikes while your family members are in separate locations so that, if it does occur, you will all be able to evacuate separately (Research Center for Disaster Prevention in the Extended Tokyo Metropolitan Area 2011).

Prof. Katada and his colleagues at the Research Center for Disaster Prevention in the Extended Tokyo Metropolitan Area therefore sent the message to the parents and guardians of children in Kamaishi that "We will provide thorough education to equip your children with the wisdom to evacuate on their own so if a tsunami does occur, we want you to trust your children and be sure to evacuate yourselves." Encouraging people to foster this mutual trust on a daily basis is an essential part of *tendenko* that is just as if not more important than behavior during the actual emergency.

Meanwhile, survey data showing that the inability to trust the behavior of loved ones effectively impeded *tendenko* demonstrate the importance of mutual trust in *tendenko* from the opposite direction. First, I will refer to the results of a tsunami evacuation survey conducted by Weathernews Inc. (2011) from May 18 to June 12, 2011, on users of the company's Internet and mobile phone service. The survey collected 5,296 responses from evacuees in Hokkaido, Aomori, Iwate, Miyagi, Fukushima, Ibaragi, and Chiba (Yamori et al. 2011). A key feature of this survey was that it consisted of one part that sought information about the respondents themselves and a second part where respondents were asked to provide information about friends and loved ones who died. The first and second parts of the survey collected 3,298 and 1,998 responses, respectively.

Of particular interest was the marked difference between the responses of the surviving respondents and those provided on behalf of their deceased love ones in a question that asked whether they left the evacuation site to return to a location endangered by the tsunami. While 23 % of the respondents claimed to have

revisited a tsunami-endangered location themselves, 60 % of their deceased loved ones purportedly returned. In a subsequent question on why the deceased persons returned to an endangered location, the most common response was "To search for family members" at 31 %. Basically, far more persons who died returned to an endangered location than the surviving respondents, and their main reason for doing so was concern over the behavior (i.e., safety) of loved ones.

A similar trend can also be identified in other data. In the aforementioned CDPC field survey (2011c) which garnered responses from 870 people, the 267 respondents who did not evacuate immediately after the tremors stopped but instead finished what they were doing before evacuating (delayed evacuees), and the 94 respondents who only evacuated after the tsunami struck while they were preoccupied with another matter (threatened evacuees) were asked why they did not evacuate immediately. The top response was "Because I had returned home" at 22 %, followed by "Because I went to look for/pick up family member(s)" at 21 % and "Because I was confirming the safety of family member(s)" at 13 %, all of which far exceeded the next most popular responses of "Because no tsunami came after previous earthquake(s)" at 11 %, "Because I was cleaning up things scattered by the earthquake" at 10 %, and "Because things appeared to be fine" and "Because it didn't occur to me that a tsunami might come" at 9 % each. These results suggest that failure (or inability) to evacuate was due more to concern for loved ones (i.e., lack of trust in the evacuation of loved ones) than underestimation of the tsunami's danger.

Based on the above survey results, the CDPC (2011c) found that the actions of "searching for family members" and "returning home" impeded swift evacuation behavior and that reducing these obstacles would help to mitigate injury and death. The secret of *tendenko* therefore lies not only in people's behavior in an emergency but also in the nature of trust built on a daily basis by all concerned. Fostering strong mutual trust concerning immediate evacuation among parents and children, teachers (schools), and guardians (families)—that is the third meaning of *tendenko*.

However, this still does not resolve the issue of the people touched upon in Sect. 5.3 who would have difficulty practicing *tendenko* let alone establishing the aforementioned relationship of mutual trust, namely, those who are expected to encounter difficulty in immediately evacuating on their own. This issue will be addressed in Sect. 5.7.

5.6 Meaning 4: Reducing Feelings of Self-Reproach Among Survivors (Message from the Dead)

Massive tsunamis have taken numerous lives and destroyed countless assets, with people and society at large helpless to stop them. The Sanriku region where *tendenko* originated has had to face this cold, hard fact on numerous occasions including the recent Great East Japan Earthquake. Still, many people have also managed to survive the critical situation posed by a tsunami. The term *tendenko* was obviously coined and handed down not by those who died but by those who survived or,

in other words, those who were determined to keep on living. In addition to representing wisdom and teachings to save lives in the event of a tsunami, *tendenko* should also convey some kind of message to those attempting to live on after the tragedy of a natural disaster. It is the author's opinion that *tendenko* has a unique psychological effect on people and local communities not only during an emergency but also after a natural disaster and that this effect is epitomized by meaning 4.

For example, let us consider the hypothetical case of a family that includes a young grandchild and a grandmother. Now let us assume that the grandchild and other family members who lived together managed to evacuate to higher ground but the grandmother who lived separately died in the tsunami. Now consider the following two scenarios.

In the first scenario, the grandchild may recall her grandmother's death by pondering how "Grandma always told us to practice *tendenko* if a tsunami came." She would say "I will practice *tendenko*, so you must do the same!" (precisely the kind of mutual trust described in the previous section). Of course, simply recalling these words could not take away all of the grandchild's pain and sadness at having lost her grandmother and would not completely erase the nagging question of why her grandma was not able to survive. However, the promise to practice *tendenko* (mutual trust) would, however slightly, also help to free the grandchild from these doubts.

The significance of this fact is easy to imagine when we consider how bereaved families and relatives likely experience protracted, unique feelings of self-condemnation at the loss of loved ones in a natural disaster. A book by Yamori (2010a), who followed the progress of a support group formed by Great Hanshin Earthquake survivors (particularly the bereaved) for 15 years, provides a valuable insight into the trauma they experienced. The authors show that even 15 years after the disaster, the bereaved are still affected to a varying degree by feelings of self-guilt for not having done something to prevent the loss of their loved ones such as "If only we had lived in a more sturdy house," "If only I had woken up a bit earlier," and "If only I hadn't told them to stay another night."

In other words, their trauma did not stem directly from the experience of a tragic event but rather from having survived in spite of it. In simpler terms, they were left wondering "Why did I survive instead of you?" or conversely "Why did you die and not me?" Such an unanswerable question lingers in the minds of survivors.

Applying this to the aforementioned hypothetical scenario, it is conceivable that the grandchild would wonder "Maybe Grandma was waiting for me to come and help her" and "I could have done more to save her" or, on the other hand, "What if she died on the way to help me?" Incorporating the above-mentioned definition of trauma, it is also possible that the grandchild would experience feelings of self-reproach for a considerable period of time.

In light of all this, it is clear that *tendenko* has a unique psychological effect on survivors in that it reduces feelings of self-reproach for not having saved loved ones despite managing to evacuate and survive one's self. This effect is not limited to individuals but also impacts towns and communities. In other words, it acts not only on small units of mutual loved ones but also on the entire community that experienced the disaster, helping to release it from feelings of self-guilt at not having done more.

Tendenko also functions as wisdom that facilitates concerted efforts to make a new start and rebuild lives and the community.

In fact, the episode involving Fumio Yamashita's father that served to raise awareness of *tendenko* (Sect. 5.2) also suggests this psychological aspect. Yamashita recounts the origins of *tendenko* in the following statement: "After I spoke of how my father had fled on his own after the 1933 Showa-Sanriku earthquake without taking me, his youngest child (I was a third-grade elementary school student at the time) by the hand, my mother kept complaining of his callousness, to which my father angrily rebuked 'What did you expect? Its *tendenko*!'"(Yamashita 2008, p 231). This episode suggests that *tendenko* had imbued Yamashita's father, who had also experienced the 1896 Meiji-Sanriku earthquake, with a vigilance of tsunamis that permeated the very marrow of his bones (i.e., the wisdom to survive) and that it also possesses the ability to assuage the unexpected emotions experienced by the survivors (i.e., unique feelings of self-reproach for having been the (only) one to survive). It also contains a message of forgiveness and encouragement from the deceased to the survivors by letting survivors know that their departed loved ones wanted them to live no matter what.

There are even data that, although indirectly, support this assertion. These data can be found in the Weathernews survey described in Sect. 5.5 (also Yamori et al. 2011). The survey contained the question "Had you made any preparations for a tsunami?" Responses to this question were noteworthy in terms of the contrast between those who replied in the affirmative with "I was familiar with the evacuation route" or "I had participated in a disaster drill" and those who replied "I had not made any preparations." Specifically, 59 % of the surviving respondents claimed not have made any preparations compared with 16 % reported for the deceased.

It is important to acknowledge that the data on the deceased persons were actually provided by the surviving respondents who answered on behalf of lost loved ones. In other words, it is essential to recognize that, instead of comparing the circumstances of the survivors and deceased in the same manner, the two datasets being compared here contain biases inherent to survivors recalling their lost loved ones. Certainly we cannot discount the possibility that the deceased may have been more enthusiastic about tsunami preparation than the survivors. For instance, it is known that some people who were familiar with the details of the local hazard map were unfortunately late to evacuate because they decided that they were not in danger

However, the marked disparity in responses should instead be attributed to the inherent bias of survivors that arises when recalling those who died. That is, the deceased did not necessarily die helplessly. Rather, the data were obtained as a result of the respondents' preference toward a retrospective account in which the loved one died helplessly despite being better prepared than the respondents themselves.

On the one hand, this bias is a manifestation of the survivors' consideration for the deceased in that they do not want them to be remembered as having died unprepared. On the other hand, the bias suggests a tendency among the survivors to try to avoid feelings of self-guilt embodied by sentiments such as "I should have done more" or "They should have been saved." *Tendenko* also permits survivors to possess sentiments similar to the above-mentioned retrospections such as "My deceased loved one died in the tsunami despite attempting to practice *tendenko*."

5.7 Summary: A Wisdom of Contradictions and Conflicts

The previous sections have shown that *tendenko* is a multilayered term (i.e., teaching) integrating diverse meanings. Of particular significance is that *tendenko* is involved in all aspects of the disaster management cycle. It is well known that natural disasters, especially the earthquakes and tsunamis addressed in this paper, have long-lasting social impacts despite their relatively short duration. Nevertheless, even in recent disaster prevention research, many studies end up discussing the themes of preparedness, response, and recovery and reconstruction as independent aspects.

Contrarily, *tendenko* is a single teaching that, despite being a relatively old concept, encompasses various elements as mentioned in Sect. 5.2. On its surface, *tendenko* is admittedly a word that focuses on a code of action for tsunami evacuation where every second counts. However, as this paper has demonstrated, *tendenko* is also a teaching with considerable implications both in terms of the nature of society prior to a natural disaster (i.e., families and communities) and, conversely, the restoration and unification of public sentiment after a disaster. Given that *tendenko* may at first glance appear to emphasize *jijo* or self-reliance but actually possesses extensive elements emphasizing the importance of *kyoujo* or mutual help, the term can also be recognized as an early precursor of the need for "comprehensive disaster risk management" (Kameda et al. 2006).

Finally, I will address the question left unanswered by previous sections, namely, the issue of tsunami evacuation for people who would presumably find it difficult to practice *tendenko* or, in contemporary terminology, *saigai jakusha* (literally people vulnerable to natural disasters) and *saigaiji youengosha* (literally people requiring assistance during a natural disaster). At this point, however, I am incapable of proposing a method that would instantly solve this problem. *The Mainichi Shimbun* article mentioned above closes with the following harsh assessment by the head of a neighborhood association within a ward devastated by the Great East Japan Earthquake: "No matter which way you look at it, a contradiction exists between *tendenko* and voluntary disaster prevention organizations" (The Mainichi Newspapers Co., Ltd. 2011). As this sentiment suggests, there are conflicts, contradictions, and divisions here that cannot be easily resolved.

This lack of an easy solution was highlighted by the tsunami-related deaths of many of the people who were implicitly or explicitly expected to provide assistance (such as firefighters, members of voluntary disaster prevention organizations, and social workers) to those within the community requiring assistance in a disaster under the motto of *kyoujo* (mutual help) amid the recent spate of deaths of the elderly in disasters prior to the Great East Japan Earthquake. For instance, according to the Fire and Disaster Management Agency (2011), a total of 254 firefighters in the three prefectures constituting the Tohoku region died in the earthquake and tsunami.

Nevertheless, one point that can certainly be raised here is that the contradictions, conflicts, and divisions surrounding this issue cannot be resolved simply by establishing rules for how to behave in the event of a tsunami. What we must now do having experienced the Great East Japan Earthquake is to confront these

contradictions, conflicts, and divisions head on, express them in a readily understood form (i.e., visualization), and develop a framework and tools to allow concerned parties and numerous others to consider measures to mitigate and resolve these issues while taking into account individual circumstances.

Therefore, as discussed above, the attitude that simply adhering to the principle of *tendenko* will magically solve all of these issues runs contrary to the true meaning of the word that Fumio Yamashita worked so hard to raise awareness of. Furthermore, when examining the aforementioned "miracle of Kamaishi" we should focus not on its outcomes but on the contradictions, conflicts, and divisions that Prof. Katada and many others encountered as well as the earnest efforts of stakeholders to resolve these issues.

Focusing on the contradictions, conflicts, and divisions essentially means that when we attempt to illustrate the lessons and knowledge of tsunami evacuation, we should not adopt simple behavioral rules based on a rigid format (e.g., do A, do not do B) and its derivatives (e.g., in case of C, do D) but should instead utilize a format that preserves the contradictions, conflicts, and divisions in their current form. An example of a disaster prevention tool based on this approach is the "Crossroads" disaster prevention game developed by Yamori (2010b) and Yamori et al. (2005).

Crossroads is a disaster prevention learning tool in which participants (i.e., players), such as residents of a local community, answer questions and then engage in a discussion. For example, one question asks: "You are a public servant at the city hall. Your house was partially destroyed in a large earthquake. Fortunately you were unharmed but your family is frightened. The trains are not running and it would take 2–3 h for you to walk to work. Would you go to work?" Players would then select either "Yes" (I would go to work) or "No" (I wouldn't go to work) and discuss their choices. The learning tool originated from the actual contradictions, conflicts, and divisions faced by local officials and disaster survivors following the Great Hanshin Earthquake. Its title refers to the dilemma-filled scenarios involved in decision making.

Another question in Crossroads is as follows: "You live in a seaside town and an earthquake has just triggered a tsunami that is expected to make landfall in as little as 15 min. You start evacuating immediately but are concerned about an elderly woman in your neighborhood, who you know well and who lives alone. Do you go to check on her?" The responses offered are "Yes" (I would check on her) and "No" (I wouldn't check on her). This question was developed based on the tsunami event referred to in Sect. 5.2 which occurred prior to the Great East Japan Earthquake and was subsequently included in Crossroads. While this is one of the tougher questions leveled at players, the Great East Japan Earthquake gave rise to even more severe situations in numerous disaster areas. As a result, a number of users expressed their hesitation in answering the question after having experienced a major earthquake.

More importantly, however, one of Crossroad's developers, Toshiko Kikkawa, reported that, after the Great East Japan Earthquake, many people who played the game at disaster prevention seminars, workshops, and the like actually requested this question (Kikkawa 2011). This suggests that rather than avoiding the contradictions, conflicts, and divisions on tsunami evacuation after a major earthquake, people actually attempt to seriously deal with these issues.

With its multilayered teachings covering a diverse range of meanings, *tendenko* is a word that symbolizes tsunami evacuation—an issue constantly plagued by contradictions, conflicts, and divisions. Today, after having experienced the Great East Japan Earthquake, there is an even greater need for steadfast, multifaceted tsunami evacuation measures that embody the spirit of *tendenko*.

References

Bungeishunju Ltd (2011) Tsunami – Hisaichi no kodomo hachijunin no sakubunshu. Bungeishunju Ltd, Tokyo

Central Disaster Prevention Council (2011a) Expert panel report on earthquake and tsunami countermeasures in light of the lessons learned from the 2011 Tohoku-Pacific Ocean Earthquake. http://www.bousai.go.jp/jishin/chubou/higashinihon/houkoku.pdf. Accessed 31 December 2011

Central Disaster Prevention Council (2011b) Expert panel report on earthquake and tsunami countermeasures in light of the lessons learned from the 2011 Tohoku-Pacific Ocean Earthquake. http://www.bousai.go.jp/jishin/chubou/higashinihon/sankou.pdf. Accessed 31 December 2011

Central Disaster Prevention Council (2011c) 7th meeting of the expert panel on earthquake and tsunami countermeasures in light of the lessons learned from the 2011 Tohoku-Pacific Ocean Earthquake (Document 1: analysis results of interview survey (residents) on evacuation behavior during the Great East Japan Earthquake. http://www.bousai.go.jp/jishin/chubou/higashinihon/7/1.pdf. Accessed 31 December 2011

Fire and Disaster Management Agency (2011) Committee for the review of firefighting activities during major natural disasters based on the Great East Japan Earthquake; Document no. 6 from the 1st committee meeting. http://www.fdma.go.jp/disaster/syobodan_katudo_kento/index.html. Accessed 31 December 2011

Inochi wo mamoru chie Production Committee (2007) Inochi wo mamoru chie – Gensai ni idomu 30 no fukei (Wisdom for protecting lives—30 scenes of efforts to mitigate damage from natural disasters). NPO rescue stock yard

Kameda H, Hagihara Y, Okada N, Tatano H (2006) Sougou bousai he no michi (The road to comprehensive disaster prevention). Kyoto University Press, Kyoto

Katada T (2006) Saigai chousa to sono kekka ni motozuku social co-learning no arikata ni kan suru kenkyu (study on disaster surveys and the state of social co-learning based on survey results), Japan society of civil engineers research division report on outcomes of 2005 priority research themes (research grant). http://www.jsce.or.jp/committee/jyuten/files/H17j_04.pdf. Accessed 31 December 2011

Katada T (2011) Higashi Nihon Daishinsai ni miru bousai no arikata (The state of disaster prevention observed in the Great East Japan Earthquake). Academia 99:6–9. http://www.jamp.gr.jp/academia/images/99_04.pdf. Accessed 31 December 2011

Katada T, Kodama S, Kuwasawa N, Koshimura S (2005) Issues of resident consciousness and evacuation from the tsunami – results of a questionnaire survey in Kesennuma City, Miyagi Prefecture, after the 2003 Miyagi-oki Earthquake. In: Proceedings of the Japan society of civil engineers, 789/II-71, pp 93–104

Kawata Y (2010) Tsunami saigai – gensai shakai wo kizuku (Tsunami disasters—building a society to mitigate damage from natural disasters), Iwanami Shoten, Tokyo

Kikkawa T (2011) Kurosurōdo no tsudoi zenkoku taikai in Shizuoka ni okeru houkoku (Report on crossroad national congress in Shizuoka), 25 December 2011

Kondo S, Yamori K, Okumura Y (2011) The reality of the 2010 Chile tsunami as a media event – content analysis of NHK-TV reporting. J Jpn Soc Disaster Info Stud 9:60–71

Ministry of Land, Infrastructure, Transport and Tourism (2011) Results of the field survey on tsunami damage from the Great East Japan Earthquake – Tsunami evacuation field survey results (summary). http://www.mlit.go.jp/common/000186474.pdf. Accessed 31 December 2011

Murai S (2011) Higashi Nihon Daishinsai no kyoukun – Tsunami kara tasukatta hito no hanashi (Lessons from the Great East Japan Earthquake—eyewitness accounts of tsunami survivors), Kokon Shoin, Tokyo

Okada Y, Takeuchi N (2011) Simulation of follow-direction method and follow-me method in emergency evacuation. Bulletin of Research Center for Computing and Multimedia Studies, vol 20. Hosei University, pp 55–62

Research Center for Disaster Prevention in the Extended Tokyo Metropolitan Area, Gunma University (2011) *Kamaishi-shi ga kore made okonatte kita tsunami bousai kyoiku* (Kamaishi City's past disaster prevention training). http://www.ce.gunma-u.ac.jp/bousai/research02_1.html. Accessed 31 December 2011

Sanriku Shimposha (2011) Kyoshin Gekiryu (3.11 Higashi Nihon Daishinsai) (Massive quake and torrent (3.11 Great East Japan Earthquake)), Sanriku Shimposha, Kesen-numa

Sugiman T, Misumi J (1988) Development of a new evacuation method for emergencies: control of collective behavior by emergent small groups. J Appl Psychol 73(1):3–10

Survey Research Center (2011) Report on the questionnaire survey of disaster areas on the Miyagi Coast. http://www.surece.co.jp/src/research/area/pdf/20110311_miyagi.pdf. Accessed 31 December 2011

The Asahi Shimbun Company (2011) Keyword search "*tendenko*" in The Asahi Shimbun (10 September 2011)

The Kahoku Shimpo (2011) "Tendoko" no atsukai de ronsen – Kamaishi City Council Special Committee *Kahoku Shimpo* (25 October 2011). http://www.kahoku.co.jp/spe/spe_sys1062/20111025_03.htm. Accessed 31 December 2011

The Mainichi Newspapers Co., Ltd (2011) Kotae denai tendenko (Jury still out on *tendenko*), The Mainichi Shimbun (3 July 2011). http://mainichi.jp/select/weathernews/20110311/shougen/archive/news/20110703ddm041040072000c.html. Accessed 31 December 2011

Weathernews Inc (2011) Higashi Nihon Daishinsai Tsunami Chousa (Chousa Kekka) (Great East Japan Earthquake & Tsunami Survey (survey results)). http://weathernews.com/ja/nc/press/2011/pdf/20110908_1.pdf. Accessed 31 December 2011

Yamashita F (1997) Tsunami (Tsunami), Ayumi Shuppan, Tokyo

Yamashita F (2005) Tsunami no kyofu—Sanriku tsunami denshou roku (Fear of tsunami—Collection of folk stories about tsunami in Sanriku region). Tohoku University Press, Sendai

Yamashita F (2008) Tsunami tendenko—Kindai nihon no tsunami shi (Tsunami tendenko—Tsunami disasters in Japanese modern history), Shin-Nihon Shuppan, Tokyo

Yamori K (2009) Bousai Ningen Kagaku (Human science of disaster prevention). Tokyo University Press, Tokyo

Yamori K (2010a) Akushon risachi—Jissen suru ningen kagaku (Action research—Human science in practice), Shinyosha, Tokyo

Yamori, K (2010b) Using games in community disaster prevention exercises. Group Decision and Negotiation (doi:10.1007/s10726-011-9227-9 Key: citeulike:8711838)

Yamori K, Kikkawa T, Ajiro T (2005) Gēmu de asobu risuku komyunikeishon—Kurosurōdo he no shoutai (Risk communication game—invitation to "Crossroads"), Nakanishiya Shuppan, Kyoto

Yamori K, Nakagami T, Unozawa T, Ueyama R, Honda S, Kasai K, Nagai Y, Iwata Y, Imamura F (2011) Large-scale survey on tsunami evacuation in the Great East Japan Earthquake (summary) – requirements for future survey analysis and information utilization. In: Proceedings of the 30th annual meeting of the Japan society for natural disaster science, pp 55–56

Chapter 6
Soil-Slide Avalanches of Pyroclastic Fall Deposits Induced by the 2011 Off the Pacific Coast of Tohoku Earthquake

Masahiro Chigira, Akito Nakasuji, Shinya Fujiwara, and Masayuki Sakagami

Abstract The 2011 Off the Pacific Coast of Tohoku Earthquake set off four soil-slide avalanches of pyroclastic fall deposits within Shirakawa (Fukushima Prefecture) and Nakagawa (Tochigi Prefecture). At Shirakawa, a seismic intensity of 6+ on the JMA scale was recorded and at Nakagawa, 6−. Predominant factors behind these slides were (1) a bedding of pyroclastic fall deposits parallel to the original slope and (2) a sliding surface of weak paleosol that, having been undercut by erosion at the bottom of the slope, lost its ability to support the soil above it. These landslides were highly mobile, as suggested by apparent friction angles of 10–16°. Many trees on them, supported by root systems, remained standing within their root–soil plate; that is, they were transported and deposited upon the underlying debris in an upright position. Similar slides have been observed to occur in numerous other earthquakes, which suggests that some pyroclastic fall deposits are highly susceptible to seismic shocks. Here, to contribute to efforts toward mitigating the earthquake-induced hazards presented by such deposits, we identify some of the characteristics of soil-slide avalanches induced by the 2011 Off the Pacific Coast of Tohoku Earthquake.

Keywords Avalanche • Halloysite • Landslide • Paleosol • Pyroclastics • The 2011 Off the Pacific Coast of Tohoku Earthquake

M. Chigira (✉)
Disaster Prevention Research Institute (DPRI), Kyoto University, Kyoto, Japan
e-mail: chigira@slope.dpri.kyoto-u.ac.jp

A. Nakasuji • S. Fujiwara • M. Sakagami
Kokusai Kogyo Co. Ltd., Tokyo, Japan

H. Kawase (ed.), *Studies on the 2011 Off the Pacific Coast of Tohoku Earthquake*,
Natural Disaster Science and Mitigation Engineering: DPRI reports,
DOI 10.1007/978-4-431-54418-0_6,

6.1 Introduction

The 2011 Off the Pacific Coast of Tohoku Earthquake (hereinafter, the Tohoku Earthquake) is the strongest seismic event (Mw9.0) ever recorded in Japan by modern methods. It struck on March 11, 2011, at 14:46:18.1, with an epicenter 24 km deep off the Sanriku coast at 38°06.22′N, 142°51.6′E (Japan Meteorological 2011a, b). The quake was particularly destructive because of its tsunami; damage from landslides and avalanches, by comparison, was limited. This said, soil-slide avalanches did occur on gentle slopes at Shirakawa (Fukushima Prefecture; seismic intensity of 6+ on the JMA scale) and Nakagawa (Tochigi Prefecture; 6−) (see Fig. 6.1). We investigated these occurrences through geological field examinations, laser surveying, X-ray mineralogical analysis, various physical property measurements, and geomorphic analysis by means of aerial photographs taken before the earthquake. In this manner, we examined the various geological characteristics of these slides for comparison against similar occurrences in past earthquakes.

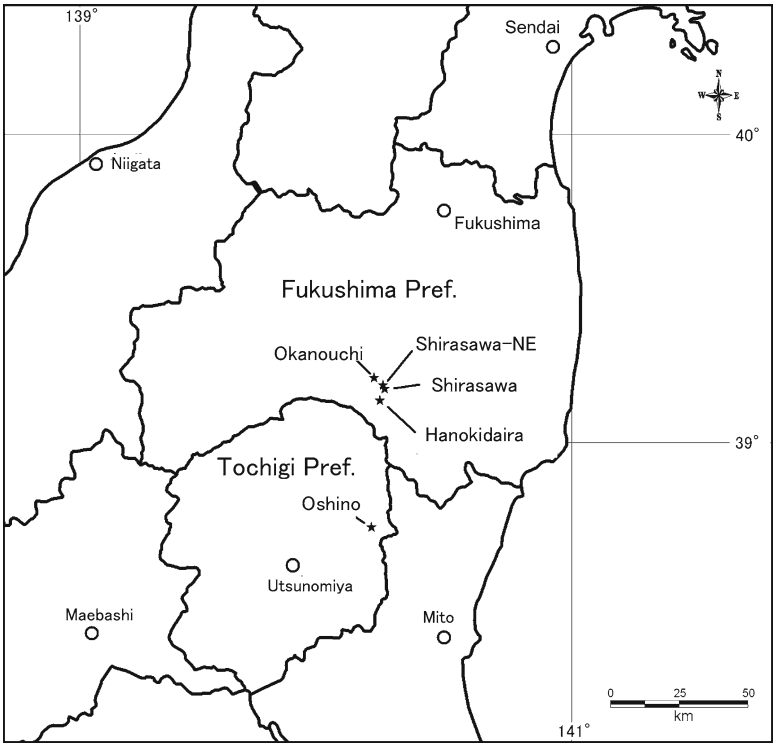

Fig. 6.1 Index map of the landslides

6.2 Landslide Distribution and Characteristics

Notable soil-slide avalanches occurred at five locations, four in Shirakawa, Fukushima Prefecture (Hanokidaira, Shirasawa, Shirasawa-NE, and Okanouchi), and one in Nakagawa, Tochigi Prefecture (Oshino). As will be described in more detail later, the Okanouchi slide involved a colluvium of weakly welded tuff. The other four were avalanches of pyroclastic fall deposits. We directly examined four of the five; a summary of their characteristics is presented as Table 6.1. We did not directly examine the Shirasawa-NE slide and thus do not include it within the table.

6.2.1 Landslide at Hanokidaira (Shirakawa, Fukushima Prefecture)

Figure 6.2 shows a schematic map of the Hanokidaira landslide. Features of that slide are outlined below.

6.2.1.1 Overview

Casualties: 12 dead, one missing

Extent: Horizontal length 251 m; height 47 m; volume [(60 m long × 50 m wide × 5 m deep) + (50 m long × 70 m wide × 4.5 m deep)] = 30,000 m^3

Apparent friction angle: 10.0°

Geology: Paleosol, pumice, scoria, and weathered ash. They are mostly from the Nasu volcano (Suzuki 1992).

Geological structure: Bedded texture roughly parallel to slope surface, burying a small valley in the Shirakawa ignimbrite; some weathered ash present in thick drifts (labeled “9 m” in Fig. 6.2).

Duration: An eyewitness mentioned the movement started just after the strongest shaking and continued 5 s.

Morphology before the event: Aerial photographs taken in 1975 by the Geospatial Information Authority of Japan showed a cup-shaped gully head at the location that later marked the bottom of the avalanched slope. Local people observed water was coming out at the gully head. We infer that the gully eroded the slope from its bottom, thus undercutting the upper portion from its bedding.

Table 6.1 A list of soil-slide avalanches induced by the 2011 Tohoku Earthquake

Locality	Damage	Apparent friction angle (°)	Horizontal length (m)	Height (m)	Volume (m^3)	Geology	Sliding surface	Depth (m)	Slope angle (°) of a source area	Morphology before the event	Slope direction
Hanokidaira	12 dead 1 missing	10	251	47	30,000	Paleosol, pumice, scorias, weathered ash	Paleosol	5–9	22	Undercut	N45°E
Shirasawa	Forest and paddy	15[a]	330	70	9,000	Paleosol, pumice, weathered ash	Paleosol	3	13	Undercut	S60°E
Okanouchi	1 dead	16	143	40	16,000	Colluvium of weakly welded tuff	Paleosol	5	18	Undercut	S
Oshino	Forest and paddy	12.7	330	75	5,500	Paleosol, pumice, weathered ash	Paleosol	4	23	Undercut	N56°E

[a]From 1/25,000 map (the others were measured)

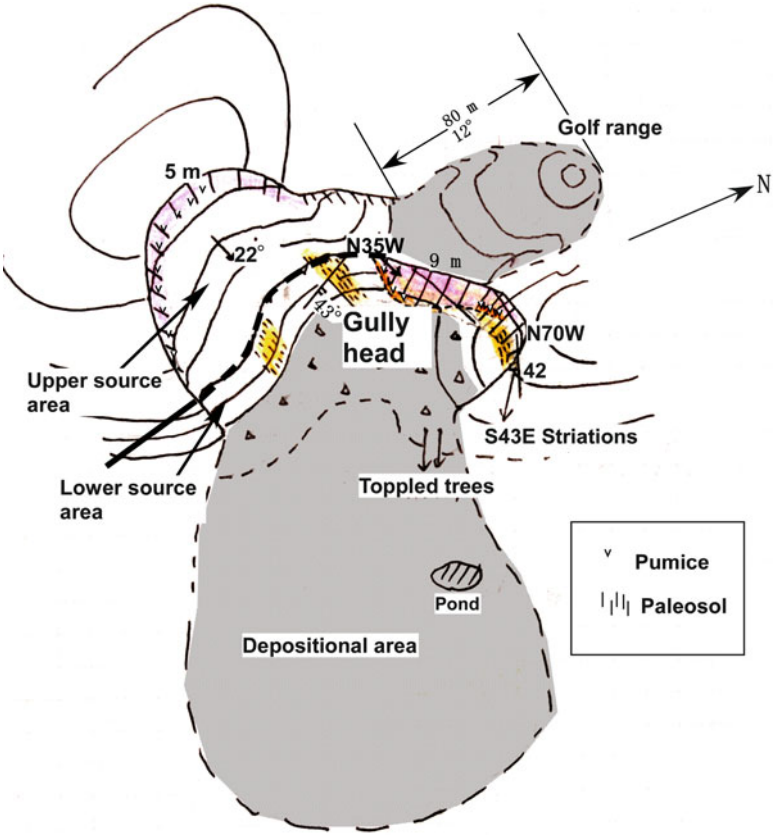

Fig. 6.2 Schematic map of the Hanokidaira landslide

6.2.1.2 Avalanche Source

The upper edge (crown) of the avalanche slope is bounded by a vertical scarp of 4–5 m in height; essentially all of the material originally within this portion was transported outside of the source area (Fig. 6.3a, c). Exposed on the scarp are weathered ash, pumice, scoria, and paleosol (Fig. 6.4). Minerals identified from these were halloysite, gibbsite, 1.4 nm mineral, cristobalite, tridymite, and quartz. Gibbsite was contained only in soil and pumice near the ground surface, and halloysite was contained only in the paleosol. Soil hardness measured by using a portable hardness tester (soil hardness meter, Yamanaka type, Daiki Rika Kogyo Co., Japan; Yokota and Iwamatsu 1999; Chigira and Yokoyama 2005) suggested that the paleosol in the depth of 3.5–4 m was the weakest, where sliding surface was formed. The source area is divided into two parts—an upper portion and a lower portion. The upper portion has a slope of 22° and is concave, opening to the east. The lower portion has a slope of 43° and is also concave, opening to the southeast (Fig. 6.2).

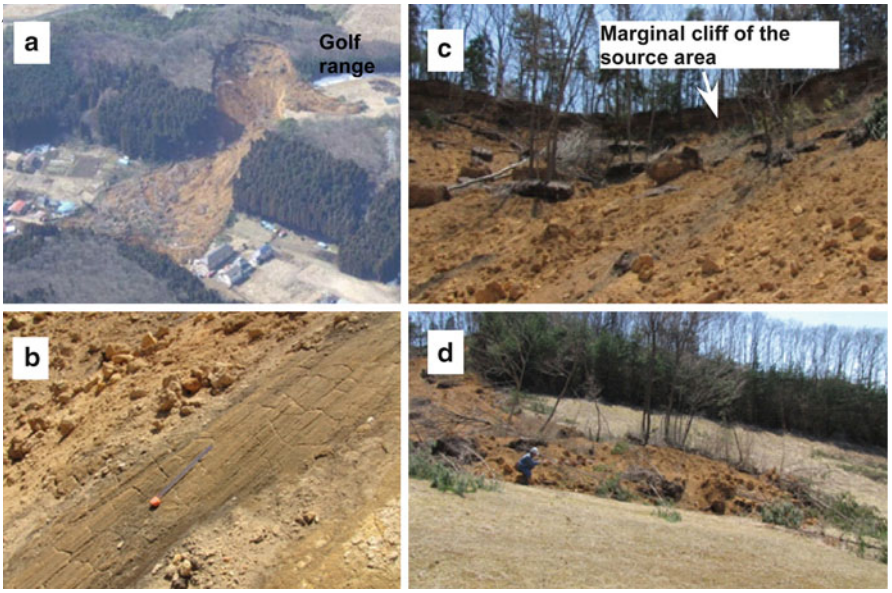

Fig. 6.3 Photographs of the Hanokidaira landslide. (**a**) Overview (photo by the Ministry of Land, Infrastructure, Transportation and Tourism); (**b**) sliding surface (**c**) standing trees remaining in the source area; (**d**) landslide deposits on the turf in a golf range

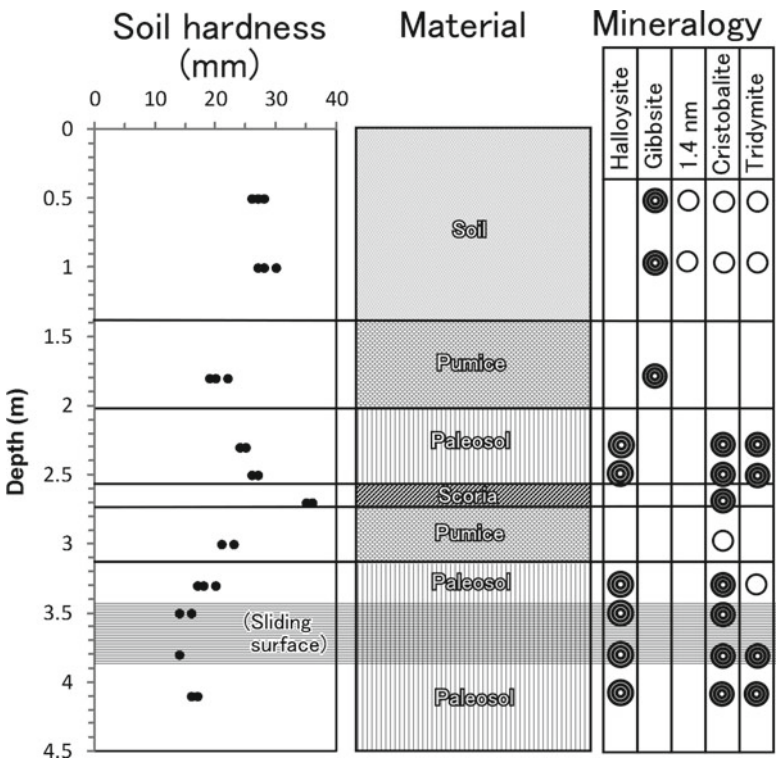

Fig. 6.4 Columnar section with soil hardness and mineralogy at the top of the marginal cliff of the Hanokidaira landslide. *Dark circles* and *white circles* indicate abundant and less-abundant minerals, respectively. Quartz is contained in all the samples including scoria

The lower portion corresponds to the location of a gully head before the slide. Trees, supported by their root networks, remain standing within thin layers of avalanched soil in the source area (Fig. 6.3c).

6.2.1.3 Sliding Surface

A sliding surface is discontinuously exposed within the source area (Fig. 6.2). Also apparent are striations scraped onto that surface (Fig. 6.3b). The surface was formed near the top of a paleosol layer which, before the slide, was located 4–9-m underground. The deep portion (9-m underground) corresponds to the hollow before the slide, which suggests that the sliding surface at that area was actually considerably shallower than 9 m (we suspect that the true depth of that portion was about 5-m underground, or roughly half that amount). A close examination of the sliding surface reveals that paleosol has lost its texture down to a depth of 1–2 cm below that surface, where visible pores are closed. The paleosol is very high in moisture and weak. It contains pumice and scoria granules and plagioclase fragments, which have transformed to clayey materials.

The paleosol is originated from loam intercalating TkP and Sr10 tephra layers in its top and KdP tephra in its base, respectively (Suzuki 1992), and the paleosol is just beneath a pumice layer of the Sr9 (Suzuki 1992). The KdP tephra is dated to be 200 ± 30 ka (Suzuki et al. 2004).

6.2.1.4 Deposited Material and Velocity

Although most of the debris was transported to the southeast, a portion moved to the north (Figs. 6.2, 6.3a). The northern slope is gentle, and much of the debris is deposited over the turf of a golf range. The underlying turf is not deformed or scraped (Fig. 6.3d). The depositional areas are up to 3 m deep, and the deposited material is dry and loose. Trees, supported by their root systems, remain standing within it, showing that they were transported in that position.

The duration time reported from an eyewitness was as short as 5 s, suggesting an average velocity to be about 180 km/h. If the time was twice of it, it suggests a velocity of 90 km/h.

6.2.2 Landslide at Shirasawa (Shirakawa, Fukushima Prefecture)

6.2.2.1 Overview

Damage: Forest and paddy

Apparent friction angle: Not measureable (calculated to be 15° from horizontal length and height)

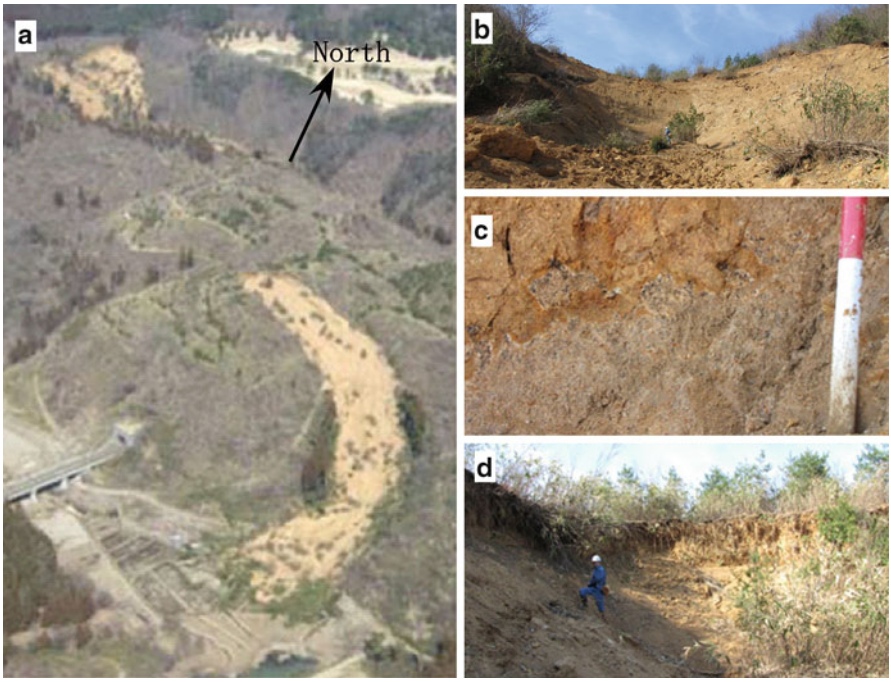

Fig. 6.5 Photographs of the Shirasawa landslide. (**a**) Oblique view from the air (Ministry of Land, Infrastructure, Transport and Tourism). (**b**) Steep slope just beneath the knickpoint along the path of debris transportation. (**c**) Paleosol with pumice grains on it at the rim cliff of the source area. (**d**) Highest part of the source area

Extent: Horizontal length 330 m; height 70 m (estimated with 1/25,000 map); volume (95 m long × 30 m wide × 3 m deep) = 9,000 m^3

Geology: Paleosol, pumice, and weathered ash. They are mostly from the Nasu volcano (Suzuki 1992).

Geological structure: Bedded roughly parallel to slope surface, burying an old small valley in the Shirakawa ignimbrite

Morphology before the event: gully head. Debris came down from head to southeast and then south (Fig. 6.5a). A clear knickpoint exists midway up the gully (Fig. 6.5b), and the avalanche occurred above it. As was the case with the Hanokidaira landslide, the bedding had been undercut at the knickpoint.

6.2.2.2 Avalanche Source

The avalanche source is a long and narrow zero-order hollow running to the southeast. It has a slope of 13° with an abrupt shift to a steep 46° at the bottom. This steep slope probably marks the head of a lower gully, erosion from which, we infer,

undercut the upper surface. The avalanche source has a horizontal length of 95 m, a width of 30 m, and a height of 20 m. The crown of the avalanched slope and both sides are bordered by an essentially vertical scarp of approximately 3 m in height (Fig. 6.5d). Exposed on the scarp is weathered ash mixed with pumice; sandwiched within it is a 15-cm layer of very fine white pumice. The pumice-containing weathered ash contacts a lower layer of paleosol at a depth of 2 m (Fig. 6.5c). Bushes remained standing on avalanched soil within the source area.

Later cutting of the source slope for slope stabilization showed that pyroclastic layers that slid had buried a small valley within the Shirakawa ignimbrite to form an apparently plunging syncline and that sliding surface was formed within the paleosol near the pumice layers of Sr8 and Sr9 and along those pumice layers. Sr9 overlies the weathered Shirakawa ignimbrite with a few tens of centimeters of paleosol in between.

6.2.2.3 Sliding Surface

A striated sliding surface was observed to be discontinuously exposed within the avalanche source. The pumice grains of Sr8 and Sr9 were heavily weathered to be clayey material. The paleosol is volcanic in origin and contains pumice. It also contains a great amount of moisture, is weak, and contains pores. The weathered ash above is relatively low in moisture. The paleosol and weathered pumice contain halloysite.

The paleosol structure has been lost down to a depth of 2 cm below the sliding surface, and gaps within it have been crushed.

6.2.2.4 Deposited Material

Debris flowed down the gully from the source area. Trees were concentrated at the toe (furthest extent) of the debris flow (Fig. 6.4a), where they remain standing on a paddy. The surface of the paddy was not deformed at all. The deposited material was dry and loose.

6.2.3 Landslide at Okanouchi (Shirakawa, Fukushima Prefecture)

6.2.3.1 Overview

Casualties: One dead, one house completely destroyed

Apparent friction angle: 16°

Extent: Horizontal length 143 m; height 40 m; volume (76 m long × 41 m wide × 5 m deep) = 16,000 m^3

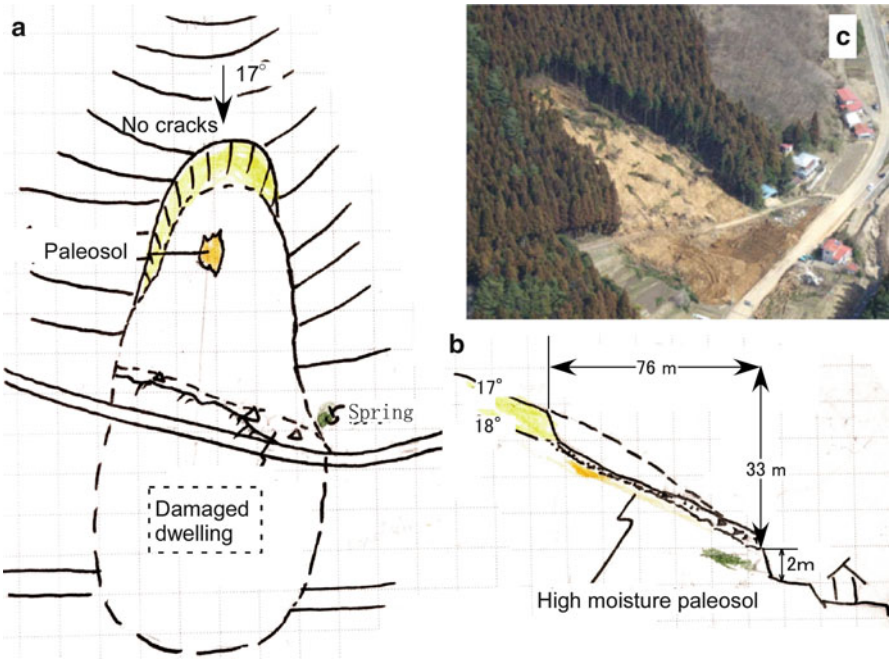

Fig. 6.6 Schematic sketch and a photograph of the Okanouchi landslide. (**a**) Plan view. (**b**) Cross section along the descending line of the slope. (**c**) Oblique view from the air (Ministry of Land, Infrastructure, Transport and Tourism)

Geology: Colluvium of weakly welded tuff (brown soil mixed with rock fragments)

Geological structure: Bedded texture roughly parallel to slope surface; strong weathering at deeper depths; high moisture; exposed weakly welded tuff alongside slope base; spring water observed flowing from cracks within it

Morphology before the event: A road runs across the bottom of the slope. The sliding surface is exposed at the road cut.

6.2.3.2 Avalanche Source

The avalanche source has a horizontal length of 76 m, a width of 41 m, and an average depth of 5 m. The slope angle is 18°. The crown of the avalanched slope is bordered by an essentially vertical scarp having a maximum height of 8 m, which shows that almost all of the material within the source has flowed away (Fig. 6.6). Exposed on the scarp is a colluvium of weakly welded tuff (Shirakawa ignimbrite). As there are no crown cracks above the avalanche source, we infer that the risk of further avalanching is low, barring seismic shocks on the level of the previous earthquake.

6.2.3.3 Sliding Surface

A sliding surface is discontinuously exposed beneath thin layers of avalanched soil, and striations are grooved into it. The soil exhibits pores, and by this we can tell it is paleosol. The paleosol structure has been lost down a depth of 3 cm below the sliding surface, and gaps have been crushed. It contained halloysite.

6.2.3.4 Deposited Material

By the time the authors had a chance to observe the deposition area, it had already been disturbed in the course of rescue efforts. Witnesses, however, report that trees were standing within the avalanched soil immediately after the slide.

6.2.4 Landslide at Oshino (Nakagawa, Tochigi Prefecture)

6.2.4.1 Overview

Damage: Forest, paddy, house (partially destroyed but no injuries)

Apparent friction angle: 13°

Extent: Horizontal length 330 m; height 75 m; volume (55 m long × 25 m wide × 4 m deep) = 5,500 m^3

Geology: Paleosol, pumice, weathered ash

Geological structure: Bedded texture roughly parallel to slope surface

Morphology before the event: Aerial photographs taken in 1975 by the Geospatial Information Authority of Japan show the northern half of the lower slope to extend to what was once the head of a steep gully. The gully apparently eroded the slope from its bottom, thus undercutting the upper portion.

6.2.4.2 Avalanche Source

The source area has a horizontal length of 25 m, a width of 55 m, a height of 35 m, and a slope of 23° (the sliding surface has a slope of 34°). The average depth is 4 m. The upper edge of the avalanched slope is bordered by an almost vertical 4-m scarp, which shows that almost all of the material on the avalanched side was transported away (Figs. 6.7 and 6.8). Exposed on the scarp are paleosol, weathered ash, and pumice. A 40-cm thick pumice layer is the KP tephra of 32 ka (Fig. 6.7, Suzuki 1993). Trees, supported by their root networks, remain standing above thin layers of debris (Fig. 6.7b).

Fig. 6.7 Photographs of the Oshino landslide. (**a**) Overview from the northeast. (**b**) Northern half of the source area with bedding of yellowish white pumice (Kanuma pumice) parallel to the slope

6.2.4.3 Sliding Surface

A sliding surface within the source area was observed to be discontinuously exposed beneath thin layers of debris, and striations are scraped onto it. The sliding surface formed near the upper surface of a paleosol layer, and its average depth was 4 m. Paleosol on the sliding surface lost its texture down to a depth of about 2 cm and, with gaps within it crushed, had been densified. The paleosol has extremely high moisture content, is weak, and has pores. It contained halloysite.

6.2.4.4 Deposited Material

Material located at the head of the gully before the slide was transported the furthest distance (Fig. 6.8). The toe (leading edge) of the deposited material covers a paddy, the surface of which is not deformed at all (Fig. 6.6a). The deposit has a maximum depth of about 3 m and is dry and loose. Trees, supported by root network layers, remain standing upon the deposit, which shows that they were transported in that position.

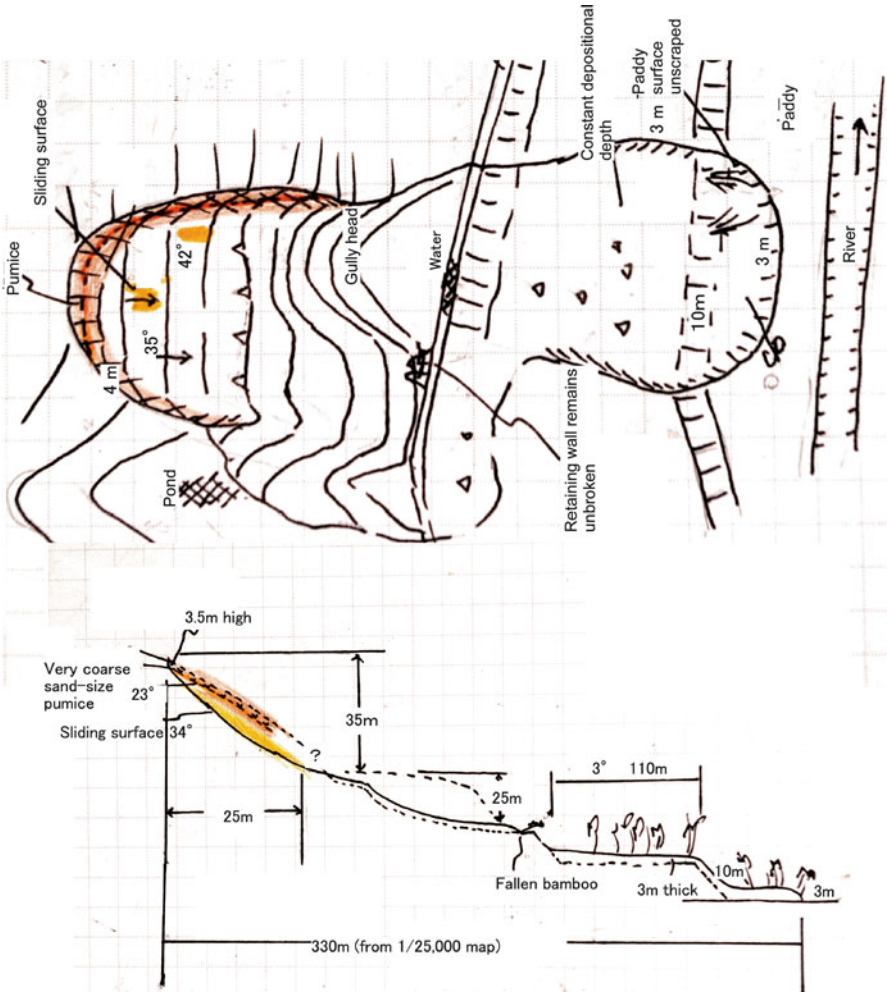

Fig. 6.8 Schematic sketch and a cross section of the Oshino landslide

6.2.4.5 Transport Behavior

According to an eyewitness account, "the landslide began and ended amid strong earthquake shocks; trees stood in place, making it look as if the entire forest was moving; it was all over in about five seconds." "Five seconds" seems a bit too short given the duration of the earthquake shocks, although this account does suggest that the slide did occur over a very short time. K-net data at Kuroiso, about 20 km from Nakagawa, indicates that shockwaves in excess of 100 Gal persisted for about 40 s. While it is uncertain when the landslide began, if we take the distance from the crown of the landslide to its toe (338 m) and divide that by 40 s, we arrive at a speed of 8 m/s (30 km/h).

6.3 Characteristics of Sliding-Surface Paleosols

Paleosols constituting the sliding surfaces of landslides induced by the 2011 Tohoku Earthquake were very moist and weak, with density measurements ranging from 1.6 to 2.1 g/cm^3 and gravimetric moisture contents ranging from 0.4 to 0.6 (Table 6.2). The density of the paleosol from the Oshino landslide is much smaller than the other two landslides, which could be attributed to the fact that the Oshino paleosol is inferred to be much younger than the other two. All the paleosols contained fine pores of a diameter of up to 1 mm. Similarly, their mineralogy can be characterized as quartz, halloysite, and cristobalite with tridymite. Halloysite is widely known to be a weathered product of volcanic glass (Aomine and Wada 1962).Cristobalite has been reported to be a weathered product of ignimbrite within the Shirakawa pyroclastic flow (Chigira et al. 2002).As for the Hanokidaira landslide, a layer of pumice (Sr9) resting above paleosol was found to be soft, easily crushable within one's fingers, and readily liquefiable; however, no halloysite was detected within it (Fig. 6.4). Pyroclastic fall avalanches of the 1986 Off Tokachi Earthquake and the 1978 Izu-Oshima-Kinkai Earthquake all entailed a sliding surface within paleosol (Inoue et al. 1970; Chigira 1982; Chigira 1995; Yoshida and Chigira 2012).The 1949 Imaichi Earthquake produced sliding surfaces in a pumice bed that had transformed into a whitish clay and were rich in halloysite (Morimoto 1951).The halloysite in a landslide induced by the 1968 Iu-Oshima-Kinkai Earthquake is interpreted to be the reaction product of gibbsite with silica in the percolating water from above beds after the burial of the paleosol (Chigira 1982), which is resilicification of gibbsite (Kleber et al. 2007). The surface soil in the Hanokidaira landslide site are dominated by gibbsite without halloysite, and the paleosol is dominated by halloysite, which suggests that the halloysite may be made by the resilicification of gibbsitic soil.

Examinations of paleosol structures in the vicinity of the sliding surfaces reveal that in all cases the structures had lost their original pores down to a depth of 1–2 cm below the sliding surface and that plagioclase/pumice particles have been crushed out of shape (Fig. 6.9). This comes as a result of strong shear deformation, to which paleosol on the bottom of the sliding surface was exposed upon the physical transport of the material. Chigira (1982) examined pyroclastic fall landslides occurring during the 1978 Izu-Oshima-Kinkai Earthquake. By means of soft X-ray photography of sliding-surface paleosols, he found that plastic deformation of paleosol occurred from a depth of several centimeters directly below the surface down to

Table 6.2 Physical properties of the paleosols

Place	Material	Moisture density (g/cm^3)	Dry density (g/cm^3)	Gravimetric water content	Gravimetric water-soil ratio
Oshino	Paleosol (halloysite)	1.66	0.75	0.55	1.20
Hanokidaira	Paleosol (halloysite)	2.03	1.20	0.41	0.68
Shirasawa	Paleosol (halloysite)	1.90	1.05	0.44	0.80
Okanouchi	Paleosol (halloysite)	–	–	–	–

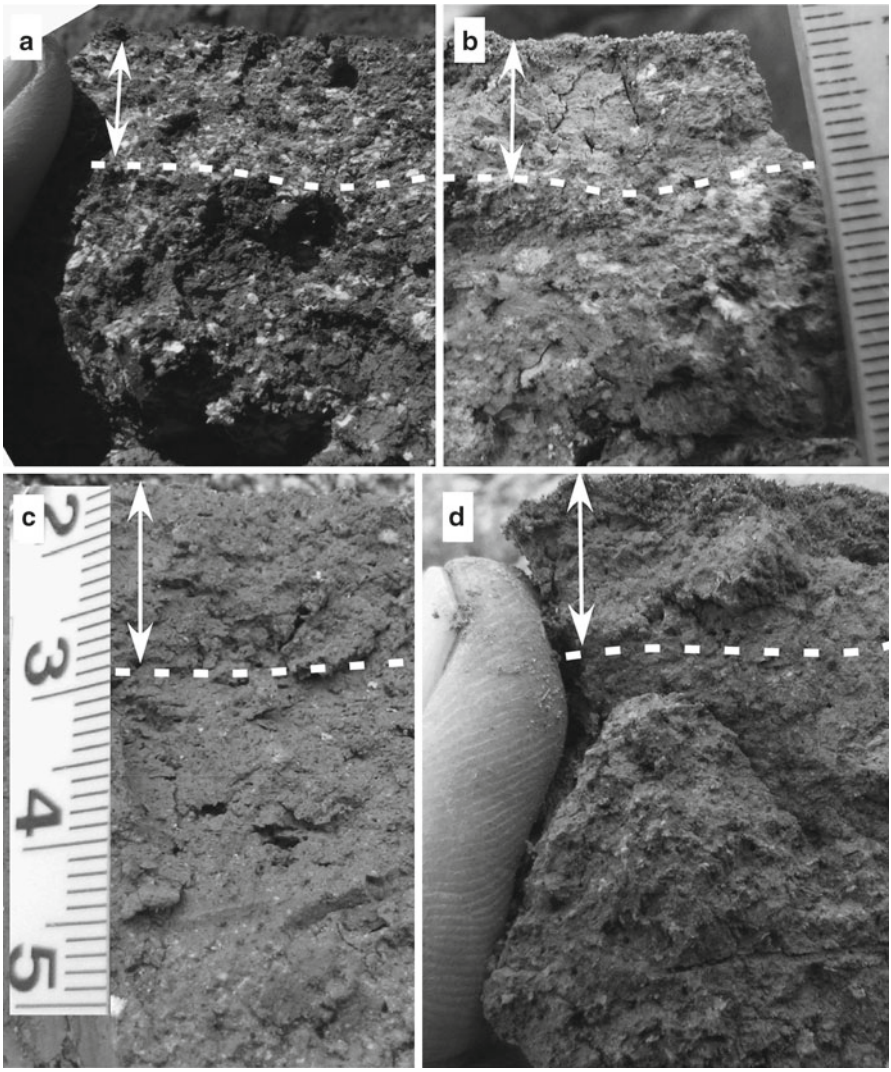

Fig. 6.9 Textures beneath a sliding surface on a vertical cross section normal to the sliding surface. Top surface of each section is a sliding surface. Original textures are lost from the sliding surface to the *dashed line*. (**a**) Hanokidaira; (**b**) Shirasawa; (**c**) Okanouchi; (**d**) Oshino

10 cm, with essentially all pores eliminated through crushing. This result indicates that deformation within a landslide is concentrated at the sliding surface and its environs. Also inferred is that the paleosol, being clay, had low moisture permeability, such that pore pressure within the area of shear deformation, unable to be released, remained at a high level. This suggests that surface liquefaction like that reported by Sassa et al. (1996) may have occurred.

6.4 Geological and Morphological Factors to Earthquake-Induced Landslides

Pyroclastic fall avalanches very similar to those of the 2011 Tohoku Earthquake occurred with considerable frequency within the 1949 Imaichi Earthquake (Morimoto 1951), the 1968 Off Tokachi Earthquake (Inoue et al. 1970; Yoshida and Chigira 2012), and the 1978 Izu-Oshima-Kinkai Earthquake (Table 3, Chigira 1982; Chigira 1995).In this section, we compare the geological and morphological characteristics of these landslides, and comment on the qualitative assessment of slope stability under seismic loading. Of the earthquakes mentioned above, the 1978 Izu-Oshima-Kinkai Earthquake produced relatively few landslides (seven occurrences), but, as they were all within a 1 km^2 area, their geographical density was high. A related factor behind their paucity was the monogenetic volcanic nature of the avalanched material, which itself was very narrowly distributed. Conversely, with regard to the 1949 Imaichi Earthquake, maps from Morimoto (1951) indicate landslides in 88 locations. Similarly, for the 1968 Off Tokachi Earthquake, landslides are reported to have occurred in approximately 150 locations (Inoue et al. 1970; Yoshida and Chigira 2012) for an average geographical density of four landslides per square kilometer.The landslides that occurred within the 2008 Iwate-Miyagi Inland Earthquake were dominated by the collapse of pumice tuff and welded ignimbrite. In other words, those slides were of a different nature than the ones discussed in this report (Hashimoto et al. 2009).

6.4.1 Surface-Parallel Bedding Structure and Slope Undercutting

Almost all the pyroclastic fall landslides induced by the four abovementioned earthquakes (Imaichi, Tokachi, Izu-Oshima, and Tohoku) occurred within a bedded structure parallel to the original slope. Also, the slopes were fairly gentle, ranging from 8°to 34° (Fig. 6.10). With regard to the Imaichi Earthquake and the Off Tokachi Earthquake, no detailed examinations were made to determine whether or not the lower portion of the slopes had been undercut. With regard to the Izu-Oshima-Kinkai Earthquake, however, it was found that all avalanched slopes had been undercut (Chigira 1982). Similarly, all avalanched slopes examined in relation to the Tohoku Earthquake were also determined to have been undercut, and, in the case of the 2004 Mid-Niigata Prefecture Earthquake, all primary landslides having an sliding surface in tuff were observed to have been undercut dip slopes (Chigira and Yagi 2005).These experiences suggest that undercut dip slopes are in a peculiar condition with respect to seismic action at the undercut and that the presence/absence of an undercut is a critical factor for the assessment of slope stability during earthquakes.

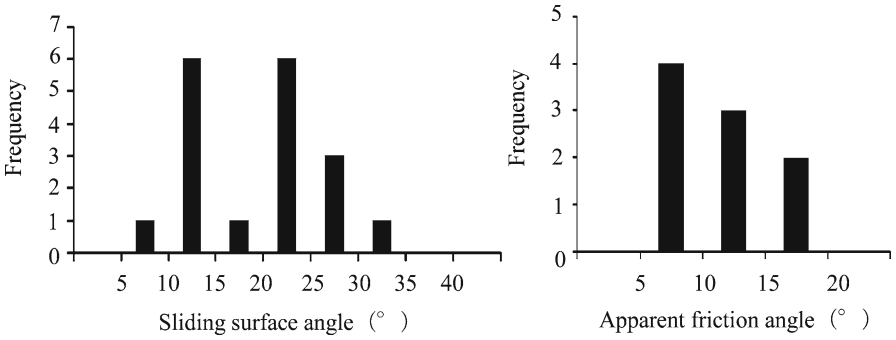

Fig. 6.10 Slope angles and apparent friction angles of soil-slide avalanches of pyroclastic fall deposits. Data: 1923 Kanto Earthquake (Kamai 1990), 1968 Off Tokachi Earthquake (Inoue et al. 1970), 1978 Izu-Oshima-Kinkai Earthquake (Chigira 1982), 1984 West Nagano Prefecture Earthquake (Oyagi 1987; Kawakami et al. 1985), and 2011 Tohoku Earthquake

6.4.2 High Mobility

The degree of landslide/avalanche mobility is typically indicated by the apparent friction angle or the equivalent coefficient of friction (Hsu 1975), which themselves are expressed as the angle of a line tying the crown of a landslide to its toe or as the tangent of that angle. A compilation of apparent friction angles for pyroclastic fall avalanches within various earthquakes, including the 2011 Tohoku Earthquake, the 1923 Kanto Earthquake (Kamai 1990), the 1968 Off Tokachi Earthquake (Inoue et al. 1970; Yoshida and Chigira 2012), the 1978 Izu-Oshima-Kinkai Earthquake (Chigira 1982), and the 1984 West Nagano Earthquake (Oyagi 1987; Kawakami et al. 1985), produces a range of 7° to 17° (Fig. 6.9), which in all cases is indicative of a high degree of mobility. These indicate a low degree of resistance not only at the source of the avalanche but also along the transport path (main track). Experience from the Izu-Oshima-Kinkai Earthquake (Chigira 1982) and the Tohoku Earthquake shows that there is little erosion on the bottom surface of the deposited material at either the transport path or the depositional area, suggesting that the material encounters little resistance along its bottom surface as it travels. While it is possible that some surface liquefaction occurred along the sliding surface as mentioned earlier, the transport mechanism over the transport path remains unknown.

6.4.3 Slope Directionality

The avalanches that occurred in the 2011 Tohoku Earthquake all faced from northeast to south (Fig. 6.11), which suggests a relation between these landslides and the direction of seismic action. A high degree of directional alignment was also noted

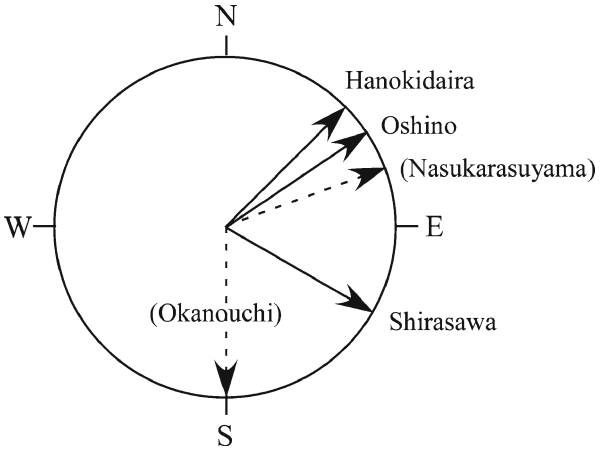

Fig. 6.11 Slope face of the soil-slide avalanches. *Solid lines*: pyroclastic fall deposits. *Dashed lines*: others

for pyroclastic fall landslides within the 1978 Izu-Oshima-Kinkai Earthquake and the 1968 Off Tokachi Earthquake, and here as well researchers have pointed to the possibility that a relation exists between such alignment and the direction of seismic action (Inoue et al. 1970; Chigira 1982).Further research is needed to examine the behavior of undercut slopes exposed to seismic forces.

6.4.4 Preceding Rainfall

Making use of AMeDAS and other rainfall data from the Japan Meteorological Agency, we compiled the cumulative rainfalls during the preceding 10 days, preceding 30 days, and preceding 60 days at sites that subsequently avalanched during various earthquakes (Table 6.3). Figure 6.12 shows a graph of the results. Preceding 10-day rainfall was heavy before the Off Tokachi Earthquake and the Iwate-Miyagi Inland Earthquake and light before the Imaichi Earthquake, the Izu-Oshima-Kinkai Earthquake, and the Tohoku Earthquake. Similarly, the preceding 30-day rainfall was relatively light before the Imaichi Earthquake and the Tohoku Earthquake, and the preceding 60-day rainfall was extremely light (less than half that of any other earthquake) before the Tohoku Earthquake. The sliding surfaces of avalanches occurring within these earthquakes consist of clayey weathered material or paleosol, all of which have a high degree of moisture retention. Such water retention appears to exert a deleterious effect on strength for roughly 30 days at least. The Tohoku Earthquake was characterized by a comparative paucity of landslides, and the dryness preceding the quake is presumably a major underlying factor. Assuming for the moment that the occurrence of such landslides is influenced by the amount of preceding rainfall, then, at least with regard to pyroclastic fall deposits, it would seem necessary to include some consideration of rainfall when assessing the stability of a slope under seismic loading. However, as it is currently impossible to forecast earthquakes with any confidence, this approach would be difficult to implement in

Table 6.3 Preceding precipitations of earthquakes that induced landslides of pyroclastic fall deposits (Iwate-Miyagi Inland Earthquake is for reference)

Earthquake	Date	Seismic intensity at the site of landslide (JMA)	Observatory	Preceding rainfall (mm)			Number of landslides	Sliding surface depth (m)	Slope-parallel bedding	Undercut
				10 days	30 days	60 days				
1949 Imaichi	26 December	5–6 (Imaichi)	Utsunomiya	22.5	80.8	255	88[a]	3–5[a]	yes	yes
1968 Off Tokachi	16 May	5 (Hachinohe)	Hachinohe	181	292	307	152[b]	<3[b]	yes	yes
1978 Izu-Oshima-Kinkai	14 January	5–6	Inatori	12	172	334	7[c] (material distribution limited)	2–6[c]	yes	yes
2008 Iwate-Miyagi Inland	14 June	5+–6+	Komanoyu	89	284.5	388	>100	–	–	Various
2011 Tohoku	11 March	6+ (Shirakawa) 6– (Nakagawa)	Shirakawa	12.5	83.5	93.5	~10	3–9	yes	yes

[a]Morimoto (1951)
[b]Inoue et al. (1970)
[c]Chigira (1982)

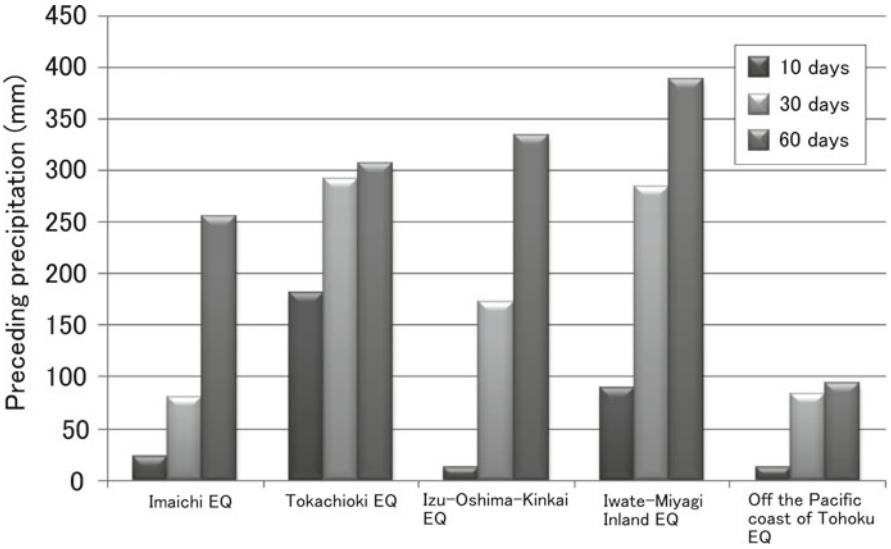

Fig. 6.12 Rainfalls preceding earthquakes that induced landslides of pyroclastic fall deposits (Japan Meteorological Agency). Observatories are located as follows: Imaichi Earthquake, Utsunomiya. Off Tokachi Earthquake, Hachinohe. Izu-Oshima-Kinkai Earthquake, Inatori. Iwate-Miyagi Inland Earthquake, Kumanoyu. Tohoku Earthquake, Shirakawa

practice. A more realistic approach would be to assess slope stability on an assumption that a certain amount of rain will fall over some period ahead of the earthquake, in which case we believe from the above that a period of approximately 30 days would be appropriate. Nevertheless, there remains a need to quantitatively assess relations among preceding rainfall, paleosol moisture content, and strength degradation.

6.5 Conclusions

The 2011 Tohoku Earthquake set off four soil-slide avalanches of pyroclastic fall deposits at Shirakawa, Fukushima Prefecture, and Nakagawa, Tochigi Prefecture. At Shirakawa, a seismic intensity of 6+ on the JMA scale was recorded and at Nakagawa, 6−. Predominant factors behind these landslides were (1) bedding of pyroclastic fall deposits parallel to the original slopes and (2) a sliding surface of weak paleosol at depths of 3–9 m below the slope surface. The paleosol consisted of weathered ash mixed with pumice, was moist and weak, was rich in halloysite, contained macropores, and liquefied when crushed between one's fingers. The transported material was dry and comprised weathered ash, pumice, and scoria; the large majority of the material flowed downhill from the source at a high speed, leading to, in the case of the Shirakawa slide, fatalities. Many of the trees growing on the slopes,

supported by root systems, remained standing within their root-soil plate; that is, they were transported and deposited upon the underlying debris in an upright position. The material was highly mobile, as suggested by apparent friction angles of 10–16°. A bedded slope structure was determined to have been undercut near the bottom of their slopes before the occurrence of a slide. Pyroclastic fall avalanches very similar to those of the 2011 Tohoku Earthquake occurred with considerable frequency in the 1949 Imaichi Earthquake, the 1968 Tokachi Earthquake, and the 1978 Izu-Oshima-Kinkai Earthquake, thus demonstrating that some pyroclastic fall deposits are extremely unstable under seismic loading. The relative paucity of pyroclastic fall landslides within the 2011 Tohoku Earthquake is thought to be attributable to a comparatively small amount of rainfall over the days preceding the quake.

Acknowledgement We thank Prof. Takehiko, Suzuki for his identifying tephra in the field. We are grateful to Maho Nakano for her help in the field. We also thank Takeshi, Shibasaki of NHK (Japan Broadcasting Corporation) for his stimulating our research.

References

Aomine S, Wada K (1962) Differential weathering of volcanic ash and pumice resulting in formation of hydrated halloysite. Am Mineralogist 47:1024–1048

Chigira M (1982) Dry debris flow of pyroclastic fall deposits triggered by the 1978 Izu-Oshima-Kinkai Earthquake: the “collapsing” landslide at Nanamawari, Mitaka-Iriya, southern Izu Peninsula. J Nat Disaster Sci 4:1–32

Chigira M (1995) Weathering and slope movement. Kinmiraisha, Naboya, 204 p

Chigira M, Yagi H (2005) Geological and geomorphological characteristics of landslides triggered by the 2004 Mid Niigata prefecture earthquake in Japan. Eng Geol 82:202–221

Chigira M, Yokoyama O (2005) Weathering profile of non-welded ignimbrite and the water infiltration behavior within it in relation to the generation of shallow landslides. Eng Geol 78:187–207

Chigira M, Nakamoto M, Nakata E (2002) Weathering mechanisms and their effects on the landsliding of ignimbrite subject to vapor-phase crystallization in the Shirakawa pyroclastic flow, northern Japan. Eng Geol 66:111–125

Hashimoto S, Chigira M, Nakasuji A et al (2009) The report of the Iwate-Miyagi Nairiku Earthquake in 2008 disaster. J Jpn Soc Eng Geol 50:98–108

Hsu KJ (1975) Catastrophic debris streams (sturzstroms) generated by rockfalls. Geol Soc Am Bull 86:129–140

Inoue Y, Honsho S, Matsushima M, Esashi Y (1970) Geological and soil mechanical studies on the slides occurred during the 1968 Tokachioki earthquake in southeastern area of Aomori Prefecture. Technical report of the central research institute of electric power industry 886:1–27

Japan Meteorological Agency (2011a) Distribution of seismic intensity induced by the 2011 off the Pacific coast of Tohoku Earthquake. 25 March 2011

Japan Meteorological Agency (2011b) Monthly report on earthquakes and volcanoes in Japan. March 2011

Kamai T (1990) Failure mechanism of deep-seated landslides caused by the 1923 Kanto earthquake, Japan. In: Proceedings of the sixth international conference and field workshop on landslides, Milano, pp 187–198

Kawakami H, Konishi J, Saito Y (1985) Mechanism of slope failures by the Naganoken-seibu earthquake 1984 and the characteristics of pumice. Tsuchi-to-Kiso 33:53–59

Kleber M et al (2007) Halloysite versus gibbsite: silicon cycling as a pedogenetic process in two lowland neotropical rain forest soils of La Selva, Costa Rica. Geoderma 138:1–11
Morimoto R (1951) Geology of Imaichi district with special reference to the earthquakes of December 26th, 1949. (II). Bull Earthquake Res Inst 29:349–358
Oyagi N (1987) The 1984 Ontake-san landslide and its movement. Trans Jpn Geomorphologic Union 8:127–144
Sassa K, Fukuoka H, Scarascia-Mugnozza G, Evans S(1996) Earthquake-induced-landslides: distribution, motion and mechanisms. Special issue of soils and foundations, pp 53–64
Suzuki T (1992) Tephrochronological study on Nasu volcano. Bull Volcanological Soc Jpn 37:251–263
Suzuki T (1993) Stratigraphy of middle Pleistocene tephra layers around Nasuno Plain, in north Kanto, Central Japan. J Geography 102:73–90
Suzuki T, Fujiwara O, Danhara T (2004) Stratigraphy and chronology of middle Pleistocene tephras in and around Aizu area, northeast Japan. J Geography 113:38–61
Yokota S, Iwamatsu A (1999) Weathering distribution in a steep slope of soft pyroclastic rocks as an indicator of slope instability. Eng Geol 55:57–68
Yoshida M, Chigira M (2012) The relation between weathering of pyroclastic fall deposits and the collapses caused by the 1968 Tokachi-oki earthquake. J Jpn Soc Eng Geol 52:213–221

Chapter 7
Estimation of Strong Motion During the 2011 Northern Nagano Earthquake and an Associated Building Damage Survey

Masumi Yamada, Masayuki Yamada, Christine Smyth, Yui Fukuda, Yoshinori Fujino, and Koji Hada

Abstract We conducted a damage survey of the wooden structures and collected very dense ambient noise measurements in the near-source region of the 2011 Northern Nagano earthquake in central Japan. The percentage of totally collapsed buildings exceeded 30 % in the Aokura and Yokokura colonies of Sakae village, Nagano prefecture. The percentage in the Mori colony, where a strong motion was recorded during the mainshock, was <10 %. We estimated the strong motion in the Aokura and Mori colonies from the ambient noise measurements and strong motion records. The estimated strong motion distribution reflects the soil conditions and varies within that small area. The correlation of the estimated strong motion and damage ratio of the wooden structures is reasonably high, which indicates that the estimated ground motions are realistic. The damage curve obtained in this research shows that the collapse ratio exceeds 50 % at around 150 cm/s of input ground motion.

Keywords Ambient noise • Building damage survey • Northern Nagano earthquake • Strong motion • Wooden structure

7.1 Introduction

The 2011 Northern Nagano earthquake, which occurred on March 12, 2011, produced strong shaking in the northern part of the Nagano prefecture, located in the central region of Honshu Island, Japan. However, because the earthquake occurred

M. Yamada (✉) • C. Smyth
Disaster Prevention Research Institute (DPRI), Kyoto University, Kyoto, Japan
e-mail: masumi@eqh.dpri.kyoto-u.ac.jp

M. Yamada • Y. Fukuda • Y. Fujino • K. Hada
NEWJEC Inc., Osaka, Japan

H. Kawase (ed.), *Studies on the 2011 Off the Pacific Coast of Tohoku Earthquake*,
Natural Disaster Science and Mitigation Engineering: DPRI reports,
DOI 10.1007/978-4-431-54418-0_7,

on the day following the great Tohoku earthquake, public attention was very low. The largest seismic intensity was 6 upper (X–XI in MMI scale) in Sakae village, Nagano prefecture, and the largest peak ground velocity (PGV) exceeded 110 cm/s. Sakae village is located between mountains, and the local settlements are very sparse. Therefore, it is important to understand the differences in the structural damage and the distribution of strong motions during the earthquake. We conducted a damage survey of the wooden houses in Sakae village in Nagano prefecture and Tsunan town in Niigata prefecture, both of which are located above the fault surface. We also performed a very dense ambient noise measurement in Sakae village and estimated the distribution of the strong motions during the earthquake on the basis of the strong motion record and ambient noise records. In this paper, we present a relationship between the estimated ground motions and damage ratio of the wooden houses, and compare this damage curve with those obtained from past earthquakes.

7.2 The 2011 Northern Nagano Earthquake and Strong Motion Records

The 2011 Northern Nagano earthquake occurred at 3:59 a.m. on March 12, 2011. The focal depth was 8 km, the JMA magnitude was 6.7, and the largest seismic intensity was 6 upper in Sakae village (Japan Meteorological Agency 2011). The fault rupture surface estimated from the aftershock distribution is northwest dipping, and the surface has dimensions of 10×20 km (Fig. 7.1).

Near-field strong motion records at the town hall of Sakae village were recorded by the government of the Nagano prefecture and are available at the website (Earthquake Research Institute 2000). Figure 7.2 shows the acceleration and velocity waveforms recorded during the mainshock. The sensor recorded ground acceleration, and we processed the original record using the following procedure. First, we removed the DC offset from the data, applied a baseline correction scheme proposed by Boore (Boore 2001), and integrated once in the time domain to obtain the velocity record. The acceleration records of both the EW and NS components exceed 900 cm/s^2, and the PGV of the EW component exceeds 110 cm/s. Figure 7.3 shows the acceleration response spectrum of the recorded data with a 5 % damping factor. The EW component has a large peak at 0.9 s, which is close to the period (1–2 s) which causes the most damage to wooden structures (Sakai et al. 2006). Based on these results, the recorded ground motion close to the source was likely to cause significant damage to wooden structures.

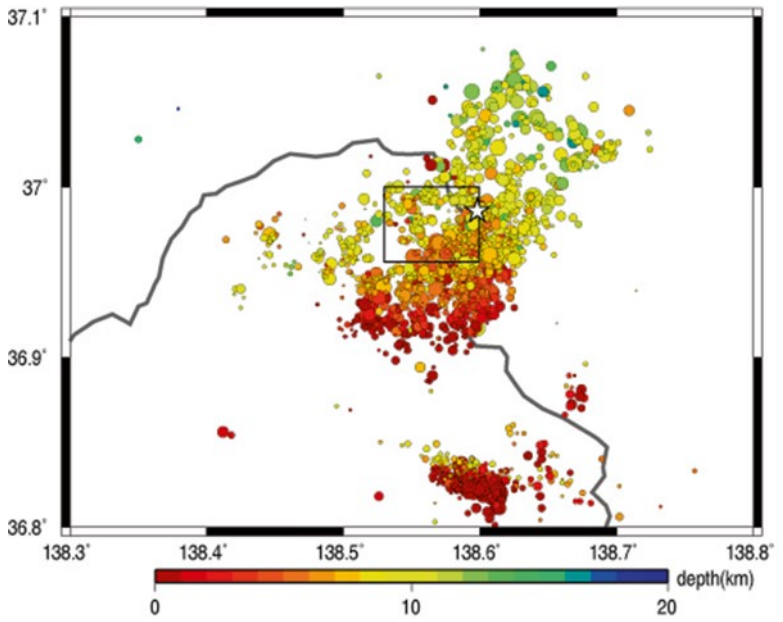

Fig. 7.1 Seismicity for the period March 1–31, 2011, obtained from the JMA unified catalog. The color of the *circles* shows the depth of the hypocenters. The *rectangle* in the center shows the area that is enlarged in Fig. 7.4, and the *star symbol* shows the epicenter of the mainshock. The *thick gray line* shows the boundary between Nagano and Niigata prefectures

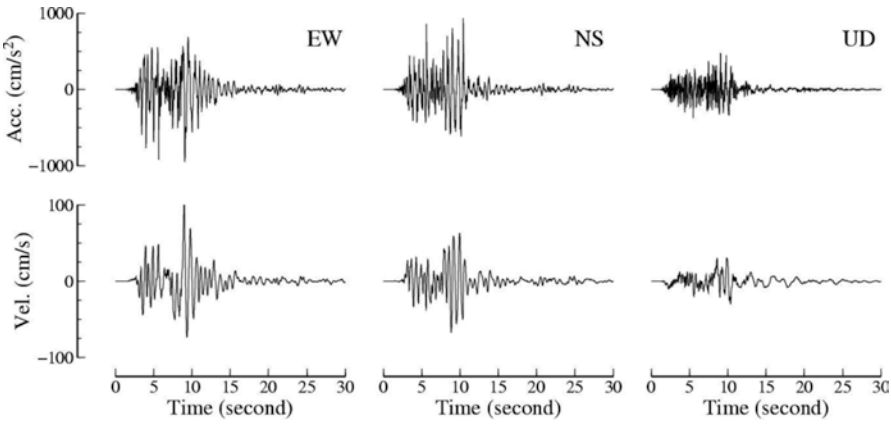

Fig. 7.2 Strong motion record of the mainshock recorded at the strong motion station in Sakae village. *Top*: acceleration waveforms, *bottom*: velocity waveforms. EW, NS, and UD components from the left

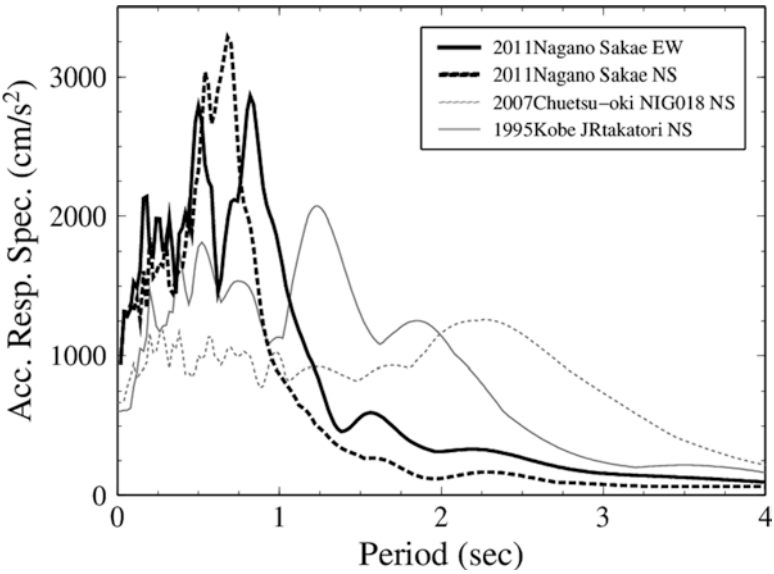

Fig. 7.3 Acceleration response spectrum of the waveform recorded in Sakae village, K-net Kashiwazaki for the 2007 Chuetsu-oki earthquake, and JR Takatori for the 1995 Kobe earthquake (all measurements have a 5 % damping coefficient)

7.3 Field Survey

7.3.1 Damage Survey of Wooden Structures

The field survey was performed on June 6–9, 2011, 3 months after the mainshock. The survey area spans the northeast area of Sakae village (the seven colonies are Mori, Aokura, Yokokura, Kotaki, Tsukioka, Minotsukuri, and Yukitsubo) and the northwest area of Tsunan town (the five colonies are Hanekura, Teraishi, Sakamaki, Kameoka, and Kodane). The size of the surveyed area is about 5 km in the east–west direction and 3 km in the north–south direction. Figure 7.4 shows the location of the target area. The fault surface is much larger than the survey area, and it encompasses all of the survey area.

We performed the survey in three groups, with two people in each group. The grade of the damage was judged according to the damage pattern chart for wooden structure proposed by Okada and Takai (1999). The criteria are D0 (no damage), D1, D2 (minor damage), D3 (half collapsed), and D4, D5 (totally collapsed). We visually investigated the damage and recorded damage levels on the local house map. We also recorded the usage of the structures (house, store, office, storage, etc.) and the type of the structures (wood, steel, RC, etc.). There were structures already cleared when we carried out the survey. We treated those structures as totally collapsed because we can assume that they were damaged beyond repair. The total number of structures we surveyed was 880.

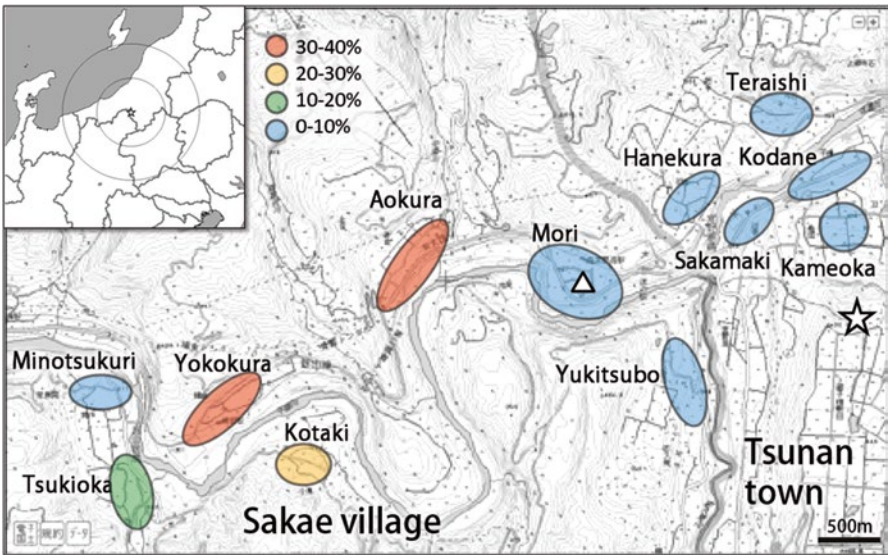

Fig. 7.4 Damage ratio of totally collapsed houses. Aokura and Yokokura colonies show more severe damage. The *triangle* in Mori colonies shows the strong motion station, and the *star* shows the epicenter

7.3.2 Dense Ambient Noise Measurement

We also performed an ambient noise measurement to evaluate the subsurface structure. We used JU210 sensors made by Hakusan and performed the measurement for 11 min at each site. JU210 includes three components, acceleration-type sensor, logger, and battery, in a casing. The sampling frequency was 100 Hz, and the cutoff frequency of the high-cut filter was 30 Hz. Measurements for the survey were taken at 40 m increments in the Aokura and Mori colonies, Sakae village. Typical 1–2 sites were measured in each of the other colonies. The peak frequencies of the H/V spectra of the ambient noise in each colony are shown in Table 7.1.

7.4 Result of the Damage Survey and Estimation of Strong Motions

7.4.1 Damage Ratio of the Wooden Structures

The damage ratio of the wooden structures in each colony was computed based on the building damage survey. In this analysis, the target structure type is wooden houses only. All other types of structures are excluded. We computed the percentage of totally collapsed houses (D4 or D5) and partially and totally collapsed houses (D3, D4, and D5). The percentage of totally collapsed houses in each colony is

Table 7.1 Damage ratios of wooden houses and results of ambient noise measurements in each colony. The damage ratio is in percentage

			House			House + store					H/V	PGA	PGV	
No	Colony	Location	D4–D5 (%)	D3–D5 (%)	*N*	D4–D5 (%)	D3–D5 (%)	*N*	Longitude	Latitude	(Hz)	(cm/s^2)	(cm/s)	JMA SI
1	Mori	Seismic station	5.4	18.9	74	11.6	26.3	95	138.577	36.988	2.64	947	111	6.41
2	Aokura	Center	32.3	46.2	65	33.8	47.1	68	138.564	36.990	1.86	1,962	216	7.14
3	Yokokura	Center	30.6	61.1	36	31.7	61.0	41	138.551	36.981	3.27	1,427	99	6.59
4	Yokokura	Damaged area	30.6	61.1	36	31.7	61.0	41	138.548	36.979	2.93	1,427	142	6.86
5	Kotaki	Center	21.1	52.6	19	20.0	55.0	20	138.557	36.977	5.25	2,247	118	6.7
6	Tsukioka	Center	13.0	46.3	54	12.3	45.6	57	138.544	36.975	6.57	946	91	6.34
7	Tsukioka	Damaged area	13.0	46.3	54	12.3	45.6	57	138.543	36.966	4.66	1,124	103	6.46
8	Minotsukuri	Center	3.6	16.1	56	6.5	17.7	62	138.541	36.981	9.13	1,105	106	6.59
9	Minotsukuri	Damaged area	3.6	16.1	56	6.5	17.7	62	138.540	36.982	5.86	1,141	110	6.6
10	Yukitsubo	Center	0.0	12.5	16	0.0	22.2	18	138.586	36.981	2.95	636	80	6.27
11	Henekura	Center	2.6	15.4	39	2.5	15.0	40	138.584	36.993	3.05	1,096	107	6.6
12	Teraishi	Center	3.7	25.9	27	3.3	23.3	30	138.592	36.998	6.74	815	82	6.32
13	Sakamaki	Center	0.0	0.0	35	0.0	0.0	44	138.588	36.991	3.00	811	81	6.23
14	Kodane	Center	0.0	15.8	19	4.2	20.8	24	138.595	36.995	4.27	823	87	6.29
15	Kameoka	Center	7.4	14.8	27	7.1	14.3	28	138.595	36.990	1.90	1,330	92	6.42

shown in Fig. 7.4. The percentage of totally collapsed houses in the Aokura and Yokokura colonies of Sakae village exceeds 30 %. This damage ratio is higher than that of the most damaged area during the 2007 Noto Hanto earthquake (Hashiride colony in Monzen town, 25 %; Arai et al. 2008). Because the percentage of totally collapsed houses in Mori colony, where the strong motion was recorded during the mainshock, is <10 %, the strong motion in the Aokura and Yokokura colonies may have been larger than the recorded strong motion. We also computed the percentage of totally collapsed houses and commercial buildings (stores and office buildings), as shown in the Table 7.1. The percentages of damaged buildings are slightly changed, but the overall pattern of the damage grades in the colonies does not change.

In order to compare damage with the site condition estimated from the ambient noise measurement completed later, the damage ratio at the sites of the ambient noise measurements was computed in the Aokura and Mori colonies. Because the ambient noise measurement was performed in a very dense spacing, we needed to identify the damage profile of the buildings near the survey site. However, if we compute the damage ratio from a small area, the variance becomes large because the number of samples in the area is insufficient. To solve this trade-off, we introduce a weighting as a function of the distance between the site of the ambient noise measurement and each building (R_i), then computed the percentage of the damaged houses within 100 m of the site of the ambient noise measurement:

$$\text{Damage Ratio}\left(\text{DR}_{\text{Dx}}\right) = \frac{\sum_{i=1}^{n} w_i f_i}{\sum_{i=1}^{n} w_i} \times 100 \tag{7.1}$$

where $f_i = 1$, if the damage to building i is greater equal to D3 or D4, $f_i = 0$, if the damage to building i is smaller than D3 or D4; $w_i = 1/R_i$, if $R_i \geq 0.02$ km, and $w_i = 1/0.02$, if R_i is <0.02 km; n is the number of the houses within 100 m of the site of ambient noise measurement.

The damage ratio with the threshold of D3 is defined as DR_{D3}, and the ratio with the threshold of D4 is defined as DR_{D4}. By applying the weighting, we can put emphasis on the damage profiles of the buildings near the site of the ambient noise measurement. We eliminated 11 points where number of the houses within 100 m was <10. The estimated damage ratio (DR_{D4}) is shown in Fig. 7.5. The center of the Aokura colony and the northeast area of the Mori colony showed the larger damage ratio. The northeast area of the Mori colony is next to the cliff to the Chikuma river, and that area was affected by a landslide due to the strong motion. We think this ground movement was an additional factor on the level of structural damage in this area, so the four points in the northeast area of the Mori colony were excluded from the following analysis (see Fig. 7.5).

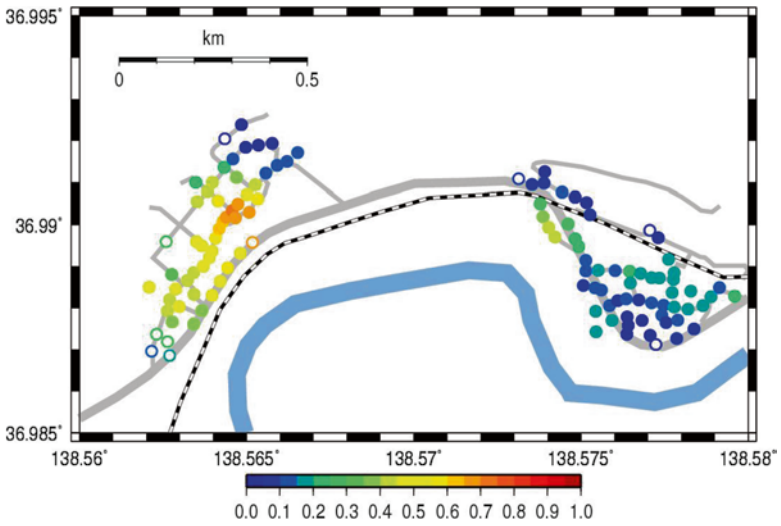

Fig. 7.5 Damage ratio of totally collapsed houses at the ambient noise observation sites in Aokura and Mori colonies. The damage ratio is higher in the center of Aokura colony and northwestern part of Mori colony. The *open circles* show a site with samples <10

7.4.2 Estimation of the Strong Motion Based on Ambient Noise Measurements

The H/V spectrum at a site is computed from the ambient noise record. The H/V spectrum was computed using the following method. First, five segments with 4,096 points (40.96 s) were randomly selected from the 11 min record, and the Fourier amplitude spectrum of each segment was computed. We repeated this selection hundred times, and a set of the five spectra with the smallest variance were selected. The horizontal component is defined as the root mean square of two components. We smoothed the spectra with a smoothing filter, Parzen window at 0.05 Hz. Table 7.1 shows the peak frequency of the H/V spectrum in each colony. Figure 7.6 shows a typical H/V spectrum in the Aokura and Mori colonies, and Fig. 7.7 shows the distribution of the peak amplitude and frequency in the Aokura and Mori colonies. The H/V spectra in the Aokura and Mori colonies are quite different, and the H/V spectrum in the Aokura colony has a larger peak and lower peak frequency.

We estimated the strong motion records at the sites of ambient noise measurement during the mainshock from the H/V spectra and the strong motion recorded in the Mori colony. Because the sites of ambient noise measurement and the strong motion station are only 1.2 km away at the maximum, we assumed that the input ground motion in the seismic bedrock is identical and obtained the estimated ground motion from the following equation:

$$A(\omega) = \frac{A_0(\omega) \times \mathrm{AMP}(\omega)}{\mathrm{AMP}_0(\omega)} \tag{7.2}$$

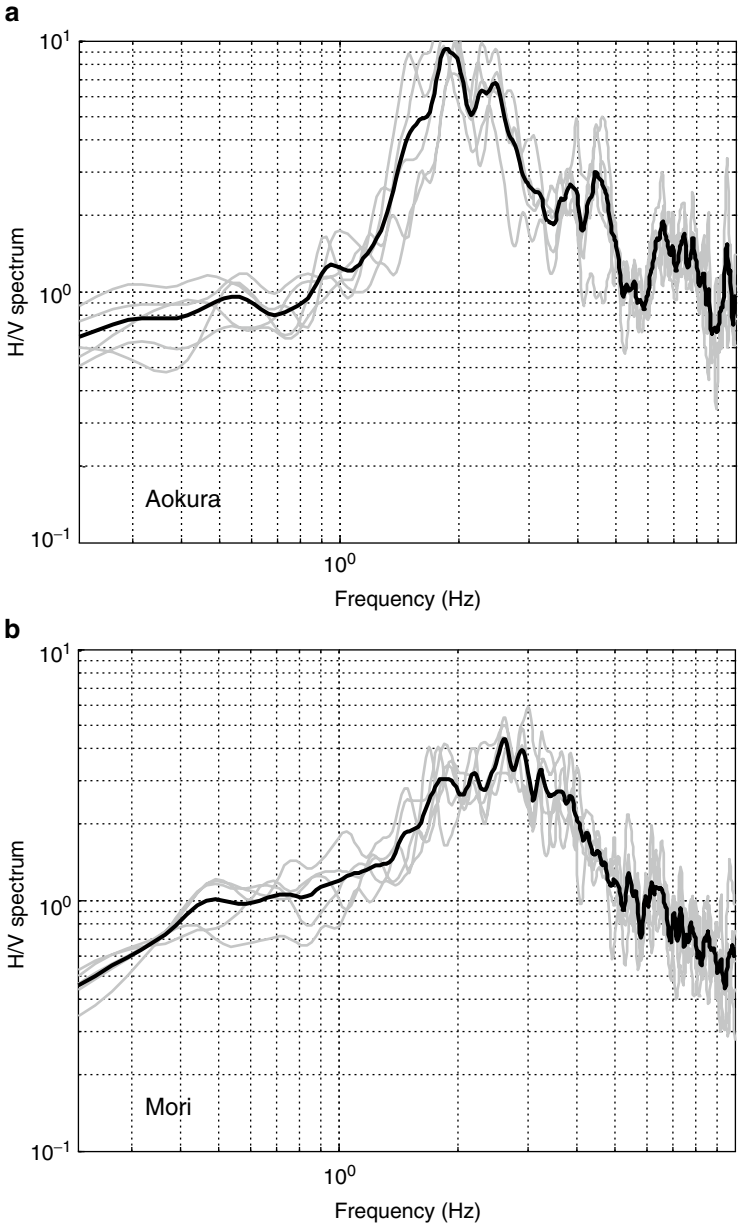

Fig. 7.6 Typical H/V spectra of ambient noise in Aokura (**a**) and Mori (**b**) colonies. The *thin lines* show the spectra of five segments, and the thick line shows the mean spectrum of five segments

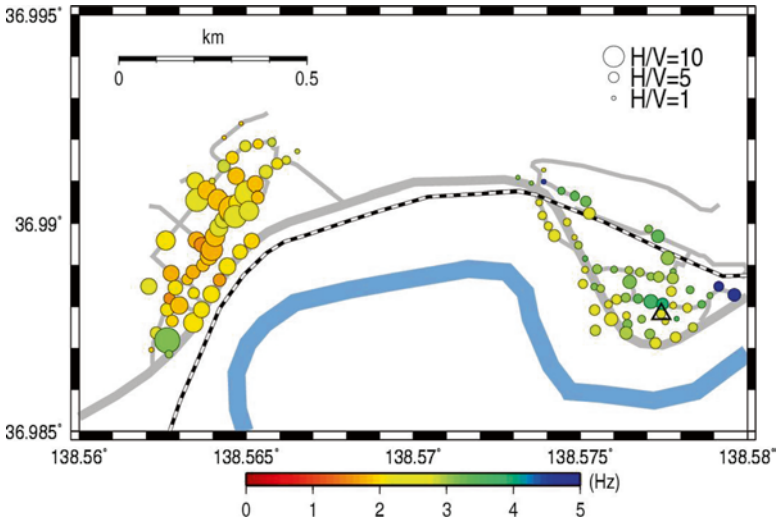

Fig. 7.7 Peak amplitudes and peak frequencies of the H/V spectrum in Aokura and Mori colonies. The size of the *circle* shows the peak amplitude, and the color of the *circle* shows the peak frequency. The *triangle* shows the location of a strong motion station

where $A_0(\omega)$ and $A(\omega)$ are the Fourier amplitude spectra of the acceleration records at the strong motion station and the site of the ambient noise measurement, respectively, and $\mathrm{AMP}_0(\omega)$ and $\mathrm{AMP}(\omega)$ are the site amplification response between seismic bedrock and ground surface at the strong motion station and site of the ambient noise measurement, respectively. That means that the strong motion record during the mainshock is corrected by the ratio of the site amplification response between the strong motion station and site of the ambient noise measurement.

The ratio of the site amplification response between the strong motion station and site of the ambient noise measurement was computed by the method proposed by Nagao et al. (2010). There are still arguments about the theoretical interpretation of the H/V spectrum, but Nagao et al. (2012) explained that ambient noises are composed of a mixture of the surface wave and body wave. Based on their interpretation, this correction scheme assumes that there is a correlation between the amplitude of the H/V spectrum and site amplification. We use the spectrum of the original strong motion data in the long-period component for the correction because the long-period component is sometimes contaminated by the noise of the H/V spectrum. To be more precise, we multiplied by 1 if the period was longer than 2 s, multiplied by the correction coefficient obtained by the approach in Nagao et al. (2010) if the frequency was <1 s, and connected those two ranges by a smooth cosine curve.

The strong motion record of the mainshock at the strong motion station includes the nonlinear effect of the subsurface soil structure. In this correction scheme, the difference in nonlinear effect at each site is not considered, and the same nonlinear effect is assumed for each ambient noise survey point. This assumption may not be true, so it is our future work to evaluate the nonlinear effect. Here, we corrected the

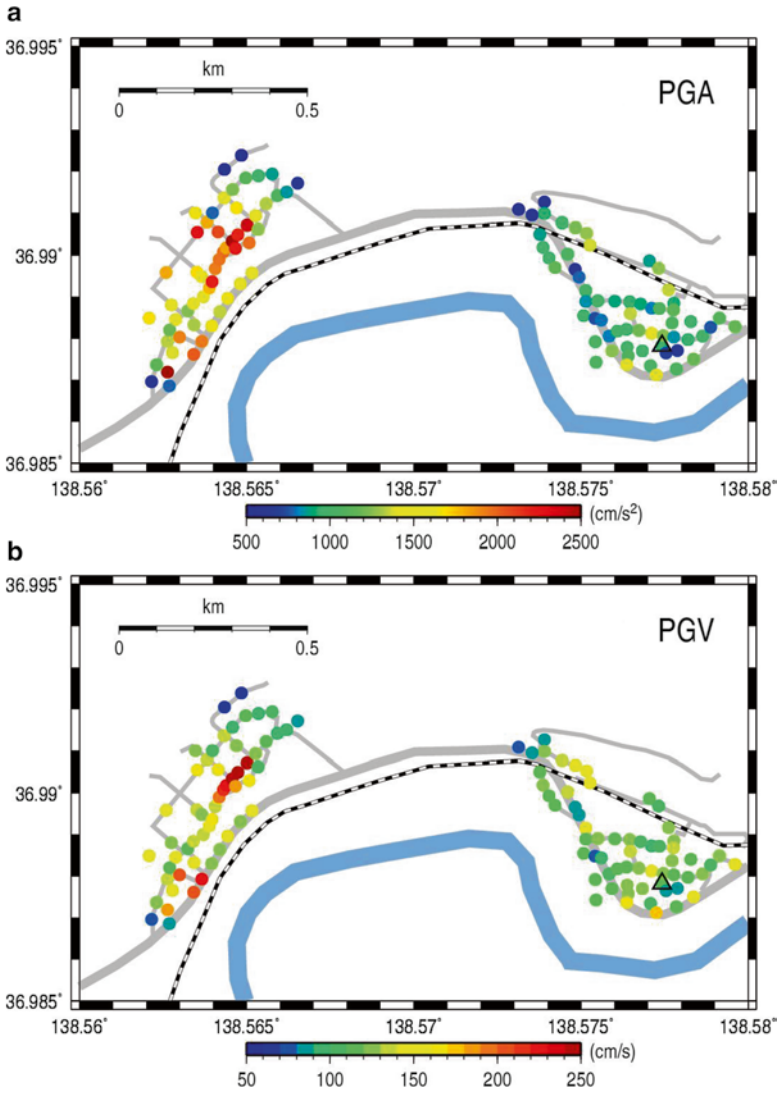

Fig. 7.8 Estimated PGA (**a**) and PGV (**b**) during the mainshock. The *triangle* shows the location of a strong motion station

amplitude of the spectrum only, but did not correct the nonlinearity and phase characteristics.

Figure 7.8 shows the estimated peak ground acceleration (PGA) and PGV at the sites of the ambient noise measurement. In this paper, the largest component of the two horizontal components is used for the PGA and PGV. In the Aokura colony, the center area shows a larger ground motion. This is consistent with the distribution of damaged wooden houses. The ground motion distribution in the Mori colony shows smaller variation than that in the Aokura colony.

7.5 Discussions

In this section, the estimated strong motion during the mainshock and damage ratio in the Aokura and Mori colonies are compared. Figures 7.5 and 7.8 show a similar distribution. For example, the center of the Aokura colony shows a large damage ratio for wooden houses and a large amplitude of estimated ground motion. In order to compare them precisely, in Fig. 7.9 we plotted the relationship between the PGA/PGV and the damage ratio of the wooden houses. The estimated ground motion and damage ratio in the Aokura colonies show a larger variation than those in the Mori colony. This implies that the site condition in the Mori colony has smaller variations, which made the distribution of the damage ratio homogeneous, while the center of the Aokura colony has a large site amplification, which caused severe damage to the wooden houses. Although the damage level of the wooden houses is affected by variation in the seismic performance of each structure, the average of the damage ratio reflects the amplitude of the ground motions. Therefore, the good correlation between the estimated ground motions and damage ratio of the wooden structures implies that the estimated ground motion is substantially reasonable.

The relationship between the damage ratio of the wooden houses and estimated ground motions is regressed as a function of the cumulative Gaussian distribution function, Φ. Because both the damage ratio of the wooden houses and the estimated ground motions include the estimation error, we obtained the regression equation by the orthogonal regression. The most probable regression equations that can explain the dataset are as follows:

$$\mathrm{PGA}: \mathrm{DR}_{\mathrm{D3}} = \Phi\left[\frac{\left(\ln\left(\mathrm{PGA}\right) - 7.276\right)}{0.551}\right] \tag{7.3}$$

$$\mathrm{PGV}: \mathrm{DR}_{\mathrm{D3}} = \Phi\left[\frac{\left(\ln\left(\mathrm{PGV}\right) - 4.978\right)}{0.393}\right] \tag{7.4}$$

$$\mathrm{PGA}: \mathrm{DR}_{\mathrm{D4}} = \Phi\left[\frac{\left(\ln\left(\mathrm{PGA}\right) - 7.491\right)}{0.535}\right] \tag{7.5}$$

$$\mathrm{PGV}: \mathrm{DR}_{\mathrm{D4}} = \Phi\left[\frac{\left(\ln\left(\mathrm{PGV}\right) - 5.133\right)}{0.381}\right] \tag{7.6}$$

The ground motions resulting in a 50 % damage ratio of totally collapsed buildings are 1,792 cm/s^2 for the PGA and 170 cm/s for the PGV. These hazard curves are compared with those obtained from the damage of past major earthquakes (Murao and Yamazaki 2002; Hayashi 2004; Sakai et al. 2006; Yamada et al. 2008). The hazard curves and the samples of the PGVs and damage ratios are shown in Fig. 7.10. The results for the Northern Nagano earthquake show a smaller damage ratio than the 1995 Kobe earthquake, but a slightly larger one than the 2000 western

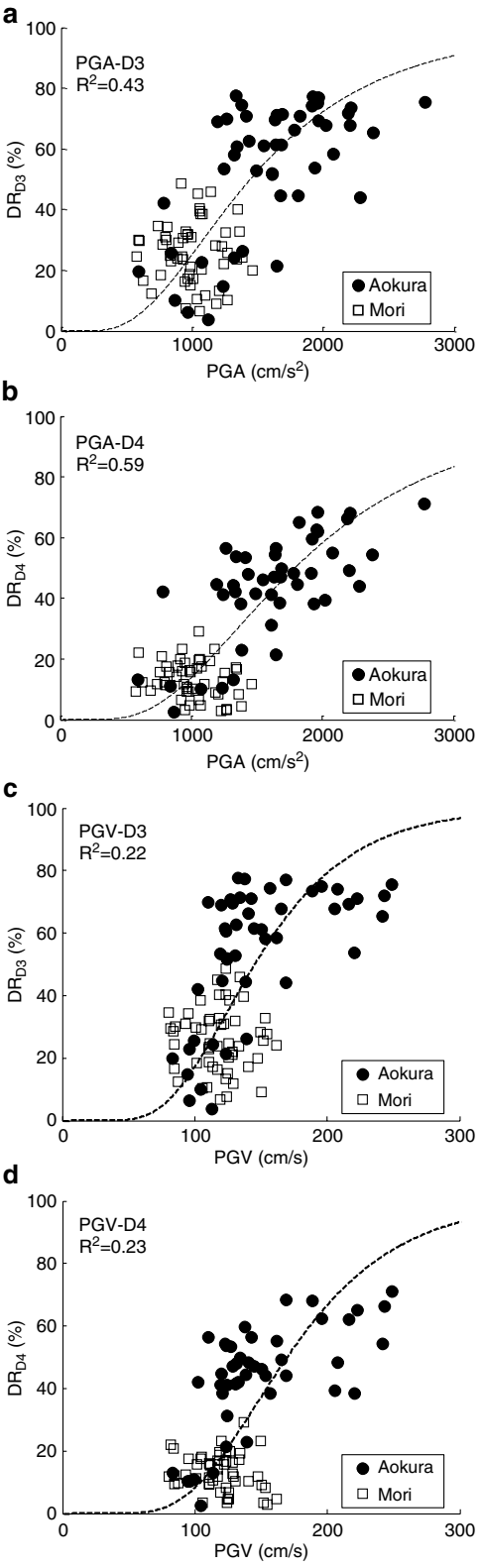

Fig. 7.9 Relationship between the damage ratio of wooden houses (DR_{D3} and DR_{D4}) and estimated PGA/PGV (**a**–**d**). *Solid circles* show the data in Aokura colony, and *open squares* show the data in Mori colony. The *regression curve*, which explains the relationship the best, is also added. R^2 is the coefficient of determination

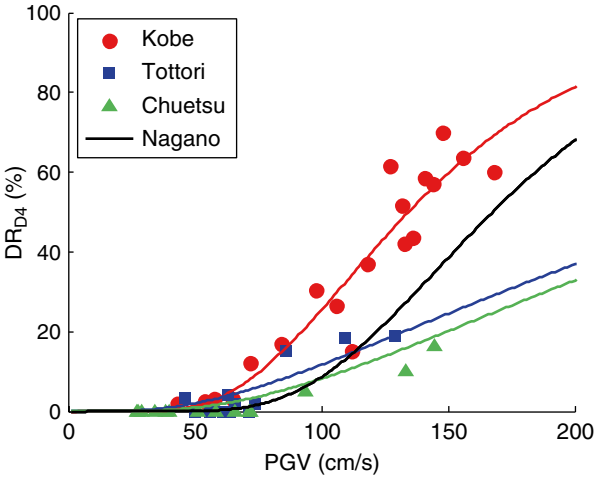

Fig. 7.10 Hazard curves (relationship between the damage ratio of wooden houses and PGV) for the past earthquakes

Tottori and 2004 Niigata-ken Chuetsu earthquakes. Sakae village has very heavy snowfall during winter (more than 3 m high), and the necessity of maintaining the houses to survive that level of snowfall may have resulted in the higher seismic performance. The hazard curve obtained from this research shows that a PGV of 150 cm/s is a threshold for severe damage to wooden houses.

7.6 Conclusions

In this paper, we conducted a damage survey of wooden structures and collected very dense ambient noise measurements in the near-source region of the 2011 Northern Nagano earthquake in central Japan. The percentage of totally collapsed buildings exceeded 30 % in the Aokura and Yokokura colonies of Sakae village, Nagano prefecture. The percentage in the Mori colony, where a strong motion was recorded during the mainshock, was <10 %. We estimated the strong motion in the Aokura and Mori colonies on the basis of the ambient noise measurements and strong motion records. The estimated strong motion distribution reflects the soil conditions and varies within the small area studied. The correlation of the estimated strong motion and damage ratio of the wooden structures is reasonably high, which indicates that the estimated ground motions are realistic. The damage curve obtained from this research shows that the collapse ratio exceeds 50 % at around 150 cm/s of input ground motion.

Acknowledgments We thank Earthquake Research Institute in University of Tokyo for providing the SK-net dataset, Japan Railway for providing the strong motion data recorded at Takatori station during the 1995 Kobe earthquake, and the National Research Institute for Earth Science and Disaster Prevention for providing the K-net and KiK-net dataset. We also acknowledge the town halls in Sakae village, Nagano prefecture, and Tsunan town, Niigata prefecture, for providing the damage data. Dr. Toshiyuki Kagawa also helped us with the damage survey. We used the Generic Mapping Tools (Wessel and Smith 1998) for mapping.

References

Arai H, Morii T, Yamada M, Shimizu H, Hayashi Y (2008) Peak ground velocity and cause of damage to wooden houses estimated in near-source area during the 2007 Noto Hanto Earthquake. J Struct Construct Eng (Trans Architectural Inst Japan) 624:227–234 (in Japanese)

Boore D (2001) Effect of baseline corrections on displacements and response spectra for several recordings of the 1999 Chi-Chi, Taiwan, earthquake. Bull Seismological Soc Am 91:1199–1211

Earthquake Research Institute (2000) SK-net. University of Tokyo. http://www.sknet.eri.u-tokyo.ac.jp/ (in Japanese)

Hayashi Y (2004) Analysis of relationship between damage ratio of wooden houses and construction years—based on damage during Hyogo-ken nanbu earthquake and western Tottori prefecture earthquake. J Archit Building Sci 119:71–75 (in Japanese)

Japan Meteorological Agency (2011) The preliminary determination of epicenters (PDE) bulletin. http://www.seisvol.kishou.go.jp/eq/mech/ini/mc201103.html (in Japanese)

Murao O, Yamazaki F (2002) Building fragility curves for the 1995 Hyogoken-Nanbu Earthquake based on CPU and AIJ'S survey results with detailed inventory. J Struct Construct Eng (Trans Architectural Inst Japan) 555:185–192 (in Japanese)

Nagao T, Yamada M, Nozu A (2010) A study on the empirical evaluation method of site amplification effects by use of microtremor H/V spectrum. J Struct Eng A 56A, CD-ROM

Nagao T, Yamada M, Nozu A (2012) A study on the interpretation of wave components in microtremor H/V spectrum. J Jpn Soc Civil Eng 68–1:48–62

Okada S, Takai N (1999) Classifications of structural types and damage patterns of buildings for earthquake field investigation. J Struct Construct Eng (Trans Architectural Inst Japan) 524:65–72 (in Japanese)

Sakai Y, Nakamura Y, Otsuki T, Kosugi S (2006) Correspondence of strong ground motions occurred in the 2004 Niigata-Chuetsu earthquake with damage to buildings. J Struct Construct Eng (Trans Architectural Inst Japan) 601:69–73 (in Japanese)

Wessel P, Smith W (1998) New, improved version of generic mapping tools released. Eos Trans 79:579–579

Yamada M, Park S, Mori J (2008) The 2007 Noto Peninsula, Japan Earthquake(Mw6.7): damage to wooden structures. Seismologic Res Lett 79–1:20–24

Chapter 8
Landslides in Urban Residential Slopes Induced by the 2011 Off the Pacific Coast of Tohoku Earthquake

Toshitaka Kamai, Hidemasa Ohta, Yasunori Ban, and Hidehiko Murao

Abstract The preliminary report on landslides in residential areas induced by the 2011 off the Pacific Coast of Tohoku earthquake (M9.0) was conducted. Many urban landslides occurred in gentle residential slopes constructed as artificial valley fills (embankments) during this earthquake, particularly in Sendai, Shiroishi, Fukushima, Iwaki, and Tokai, from southern Tohoku to northern Kanto province. The landslides are mainly described based on the field investigations and are classified into five types. Some of the landslides that initiated in 2011 overlap with landslides induced by the earthquake in 1978. The repeated landslides at the same sites indicate that recent urban development and planning did not learn from the past disasters. Although countermeasures were constructed for landslides induced by the 1978 earthquake, serious landslides were found in same place in 2011. The disasters in 2011 have far-reaching ramifications for urban planning in Japan. We need a new design concept for urban development to minimize artificial geomorphological changes. The conceptual model of a "Counter line city" should both minimize risk of disasters and create a favorable natural environment in new urban regions along the Tohoku coast.

Keywords Artificial fill • Landslides • Residential slope • The 2011 off the Pacific coast of Tohoku Earthquake

T. Kamai (✉) • Y. Ban
Disaster Prevention Research Institute (DPRI), Kyoto University, Kyoto, Japan
e-mail: kamai.toshitaka.3z@kyoto-u.ac.jp

H. Ohta
Ohta Geo-Research Co., Ltd., Nishinomiya, Japan

H. Murao
Murao Chiken Co., Ltd., Toyama, Japan

H. Kawase (ed.), *Studies on the 2011 Off the Pacific Coast of Tohoku Earthquake*,
Natural Disaster Science and Mitigation Engineering: DPRI reports,
DOI 10.1007/978-4-431-54418-0_8,

8.1 Introduction

The 2011 off the Pacific coast of Tohoku earthquake (Mw9.0; Depth, 24 km; PGA, 2,933 gal) on 11 March struck Pacific coast of east Japan in the region of Iwate, Miyagi, Fukushima, and Ibaraki prefectures. This region has experienced many great earthquakes with magnitudes ≥8 as well as numerous major earthquakes with magnitudes ≥7. The recurrence interval of the great earthquakes is several hundred years and is caused by the subduction of the Pacific Plate under the Eurasian Plate. The most recent earthquake of this type ($M \geq 8$) occurred in 1933 with magnitude 8.3 (Sanriku Offshore Earthquake of 1933). Although serious tsunami disasters were caused by the large energy releases during these earthquakes, damage due to ground shaking in the urban regions has generally been low because of their distance from the hypocenters and the less densely populated urban areas in Tohoku province prior to the era of rapid economic growth.

However, the events in 2011 followed similar patterns of damage, except for more serious impacts in urban regions compared to those experienced during past great earthquakes in eastern Japan. The difference in the level of damage in urban regions was attributed to urban expansion of Sendai City and its surrounding communities after World War II and subsequent changes in the living environments.

In the shadow of the serious damage caused by tsunami waves, more than 200 residential lots in Sendai City were damaged. Among these, at least 50 residential lots were damaged by landslides in the urban residential region, and several hundred houses were destroyed by the landslides. This preliminary report mainly describes the basic characteristics of these landslides in urban residential regions caused by the 2011 earthquake, i.e., the distributions, classification, results of prediction methods, and effects of counter measures.

8.2 Landslides in Urban Region Induced by the 2011 Earthquake

8.2.1 Distribution of Landslides

Fifty urban landslide sites induced by the 2011 earthquake in eastern Japan were inspected (Figs. 8.1 and 8.2). These landslides were distributed from the southern Tohoku Province to Tokai village, the Pacific coast side of the northern Kanto region; however, landslides were concentrated in the suburbs of Sendai City, the largest city in the Tohoku province.

While long recurrence interval great earthquakes ($M \geq 8$) have been located off of the eastern coast of Japan, the smaller major earthquakes with $M \geq 7$ have struck much closer to the mainland with increased frequency and caused far more severe damage in these urban regions. Especially, the disaster caused by the 1978 Miyagi Prefecture Offshore Earthquake is the first case when a modern large city with satellite communities was affected by a major earthquake. Even after the 1978 Miyagi

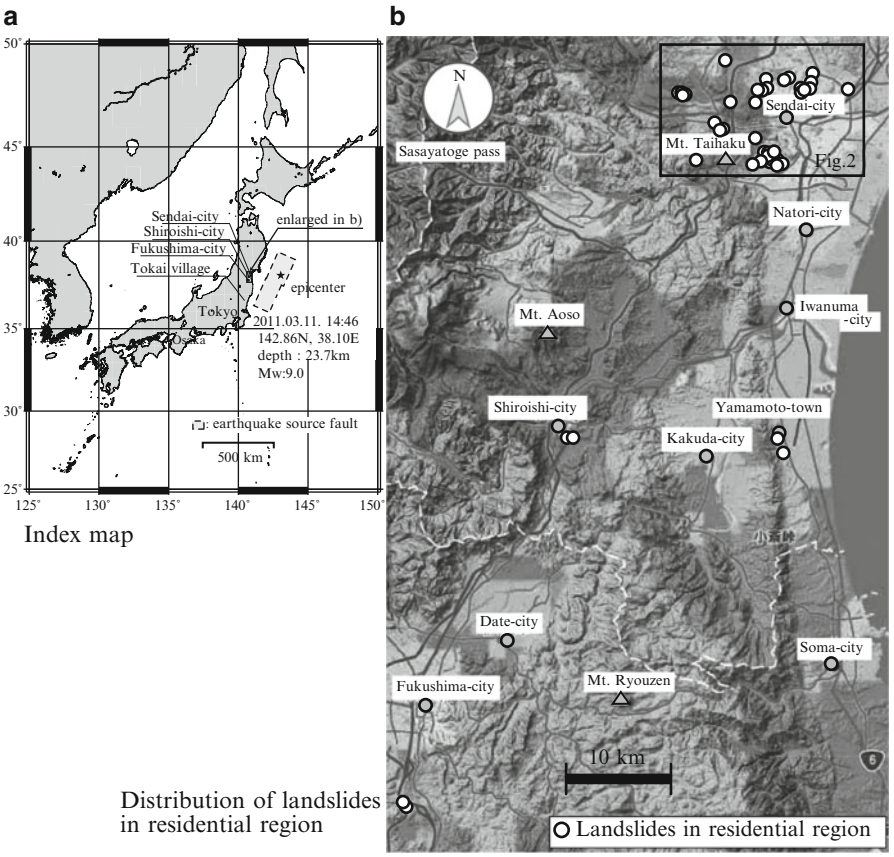

Fig. 8.1 Distribution of landslides in urban residential region of southern Tohoku province. (**a**) Index Map, (**b**) distribution of landslides in residential region

Prefecture Offshore Earthquake, the urban region of Sendai City has expanded to hillsides with population growth, especially during the bubble economy in Japan (1985–1995). In contrast, in other smaller cities, the lesser population growth precluded the need for extensive fill construction for residential lots. Thus, the population dynamics and the process of urban development in the Tohoku province during this half century are reflected in the distribution of urban landslides induced by the 2011 earthquake.

8.2.2 Types of Landslides

Features of ground surface deformation (i.e., cracks, subsidence, uplifting, and sand boiling) are important evidence to understand the state of landslide movements. These ground surface deformations appeared in conjunction with differences in thickness of fill, age of filling that affects the quality of fills, groundwater level, and

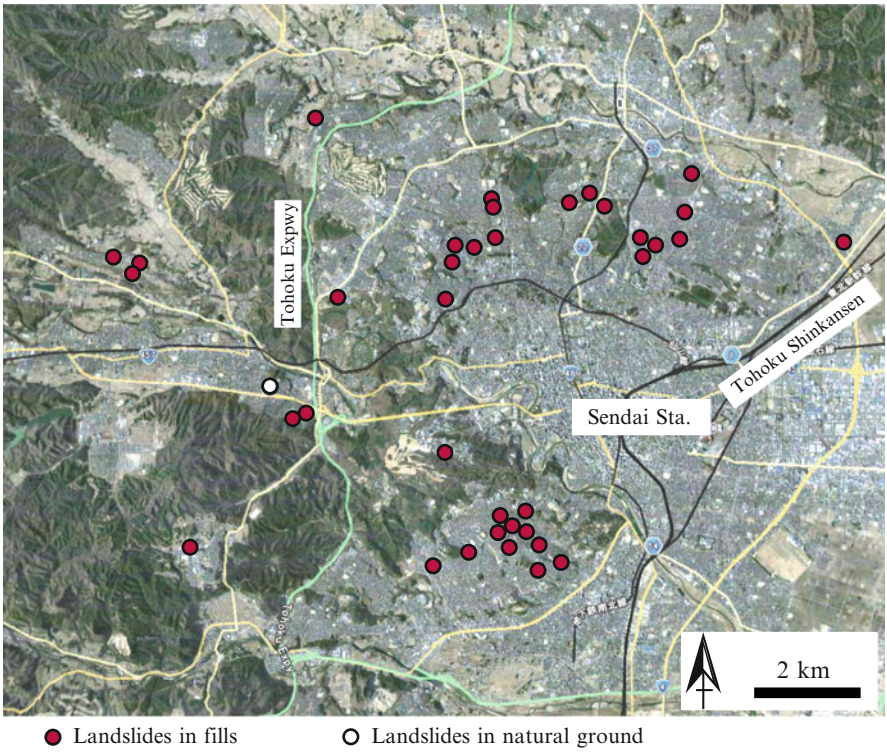

Fig. 8.2 Distribution of landslides in Sendai urban region

existence or nonexistence of landslide prevention works. Thus, the following five types of landslides in urban residential fills caused by the 2011 earthquake were recognized at this time:

Type 1 "Valley-fill type landslide"
Type 2 "Widening-fill type landslide"
Type 3 "Failure and deformation in steep sloping fill"
Type 4 "Complex type of valley-fill type landslide and failure in steep sloping fill"
Type 5 "Surficial landslide"

Figure 8.3 shows slope movement classification of fill slopes from Type 1–5, with "thickness of movement mass" on the *x*-axis and "position of slip surface" on the *y*-axis.

Among the fifty investigated sites, at least seven sites (about 20 %) are known to have been damaged by the 1978 the Miyagi Prefecture Offshore Earthquake, indicating that the remediation of slope stability of fills was not adequate even after the 1978 earthquake. Landslides also occurred at relatively new developed housing lots that were constructed after 1990. Landsliding of fills constructed after the 1980s was rare during past earthquake disasters; thus, urban landslides in newly developed housing lots are one of the characteristic damages associated with the 2011 earthquake.

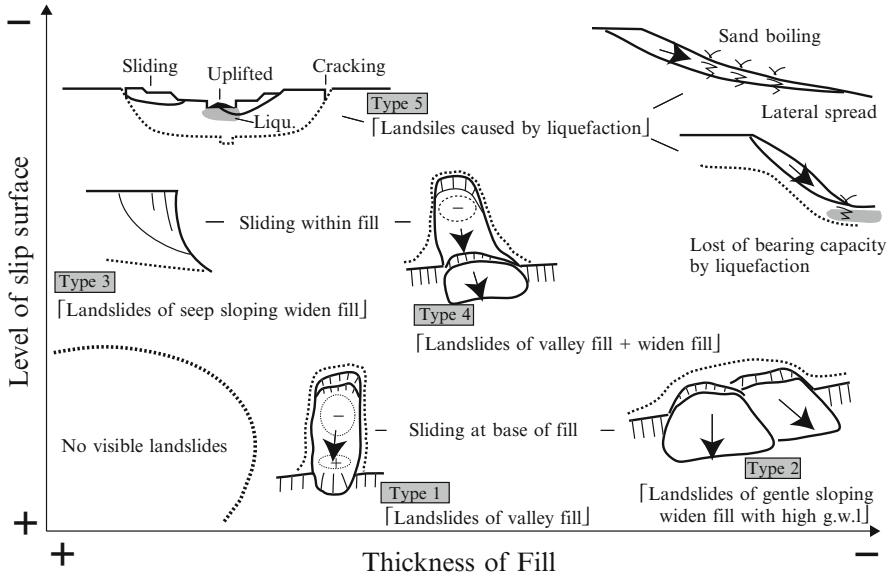

Fig. 8.3 Types of landslides in urban region caused by the 2011 Tohoku earthquake

Type 3 landslides were common in relatively new developed housing lots during the 2011 earthquake, while Type 1 and 2 landslides were mainly distributed in areas developed before 1970. Thus, it appears that ground conditions conducive to sliding existed at the bottom of older fills and these helped generate Type 1 and 2 landslides.

8.3 Typical Landslides in 2011

8.3.1 Valley-Fill-Type Landslides (Type 1)

Typical valley-fill-type landslides occurred in Oritate 5-chome (Oritate #5) of Sendai City. The development of the Oritate residential area started from 1972 by Miyagi Prefecture office. While other housing lots were affected by serious landslide disasters during the 1978 earthquake, Oritate did not suffer damage in 1978.

Figure 8.4 shows plan view of Oritate #5 indicating the distribution of ground cracks and landsliding area. Based on topographic maps and air photos before 1972, it was clear that the landslides in Oritate #5 developed along the valley that existed prior to construction of the fills. Distribution and characteristics of cracks revealed the pattern of movement caused by the landslide. Vertical displacement at the head of the landslide is small as the size of the landslide; however, major tension cracks with continual opening displacement developed along the head. As a sum of horizontal displacement of tension cracks, severe compressive deformation appeared at the toe of the landslide (Fig. 8.5).

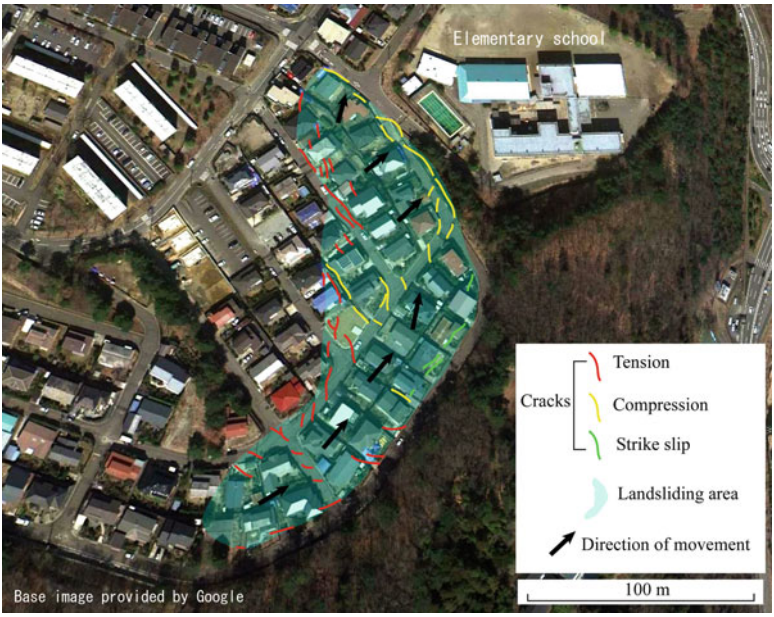

Fig. 8.4 Plan view of the landslide of the Oritate #5 subdivision

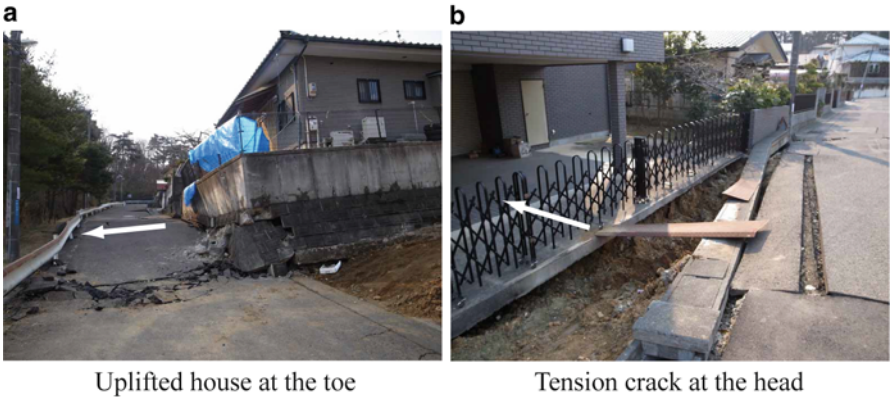

Fig. 8.5 Ground deformation induced by the Oritate #5 landslide. (**a**) Uplifted house at the toe, (**b**) tension crack at the head

The thickness of fills checked by Swedish weight sounding tests (SWS) and boring core sampling (conducted by Sendai City office) was 9–11 m at middle part of the landslide. The slip surface is supposed at the bottom of the fill. The bedrock of this area consists of highly weathered Tertiary tuff and mudstone which is weak as consolidated clay. Therefore the contrast of strength indicated by SWS values between the bottom of the fill material and original ground surface is not clear. Observations at bore holes revealed that the groundwater level was very high, and discharged water at

the toe of the landslide continued until 6 months after the 2011 earthquake. Such evidence suggests that abundant groundwater existed in the fill of the landslide during the 2011 earthquake; however, no groundwater was found in the SWS borings that were opened in January 2012, 10 months after the earthquake. Thus the shape and pattern of surface deformation of the Oritate #5 landslide looks like a typical simple valley-fill landslide, in spite of the complicated groundwater storage.

8.3.2 Landslides in Widening Fills (Type 2)

Widening fills represent embankments constructed to increase the extent flatland by cutting terraces and creating artificial ground surfaces. The bottom portion of widening fill has a steeper angle compared to valley fills under normal conditions.

The Midorigaoka District is an older subdivision that was constructed in a staircase fashion located in the southern part of Sendai City. This area is underlain by Pleistocene volcanic ash deposits (loam textured soils), Pleistocene marine terrace deposits and Pliocene sandstone and mudstone are the basement rocks. The grading operations consisted of balanced cuts and fills. The Midorigaoka 4-chome (Midorigaoka #4) subdivision sprawled across the flatland stretching between the terrace and valley floor. Based on comparisons of previous topographic maps, the development of the Midorigaoka #4 residential area started in 1968 by a private developer in Tokyo. The foundation ground of the upper part of the Midorigaoka #4 is cut; however, the lower part is typically widening fills. The large landslides occurred in the widening fills.

Figure 8.6 shows the plan view of the Midorigaoka #4 landslide. Tension cracks were aligned along elevation counters at the boundary between the cut and fill. Compressive deformation (e.g., compression cracks, uplifting, and deformation of retaining walls) appeared at the foot of the fill slope on the alluvial valley floor (Fig. 8.7). After the 2011 earthquake, three boring cores were taken in the central part of the landslide by DPRI, Kyoto University. Figure 8.8 shows the geologic column with *N*-values of Standard Penetration Tests (SPT). The fill was loose and very soft with *N*-values from 0 to 4. Some positions of *N*-values >5 in the columnar sections indicate the existence of large blocks of bedrock. The bedrock consists of Tertiary sedimentary rocks (i.e., pumice tuff, sandstone, and siltstone) and contains intercalated thin lignite beds. The bedrock is hard with *N*-values ranging from 40 to >50 except for the lignite beds.

The fills consist of mixed bedrock material, sand, clay, and sandy silt with gravel. The humid topsoil of original ground surface was found at the boundary of the fill and bedrock. The groundwater level was very shallow—0.5–1.1 m below the ground surface—indicating that the fills were nearly saturated by groundwater. The contrast in strength between the fill and bedrock is clear, and soft topsoils exist at the boundary. Thus, the landslide is thought to move along the bottom of the fill. Observations of landslide movements, pore water pressure changes, and seismic response of fills were conducted in this landslide.

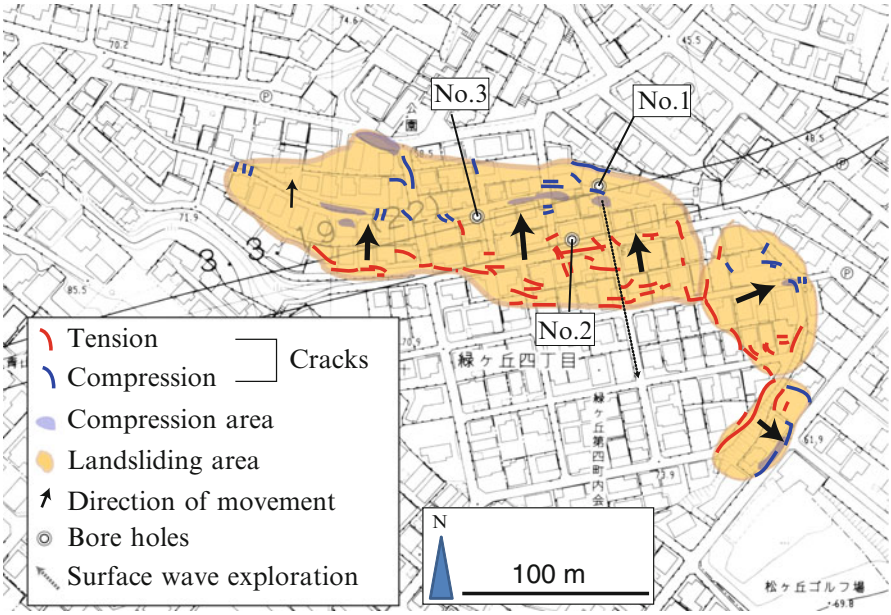

Fig. 8.6 Plan view of the landslide of the Midorigaoka #4 subdivision

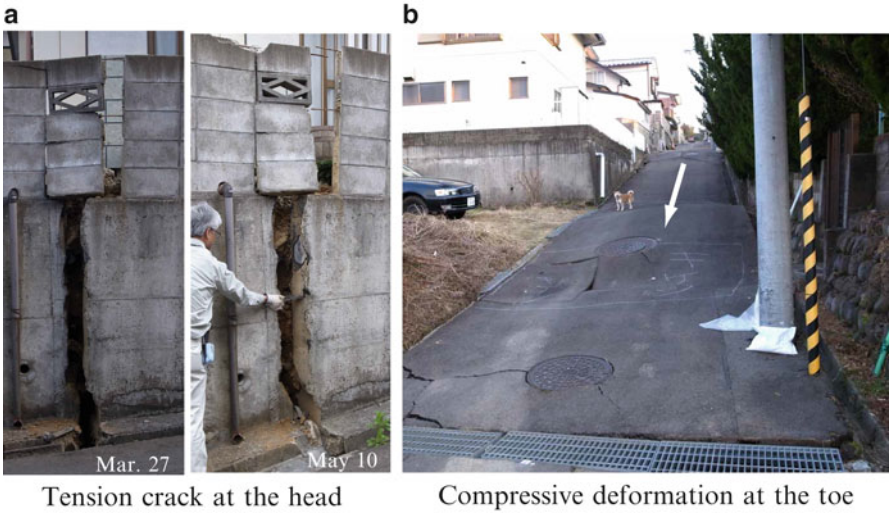

Fig. 8.7 Ground deformation induced by the Midorigaoka #4 landslide. (**a**) Tension crack at the head, (**b**) compressive deformation at the toe

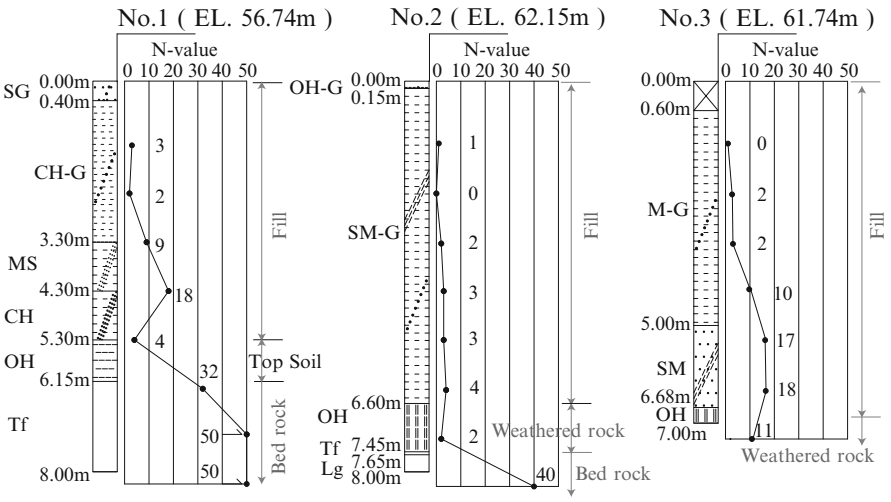

Fig. 8.8 Columnar section of bore holes in the Midorigaoka #4 landslide

8.3.3 Failure and Deformation in Steep Sloping Fill (Type 3)

When the front slope of widening fills was steepened, residential lots were considered to be at risk for slope failures in fills. Slope failures on the steep sloping fills located around the outer edge of the residential lot increased in association with resent urban development trends outside of the city.

Where development occurred in regions of higher elevation relative to the river (e.g., higher river terrace, hillside, and volcanic plateau), steep sloping fills commonly appear at the margin of the developed region. Recent technical progress on slope conservation works (e.g., new styles of retaining walls, reinforced soil walls, and ground anchors) has supported the construction of the steep gradient fills. Takanohara in the western part of Sendai is a typical residential development in an upland region constructed from the 1990s by a private developer.

Takanohara is a new housing project located on flatlands of the higher terrace of the Hirose River. Figure 8.9 shows a plan view of the northern slope of Takanohara. Tension cracks with vertical displacement of tens of cm were found at the upper boundary of fill along the outer edge of the housing project. The horizontal boundary between fills and cutting area was undulated at the edge of the residential area. In other words, the thickness of fills should be irregular at the edge of developed region. Several small deformations (landslides) were found where the boundary curved toward the inside of the residential development. Thus, small, steep valley fills were formed at the edge, and the mass of fills moved as landslides. Fortunately, the groundwater level was below the slip surface, so the slope did not collapse; landslides were mostly induced by the strong acceleration (force) of the earthquake on 11 March.

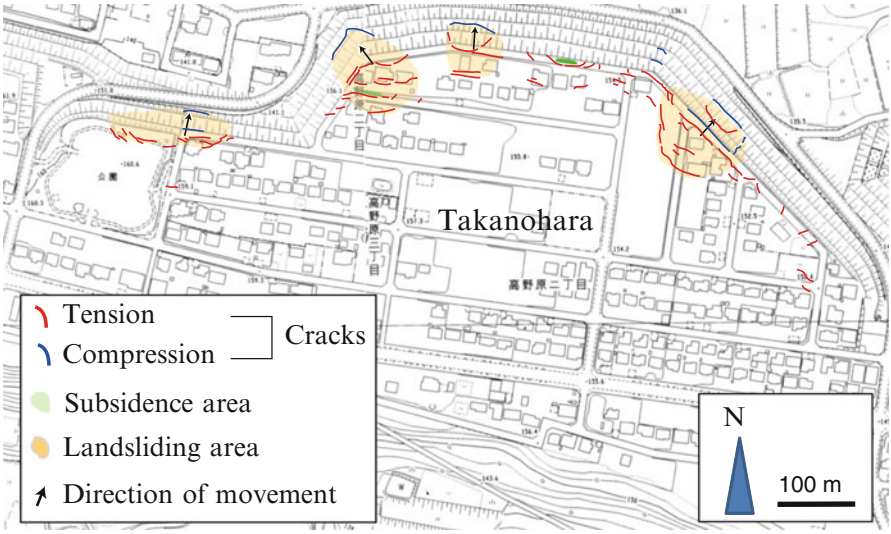

Fig. 8.9 Plan view of the landslides in the Takanohara housing lot

8.3.4 Complex Type of Valley-Fill Landslides and Failures in Steep Sloping Fills (Type 4)

Steep sloping fills were often constructed near the outlet slope (end of downstream) of large-scale valley fills. Serious damage to residential lots occurred by collapse of steep sloping fills and spreading of deformation in valley fills.

The Asahidai landslide in Fukushima City is a representative case of the complex of Type 1 and Type 3 failures. Part of collapse, 60 m wide, 80 m long, and 5–10 m thick, blocked the National Route #4 for one day on 11 March (Fig. 8.10). This highway is an important route between Tokyo and Tohoku. Groundwater existed in the collapsed fill, and its level was estimated about 4 m below the ground surface. Vertical displacement was up to 10 m at the head scarp of the collapsed fill, and the deformation of ground (e.g., cracks and subsidence) was traced along the valley fill (100 m long; 80 m wide) from the head scarp of collapsed part to inside of the residential area (Fig. 8.11). Such evidence indicates that the steep sloping fill and valley fill in the Asahidai division were interlocked during the 11 March movement.

The Asahidai subdivision was developed up until 1974 during the period when Fukushima City sprawled toward the southern suburbs. There was no obvious damage in the other massive residential developments of similar age in this region during the March earthquake. Therefore, the landslide in the Asahidai subdivision was unique and raised serious issues in the community.

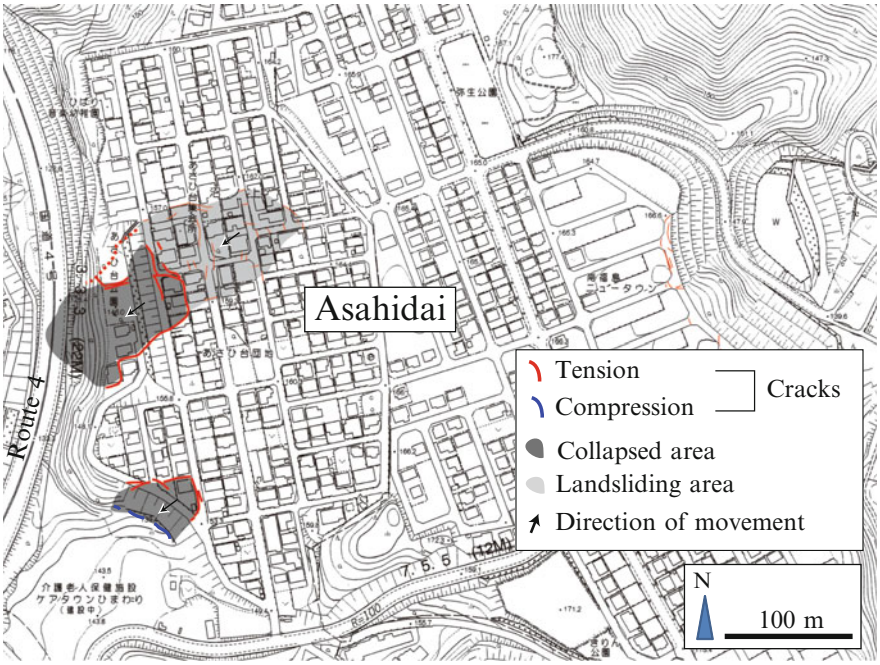

Fig. 8.10 Plan view of the landslides in the Asahidai housing lot

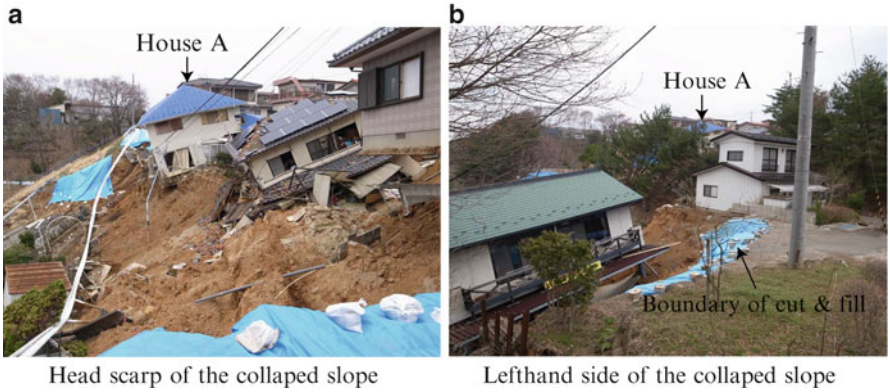

Fig. 8.11 Ground deformation induced by the landslide of Asahidai housing lot. (**a**) Head scarp of the collapsed slope, (**b**) left-hand side of the collapsed slope

8.3.5 *Surficial Deformation and Sliding Caused by Liquefaction (Type 5)*

Shallow landslides of fills (i.e., relatively small scale) can be classified into two types: (1) landslides in steep sloping fills (Type 3) and (2) landslide related to liquefaction (Type 5). Elevated groundwater levels are a significant factor related to Type 5 landslide movement (Hamada 2001).

Figure 8.12 shows distribution of surface deformation in the Nankodai District. The Nankodai District was developed in the late 1960s. Like the Midorigaoka District, the grading involved massive balanced cuts and fills. Ponds and reservoirs that once existed at the bottoms of valleys were filled. Fills in this area are relatively thick (up to 20 m) compared to the Midorigaoka District. Due to differential settlement, cracks and sites of ground subsidence developed along the cut and fill transition zones causing serious damage to houses; several small landslide blocks developed in the fills of the branch valleys. These small landslide blocks represent gently sloping mass movements caused by liquefaction. Compressive deformation causing upheaval associated with boiling sand was especially pronounced in this type of landslide.

Damages to lifelines by cracks that developed along the boundary between the region of cuts and fills were caused by the Miyagi Prefecture Offshore Earthquake in 1978. However, there were no incidences of landslides by liquefaction during this 1978 event as observed on March 11, 2011. The main shock of the earthquake on March 11, 2011, was obviously larger than the earthquake in 1978 but also the strong shaking in 2011 continued for more than 3 min at Sendai. This long-term strong oscillation likely caused ground liquefaction.

8.4 Discussion

8.4.1 *Brief History of Landslide Disasters in Urban Regions: Background of the 2011 Disaster*

Throughout Japan, large-scale residential development on hillsides accompanied by massive grading operations in the suburbs of large cities started in the 1960s. According to Tamura (1977), the evaluation of whether the expansion of residential areas into hillsides was an environmentally sound choice was not adequately addressed. The concept of a flat residential lot, which prevailed during the last 2,000 years in Japan, was maintained. Thus, residential development into the hillsides consisted of massive grading to create flatland. To accomplish this objective, the process included the removal of hilltops and filling in valleys. Such massive grading operations often resulted in inadequate compaction of fill materials creating soft and weak ground. This type of practice resulted in dangerously soft and weak ground within cities throughout Japan. In recent years, a significant number of cases

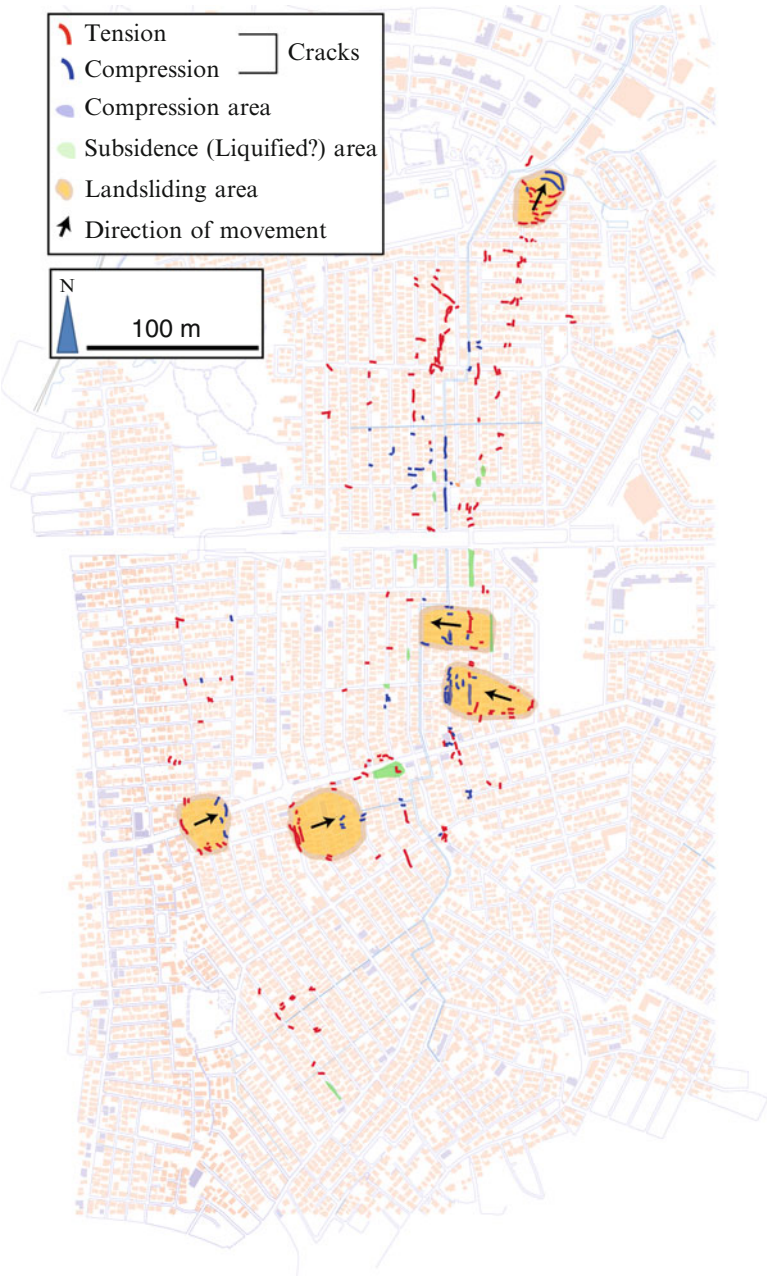

Fig. 8.12 Distribution of ground deformation in the Nankodai housing lot

of valley-fill failures and fill slope failures have been reported during large earthquakes which centered in large cities (Kamai and Shuzui 2002). One of the first landslides resulting in a valley-fill failure was recognized in a suburb of Sendai City

during the Miyagi Prefecture Offshore Earthquake of 1978 (Institute of Geology and Paleontology, Tohoku University 1979). This trend followed with the Kushiro Offshore Earthquake of 1993 and the Southern Hyogo Prefecture Earthquake of 1995 (Kamai 1995). These failures include (1) failures of most or all of the valley fill, (2) lateral spreading associated with liquefaction, and (3) development of cracks along the cut and fill transition zones (Tamura et al. 1978; Kamai et al. 2000a; Kamai et al. 2004). These disasters revealed that (1) many sites within cities were created that have a very high potential for failure and (2) there is a good possibility that such sites will increase in number. Thus, similar disasters could be repeated if large earthquakes occur near large cities. This is a universal phenomenon associated with large-scale disasters that can also be observed overseas; Ku-Lin-Ton and Chiuan-Chia-Fu during the Chi-Chi Earthquake in Taiwan are some such examples (Kamai et al. 2000b).

8.4.2 Lesson Learned from the Past Earthquake Disaster in 1978

The magnitude 7.4 earthquake with an epicenter off the shore of Miyagi Prefecture, northeastern Japan, struck on June 12, 1978, and caused widespread damage to Sendai City and surrounding cities and communities. Damages included 28 deaths, 11,028 injuries, and 179,255 damaged structures. Although the overall damage was mild, there were a few notable exceptions: (1) damage to the lifelines, (2) fill and cut slope failures, and (3) failure of masonry walls. The first two damage types have been repeated in all of the earthquakes affecting urban areas in Japan. This illustrates the unique nature of the Miyagi Prefecture Offshore Earthquake in 1978.

Landslides in cut and fill slopes during the 1978 earthquake occurred largely in the Midorigaoka and Nankodai Districts of Sendai City and the Kotobukiyama #4 Subdivision in Shiroishi City. These areas almost overlap with the sites of landslides in 2011. Figure 8.13 shows the distribution of landslides in Midorigaoka District in 2011. In this region, landslides in 1978 were recorded in Midorigaoka #1, #2, #3, and #4 (Institute of Geology and Paleontology, Tohoku University 1979). Among these areas, only the Midorigaoka #1 area was immune to landslide damage in 2011. In Midorigaoka #4, deformations of ground in 2011, distribution of cracks, areas of subsidence, and uplifting areas experienced almost the same positions and patterns as in the 1978 earthquake. Thus, these landslides should have been expected and preventable if appropriate responses were made after the earthquake in 1978.

8.4.3 Verification on Countermeasures for Landslides

In spite of countermeasures constructed for landslides induced by the 1978 earthquake, serious damages by landslides were found in Midorigaoka #3 of Sendai City and Midorigaoka #1 of Shiroishi City in 2011. Many countermeasures against

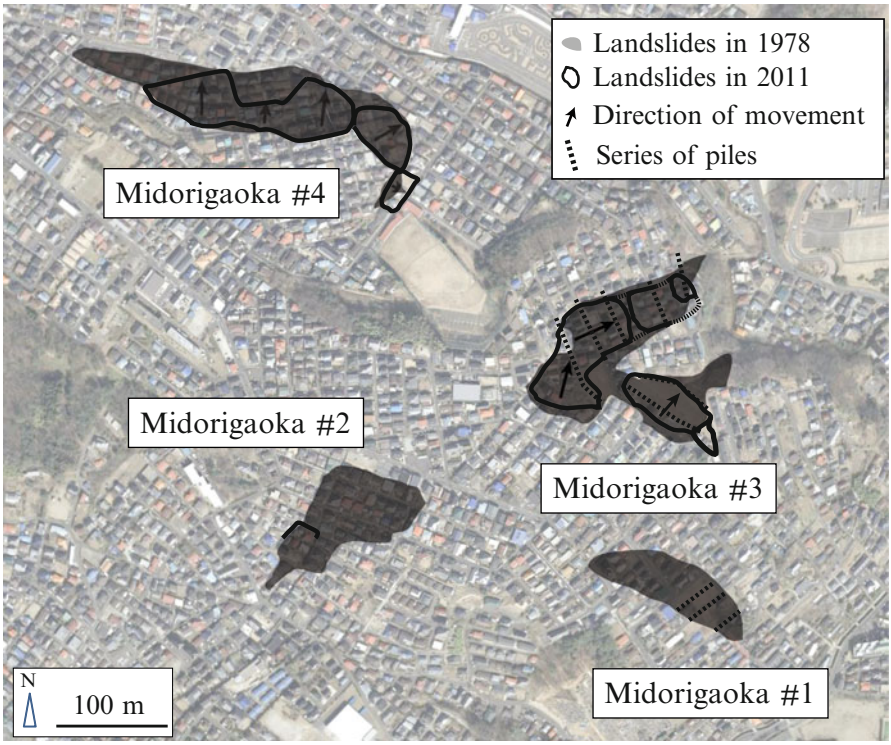

Fig. 8.13 Distribution of landslides in the Midorigaoka area

landslides on natural slopes have been implemented based on the Landslides Controlling Act of Japan; however, countermeasures intended for landslides in residential fills were only made after the 1978 earthquake in the Midorigaoka region of Sendai and Shiroishi City by the Miyagi Prefecture Office. Therefore, the 2011 earthquake provides the first opportunity to verify the effects of countermeasures for landslides in residential fills.

As shown in Fig. 8.14, about twenty houses were damaged, and ten houses were destroyed in the Midorigaoka #3 of Sendai City. Cross sections of the 1978 landslides are compared with the 2011 landslides (Fig. 8.15). In 1978, the sliding surface in Midorigaoka #3 was along the bottom of the fill. To protect against further displacement along this slip surface, the countermeasures were constructed—five series of steel piles (about 30 cm in diameter each) and several drainage wells with horizontal drainage borings. In 2011, several small surficial landslides developed between the series of piles constructed in 1978. The heads of these landslides (i.e., the tension zone) were formed at the downslope side of the piles, and the compressive deformation occurred at the toe of the landslides on the upslope side of the piles. Thus, these countermeasures prevented the total collapse of the fills; however, the countermeasures did not entirely prevent ground deformation near the housing lots in Midorigaoka #3 that was induced by surficial landslides from.

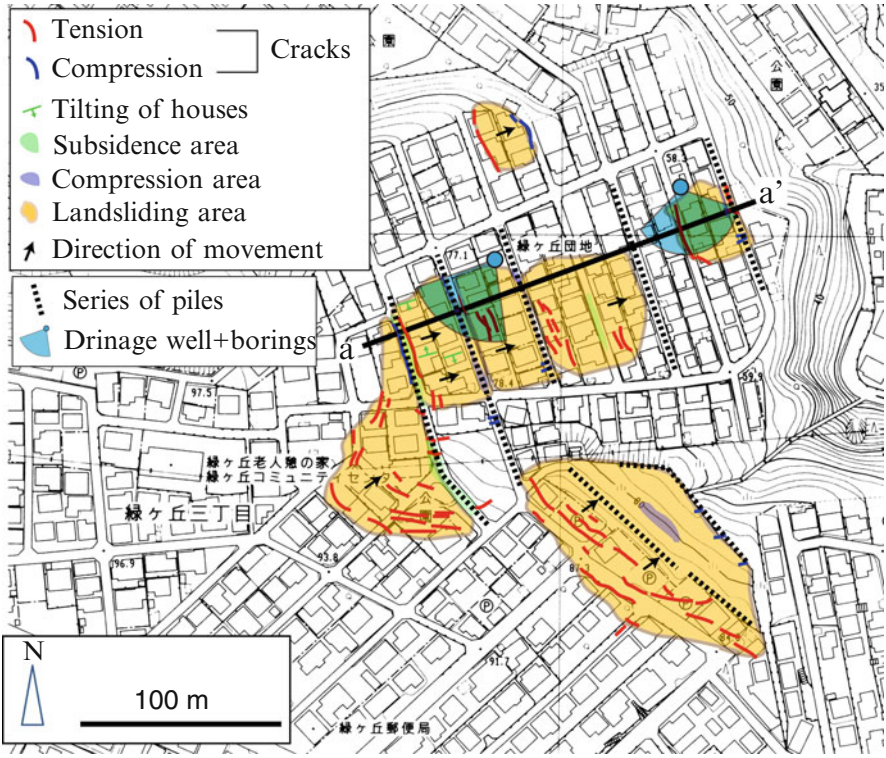

Fig. 8.14 Ground deformation in 2011 and the previous prevention works in the landslide of Midorigaoka #3 subdivision

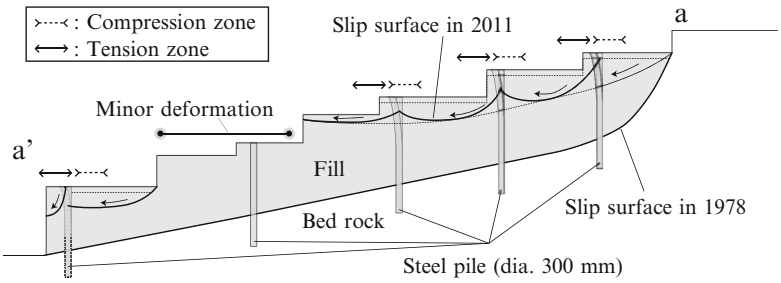

Fig. 8.15 Thematic cross section of the Midorigaoka #3 landslide in Sendai City

Limitations of countermeasures for landslide control in urban residential fills were evident in another case in 2011. The Midorigaoka #1 (called "the Kotobukiyama #4" in 1978) of Shiroishi City is located about 40 km south southwest of Sendai City and was developed between 1972 and 1975. During the 1978 Miyagi Prefecture

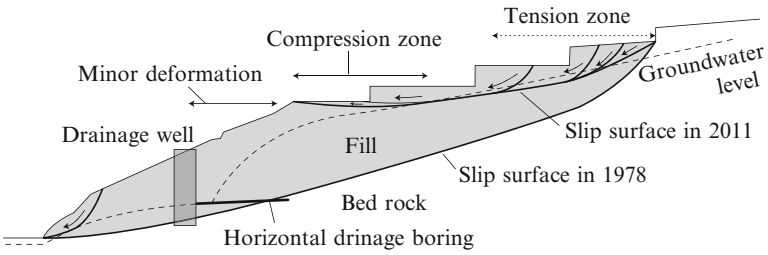

Fig. 8.16 Thematic cross section of the Midorigaoka #1 landslide in Shiroishi City

Offshore Earthquake, the entire valley fill in Midorigaoka #1 (approximately 80,000 m^3 with a maximum thickness of about 25 m) failed, killing one person. After the disaster in 1978, countermeasures (two drainage wells with horizontal borings) were installed in the fill slope; however, the valley-fill landslide in 2011 occurred at the same position as the 1978 landslide.

Figure 8.16 shows the thematic cross section of the fill slope of the Midorigaoka #1 of Shiroishi City and the relationship between the 1978 and 2011 landslides. The geology of the region consists of upper Miocene pumice tuff; therefore, the fill contains a high proportion of disassembled pumice blocks as fill materials and has high groundwater levels. The cause of the entire collapse of the fill in 1978 is suspected to be the reduction of shear strength due to liquefaction. In 2011, the occurrence of landslide features was limited to the upper part of the fill slope compared to the case in 1978; there were no landslide features around the drainage wells located at the lower part of the slope. This suggests that the drainage system for groundwater in the fill was functional causing a lowering of the groundwater level; however, the effectiveness of this drainage was limited to the proximity of the horizontal drainage borings. As such, many more drainage wells or subsurface drains would be needed for this area to prevent deeper landslides within the fill during the earthquake.

The two cases, the Midorigaoka #3 of Sendai and the Midorigaoka #1 of Shiroishi, indicate the uncertainty and limitations of countermeasures for landslides in urban residential fills. Countermeasures with steel piles and drainage wells are common methods to protect against landslides caused by intensive precipitation in Japan. Countermeasures were designed according to the technical standards authorized by the government under the Landslides Controlling Act of Japan; however, this does not consider the conditions during earthquakes for prevention of landslide damage to urban housing areas constructed in fills. Compared to cases of landslides in natural slopes, the urban residential slopes are strictly affected by deformation of fills during earthquakes. Thus, we need new design standards to maintain the stiffness of ground in urban housing lots during earthquakes and to effectively drain groundwater from fills.

In contrast with Midorigaoka #3 of Sendai City, there were no damages in the fills of Midorigaoka #1 of Sendai City. It could be concluded that countermeasures installed in the Midorigaoka #1 of Sendai City (two series of steel piles and a drainage well) performed effectively during the 2011 earthquake. The cross-sectional

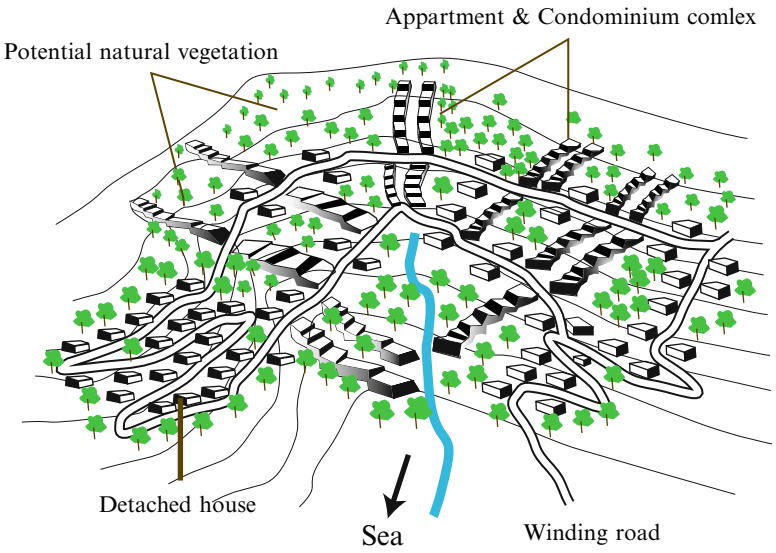

Fig. 8.17 Thematic drawing of the "Counter line city" (the drawing was modified after Nagasaka 2000)

distribution of S-wave velocity shows that high stiffness parts of fills continued from the bottom to the surface to segmentalize the fill. This inside structure of the fill might be formed by chance, but it was effective to increase friction between segments in the fill during the earthquake strong motion. Thus, the case of Midorigaoka #1 of Sendai City suggests effective methods of countermeasures for landslides in urban residential fills.

8.4.4 Contour Line City

The investigation results from the March 11th disaster suggest the intractability of the landslide hazard problem in urban residential fills. Even if artificial valley fills are appropriately designed and constructed, they will continue to be at risk in urban residential regions in the future. Thus, urban residential lots should be designed to minimize artificial changes in geomorphology, especially avoiding valley fills. In other words, we have to build our houses along the counter lines of hill slopes.

Figure 8.17 shows a thematic drawing of the "Contour line city" (modified after Nagasaka; 2000). Winding roads connect detached houses aligned along the contour lines, and apartment and condominium complexes will be built along surface water streams as the walking pass ways continuing the roads. The foundation of buildings should be laid on the stiff original ground. Forested areas consist of native vegetation that are planted in spaces between buildings. Risk mitigation of slope disaster in urban residential regions should lead to a favorable natural environment in the "Contour line city."

8.5 Conclusions

The 2011 off the Pacific coast of Tohoku Earthquake caused landslides in urban residential regions from Tohoku to northern Kanto province. As the result of urbanization, most of landslides occurred in fills of residential lots in Sendai, the largest city in Tohoku which has been growing rapidly during the past half century. Results of this investigation on these landslides are summarized as follows:

1. Landslides of fills in residential regions induced by the 2011 earthquake are classified into five types based on the combination of "thickness of movement mass" and "position of slip surface."
2. Some of landslides in 2011 are overlapped in space with landslides in 1978. These landslides are "predictable and preventable disasters" if appropriate responses were made after the earthquake in 1978.
3. Although countermeasures were constructed for landslides induced by the 1978 earthquake, serious landslides were found in the same location in 2011. Thus, new design standards to maintain the stiffness of the ground in urban housing lots during earthquake are needed.

Considering risk mitigation against landslides in residential lots, urban development should be designed to minimize artificial changes in geomorphology, especially avoiding valley fills. A new concept of a "Counter line city" is proposed that includes both minimization of risk and creating a favorable natural environment.

Acknowledgments We appreciate the helpful comments on an earlier draft of this manuscript from Dr. Roy C. Sidle. We appreciate the support of our research by Mr. Nobuhiro Sato and Mr. Kastsushiro Takahashi. This work was supported by KAKENHI (No. 23310125).

References

Hamada M (2001) A study on flow characteristics of liquefied soil. In: Proceedings of the U.S–Japan cooperative research on urban earthquake disaster mitigation. U.S–Japan joint workshop and third grantees meeting, Seatle, USA, pp 89–96

Institute of Geology and Paleontology, Tohoku University (1979) Phenomena and disasters associated with the Miyagi-ken-Oki earthquake of 1978 in the East-Central Part of Northeast Honshu, Japan. Tohoku Univ Inst Geol Pal Contr 80:1–96

Kamai T (1995) Landslides in the Hanshin Urban region caused by the 1995 Hyogoken-Nanbu earthquake, Japan. Landslide News 9:12–13

Kamai T, KobayashiY, Jinbo C et al (2000a) Earthquake risk assessments of fill slope instability in urban residential areas in Japan. In: Proceedings of the 8th international symposium landslide), Thomas Telford, pp 801–806

Kamai T, Wang WN, Shuzui H (2000b) The landslides disaster induced by Taiwan Chi-Chi earthquake of 21 September 1999. Landslide News 13:8–12

Kamai T, Shuzui H (2002) Landslides in urban region. Riko-tosho, Independent book published in Tokyo, pp 1–200

Kamai T, Shuzui H, Kasahara R et al (2004) Earthquake risk assessments of large residential fill-slope in urban areas. J Jpn Landslide Soc 157:29–39 (in Japanese)
Nagasaka D (2000) Recycled Urban Space (Nagasaki Project) model/the project for public space in NAGASAKI /1999. SHINKENCHIKU 2000(4):180–185
Tamura T (1977) Regional developments. Shokokusha, Tokyo, pp 1–73 (in Japanese)
Tamura T, Abe T, Miyagi T (1978) Housing construction in hillside and earthquake disaster. Gen Urban Res 5:115–131 (in Japanese)

Chapter 9
Soil Amplification and Nonlinearity Studies at K-Net Sites in Miyagi Prefecture, Tohoku, Japan Based on H/V Spectral Ratios for Earthquake Ground Motions

Fumiaki Nagashima, Hiroshi Kawase, Shinichi Matsushima, Francisco J. Sánchez-Sesma, Takashi Hayakawa, Toshimi Satoh, and Mitsutaka Oshima

Abstract We have proposed an optimal way to use horizontal-to-vertical (H/V) spectral ratios for underground structure exploration, which is based on diffuse field concepts (Kawase et al. (2011) The optimal use of horizontal-to-vertical spectral ratios of earthquake motions for velocity inversions based on diffuse-field theory for plane waves. Bull Seismological Soc Am 101(5): 2011–2014). This approach is applicable to earthquake and microtremor ground motions. We show here analysis on the observed data around K-NET station in Japan where very large peak ground acceleration was observed. We compare H/V spectral ratios of the strong motions during the Off the Pacific Coast of Tohoku Earthquake of March 11, 2011, with those averaged over several weak motions to see soil nonlinearity effects on the H/V spectral ratios. After we determine detailed velocity structures based on the H/V spectral ratios of the seismic motions, we estimate deconvolved bedrock motions during main shock considering nonlinearity and then simulate strong motions around the K-NET station.

Keywords Diffuse field • Directional dependence • H/V spectral ratio

F. Nagashima • H. Kawase (✉) • S. Matsushima
Disaster Prevention Research Institute (DPRI), Kyoto University, Kyoto, Japan
e-mail: kawase@zeisei.dpri.kyoto-u.ac.jp

F.J. Sánchez-Sesma
Institute of Engineering, UNAM, Mexico City, Mexico

T. Hayakawa • T. Satoh • M. Oshima
Institute of Technology, Shimizu Corporation, Tokyo, Japan

H. Kawase (ed.), *Studies on the 2011 Off the Pacific Coast of Tohoku Earthquake*,
Natural Disaster Science and Mitigation Engineering: DPRI reports,
DOI 10.1007/978-4-431-54418-0_9,

9.1 Introduction

During the 2011 Off the Pacific Coast of Tohoku earthquake that occurred on March 11, 2011, the maximum acceleration of 2,700 cm/s^2 in the NS component and JMA seismic intensity 7 was recorded at K-NET Tsukidate (MYG004) station, Miyagi, Japan, of the K-NET strong motion network (for the network description, see Kinoshita 1998). However, damages near the observation site were quite limited. The authors, therefore, observed aftershocks around MYG004 in order to identify factors for generating high acceleration and investigate the relationship between high acceleration and damages in the vicinity. Also, prior to the aftershock observation, we measured microtremors to focus on the effect of cliff topography near MYG004. The H/V spectral ratios (HVRs) of these data were compared to identify the ground motion characteristics of the area, and the HVRs of ground motion records were used to identify the soil structure around MYG004. We estimated the bedrock seismic motion of the main shock using deconvolution analysis and simulated the strong motions at the temporary observation sites.

9.2 Temporary Aftershock Observation at Tsukidate

On April 29 and 30, 2011, four survey sites were deployed around MYG004. One site was set at the center and other three sites were set on the circumference of a circle with a diameter of approximately 400 m around MYG004. Figure 9.1 shows

Fig. 9.1 Locations of the observation sites in Tsukidate, Kurihara City

the locations of MYG004 and temporary aftershock observation sites (TKDZ01–TKDZ04). At these sites, data have been continuously recorded using SMAR-6A3P (Mitutoyo Corporation), in which the data logger was replaced by LS8800 (Hakusan Corporation). These sites were set under eaves of residential properties with AC power. GPS was used for time correction and data sampling had been performed at 100 Hz.

9.3 Influence of the Cliff Topography

9.3.1 Microtremor Observation

Before deploying the temporary aftershock observation sites, in order to determine the effects of the cliff topography near MYG004, microtremor array observation was performed at five sites: two sites were set on top of the cliff and three sites were set at the base of the cliff. Figure 9.2 shows the array arrangement. M01 and M02 were set on top of the cliff with M02 located right in front of MYG004, and M01 was set approximately 10 m south of M02. M03, M04, and M05 were set at the base of the cliff with M03 located immediately beneath the cliff and M04 and M05 located 10 and 30 m apart from M03, respectively. Microtremors were recorded for 30 min.

9.3.2 Microtremor HVRs

HVRs were computed for the NS and EW components from average Fourier spectra, separately. Figures 9.3 and 9.4 show the HVRs for NS/UD and EW/UD, respectively. While the HVRs at all the five sites were similar to each other up to 7 Hz, for frequencies higher than 7 Hz, the HVRs for the cliff-top sites (M01 and M02) were two to three times as high as the HVRs for the cliff-base sites. This is believed to be the effect of the cliff topography.

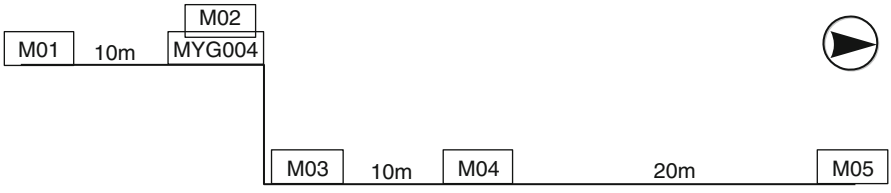

Fig. 9.2 Schematic figure of microtremor array arrangement across the cliff near MYG004

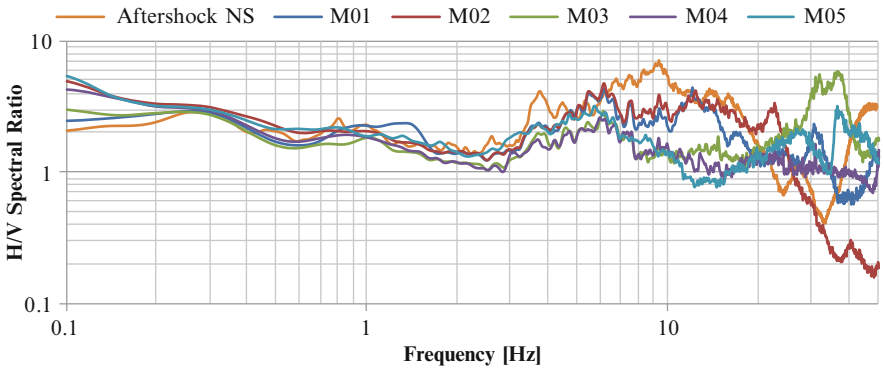

Fig. 9.3 Microtremor HVRs of the linear array with aftershock HVR for MYG004 (NS/UD)

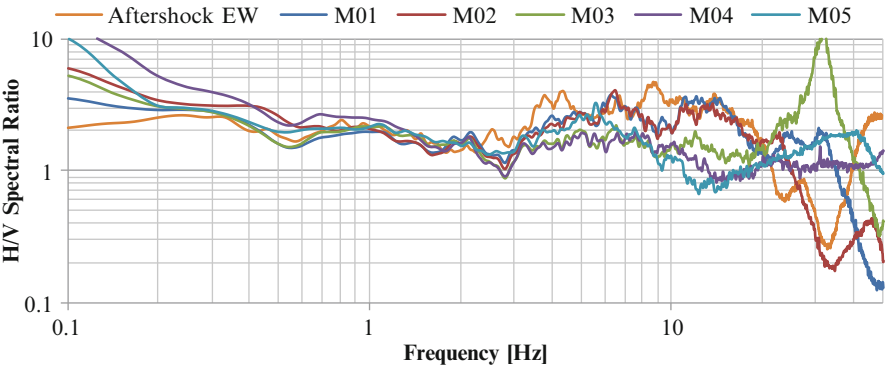

Fig. 9.4 Microtremor HVRs of the linear array with aftershock HVR for MYG004 (EW/UD)

9.4 Aftershock Data at Tsukidate

9.4.1 Comparison of Weak Motion HVRs at Temporary Observation Sites

From the aftershock data recorded between April 30 and September 20, 2011, at four temporary observation sites shown in Fig. 9.1, a time window of 81.92 s from the onset of the S-wave was extracted, and the average Fourier spectrum of each component was computed to determine the HVRs, that is, NS/UD and EW/UD, for the 77 earthquakes recorded at MYG004. Figures 9.5 and 9.6 show the aftershock

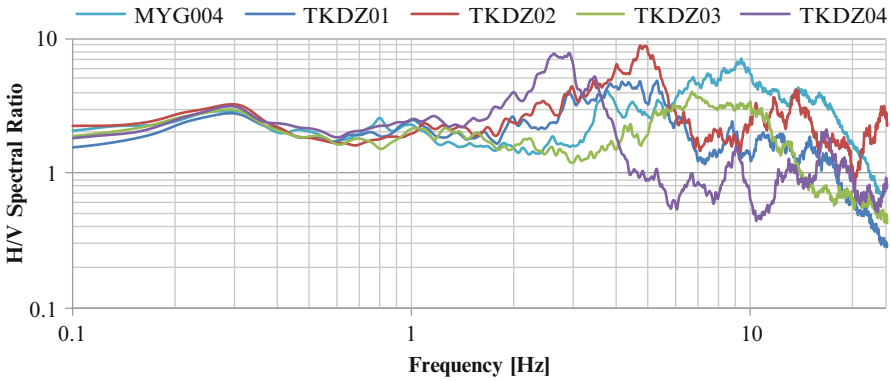

Fig. 9.5 Aftershock HVRs in Tsukidate (NS/UD)

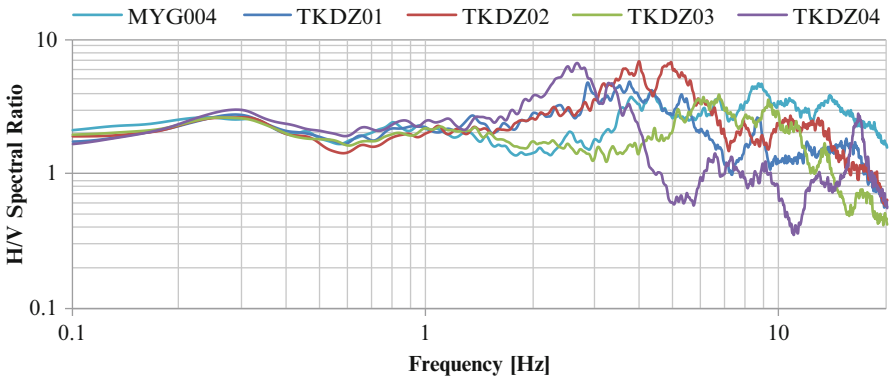

Fig. 9.6 Aftershock HVRs in Tsukidate (EW/UD)

HVRs for NS/UD and EW/UD as well as those for MYG004, respectively. The aftershock HVRs have peaks at around 0.3 and 1.0 Hz at all five survey sites including MYG004, which seems to be the effect of the deep soil structure. On the other hand, at frequencies higher than 1.5 Hz, HVRs are significantly different among the observation sites, except for TKDZ01 and TKDZ02. The NS component at MYG004, in particular for 7–10 Hz, showed higher HVRs than those at other observation sites. This is consistent with the results discussed in the previous section, where the effects of the cliff topography were apparent at frequencies higher than 7 Hz. Note that at TKDZ04 where there were some damages occurred to buildings, a peak can be seen at around 2.5 Hz, indicating the relationship between dominant frequency and damages.

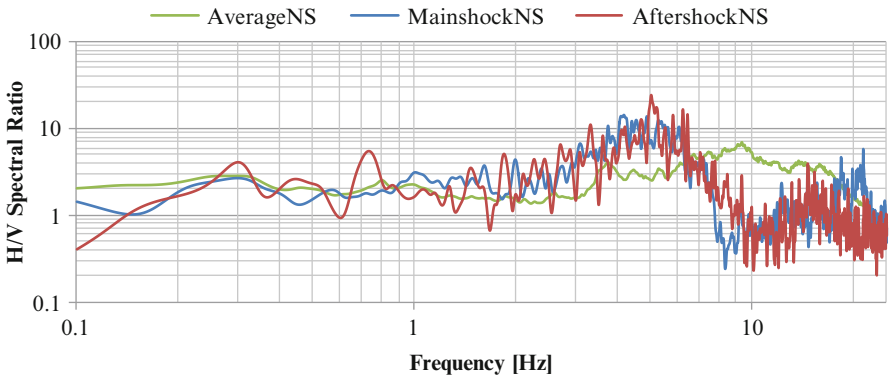

Fig. 9.7 HVRs of main shock, largest aftershock, and average of other aftershocks at MYG004 (NS/UD)

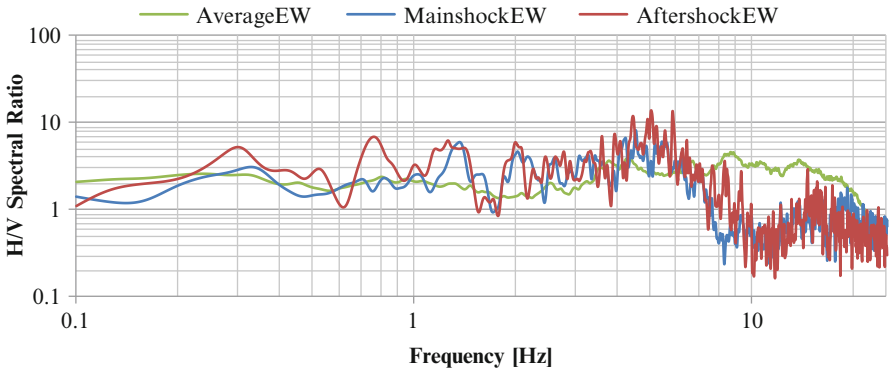

Fig. 9.8 HVRs of main shock, largest aftershock, and average of other aftershocks at MYG004 (EW/UD)

9.4.2 Comparison Between the Main Shock, the April 7 Largest Aftershock, and Average of Other Aftershocks at MYG004

Next, we compare the strong motion HVRs of the main shock and the largest aftershock that occurred at 23:32 on April 7 (M7.1) with average weak motion HVRs of other aftershocks. Figures 9.7 and 9.8 compare NS/UD and EW/UD of these HVRs, respectively. With regard to the maximum acceleration (PGA), the NS and EW components for the main shock were 2,700 and 1,268 cm/s^2, respectively, and those for the April 7 aftershock were 1,242 and 886 cm/s^2, respectively, showing large differences between the two events (1.5–2 times), but the HVRs were similar

between them. Compared with the weak motion HVRs, the peaks of the strong motion HVRs were shifted to lower frequencies, indicating the effect of nonlinearity. The peak frequency was shifted from 9 to 4–5 Hz for strong motion HVRs in comparison to weak motions HVRs, and shear rigidity may have dropped to approximately 25 % of the linear values during the strong shaking.

9.5 Identification of the Soil Structure

9.5.1 Identification at MYG004

Identification of the soil structure immediately below MYG004 was attempted based on the HVRs of weak motion data recorded at the site. First, for the 55 waves observed between March 9 and May 17, 2011, average HVRs of the EW components, which are believed to be less influenced by the cliff topography, were used as a target to identify the soil structure at MYG004, by making the residual sum of squares smallest with theoretical HVRs. For the initial model, the data published by the National Research Institute for Earth Science and Disaster Prevention (NIED 2011) were used for shallow soil layers, and the results of previous study (Kawase and Matsuo 2004) were used for deep soil layers. Layers 2 and 3 of the eight-layered model of Kawase and Matsuo (2004) had similar PS logging results and densities, so they are treated as one layer to make a seven-layered model (the Initial Model in Table 9.1).

The theoretical HVRs were calculated based on the concept of Kawase et al. (2011) and were identified by changing the thickness of layers 1–6. As a result, the velocity structure that explains the observed HVRs well was identified as shown in Fig. 9.9. The velocity structure model is shown in Table 9.1 and Fig. 9.10. Comparing the identified model with the initial model, layers near the surface got thinner and layers 5 and 6 got thicker, creating peaks at 0.3 and 1.0 Hz, and hence quite nicely reproducing the observed HVR as shown in Fig. 9.9.

Table 9.1 Velocity structure of the initial and identified model

Initial model				Identified model	
No	Vs (m/s)	Thickness (m)	Depth (m)	Thickness (m)	Depth (m)
1	100	1	1	0.4	0.4
2	240	3	4	1.12	1.52
3	550	6.25	10.25	14.25	15.77
4	1,364.29	20	30.25	71.4	87.17
5	2,075.17	110	140.25	1,624.7	1,711.67
6	2,874.27	50	190.25	1,200	2,911.67
7	3,400	–	–	–	–

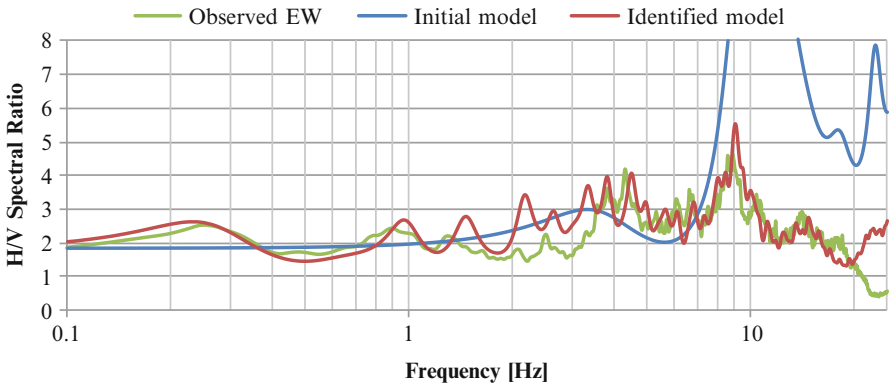

Fig. 9.9 Comparison of HVRs for observed EW/UD, initial model, and identified model

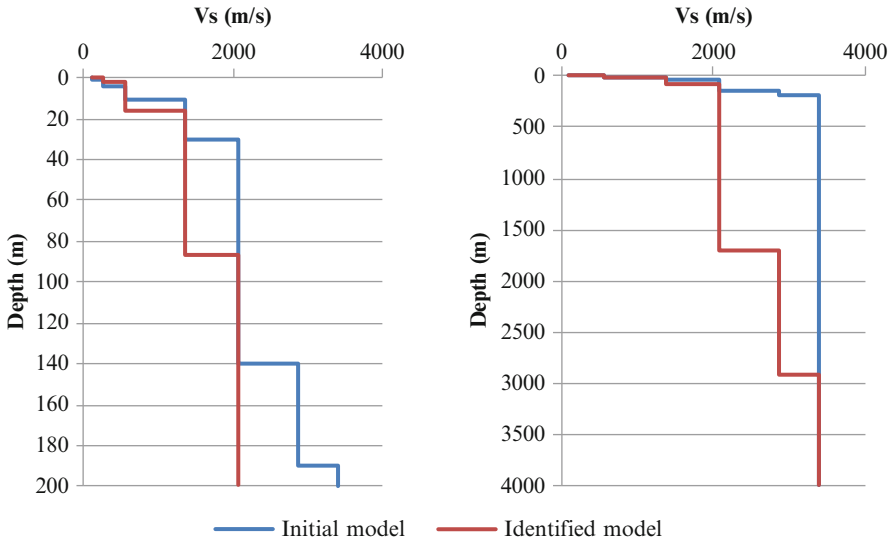

Fig. 9.10 Shallow and deep part of the initial and identified velocity structures

9.5.2 Identification at Temporary Observation Sites

Using the same approach adopted for MYG004, the soil structures at the temporary aftershock observation sites are identified so as to minimize the square sum of the residual difference between the observed and theoretical HVRs. For analysis of the temporary aftershock observation sites, however, a grid search is executed with the S-wave velocity as a variable in addition to the layer thickness. If there is an occurrence of an inverted layer in the S-wave velocity, such a model is discarded. The initial model was based on the model identified for MYG004 but with the following differences. The depth of the first layer was made to be very thin, at 0.4 m, and the first layer was coalesced with the second layer under the assumption that the

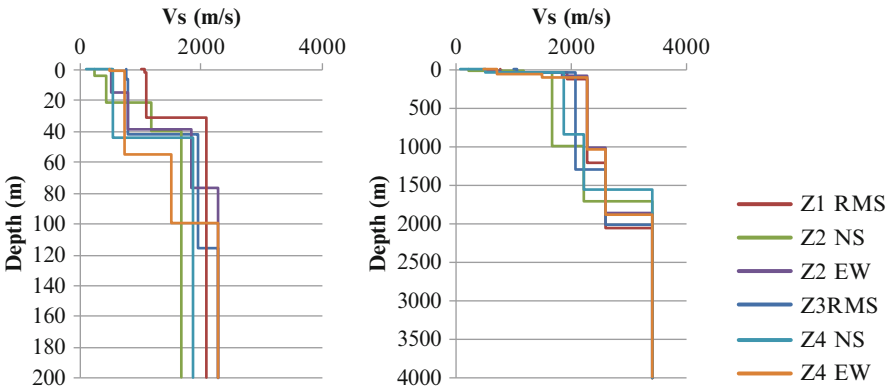

Fig. 9.11 The velocity structure at temporary aftershock observation sites

influence of these two different layers in the frequency range between 0.1 and 20 Hz used in the computation would be negligible, thus providing an initial model with a total of six layers.

The observed HVR computed at each observation site from the aftershock data was used for calculating the residual difference. There is a difference in the amplification of the peaks between NS and EW directions for observation sites TKDZ02 and TKDZ04, the mean square sum of NS and EW was used for TKDZ01 and TKDZ03, while square sums for NS and EW were used independently for TKDZ02 and TKDZ04.

The soil structures identified at the temporary aftershock observation sites are shown in Fig. 9.11. The comparison is omitted here, but we were able to obtain a model that explains the observed data very well at all observation sites. In the present analysis, the velocity structure has been identified to match each observed data. While the peaks at 0.3 and 1 Hz are commonly observed across all observation sites, their power is weak, and there is insufficient resolution to determine an identical deep layer structure across all observation sites. Thus, the deep layer structure in the identified model significantly varies within short ranges. For future analyses, an identification of a model with an identical deep velocity structure would be required.

9.6 Deconvolution Analysis of Incident Waves on Bedrock with Nonlinearity Considerations

9.6.1 Derivation of Bedrock Seismic Motion Using Deconvolution Analysis

Deconvolution analysis was performed to estimate the seismic bedrock wave, taking the nonlinearity of the soil structure into consideration. First, equivalent linear analysis was performed using the deconvolved wave, in which the effect of soil layers was stripped from the observed wave using the linear transmission function, as an input to obtain the equivalent linear transmission function on the ground surface.

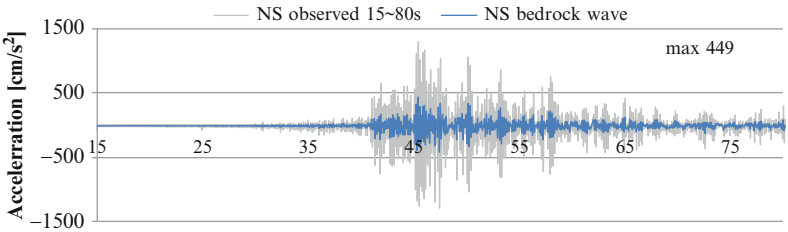

Fig. 9.12 Deconvolved bedrock motion in the NS direction

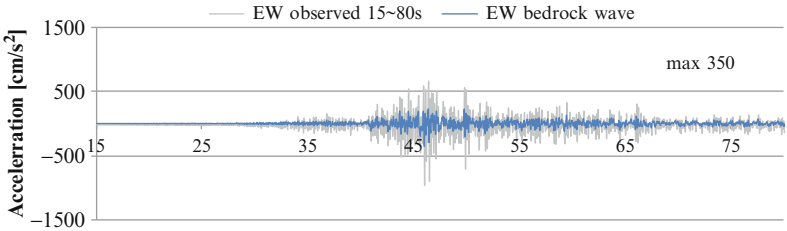

Fig. 9.13 Deconvolved bedrock motion in the EW direction

The observed wave was then deconvolved using the obtained transmission function, which was then reinjected and excited again. The above operation was repeated until a stable dynamic shear modulus, G, and damping coefficient, h, were obtained. When the changes in G and h between iterations were <5 % for all elements, the resulting deconvolved wave was considered as the seismic wave incident to the bedrock.

9.6.2 Deconvolution Analysis of the Main Shock Record at K-NET Tsukidate

One-dimensional deconvolution analysis was performed on the main shock record observed at K-NET Tsukidate to obtain the deconvolved bedrock seismic wave. The deconvolution analysis was performed by applying a filter of 0.1–20 Hz to both the NS and EW elements of the main shock data. A report has attributed the pulse-shaped acceleration at around the 100 s mark of the main shock data to rocking of the bedrock at the observation site. Thus, for the present analysis, an initial S-wave part with 65-s duration was extracted between 15 and 80 s from the start of the record.

Boring records indicate that there is soft, viscous soil up to 1.2 m in depth. This corresponds to an S-wave velocity in layers 1 and 2; thus, the nonlinear characteristics of clay (Imazu and Fukutake 1986) were used for layers 1 and 2. Layers 3–6 are equivalent to solid rock; therefore, the nonlinear characteristics of solid rock (Fujikawa et al. 2001) were used for these layers.

Figures 9.12 and 9.13 show the obtained deconvolved bedrock waves in blue on top of the observed surface waves. Maximum acceleration in the NS direction was 449 and 350 cm/s^2 in the EW direction.

9.7 Strong-Motion Simulation Near K-Net Tsukidate

9.7.1 Simulation Methodology for Strong Motion

A general-purpose soil response analysis code, SoilPlus (Itochu Techno Solutions), was used for computing the seismic motion at the ground surface. The identified soil structure of the temporary observation site was used to derive a one-dimensional model and the acceleration response at the ground surface was calculated using the deconvolved bedrock motion as input. In almost all sites along the identified structure at the temporary observation site, the S-wave had large velocity at the topmost layer, and the structure is thought to be a hard solid rock. Therefore, linear analysis was performed without taking the nonlinearity of the soil into consideration. The bedrock motions were injected in both NS and EW directions and analysis was performed.

9.7.2 Observations on the Correspondence Between Analysis Results and Actual Damages

Tables 9.2, 9.3, and 9.4 list the maximum acceleration, maximum velocity, maximum displacement, and JMA seismic intensity in the NS and EW direction of the observed data (top low), as well as those acquired from the strong-motion simulation (Z01–Z04). At TKDZ02, with a soil structure similar to K-NET Tsukidate,

Table 9.2 Maximum acceleration, velocity, displacement, and JMA seismic intensity (NS)

	Maximum acceleration (cm/s^2)	Maximum velocity (cm/s)	Maximum displacement (cm)	JMA seismic intensity
Main shock 15–80 s	1,300	41.0	6.74	6.09
Bedrock wave	449	18.1	7.95	5.10
Simulation at Z01	954	37.9	9.02	5.77
Simulation at Z02	1,473	50.8	11.0	6.15
Sivulation at Z03	572	33.0	9.41	5.41
Simulation at Z04	560	32.0	8.39	5.52

Table 9.3 Maximum acceleration, velocity, displacement, and JMA seismic intensity (EW)

	Maximum acceleration (cm/s^2)	Maximum velocity (cm/s)	Maximum displacement (cm)	JMA seismic intensity
Main shock 15–80 s	958	49.3	10.9	5.62
Bedrock wave	351	30.1	10.4	4.93
Simulation at Z01	622	44.1	11.9	5.41
Simulation at Z02	763	61.3	11.3	5.57
Simulation at Z03	402	43.8	12.2	5.14
Simulation at Z04	596	57.9	11.3	5.41

Table 9.4 Maximum acceleration, velocity, displacement, and JMA seismic intensity (vector sum)

	Maximum acceleration (cm/s^2)	Maximum velocity (cm/s)	Maximum displacement (cm)	JMA seismic intensity
Main shock 15–80 s	1,511	58.1	11.0	6.15
Bedrock wave	476	30.9	12.0	5.24
Simulation at Z01	1,009	50.6	12.1	5.85
Simulation at Z02	1,498	64.3	12.3	6.18
Simulation at Z03	620	47.7	12.4	5.53
Simulation at Z04	633	59.1	11.4	5.68

large acceleration, velocity, and displacement are observed; however, although acceleration exceeds 1 g, the velocity is in the vicinity of 50 cm/s, and displacement was only 10 cm. The seismic intensity was slightly greater than 6.0 at TKDZ02 but was lower than 6.0 at other observation sites. Although the shaking at the Tsukidate region that resulted from the initial half of the main shock had a large maximum acceleration and seismic intensity, the velocity and displacement was not so great, and it is thus believed that it did not have a large impact on building damage.

9.8 Summary and Conclusions

Temporary aftershock observation was undertaken near the K-NET Tsukidate in order to investigate the factors causing large acceleration near K-NET Tsukidate, as well as to understand the relationship of the large acceleration to building damages in the surrounding area. The amplification characteristics of the nearby soil structure were studied based on the H/V spectral ratio (HVR) of the observed data.

A clear directional dependence was observed in the HVR at K-NET Tsukidate, which is indicative of the effect of topography. Small peaks at 0.3 and 1.0 Hz were consistently observed near K-NET Tsukidate, which is attributed to the effect of the deep soil structure. While varying wave shapes were observed at each observation site above 1.5 Hz, waves of 7–10 Hz at MYG004 were the greatest among all observation sites. This corresponds to the amplification that can be seen in a linear microtremor array across the cliff for waves of frequencies above 7 Hz. Comparisons were made between the main shock on March 11th as well as the maximum aftershock on April 7th. Prolongation of peak period was observed, which can be attributed to the effect of the nonlinearity of the soil structure.

The one-dimensional soil structure at K-NET Tsukidate was also identified based on the diffuse field theory. We were able to reproduce the peaks at 0.3 and 1.0 Hz by increasing the depth of the layer with Vs = 3,400 m/s to 2,900 m, resulting in the identification of a structure that matches the observed data very well. The soil structures at the temporary aftershock observation sites near Tsukidate were also identified. Although we were able to identify soil structures that match the observed data very well, there are differences in the deep soil structures and further identification is needed to obtain a homogeneous deep soil structure.

One-dimensional deconvolution analysis was applied to derive the incident seismic wave on the bedrock, which was found to have a maximum acceleration of 449 cm/s^2 in the NS direction and 350 cm/s^2 in the EW direction for the initial half of the whole duration. However, the actual soil structure is three dimensional, and a detailed study would be needed to see two- and three-dimensional site effects. Based on strong-motion simulation using the deconvolved incident wave at the bedrock during the main shock at the temporary observation sites, it is estimated that despite a significant seismic intensity at the Tsukidate area due to large acceleration, the seismic motion did not cause structural damage to buildings because the main component of the motion was amplified only in the high-frequency range. The present strong-motion simulations only used the initial half of the recorded data from the main shock, and further simulations that consider the whole wave would be needed to perform in future.

Acknowledgement We would like to thank all the people in Kawase-Matsushima laboratory in DPRI who cooperated in the measurement of aftershocks. We also thank the National Research Institute for Earth Science and Disaster Prevention (NIED) for allowing us to access to their K-NET data. Some of the figures were made using "Google Map."

References

Fujikawa S, Hayashi Y, Fukutake K (2001) The Effect of The Nonlinearity of Diluval Deposit and Deep Sediment on The Earhquake Responses of Surface Ground and Buildings. J Struct Constr Eng AIJ 545:71–77 (in Japanese)

Imazu M, Fukutake K (1986) Dynamic shear modulus and damping of gravel materials, Proceedings of the 21th Japan National Conference on Soil Mechanics and Foundation Engineering, 509–512 (in Japanese)

Kawase H, Matsuo H (2004) Separation of source, path, and site effects based on the observed data by K-NET, KiK-net, and JMA strong motion network. J JAEE 4(1):33–52 (in Japanese with English abstract)

Kawase H, Sanchez-Sesma FJ, Matushima S (2011) The optimal use of horizontal-to-vertical spectral ratios of earthquake motions for velocity inversions based on diffuse-field theory for plane waves. Bull Seismological Soc Am 101(5):2011–2014

Kinoshita S (1998) Kyoshin net (K-Net). Seismolgical Res Lett 69:309–334

National Research Institute for Earth Science and Disaster Prevention (2011) A strong-motion seismograph networks Portal site. http://www.kyoshin.bosai.go.jp/index_en.html. Accessed 28 February 2012

Chapter 10
Soil Liquefaction Along the Tokyo Bay Coast Induced by the 2011 Off the Pacific Coast of Tohoku Earthquake

Shuji Tamura

Abstract The 2011 Off the Pacific coast of Tohoku earthquake resulted in widespread soil liquefaction along the coast of Tokyo Bay and the Tone River basin, causing extensive damage. This paper reports on cases of damage from soil liquefaction, with a primary focus on the results of investigations performed immediately after the earthquake (13th–17th of March) in mainly Urayasu City, Chiba Prefecture, the damage to detached houses implemented soil cement columns, and the restoration methods of tilting detached houses. Predominant features of liquefaction damage include (1) a long duration of ground motion, (2) expanded liquefaction damage during aftershocks, (3) liquefaction of low-plasticity silt (dredged silt in particular), (4) sinkage and tilting of a majority of detached houses, and (5) an extended period of water and sewage service stoppage. The damage to detached houses complemented soil cement columns depending on the depth of the soil cement column base and the filling soil layer.

Keywords Detached house • Restoration method • Soil cement column • Soil liquefaction

10.1 Soil Liquefaction in Urayasu City

10.1.1 Ground Conditions and Ground Motion in Urayasu City

Urayasu City conducted extensive land reclamation through dredging in the 1960s and 1970s. The ground surface of landfill areas is composed primarily of sand and sandy silt. The depth to the gravel of the Paleo-Tokyo River is 20 m at the shallowest points,

S. Tamura (✉)
Disaster Prevention Research Institute (DPRI), Kyoto University, Kyoto, Japan
e-mail: tamura@sds.dpri.kyoto-u.ac.jp

H. Kawase (ed.), *Studies on the 2011 Off the Pacific Coast of Tohoku Earthquake*,
Natural Disaster Science and Mitigation Engineering: DPRI reports,
DOI 10.1007/978-4-431-54418-0_10,

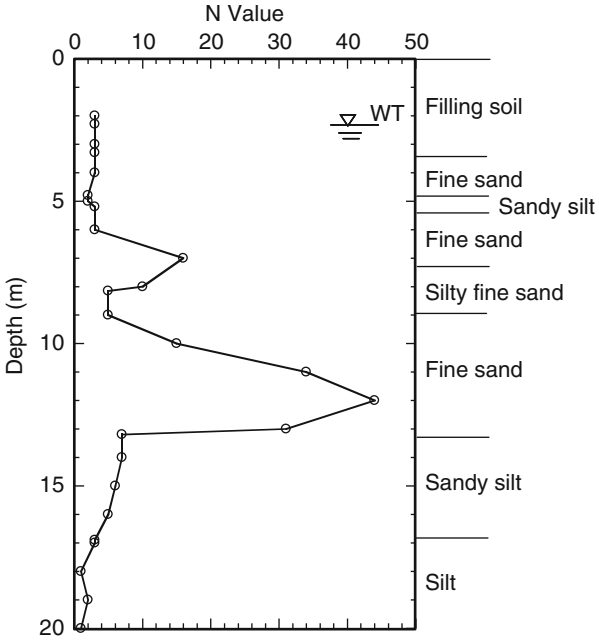

Fig. 10.1 Soil profiles in the Maihama 3-chome area, Urayasu City

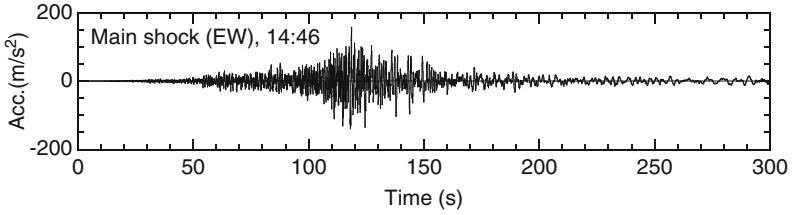

Fig. 10.2 Acceleration waveform (EW component) of the main shock (14:46) as measured by K-NET Urayasu

over 30 m in most locations within the city limits, and up to 60 m in some places (Urayasu City 2012). Figure 10.1 shows the results of a standard penetration test in the 3-chome area of the Maihama district in Urayasu City (Chiba Prefectural Environmental Research Center 2012). Ground strata near the surface are approximately 5 m accumulations of fine, loose sand with *N*-values between 2 and 3. The groundwater level is 2.2 m, resulting in ground conditions prone to soil liquefaction.

The 2011 Tohoku earthquake occurred at 14:46 on 11th of March. Figure 10.2 shows the acceleration time history of the main shock, as recorded by K-NET Urayasu (National Research Institute for Earth Science and Disaster Prevention 2011). The peak east–west (EW) horizontal acceleration was 157 cm/s^2, and the

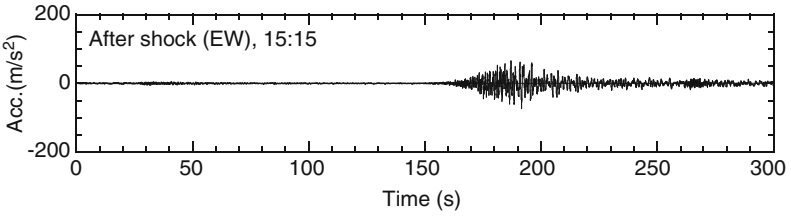

Fig. 10.3 Acceleration waveform (EW component) of an aftershock (15:15) as measured by K-NET Urayasu

duration of continuous ground motion exceeded 5 min. During that time, ground motion with acceleration amplitude exceeding 50 cm/s^2 lasted for approximately 1 min. K-NET Urayasu is located inland and, thus, did not experience sand boils or similar phenomena. Areas in which soil liquefaction occurred are thought to have experienced peak horizontal accelerations of approximately 150–200 cm/s^2.

Figure 10.3 shows the EW acceleration time history of an aftershock that occurred at 15:15, approximately 30 min after the main shock. Peak acceleration in that case was 73 cm/s^2. Soil liquefaction is generally considered not to occur under peak accelerations of 100 cm/s^2, but Urayasu City residents gave reports of sand boils with increased intensity during aftershocks, and these reports have been verified by using surveillance camera video. Therefore, it is highly likely that aftershocks contributed to the damage caused by soil liquefaction.

10.1.2 An Overview of Soil Liquefaction

Severe liquefaction events occurred in Urayasu City during the 2011 Tohoku earthquake. Roads were covered with sand from sand boils (Fig. 10.4), with depths reaching up to 55 cm in some locations (Fig. 10.5). Sand boils buried automobiles and bicycles in many locations (Fig. 10.6), and sidewalks were severely deformed (Fig. 10.7). Primary causes for the numerous sand boils under peak horizontal accelerations of approximately 150 cm/s^2 are the shallow groundwater level, the loose sand surface layer with an N-value of <10, the extended duration of ground motion, and the aftershock.

Figure 10.8 shows a map of locations where liquefaction damage occurred, based on a damage survey performed immediately after the earthquake (Tokimatsu et al. 2012). Liquefaction damage was not seen in areas north of the circa 1964 coastline. Within landfill areas, liquefaction damage was seen in some locations, but not in others. The presence or absence of liquefaction damage is clearly demarked by area, with likely causes being differences in ground conditions including the depth of water table and whether improvements to ground conditions had been performed. Only partial information is available as to what improvements have been made in what areas, and so such details remain unclear.

Fig. 10.4 Residential area covered by sand from a sand boil

Fig. 10.5 55 cm accumulation of sand

Fig. 10.6 Bicycles buried in sand

Fig. 10.7 Damage to a sidewalk

10.1.3 Damage to Large Buildings

Large buildings supported by pile foundations generally did not show any signs of settlement or structural damage, but separations with the surrounding ground of up to approximately 50–60 cm were seen (Fig. 10.9), indicating ground sinkage of this

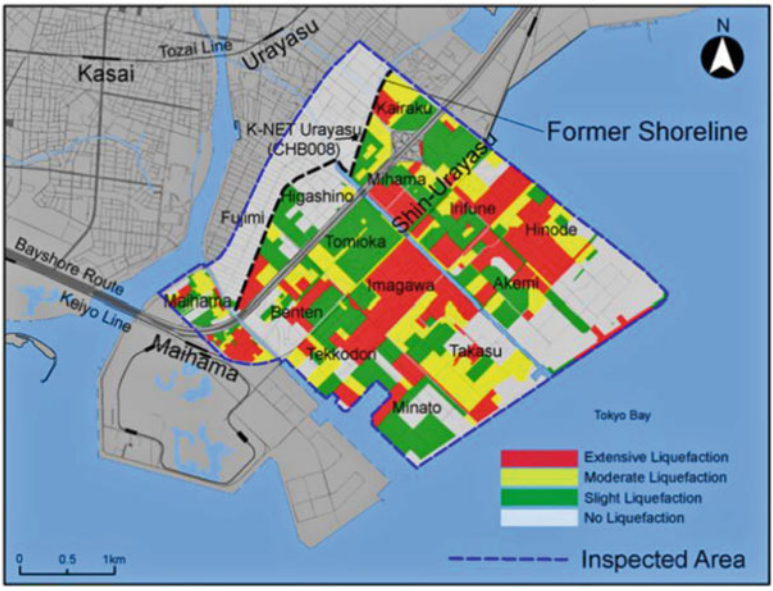

Fig. 10.8 Liquefaction damage map

Fig. 10.9 Ground sinkage around a pile foundation building

magnitude. This sinkage resulted in numerous cases of lifeline damage at the border between buildings and the surrounding ground (Fig. 10.10). Such damage did not occur in buildings that used flexible joints as a measure against consolidation settlement (Fig. 10.11), indicating the effectiveness of flexible joints as connectors between pile foundation buildings and lifelines during liquefaction events.

Fig. 10.10 Severed lifeline at the border between the building and the ground

Fig. 10.11 Flexible joint

10.1.4 Damage to Lifelines

In areas that experienced liquefaction, cases were found of utility poles sinking or tilting (Fig. 10.12), manhole uplift (Fig. 10.13), inflow of sand into manholes (Fig. 10.14), and water pipe ruptures. In places where water pipes ruptured (Fig. 10.15), sediment erosion was severe, as was sinking and tilting of detached

Fig. 10.12 Sinkage at a utility pole

Fig. 10.13 Protruding manhole

houses. Lifeline recovery dates were 11th of March for electricity, 30th of March for gas, 6th of April for water, and 15th of April for sewage (Urayasu City 2011). Hence, considerable time was required for water and sewage facilities to be restored, resulting in daily life interruptions even for residents of apartment buildings that escaped structural damage. Water and sewer line stoppages forced the city to

Fig. 10.14 Sand flown into a manhole (photo by Mr. Y. Kamiya)

Fig. 10.15 Sediment erosion due to a ruptured water pipe

provide portable toilets and water supplies in local parks (Fig. 10.16). Sewage facility restoration was severely delayed because ground deformation and sinkage caused sewer lines to rupture and fill with sand and because restoring sewer line gradients took a substantial amount of time.

Fig. 10.16 Long line at a drinking water supply station

10.1.5 Damage to Detached Houses

Over 8,700 houses in Urayasu City were damaged by the earthquake. According to Urayasu City reports (Japan Society of Civil Engineering 2012), 18 houses were completely destroyed (tilting of 1/20 or more), 1,541 were severely damaged (tilting of 1/60 or more), 2,121 were significantly damaged (tilting of 1/100 or more), and 5,096 showed some damage. Only 1,105 houses showed no damage at all. By these figures, 89 % of detached houses in Urayasu City experienced damage due to liquefaction.

Liquefaction caused sinkage or tilting in many detached houses (Fig. 10.17). Damage to upper structures was generally minor. A tilt angle of 1° (equivalent to 1/60) is, however, enough to cause discomfort to occupants.

According to residents in areas affected by liquefaction, the earthquake felt like "riding on a boat." Reports also suggest that furniture did not fall over. This finding seems to corroborate the reduced response acceleration and lengthened periodicity of the ground motion under soil liquefaction. Sand boils occurred for the duration of ground motion, and reports are that sand boiling continued to flow for approximately 1 h after the earthquake.

Some detached houses used soil cement columns as a measure against consolidation settlement (Fig. 10.18). Figure 10.19 shows the damage distribution of houses that implemented soil cement columns (Tokimatsu and Matsushita 2012). In the Higashino and Kairaku areas, landfill was approximately 4 m deep and soil cement column was approximately 3.5–7 m deep. Approximately 70 % of detached houses with soil cement columns were undamaged. In contrast, in the Imagawa, Irifune, Takasu, and Hinode areas, landfill was approximately 8 m deep and soil cement

Fig. 10.17 Tilting houses

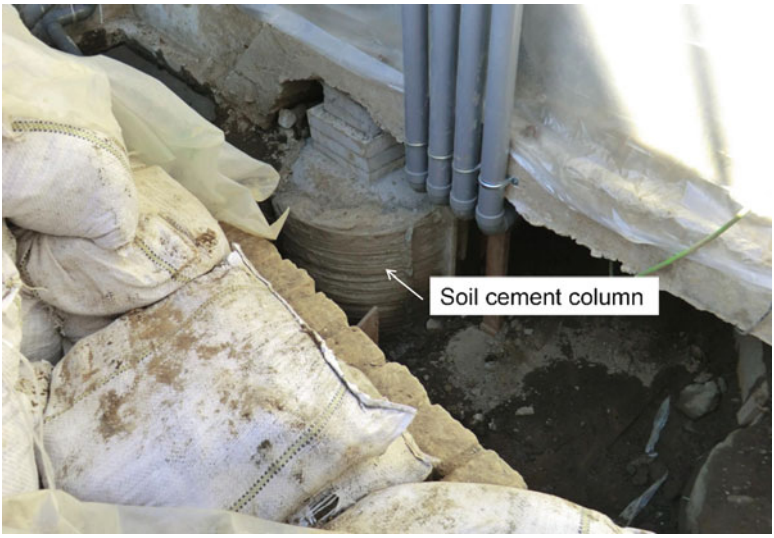

Fig. 10.18 Soil cement column

columns was approximately 3.5–8 m deep. In those areas, approximately 50 % of detached houses with soil cement columns experienced severe sinking or tilting damage. These results indicate that soil cement columns that extended below the landfill layer typically prevented damage to detached houses, but in cases where soil cement columns were shallower than the landfill layer, considerable tilting of the houses often occurred. The reason for this difference is likely to be the inability of

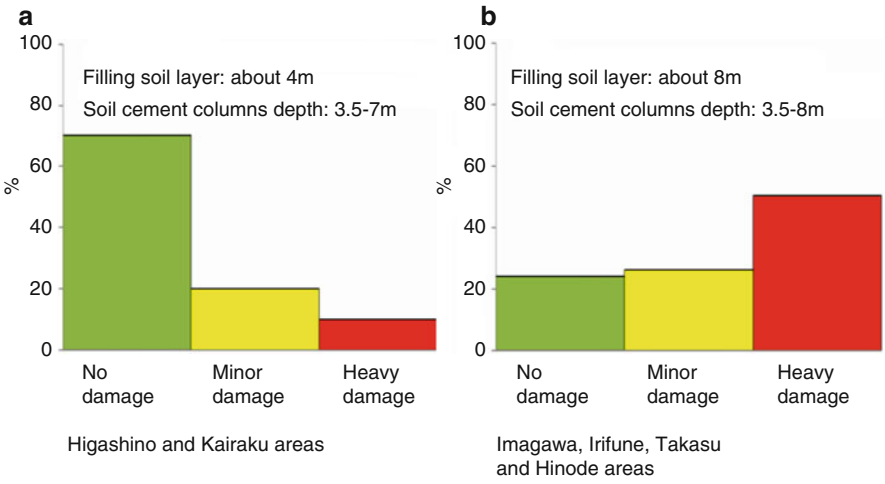

Fig. 10.19 Damage to small buildings implemented soil cement columns. (**a**) Higashino and Kairaku areas; (**b**) Imagawa, Irifune, Takasu, and Hinode areas

soil cement columns to support detached houses when the ground beneath the soil cement columns experiences liquefaction. Thus, when using soil cement columns as a tilting prevention measure in detached houses, precise estimation is needed of the depth of layers in which liquefaction might occur, and care must be taken to ensure that soil cement columns are supported by soil layers that will not liquefy.

10.1.6 Restoration of Detached Houses After Tilting

The cost of soil cement columns is often considerable for small structures such as detached houses. An alternative approach is the use of rigid mat footing or highly rigid strip foundation that enables restoration of houses experiencing sinkage or tilting due to liquefaction. Figure 10.20 shows an example of damage to a detached house with an unreinforced strip footing foundation after the 1993 Southwest-off Hokkaido earthquake. Ground deformation caused extensive damage to the foundation and even to the upper parts of the structure. Restoration of houses in such cases is difficult.

The majority of detached houses in Urayasu City used a rigid mat footing or a highly rigid strip foundation, and structural damage to the upper part of these houses was minor. Tilting in houses can cause health problems such as dizziness and nausea, and reports have stated that tilting of greater than 1/125 can be strongly felt (Fujii et al 1998). To address this issue, restoration was performed on many detached houses to eliminate tilting. As Fig. 10.21 (Architectural Institute of Japan 2008) shows, restoration methods can be largely divided into two types: jack-up techniques and chemical grouting techniques. Jack-up techniques use jacks to lift

Fig. 10.20 Damage to unreinforced strip foundations

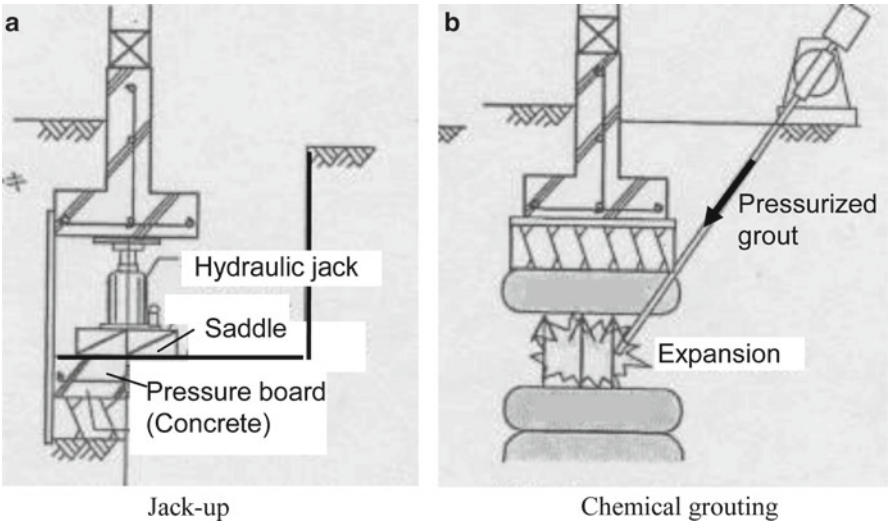

Fig. 10.21 Reconstruction methods for tilting detached houses. (**a**) Jack-up; (**b**) chemical grouting (Architectural Institute of Japan 2008)

foundations (Fig. 10.22) and can be applied to both a mat footing and a strip foundation. Jack-up requires care in its implementation, however, as an insufficient number of jacks can result in large stresses that can damage or destroy foundations. Chemical grouting techniques, on the other hand, can only be applied for relatively small amounts of sinkage and cannot be used with some strip foundations.

Fig. 10.22 Example of jack-up technique

These restoration methods are expensive, costing 2–10 million yen (US$20,000–100,000) depending on the type of foundation and the amount of tilt. The probability of a recurrence of liquefaction during future earthquakes also remains high. Given this high cost and high likelihood of recurrence, there is a strong need for improved restoration methods or methods for inexpensive soil improvements for exiting detached house that can accommodate future liquefaction events.

10.2 Liquefaction in Shinkiba District

Shinkiba district in Tokyo's Koto Ward is a landfill area occupied by office buildings, distribution centers, and wholesalers and is located approximately 7 km west of Urayasu City. As in the case of Urayasu City, the district experienced extreme liquefaction during the 2011 Tohoku earthquake. The Shinkiba train station did not suffer any structural damage, and by the 13th of March, electricity, water, and sewage services were operational.

As shown in Figs. 10.23 and 10.24, roads in the 1-chome area of Shinkiba were covered by approximately 30 cm of silt from sand boils. Reinforced concrete buildings also experienced sinkage and tilting (Fig. 10.25).

Many businesses performed cleanup operations and made minor repairs after the sand boils. Several businesses were affected by the soil liquefaction slightly even in areas where liquefaction was severe and performed normal operations. This small impact was likely due to the extensive soil improvements that had been made,

Fig. 10.23 Sand accumulated on a sidewalk

Fig. 10.24 Tires submerged in sand

showing the effectiveness of soil improvements as a measure against liquefaction and in keeping businesses operational after an earthquake. In buildings in which pilings were thought to be used in their construction, the surrounding ground sank approximately 50 cm, causing a gap between foundations and the surrounding ground (Fig. 10.26). No tilting or structural damage was seen in any of the buildings.

Fig. 10.25 Sunk and tilted two-storey reinforced concrete building

Fig. 10.26 Ground sinkage around a pile foundation building

10.3 Characteristics of Liquefaction

This section describes the characteristics of liquefaction during this event, according to the Architectural Institute of Japan's (2001) *Recommendations for Design of Building Foundations* (hereinafter called the "Recommendations").

10.3.1 Duration of the Earthquake

Ground motion measured in Urayasu City during the 2011 Tohoku earthquake showed a peak acceleration of approximately 150 cm/s^2, which is not considered to be a large value. The predominant feature of the ground motion was instead its duration. The recommendations use a correcting factor r_n for the number of cyclic shear stress ratio corresponding to the magnitude of the earthquake. For a magnitude 7.5 earthquake the value of r_n is 0.65, but the value is 0.80 for a magnitude 9.0 earthquake, equivalent to a 23 % increase in the shear stress ratio. We expect that the effects of the duration of ground motion will be considered in future damage case investigations. Furthermore, as described above, reports stated that sand boils intensified in Urayasu City during aftershocks. Previous liquefaction studies have focused on main shocks only, but since magnitude 9.0 earthquakes can have magnitude 7-class aftershocks, important structures must also take measures against liquefaction that may occur during aftershocks.

10.3.2 Low-Plasticity Silt

Sand boils in Urayasu were noted to have produced extremely fine grains (Tokimatsu et al. 2012). It is generally understood that ground soil with a high proportion of fine grains (cohesive soil) does not experience liquefaction, because silt and clay lead to stronger cohesive forces. In land that was formed by dredging, however, cases have been discovered where the mud expelled from sand pumps precipitates, separating even very fine particles and causing them to lose cohesion. Hence, liquefaction may occur even in fine-grained soils.

Permeability is small when liquefaction occurs in fine-grained soils, making dissipation of excess pore water pressure difficult and therefore leading to the risk of liquefaction for extended durations. Reports made of liquefaction of low-plasticity silt in landfill areas during the 2000 western Tottori earthquake have led the Recommendations to suggest that "In landfill areas having <10 % clay content, and in landfill and embankments having a plasticity index of <15 %, the potential for liquefaction should be investigated." Testing for liquefaction when building constructions on landfill areas is thus necessary; we cannot simply assume that liquefaction will not occur because the landfill content is silt.

10.3.3 Assessment of Liquefaction

Assuming a peak ground surface acceleration of 150 cm/s^2, the equivalent cyclic shear stress ratio used in the Recommendations is approximately 0.1–0.15. Figure 10.27 shows this shear stress ratio in terms of the relation between the corrected *N*-value and liquefaction resistance (shaded). As can be seen, the shear stress

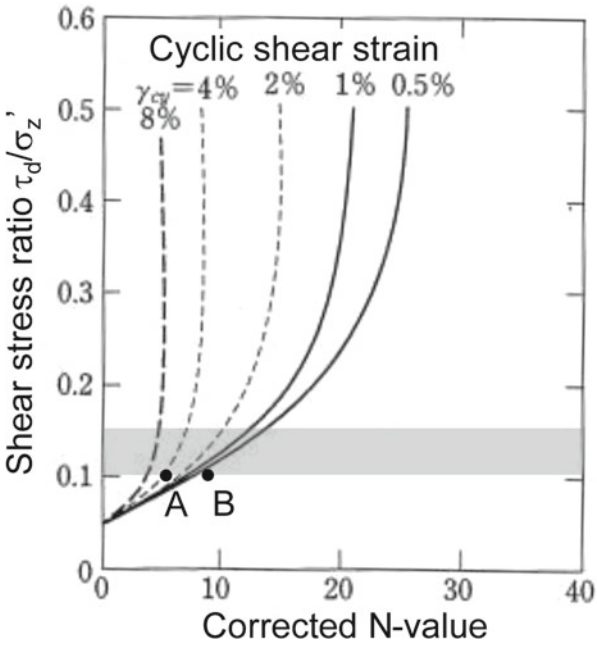

Fig. 10.27 Corrected *N*-value vs. shear stress ratio (from Architectural Institute of Japan (2001))

ratio experienced in Urayasu City was equivalent to the minimum required to result in liquefaction. Under such low shear stress ratios, the curves describing the amplitudes of shear strain begin to converge. In the shaded portion of the graph, point A (with a corrected *N*-value of 5) indicates extensive liquefaction (the cyclic shear strain amplitude is 4 %), but at point B (with a corrected *N*-value of 9) there is no liquefaction. From this result, selective extreme liquefaction is predicted for those sections of Urayasu City with loose sand, and such a prediction is borne out by the existence of areas in which liquefaction damage occurred and those in which none occurred.

10.4 Conclusions

This paper reports on cases of damage from soil liquefaction, with a primary focus on the results of investigations performed immediately after the earthquake (13th–17th of March) in mainly Urayasu City, Chiba Prefecture, the damage to detached houses implemented soil cement columns, and the restoration methods of tilting detached houses. Predominant features of liquefaction damage in Urayasu City during the 2011 Tohoku earthquake include (1) a long duration of ground motion, (2) expanded liquefaction damage during aftershocks, (3) liquefaction of low-plasticity silt (dredged silt in particular), (4) sinkage and tilting of a majority of detached houses, and (5) an extended period of water and sewage service stoppage. The

damage to detached houses complemented soil cement columns depending on the depth of the soil cement column base and the filling soil layer. Restoration work on houses in Urayasu City continues even today, 1 year after the occurrence of the earthquake. Liquefaction measures must be considered not only for new constructions but also for existing houses.

Research regarding liquefaction began in the 1960s and has yielded many results related to the mechanism by which liquefaction occurs, the characteristics of liquefaction in laboratory tests, assessment of liquefaction resistance using standard penetration tests and static cones, predictions by effective stress analysis, and construction methods for liquefaction prevention through ground improvements. Most local governments have also published hazard maps indicating areas of possible liquefaction, increasing awareness of the dangers. Nonetheless, the 2011 Tohoku earthquake caused extensive damage, predominantly to detached dwellings. Pile foundation destruction and lateral spreading were also major problems in the 1995 Great Hanshin (Kobe) earthquake. We can expect further damage during future large earthquakes, and preemptive countermeasures must be developed.

Acknowledgments Tokyo Institute of Technology Professor Tokimatsu K. provided invaluable information and Mr. Kamiya Y. offered photos. We used K-NET data of NIED. I greatly appreciate their support and cooperation.

References

Architectural Institute of Japan (2001) Recommendations for design of building foundations. Architectural Institute of Japan (in Japanese)

Architectural Institute of Japan (2008) Recommendations for design of small building foundations. Architectural Institute of Japan (in Japanese)

Chiba Prefectural Environmental Research Center (2012) Soil boring log. http://wwwp.pref.chiba.lg.jp/pbgeogis/servlet/infobank.index. Accessed 3 March 2012

Fujii M, Ijuin H, Tamura M, Ina K (1998) Damage and restoration of foundation for houses in liquefied areas by the Hyogo-ken Nanbu earthquake: concept for restoration of foundation for houses. Tsuchi-to-kiso 46(7):9–12 (in Japanese)

Japan Society of Civil Engineering (2011) Report meeting of soil liquefaction and countermeasure at Urayasu city. http://committees.jsce.or.jp/2011quake/node/125. Accessed 3 March 2012

National Research Institute for Earth Science and Disaster Prevention (2011) Kyoshin Net-work K-NET. http://www.k-net.bosai.go.jp/k-net/. Accessed 27 October 2011

Tokimatsu K, Matsushita K (2012) Damage of small buildings supported by deep soil mixing. http://committees.jsce.or.jp/2011quake/node/125. Accessed 3 March 2012

Tokimatsu K, Tamura S, Suzuki H, Katsumata K (2012) Building damage associated with geotechnical problems in the 2011 Tohoku Pacific Earthquake, Special Issue for the East Japan Great Earthquake, Soils and Foundations, Japan Geotechnical Society, 52(5), pp 956–974

Urayasu City (2011) http://www.city.urayasu.chiba.jp/. Accessed 25 April 2011

Urayasu City (2012) Geography and geology of Urayasu city. http://www.city.urayasu.chiba.jp/menu3185.html. Accessed 3 March 2012

Chapter 11
Sediment-Related Disasters Caused by the Nagano-ken Hokubu Earthquake in the Heavy Snow Season

Sumio Matsuura, Masahiro Chigira, Yuki Matsushi, and Takashi Okamoto

Abstract Mountain slopes covered in deep snow were hit by seismic motions during the Nagano-ken Hokubu Earthquake on March 12, 2011, resulting in avalanches, slope failures, and deep-seated landslides. Sediment-related disasters occurred at places which had geologically weak structures such as faults and fractured rock masses and/or topographical features that were prone to receiving concentrated earthquake acceleration. However, the key characteristic was the interaction between snow cover and sediment-related disasters during and after the earthquake. Fast-moving layers of air and suspended snow particles were also produced when fast debris flows crashed into accumulated snow, destroying peripheral areas along the path of the debris flows. Furthermore, a landslide occurred about 1 month after the earthquake on a slope that was likely to have been loosened by the seismic motions. The numbers of slope failures and landslides were very small compared to the Niigata-ken Chuetsu Earthquake of a similar scale, which was probably attributable to the physical and/or mechanical properties of snow cover.

Keywords Deep snow cover • Interactions • Sediment-related disasters • Snow effects • The Nagano-ken Hokubu Earthquake

S. Matsuura (✉) • M. Chigira • Y. Matsushi
Disaster Prevention Research Institute (DPRI), Kyoto University, Kyoto, Japan
e-mail: matsu03@scs.dpri.kyoto-u.ac.jp

T. Okamoto
Forestry and Forest Products Research Institute (FFPRI), Tsukuba, Japan

H. Kawase (ed.), *Studies on the 2011 Off the Pacific Coast of Tohoku Earthquake*,
Natural Disaster Science and Mitigation Engineering: DPRI reports,
DOI 10.1007/978-4-431-54418-0_11, © Springer Japan 2014

11.1 Introduction

On the next day of the 2011 off the Pacific coast of Tohoku earthquake (March 11, 2011), a strong earthquake occurred near the prefectural border of northeastern Nagano and Niigata and caused slope failures, landslides, avalanches, etc. in mountainous areas. The earthquake-induced disasters, which occurred in the snowy season, showed characteristic interactions between snow covers and sediment-related disasters, which were not observed during the Niigata-ken Chuetsu Earthquake in 2004 and the Iwate and Miyagi Inland Earthquake in 2008.

In the past, the Kambun Takada Earthquake (February 1, 1666) occurred in the snowy season and was recorded to have destroyed houses and killed a number of people in the castle town of Takada. However, the actual states of sediment-related disasters in mountainous areas are not understood due to the long lapse of time. Therefore, the sediment-related disasters caused by the earthquake on March 12, 2011, provide precious information for understanding what disaster is likely to occur when snow-covered mountain slopes receive earthquake motion, what roles snow cover plays in the generation mechanism of disaster, and how the effects of an earthquake are manifested in spring snowmelt seasons.

11.2 Overview of the Nagano-ken Hokubu Earthquake and Snow Environment

The Nagano-ken Hokubu Earthquake (M6.7 on the Richter scale) occurred at 3:59 AM on March 12, 2011, near the prefectural boarder of Nagano and Niigata at a depth of about 8 km (Fig. 11.1). The Miyanohara Fault near the epicenter was likely to have caused the earthquake (Matsuta et al. 2011). It has also been pointed out that the earthquake was triggered by the 2011 off the Pacific coast of Tohoku Earthquake, which occurred on the previous day. During the earthquake on March 12, very strong motion of 6-upper on the Japanese seven-stage seismic scale was recorded in Sakae-mura, Nagano Prefecture, and an intensity of 6-lower was recorded in Tsunan-machi and Tokamachi City, Niigata Prefecture. The earthquake killed or wounded 70 people and damaged 2,465 buildings.

During this winter, Japan was covered interruptedly by southing strong cold air masses since the end of December 2010. It snowed heavily over a large area along the Sea of Japan until early February. On January 31, the maximum snow depth of the season of 260 cm was recorded at Yasuzuka AMeDAS Station (elevation: 126 m) of the Japan Meteorological Agency (JMA), which is about 18 km northwest of the epicenter. At Busuno Observation Station (elevation: 567 m) of the Forestry and Forest Products Research Institute (FFPRI), which is about 14 km west-northwest of the epicenter, a snow depth of 471 cm was recorded (January 30),

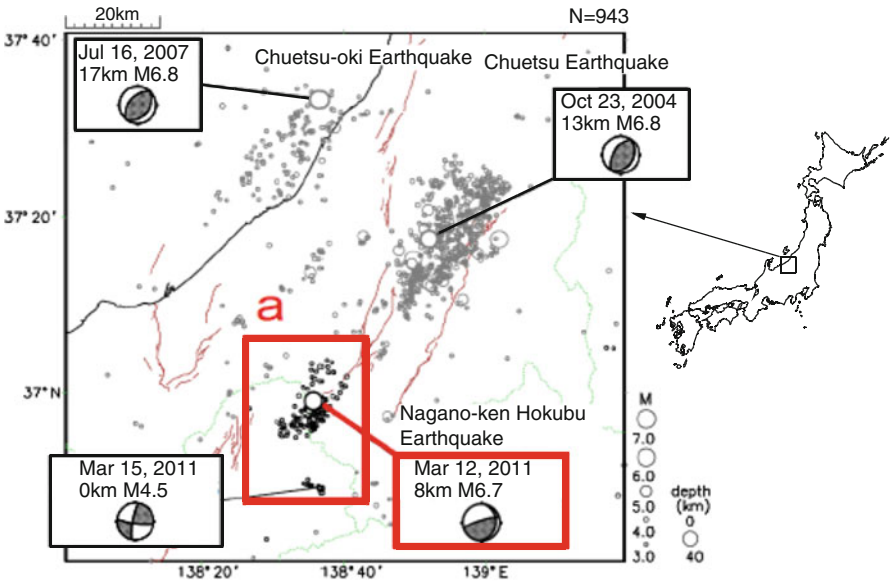

Fig. 11.1 Nagano-ken Hokubu Earthquake and major earthquakes in the region (Prepared based on the reference by the Headquarters for Earthquake Research Promotion (2011))

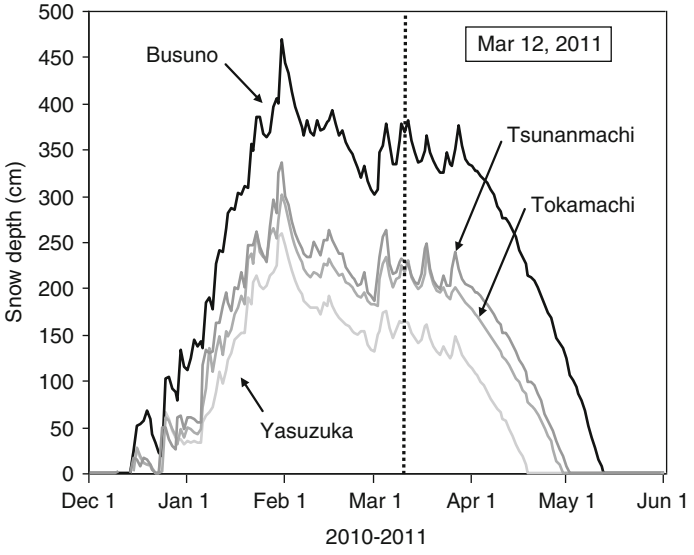

Fig. 11.2 Snow conditions in 2010/2011 in the mountain areas of Niigata Prefecture

which was deeper compared to average years. It became relatively warm in the mid to end February, and the snow started to melt. However, in March, cold air masses arrived again and brought snow. On March 12, snow depths of 163 and 381 cm were recorded at Yasuzuka and Busuno, respectively (Figs. 11.2 and 11.3), suggesting

Fig. 11.3 Snow survey at Busuno Observation Station 5 days before the earthquake

that there was snow cover of at least 1 m, and 4–5 m in deep sites, on the mountain slopes affected by the earthquake.

11.3 Distribution and Examples of the Sediment-Related Disasters Caused by the Earthquake

11.3.1 Distribution Characteristics of the Sediment-Related Disasters

The earthquake caused rockfalls, slope failures, deep-seated landslides, movement of reactivated landslides, avalanches, and movements of slope constituents. They concentrated on the hanging wall side of the earthquake source fault, such as the terrace cliffs along the banks of the Shinano River and adjacent mountain slopes and mountain areas in Niigata Prefecture (Fig. 11.4). The results agree with the so-called hanging wall effect (Abrahamson and Somerville 1996).

The relatively large sediment-related disasters that occurred simultaneously with the earthquake were mainly distributed within about 10 km from the estimated surface earthquake fault (Miyanohara Fault) with the farthest failure observed at about 18 km from the fault. The accelerations, which were calculated using the Joyner-Boore attenuation relationship (Joyner and Boore 1981), were about 260 gal at 10 km from the fault and about 160 gal at 18 km, where the furthest affected point was located (Fig. 11.5).

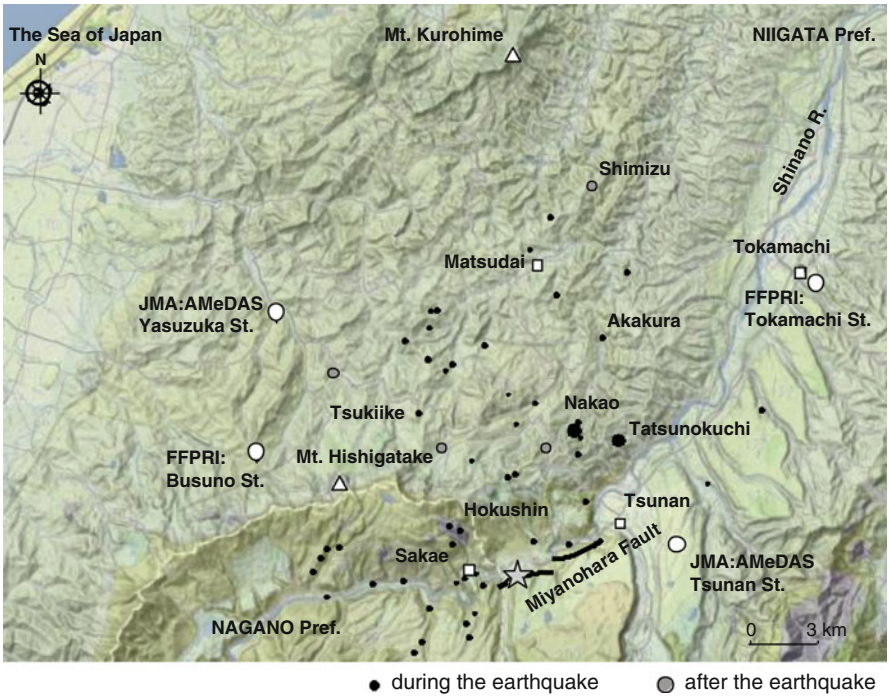

Fig. 11.4 Distribution of sediment-related disasters during the Nagano-ken Hokubu Earthquake (The locations of the sediment-related disasters were prepared based on the references by Niigata and Nagano Prefectural governments, and the map was prepared based on the map (2010) edited by the Geological Survey of Japan, National Institute of Advanced Industrial Science and Technology)

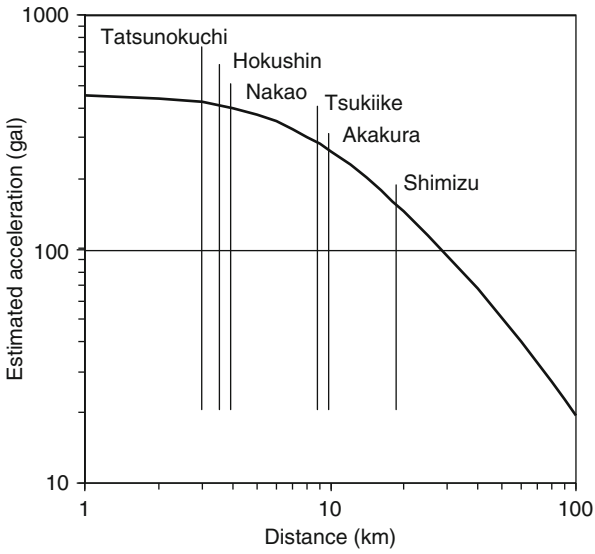

Fig. 11.5 Distance from the surface earthquake fault and estimated acceleration

Fig. 11.6 Deep-seated landslide on the left bank of the Higashi-irisawagawa River

11.3.2 Deep-Seated Landslides (Hokushin, Sakae-mura, Nagano)

A large-scale deep-seated landslide (width, 220 m; length, 350 m; landslide volume, 1.10 million m^3) occurred on a steep slope on the left bank of the Higashi-irisawagawa River, a branch of the Nakajogawa River (Fig. 11.6). The site was located on the hanging wall of the earthquake fault at a short distance of only about 4 km. A large landslide also occurred on the left bank in the upper reaches of the river.

The slope consisted of tuff and andesite of the Pliocene to Pleistocene epochs. Developed and open cracks were observed in some andesite strata (Fig. 11.7). According to the landslide distribution maps of the National Research Institute for Earth Science and Disaster Prevention (NIED), there are many landslide-prone landforms throughout the area. The slope that collapsed during the earthquake was at one end of a large landslide-prone landform. The lower part of the slope had already collapsed before the earthquake, and the earthquake expanded the landslide further. The landslide moving body struck the opposite bank, creating a landslide dam that blocked the river, but relatively little water accumulated due to the steep river bed. A part of the landslide moving body flowed about 900 m down the river, swallowing the snow cover along the river and travelled another 100 m along the Nakajogawa River.

11.3.3 Movement of Reactivated Landslide (Nakao, Matsunoyama, Niigata)

An example of the movement of reactivated landslide was observed in Nakao, Matsunoyama. The landslide was likely to have been reactivated because there are

Fig. 11.7 Tuff and andesite with developed cracks exposed at the head scarp

flatlands scattered around the site and landslide topography in the upper slope that was likely to have moved in the past. The landslide was on a slope facing southeast of a ridge extending from west to east. During the earthquake, the landslide mass, which was about 70 m wide, about 170 m long, and 14 m deep (Fig. 11.8), moved about 40 m together with the houses that were built on the slope (Fig. 11.9). A main scarp that was 10 m or higher was formed at the head (Fig. 11.10). It was estimated that the area was covered by at least 3 m of snow on the day.

Although there was highly weathered colluvial deposit on the left bank, relatively fresh bedrock was exposed on the right bank, suggesting that part of the landslide moving body may have been intact rock engulfed by landslide. Although Neogene Tamugigawa siltstone of the Pliocene epoch was dominant in the soil, the slip surface had probably formed within the highly weathered sandy mudstone. Although there were a number of reactivated landslides near the site, only this landslide was reactivated during the earthquake.

11.3.4 Landslide Mainly Attributable to Topographical Characteristics (Matsunoyama Akakura, Tokamachi City, Niigata)

The northern slope of a ridge, which was with a uniform height and ran east to west, collapsed for a width of 40–50 m and a length of about 80 m. Consequently, landslide moving body dammed up the the Higashigawa River temporarily. The rock was Pliocene Higashikawa formation. Since weathered silt rocks were exposed on the 5-m-high head scarp that was formed by the landslide and round gravel was

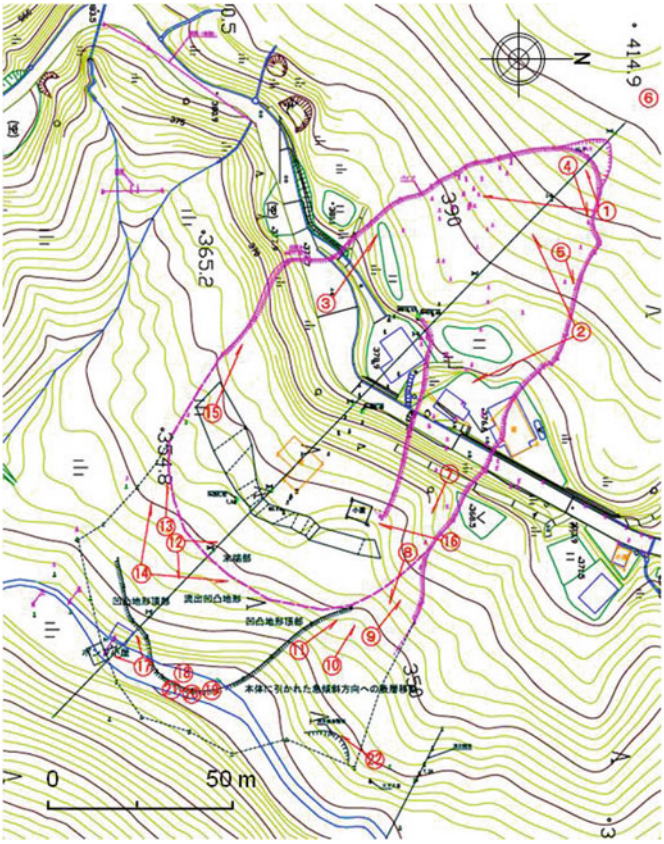

Fig. 11.8 Plan of Nakao landslide (Niigata Prefectural Government (2011))

Fig. 11.9 Reactivated landslide moved approximately 40 m during the earthquake

Fig. 11.10 Head scarp and landslide moving body remaining on a hillock

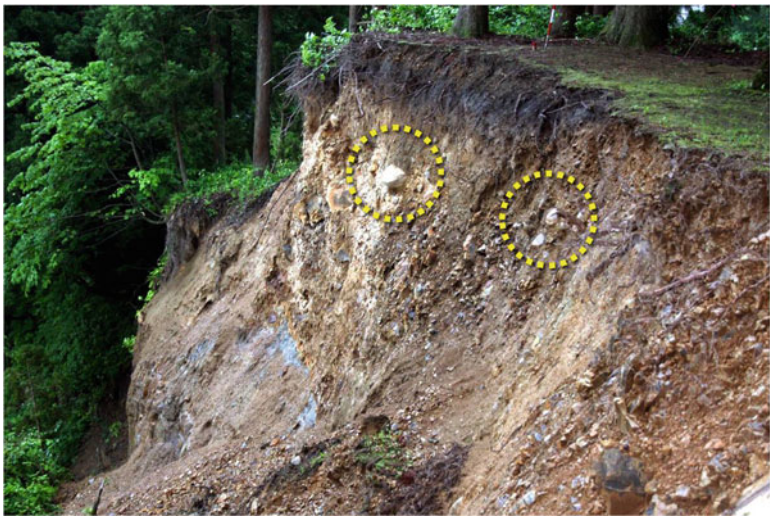

Fig. 11.11 East end of the summit-level accordance ridge and round gravel on the top of scarp

observed on the top of the eastern scarp (Fig. 11.11), the short ridge was estimated to have been river terrace and meander core (Fig. 11.12). Today, the Higashikawa River flows along the northern slope of the ridge toward the west and turns north at the toe of the slope (Fig. 11.13). Since it is an undercut slope of the river, the slope is steep. The area was located about 10 km from the surface earthquake fault and

Fig. 11.12 Akakura landslide after earth removal works (view from the south)

Fig. 11.13 River course of the Higashikawa River and the northern slope

was estimated to have received an acceleration of about 260 gal. This weak acceleration was sufficient to cause the landslide likely because the eroded toe was unstable and was a meander core, which is topographically prone to the concentration of seismic acceleration. The geological inclination of about 20° to the northeast may have been another factor. There was an old shrine and tall, straight Japanese cedar trees of at least 50–60 cm in diameter at breast height growing on the ridge, suggesting that this was the first time for the slope to collapse.

Fig. 11.14 Side view of the landslide in Tsukiike

Fig. 11.15 Front view of the landslide in Tsukiike

11.3.5 Landslide Mainly Attributable to Geological Structure (Matsunoyama Tsukiike, Tokamachi City, Niigata)

A landslide with a maximum width of about 80 m and length of about 100 m occurred on a north-facing slope along National Highway Route No. 405 near the border between Tokamachi and Joetsu Cities. The upper slope of the right scarp of a large previous landslide collapsed, involving the old landslide mass, and the moving body travelled more than 10 m (Figs. 11.14 and 11.15). The rock was Pliocene Higashikawa

Fig. 11.16 Head scarp formed along the fault

formation, in which highly cracked silt rocks were dominant. The resultant head scarp appeared in the middle of the old landslide, extending linearly west-northwest along a fault (N75W/75N) in the silt rocks (Fig. 11.16). Clear striations on the surfaces showed horizontal displacements. This area was also located about 10 km from the earthquake fault and was estimated to have received acceleration of a similar magnitude to that in Akakura. The slope in Tsukiike had topographical characteristics vulnerable to the concentration of earthquake acceleration, such as the ridgelike lateral scarp on the right bankside of the old landslide, but the main factor was probably the existence of the fault, which crossed the small ridge almost perpendicularly.

11.4 Interactions Between Snow Covers and Sediment-Related Disasters

11.4.1 Characteristics of the Sediment-Related Disasters During the Nagano-ken Hokubu Earthquake

Before the earthquake on March 12, this area had been hit by the Niigata-ken Chuetsu Earthquake (M6.8) in October 2004 and the Niigata-ken Chuetsu-oki Earthquake (M6.8) in July 2007 (Fig. 11.1) (The Headquarters for Earthquake Research Promotion 2011). Particularly the former caused 2,902 slope failures and landslides mainly in hilly and mountainous regions of the former Yamakoshi-mura Village (Yagi 2007).

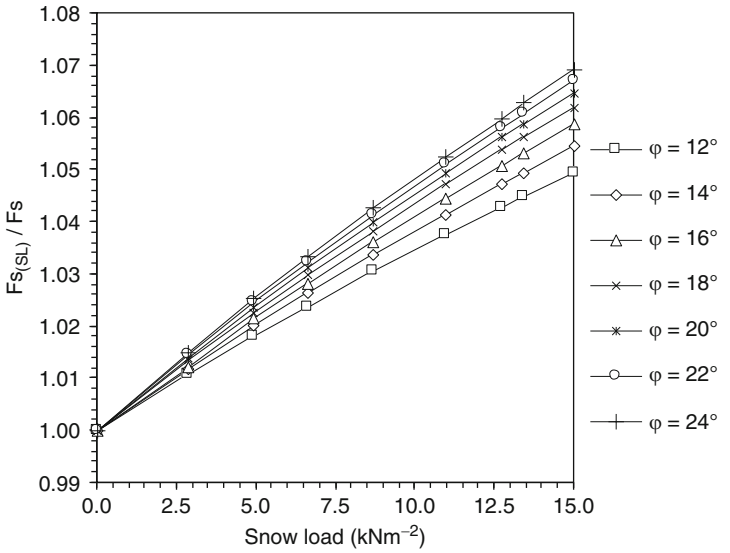

Fig. 11.17 Effects of snow load on safety factor

Field surveys have revealed that the earthquake on March 12 affected landforms that are prone to receiving concentrated seismic motion, such as ridges, and geological weak structures represented by faults and joint systems. However, the number of slope failures and landslides was much less than those caused by the Niigata-ken Chuetsu Earthquake although the two earthquakes were similar in scale. During the Niigata-ken Chuetsu Earthquake, a large number of reactivated landslides moved. On the other hand, there were almost no reactivated landslides during this earthquake except the one in Nakao described above. Even in Matsunoyama Kamiebiike, Amamizukoshi, and Amamizushima Districts of Tokamachi City, where many reactivated landslides are densely distributed, almost no landslide showed marked conspicuous movement.

11.4.2 Effects of Snow Cover on the Slope

The deep snow cover during the earthquake was a possible factor that suppressed slope failures and large displacements of reactivated landslides. Snow cover has been reported to increase the effective normal stress on gentle slopes, although the effect may vary by the inclination of the slip surface and internal friction angle (Matsuura et al. 2003). Therefore, a stability analysis was conducted using a model of a small-scale reactivated landslide, which had a length of about 110 m, width of about 40 m, and slip surface depth of 6–7 m, to investigate increase in effective normal stress by snow load. A snow load of 10 kNm^{-2} was found to increase the safety coefficient by 3–4 % (Fig. 11.17). However, such a small increase in safety coefficient is unlikely to be effective against seismic motion.

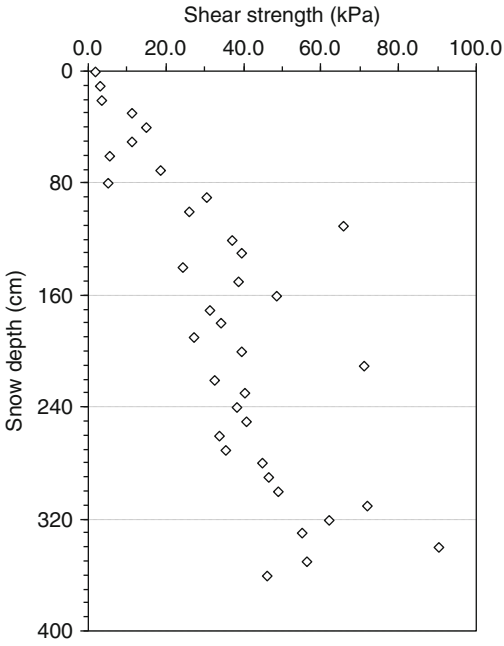

Fig. 11.18 Changes in shear strength within snow cover

Therefore, there must be factors involved other than snow load, including the mechanical properties of snow cover. When the ground is covered by snow, the shear strength and tensile strength of the snow cover act on the ground and are likely to somewhat stabilize landslides (Shibasaki et al. 2008).

The shear strength of snow cover was surveyed at Busuno Observation Station 5 days before the earthquake. The shear strength of newly formed snow cover was relatively low with 1–15 kPa and had little strengthening effect. On the other hand, deep and densely packed snow covers showed strong shear strength of 25–90 kPa (Fig. 11.18) although the value varied by the effects of ice layers. The shear strength plus the compressive strength at the toe of a landslide were likely to have prevented the reactivated landslide from moving or the slope surface from collapsing. Further studies are required to understand precise mechanisms.

11.4.3 Generation of Suspension Layers of Air and Snow Particles by Landslide

In Tatsunokuchi, Tsunan-machi, the northern slope collapsed on the ridge that extended from Eboshigata-yama toward the west. The landslide moving body flowed down along a stream toward east-northeast, passed over National Highway

Fig. 11.19 Natural levee of earth and snow formed along the debris flow

No. 353, and reached the Funatsugigawa River. The slope that fell consisted of sandstones, mudstones, and conglomerates of Pliocene to Pleistocene epochs, which formed strata of opposite dip. The dimensions were 100–130 m in width and about 150 m in length. The horizontal length from the head to the toe was about 800 m, and the elevation difference was 270 m.

The landslide was likely to have travelled fast through the valley, where the snow debris of an avalanche on the right bankside accumulated deep and pushed out the snow. Therefore, natural levee consisting of mixture of earth and snow was formed along the edges of the debris flow (Figs. 11.19 and 11.20). Snow was dominant on the edges of the bank, and earth was dominant inside.

Outside the curves toward the hills, trees were found fallen over a distance of about 20 m from the path of the debris flow (Fig. 11.21). The trees were likely to have been smashed down by snow smoke, which was produced by the debris flow breaking into snow cover at very high speeds. Snow smoke is a suspension layer of air and snow particles and has very strong destructive power. A similar phenomenon has been reported in Alps when bedrocks fell on a glacier (Barla et al. 2000).

11.4.4 Landslide Caused by Snowmelt After the Earthquake

On April 19, or about 1 month after the earthquake, a slope collapsed for about 100 m in width and 400–500 m in length in Matsudai Shimizu District of Tokamachi City and destroyed about 1.6 ha of the famous and tourist-attracting terraced rice

Fig. 11.20 Close-up view of natural levee consisting of mixture of earth and snow

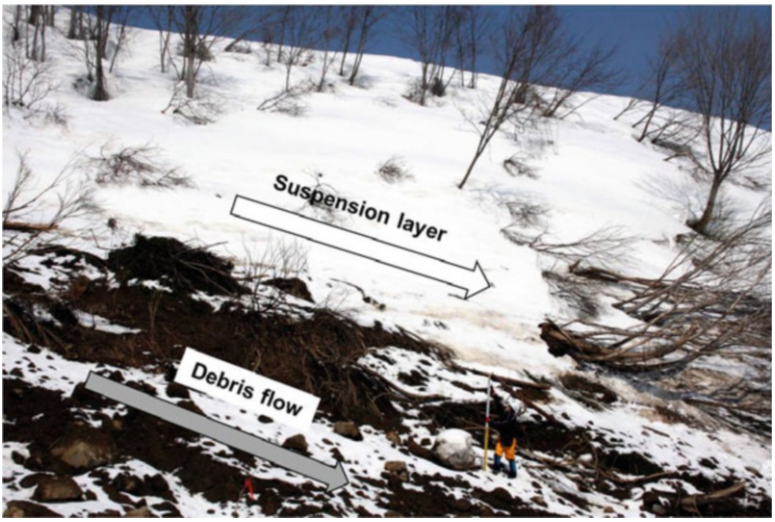

Fig. 11.21 Trees smashed down by suspension layer of air and snow particles on the upper slope of the debris flow

Fig. 11.22 Landslide in "Shimizu-no tanada" 1 month after the earthquake (views before and after the landslides)

fields, known as "Shimizu-no tanada" (Fig. 11.22). Shimizu District is located about 20 km from the surface earthquake fault and was estimated to have received seismic acceleration of approximately 150 gal. Such acceleration is insufficient for causing immediate landslides but may have loosened structurally weak slopes. A lateral main scarp was observed on the right bankside of the landslide, which was estimated to be an old fault. Therefore, it was likely that the earthquake motion decreased the initial safety factor, and a large amount of meltwater infiltrated into the ground and triggered the landslide.

The effects of the seismic motion were quantitatively assessed by estimating the amount of meltwater and/or rainfall that reached the ground surface (MR) each day in Shimizu District during the seven snow seasons from 2004/2005, which was a year of heavy snow, to 2010/2011 from the data monitored at Yasuzuka AMeDAS Station and Busuno Observation Station. From the daily MR data, the effective MR (half-life: 72 h) was calculated from the day of the maximum water equivalent of snow to the day when the snow disappeared for each snow season.

The maximum effective MR was recorded in the winter of 2005/2006, when there was heavy snow, followed by 2004/2005 (Fig. 11.23). During both seasons, Shimizu District was likely to have been covered by almost 4 m deep snow, storing over 1,500 mm of water on the ground surface. No landslide occurred in Shimizu District in neither of the seasons although one of which was the spring that followed the Niigata-ken Chuetsu Earthquake in October 2004. The reason is not fully understood, but this was possibly because the earthquake did not loosen the ground sufficiently to reduce the safety factor below 1.0 during the spring snowmelt period. Winter of 2010/2011 marked the third largest value in the past seven seasons. The landslide was estimated to have occurred by an effective MR of about 120 mm. Therefore, the effect of the seismic motion was equivalent or more to 140 mm in effective MR, which is the difference between the maximum value in 2004/2005 and 2010/2011 (Fig. 11.24).

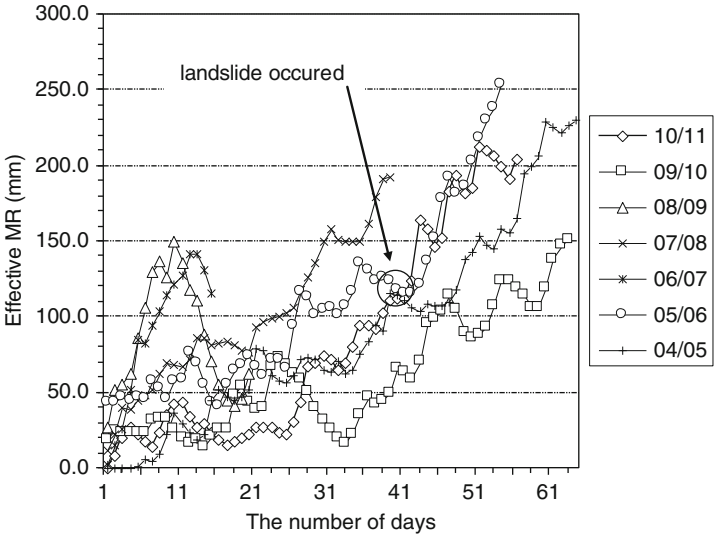

Fig. 11.23 Changes in effective MR in seven snow seasons from the day of the maximum water equivalent of snow to the day of snow disappearance

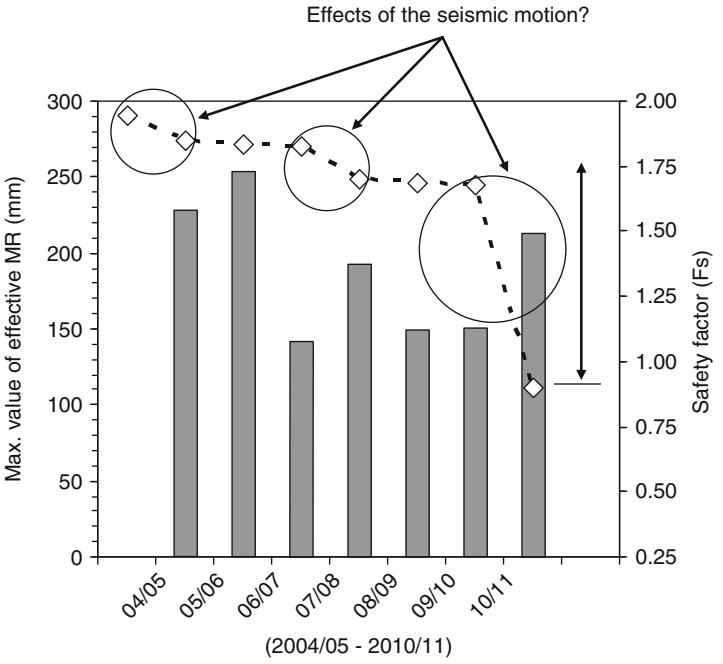

Fig. 11.24 Changes in maximum effective MR in seven snow seasons and concept of safety factor reduction against seismic motion

11.5 Conclusions

The Nagano-ken Hokubu Earthquake, which occurred in winter in a snowy area, caused avalanches, slope failures, deep-seated landslides, and movements of slope constituents. Sediment-related disasters occurred at the places having geological and topographical features of vulnerability similar to the earthquake-induced landslides in the non snow-covered season. However, the number of slope failures and landslides was significantly small compared to the Niigata-ken Chuetsu Earthquake of a similar scale. This was likely attributable to the increase of the effective normal stress by the snow load and enhanced shear strength of the ground by the snow cover. Fast-moving snow smoke, which was a mixture of snow and air, was also produced when a fast landslide moving body crushed against snow accumulation and destroyed the periphery along the path of the debris flow. Natural levee of snow and earth peculiar to snow season was also formed by a debris flow that moved through a snow cover while dragging in the snow, flowing as a mixture of earth and snow, and bulldozing the deep snow cover. Furthermore, a landslide occurred about 1 month after the earthquake on a slope that did not collapse with a large amount of meltwater in the past. The earthquake was likely to have loosened the slope, and thus, the landslide occurred even with the less amount of meltwater.

References

Abrahamson NA, Somerville PG (1996) Effects of the hanging-wall and footwall on ground motions recorded during the Northridge earthquake. Bull Seimo Soc Am 86(1B):S93–S99

Barla G, Dutto F, Mortara G (2000) Brenva glacier rock avalanche of 18 Jan 1997 on the Mount Blanc range, Northwest Italy. Landslide News 13:2–4

Joyner WB, Boore DB (1981) Peak horizontal acceleration and velocity from strong motion records including records from the 1979 Imperial Valley, California, earthquake. Bull Seism Soc Am 71:2011–2038

Matsuta N, Sugito N, Hirouchi D (2011) Deformation of the ground surface near the prefectural border of Nagano and Niigata during the earthquake on March 12, 2011 (prompt report). http://www.seis.nagoya-u.ac.jp/INFO/tohoku20110311/chihyou_110317. Pdf. (in Japanese)

Matsuura S, Asano S, Okamoto T, Matsuyama K, Takeuchi Y (2003) Characteristics of the displacement of a landslide with shallow sliding surface in a heavy snow district of Japan. Eng Geol 69:15–35

Niigata Prefectural Government (2011) Report on the Nakao landslide disaster and its mitigation works, 104 pp (in Japanese)

Shibasaki T, Shinoda K, Yamasaki T (2008) Possible mechanism to explain various landslide behaviors during snow season. In: International conference on management of landslide hazards in the Asia-Pacific Region, Sendai, Japan, pp 809–817

The Headquarters for Earthquake Research Promotion (2011) Earthquake near the Border between Nagano and Niigata Prefectures on March 12, 2011. http://www.jishin.go.jp/main/chousa/11apr/p18.htm

Yagi K (2007) Characteristics of landslide distribution in the study area, earthquake-induced landslide disasters in middle mountains – study report on the 2004 Mid-Niigata earthquake part I – geomorphology & geology. Jpn Landslide Soc 84–89 (in Japanese)

Chapter 12
High-Resolution Local-Scale Simulations of Meteorological Conditions and Wind Fields over the Fukushima Region in March 2011

Tetsuya Takemi and Hirohiko Ishikawa

Abstract After the great Tohoku earthquake occurred on 11 March 2011, the dispersion of radioactive materials in the atmosphere from the Fukushima Daiichi nuclear power plant induces serious environmental pollution that is enhanced in the eastern part of Fukushima Prefecture. Considering that nuclear power plants in Japan locate over and/or near complex and complicated terrains, it is critical to understand local-scale wind systems over such complex terrains. This study investigates the characteristics of local-scale wind fields over the complex terrain of Fukushima by conducting high-resolution meteorological simulations that represent small-scale terrain features focused in the eastern area of Fukushima. The analyses are made for the relationship between the complex terrain and the low-level wind fields. The effects of the complex terrains are clearly demonstrated for winds near the surface. It is emphasized that resolving small-scale terrain features at the resolution on the order of 100 m is critically important in accurately simulating low-level winds over complex terrains.

Keywords Complex terrain • Fukushima Daiichi nuclear power plant • Local wind

12.1 Introduction

The 2011 off the Pacific Coast of Tohoku Earthquake that occurred on 11 March 2011 induces various types of disasters including the loss of human lives; damages to houses, buildings, and social infrastructures; devastating damages due to tsunamis and landslides; and serious damages to a nuclear power plant. The damage to the nuclear power plant, the Fukushima Daiichi nuclear power plant, caused the dispersion of

T. Takemi (✉) • H. Ishikawa
Disaster Prevention Research Institute (DPRI), Kyoto University, Kyoto, Japan
e-mail: takemi@storm.dpri.kyoto-u.ac.jp

H. Kawase (ed.), *Studies on the 2011 Off the Pacific Coast of Tohoku Earthquake*,
Natural Disaster Science and Mitigation Engineering: DPRI reports,
DOI 10.1007/978-4-431-54418-0_12, © Springer Japan 2014

radioactive materials in the atmosphere not only in the local scales (on the order of 10 km) but also in the regional scales (on the order of 100 km) and beyond. Significant efforts have been made to understand the amount of release of radioactive materials, the atmospheric transport not only in the local ranges but also in the longer ranges, and the deposition onto the ground surface (e.g., Chino et al. 2011; Morino et al. 2011; Takemura et al. 2011; Yasunari et al. 2011; Stohl et al. 2012).

The Pacific coast of Tohoku is known to be a region where the activity of earthquakes is high. If another great earthquake occurs over the Tohoku region within the next tens of years, it will induce serious damages to the Fukushima Daiichi nuclear power plant, which has a high risk of releasing radioactive materials from the power plant. Therefore, continuous efforts are required in order to accurately assess the amount of release of radioactive materials from the Fukushima power plant, the dispersion in the atmosphere, and the deposition onto the ground. For this purpose, approaches from a wide range of scientific and engineering perspectives should be examined and evaluated through considering a worst scenario and/or some extreme cases.

The numerical simulations of the atmospheric transport done so far have been performed in the regional scales and/or the global scales. Owing to the large areal coverage for the numerical analyses, the horizontal resolutions of the computational domains are limited to a few kilometers at their finest. The sizes of the computational domain and the computational resolution are a trade-off, which is determined by computational resources available. However, it is obvious that the grid resolution of larger than 1 km is not sufficient to resolve the small-scale features of complex and complicated topography. Since the land of Japan is characterized by steep mountains and complex terrains, the numerical simulations of airflows over such complex terrains should adequately resolve the complex terrain features. In fact, most of the nuclear power plants in Japan are located over and/or near complex terrains. Therefore, the dispersion of radioactive materials accidentally released from nuclear power plants located in complex terrain should be assessed by high-resolution numerical simulations in which terrains are adequately represented.

The importance of the representation of terrains in simulating the spatial and temporal variability of surface winds near the surface and in the atmospheric boundary layer has been emphasized by the boundary-layer meteorological community (e.g., Jimenez et al. 2008; Jimenez and Dudhia 2012); Takemi (2009) and Takemi et al. (2010) incorporate a high-resolution elevation dataset in simulating strong winds over a land which is characterized by a complex of flat surfaces, hills, and steep mountains that are characterized by various categories of land use and land cover. Their studies emphasized that an accurate representation of complex terrains is important in simulating the spatial and temporal variability of surface winds over such terrains. Furthermore, it is also pointed out that the representation of surface slopes affects quantitative estimates of surface wind variability in complex terrains (Oku et al. 2010).

It is obvious that the dispersion of materials released from the surface into the atmosphere is strongly regulated by the variability of winds near the surface and in the atmospheric boundary layer. Therefore, to numerically investigate atmospheric dispersion for a case in complex topography (like the one that we have seen at the

Fukushima Daiichi nuclear power plant), the representation of surface wind variability over complex terrains in a numerical simulation is critical. Our philosophy for the need of a high-resolution modeling is to properly resolve small-scale, complex undulations of terrains in representing the variability of wind fields near the surface and in the boundary layer, which strongly affects instantaneous gusty winds, turbulent features of winds, and turbulent diffusion.

In this study, we perform a high-resolution numerical simulation of wind fields over the Fukushima region in March 2011 by using a non-hydrostatic, regional meteorological model at the horizontal resolution of 400 m. We compare the results obtained from the high-resolution simulation with those from a coarser-resolution simulation and thereby emphasize the importance of the representation of complex terrains at a resolution of at least the order of 100 m.

12.2 Numerical Model and Simulation Methodology

The numerical model for regional meteorological simulations conducted in this study is the Weather Research and Forecasting (WRF) model, specifically, the version 3.1.1 of the Advanced Research WRF (ARW) (Skamarock et al. 2008). This model is a community model developed mainly by the National Center for Atmospheric Research, USA, and has been widely used not only by research communities but also by operational communities around the world. The WRF model has a nesting capability that is useful in both capturing synoptic-scale meteorological conditions and downscaling the meteorological structure at a high resolution. The gridded analysis and/or forecast data created by operational weather-forecasting centers are used to drive the WRF model.

We employ the nesting capability in order to resolve the area of interest at a fine resolution. In the present simulations, we set three multi-nested computational domains with the boundary conditions of the inner two domains being given by their parent domains (i.e., one-way nesting). The three domains have areas of 1,800 km by 1,600 km (which covers the most part of the Japanese main islands) at 10-km grid, 560 km by 800 km (which covers the Tohoku and the Kanto region) at 2-km grid, and 100 km by 150 km (which covers the eastern part of Fukushima Prefecture) at 400-m grid (Fig. 12.1). The top of the computational domain is fixed at the 50-hPa level. The vertical structure of the atmosphere is resolved by 45 levels, with 14 levels in the lowest 1-km depth; thereby the atmospheric boundary layer is represented at a fine resolution. The vertical coordinate system is a terrain-following system.

In order to generate accurate terrain features in the computational domains, we need to use high-resolution elevation dataset. Taking into account the size of the horizontal grid spacing of each domain, we use the global 30-s data (GTOPO30) from the US Geological Survey for the outer 2 domains and the 50-m mesh digital elevation dataset by the Geographical Survey Institute of Japan for the innermost domains. The land-use/land-cover information is obtained from the 100-mesh dataset provided by the Ministry of Land, Infrastructure, Transport and Tourism of Japan.

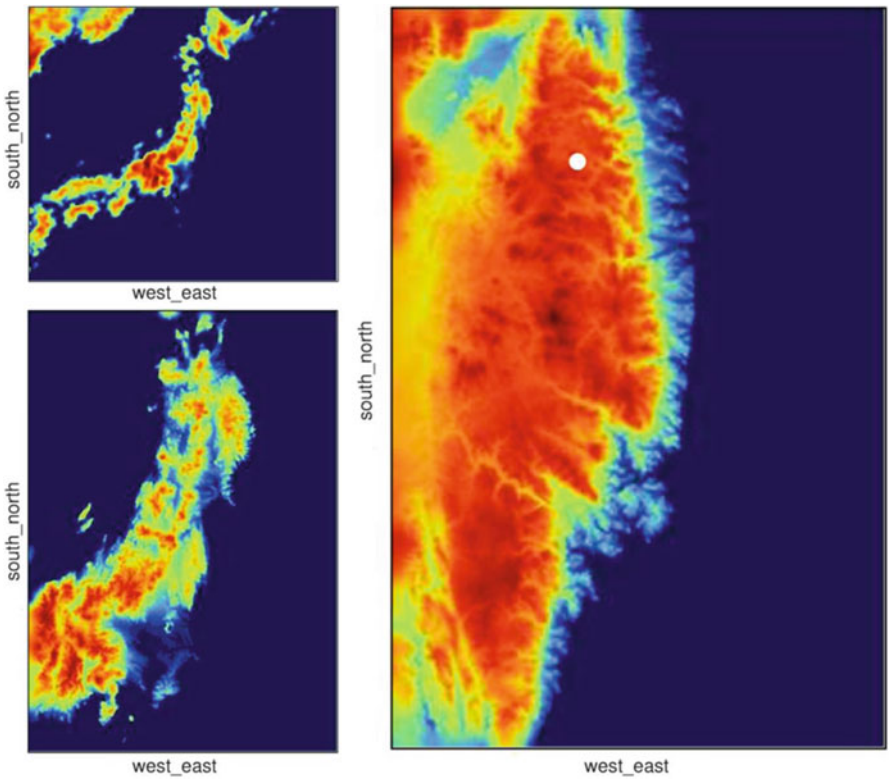

Fig. 12.1 The computational areas with the 10-km grid (*upper left*), the 2-km grid (*lower left*), and the 400-m grid (*right*). The color shading indicates the surface elevation scaled by the maximum heights (2,253 m for the 10-km grid, 3,200 m for the 2-km grid, and 1,150 m for the 400-m grid). The *white dot* in the 400-m domain indicates the location of the Iitate observation point

In order to perform regional meteorological simulations, we need the initial and boundary conditions adapted to the computational domains. These conditions are determined by gridded meteorological analyses generated by operational weather-forecasting centers. In this study, we use 6-hourly Mesoscale Analysis data (MANAL) of Japan Meteorological Agency (JMA), 6-hourly Final Analysis data of the US National Centers for Environmental Prediction (NCEP), and daily Merged Sea Surface Temperature (MGDSST) analysis data of JMA. The horizontal resolutions of MANAL and MGDSST are 10 km and 0.25°, respectively, which are useful for high-resolution regional simulations. Six-hourly SST data are made by interpolating in time the daily MGDSST analyses. These 6-hourly data are ingested to the WRF model as the boundary conditions at the lower and the lateral boundaries of the outermost domain as well as the initial condition for the outermost domain.

Meteorological simulations under real situations are realized with proper formulations for physics processes. A physics process that is closely relevant to the simulation of wind fields is a planetary-boundary-layer mixing parameterization.

We chose a Mellor-Yamada Level 2.5 model (Janjic 2002). This scheme, formulated based on a Reynolds-averaging approach, solves a prognostic equation for turbulent kinetic energy that determines the vertical components of the coefficients of eddy viscosity and diffusivity with a diagnostic equation of length scale.

The model is initialized at 0000 UTC 11 March 2011 and integrated until 0000 UTC 1 April 2011. The simulated outputs are saved at 10-min interval.

12.3 Results

The difference in the representation of wind fields in simulations with different horizontal resolutions can be easily seen by the temporal variation of wind speed at a certain location in an area with complex terrains. Owing to the great earthquake and the accident at the Fukushima nuclear power plant, most of the meteorological observational sites of JMA were unavailable and were not recovered during March 2011. Thus, the observational data are not sufficient to be used for the comparison of the simulated results at many observational points. The observational point with a relatively small amount of missing data in complex terrains is the Iitate AMeDAS (Automated Meteorological Data Acquisition System) site, located at 37°41.7′N and 140°44.8′E (see Fig. 12.1). Hence, the simulated results obtained at the grid point nearest the Iitate AMeDAS site are compared with the observation.

Figure 12.2 shows the temporal variations of wind speed obtained by the simulations in the inner domains with 400-m grid and 2-km grid and compares them with the observational data. It is clearly seen that the simulation in the 400-m grid domain indicates temporal changes at shorter timescales than that in the 2-km domain. In addition, the result obtained in the 400-m grid domain shows a larger range of the

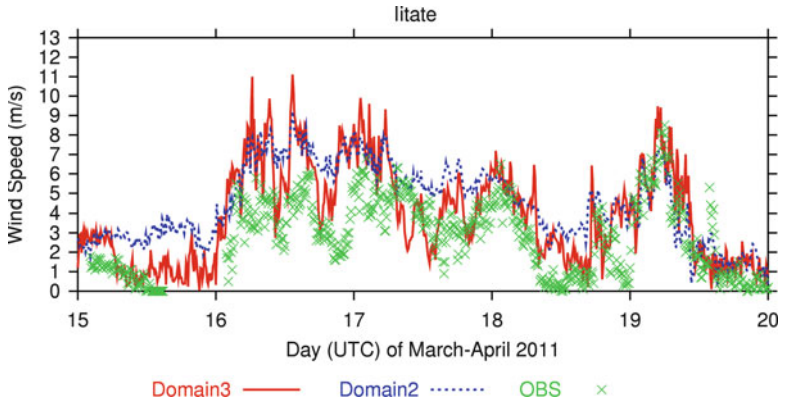

Fig. 12.2 Time series of wind speed at the Iitate point during 0000 UTC 15 and 0000 UTC 20 March 2011. The *red line* denotes the wind at the 10-m height above-the-ground level simulated in the 400-m grid domain, the *blue line* that in the 2-km grid domain, and the *green crosses* denote the surface wind observed at the Iitate AMeDAS point

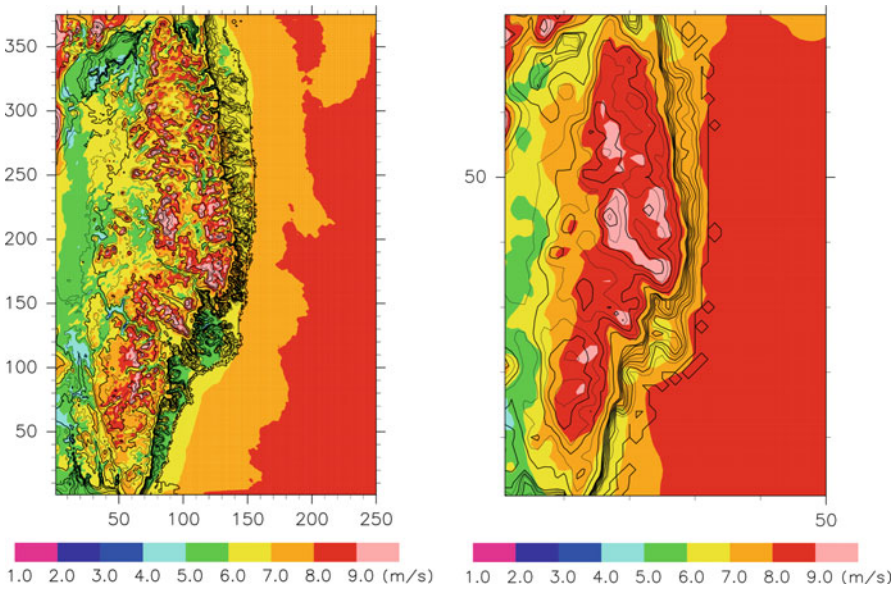

Fig. 12.3 The spatial distribution of the average from the time series of wind speed at the 50-m above-the-ground level at each grid point obtained by the simulations with the 400-m grid (*left panel*) and the 2-km grid (*right panel*). The *contour lines* indicate the modeled surface elevation at 100-m interval. The numbers in the horizontal and vertical axes indicate the grid number

temporal change, with more enhanced values of local maxima and minima, than that in the 2-km domain. In general, the simulated change in the 2-km case is more smoothed than that in the 400-m case. In this way, the dependence of the simulated results to resolution, which reflects the difference in the representation of terrain, is clearly identified by the change of surface wind in complex terrain.

In order to further demonstrate the resolution dependence, we examine the spatial distribution of the characteristics of wind speed variability simulated in the 400-m and the 2-km domain. For this purpose, average value and standard deviation from the time series at each grid point during the simulated time period are computed. Figure 12.3 demonstrates the spatial distribution of the temporal averages of the wind speed at the 50-m above-the-ground level simulated in the 400-m grid and the 2-km grid domain. Although the results from the two domains in general indicate that the wind speed increases with height, it is clearly seen that the spatial variability of the mean wind speed in complex and mountainous terrain is more significant in the 400-m case. Specifically, the mean wind speed in small-scale valley areas is more reduced in the 400-m case than in the 2-km case.

The variability of wind speed is further examined by the standard deviation, which is divided by the temporal average of the time series at each grid point. From Fig. 12.4, it is demonstrated that the representation of wind speed variability is significantly affected by the modeled terrain in each resolution case. An overall appearance indicates that the normalized standard deviation becomes smaller with height,

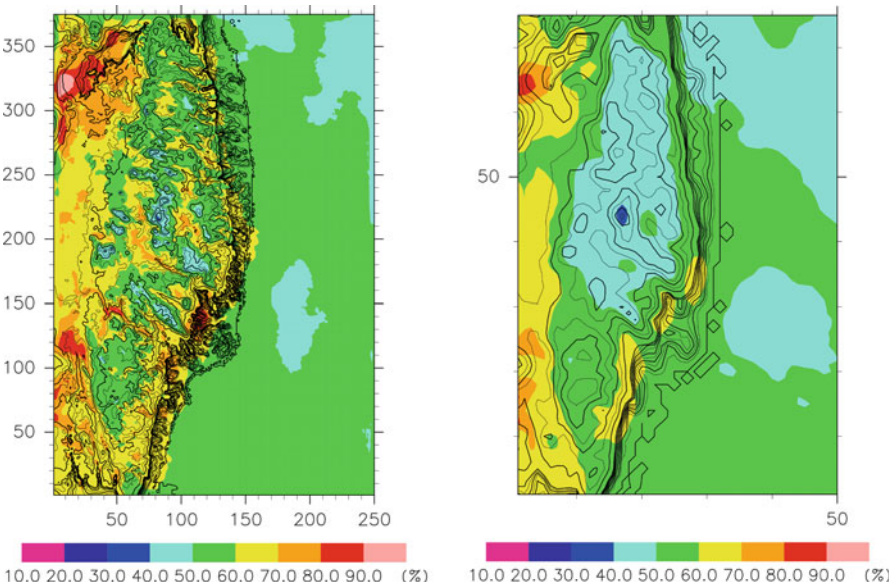

Fig. 12.4 The same as Fig. 12.3, except for the standard deviation normalized by the temporal average at each grid point

but again the spatial distribution has a larger variability in the 400-m case than in the 2-km case. In contrast to the mean wind speed, the standard deviation in small-scale valley areas in the mountainous region is more enhanced in the 400-m case than in the 2-km case. The percentage of the normalized standard deviation amounts to about 80 %, found in the valley areas in the 400-m case, which means that the range of wind variation is almost the same as the mean wind speed. Such large variability is not seen over the mountainous region in the 2-km case.

One might argue that the comparison shown in Figs. 12.3 and 12.4 is indicating not the dependence to the terrain representation but just the dependence to the horizontal resolution. Of course, the different resolution reflects not only the representation of terrains but also the representation of atmospheric processes. It is expected that higher resolution would produce small-scale variability of wind speed and other meteorological variables induced by resolved atmospheric processes. To answer this question, the simulation with the 400-m grid by creating the model terrain from a coarser-resolution elevation dataset should be conducted. For example, the GTOPO30 dataset can be used to create the model terrain in the 400-m domain. We have not conducted such a simulation for the present Fukushima case, but we did such comparative simulations for other meteorological events (Takemi 2010). Although the cases examined were severe rain events, it was indicated that peak wind speeds near the surface are represented more enhanced in using finer-resolution elevation data than in using coarser-resolution data. Therefore, it is stressed that the more accurate representation of complex terrains at a higher resolution is desirable in investigating the small-scale variability of wind speed near the surface.

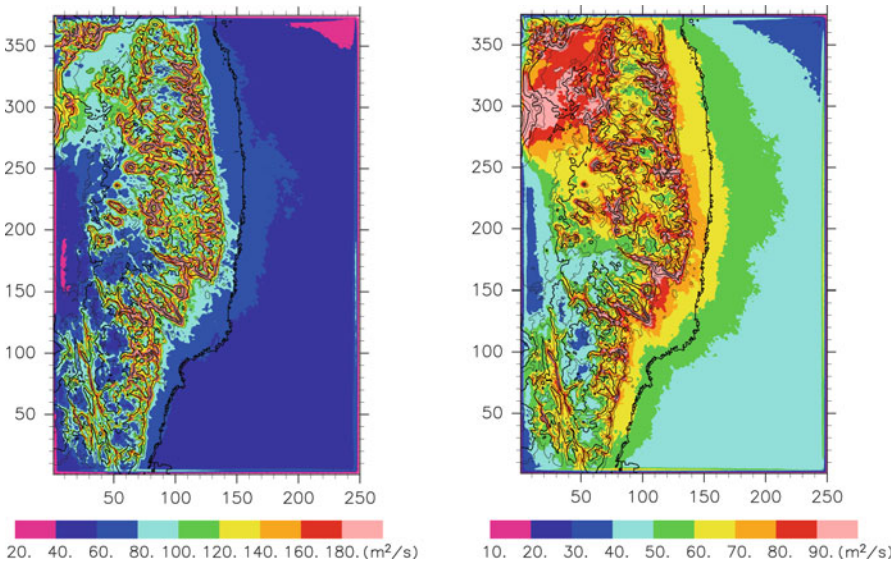

Fig. 12.5 The horizontal distribution of the temporal mean values of horizontal eddy diffusivity coefficients, averaged in time during the simulated period, at the heights of 50 m (*left panel*) and 200 m (*right panel*) above-the-ground level

Finally, the representation of the horizontal component of eddy diffusivity that is closely relevant to the dispersion of airborne materials is examined. The horizontal eddy diffusivity is computed via eddy viscosity that is determined by a standard Smagorinsky model. Figure 12.5 indicates the spatial distribution of the averaged values of horizontal eddy diffusivity coefficients at the heights of 50 and 200 m. The values are averaged in time during the simulated period from the time series at each grid point. Higher values of the eddy diffusivity coefficient are found at locations surrounding mountain peaks, that is, the locations with steep slopes and the valley areas in the mountainous region. Combining the variability of eddy diffusivity in complex terrain and the variability of wind speed near the surface seen previously, we expect that high-resolution numerical simulations by adequately representing complex terrain features should improve the assessment of material dispersion not only in the local scales but also in the regional scales and larger.

12.4 Concluding Remarks

Considering that the Pacific region off the Tohoku coast is the active area of subduction-zone earthquakes and that it is anticipated that there is a high risk of major earthquakes within next 30 years, we should continuously make efforts to assess the emission of radioactive materials from the Fukushima Daiichi nuclear power plant and the atmospheric dispersion in the complex terrain of Fukushima

and its surroundings by assuming a possible outbreak of another major earthquake. As demonstrated in this study, high-resolution meteorological modeling is critically important to accurately assess wind field and diffusion characteristics in the complex terrain.

Since the emission and dispersion of materials is strongly controlled by unsteady, turbulent flows in the atmosphere, a large-eddy simulation (LES) approach that explicitly resolves most of energetic turbulent eddies is promising. However, an LES model requires an intensive use of computational resources, and thus reducing a computational cost is a challenging task. Coupling a meteorological model for scales of weather phenomena and an LES model for scales of surface roughness such as buildings, structures, and vegetations is considered to resolve the computational issue, because both meteorological conditions and local-scale turbulent fields can be represented. An approach developed by Nakayama et al. (2012) enables to incorporate the meteorological effects simulated by a meteorological model into an LES model. An LES modeling not only for flows over complex terrains but also for flows over roughness obstacles, that is, urban areas (Nakayama et al. 2011), is also required in order to assess turbulent flows at building scales (i.e., flows around the power plant). Further improvements of the method of Nakayama et al. (2012) are now undertaken.

It is noted that the time period of 30 years coincidentally corresponds to the radioactive half-life period of cesium-137. With a great earthquake anticipated to occur off the Pacific coast of the Tohoku region within the next 30 years, there is a risk of a critical accident at the Fukushima Daiichi power plant. In addition to the efforts ahead to remove the radioactive materials contained in the Fukushima power plant and to dismantle the power plant itself, we need to carefully examine and evaluate the measures on emergency responses and environmental assessments. We should be prepared for a disastrous event by assuming the worst scenario.

Acknowledgments This work was partly supported by a grant for the urgent researches on the 2011 off the Pacific Coast of Tohoku Earthquake from Disaster Prevention Research Institute, Kyoto University.

References

Chino M, Nakayama H, Nagai H, Terada H, Katata G, Yamazawa H (2011) Preliminary estimation of release amounts of 131I and 137Cs accidentally discharged from the Fukushima Daiichi nuclear power plant into the atmosphere. J Nuclear Sci Tech 48(7):1129–1134

Janjic ZI (2002) Nonsingular implementation of the Mellor-Yamada level 2.5 scheme in the NCEP Meso model. NCEP office note, 437, 61 pp

Jimenez PA, Dudhia J (2012) Improving the representation of resolved and unresolved topographic effects on surface wind in the WRF model. J Appl Meteor Climatol 51:300–316

Jimenez PA, Gonzalez-Rouco JF, Montavez JP, Navarro J, Garcia-Bustamante E, Valero F (2008) Surface wind regionalization in complex terrain. J Appl Meteor Climatol 47:308–325

Morino Y, Ohara T, Nishizawa T (2011) Atmospheric behavior, deposition, and budget of radioactive materials from the Fukushima Daiichi nuclear power plant in March 2011. Geophy Res Lett 38:L00G11

Nakayama H, Takemi T, Nagai H (2011) LES analysis of the aerodynamic surface properties for turbulent flows over building arrays with various geometries. J Appl Meteor Climatol 50:1692–1712

Nakayama H, Takemi T, Nagai H (2012) Large-eddy simulation of urban boundary-layer flows by generating turbulent inflows from mesoscale meteorological simulations. Atmos Sci Lett 13: 180–186

Oku Y, Takemi T, Ishikawa H, Kanada S, Nakano M (2010) Representation of extreme weather during a typhoon landfall in regional meteorological simulations: a model intercomparison study for Typhoon Songda (2004). Hydrol Res Lett 4:1–5

Skamarock WC, Klemp JB, Dudhia J, Gill DO, Barker DM, Duda MG, Huang XY, Wang W, Powers JG (2008) A description of the advanced research WRF version 3. NCAR/TN-475+STR, 113 pp

Stohl A, Seibert P, Wotawa G, Arnold D, Burkhart JF, Eckhardt S, Tapia C, Vargas A, Yasunari TJ (2012) Xenon-133 and caesium-137 releases into the atmosphere from the Fukushima Dai-ichi nuclear power plant: determination of the source term, atmospheric dispersion, and deposition. Atmos Chem Phys 12:2313–2343

Takemi T (2009) High-resolution numerical simulations of surface wind variability by resolving small-scale terrain features. Theor Appl Mech Jpn 57:421–428

Takemi (2010) The 100-m mesh numerical simulations of severe local rainstorms by representing complex terrain features. Ann Disas Prev Res Inst Kyoto Univ 53B:337–343, http://www.dpri.kyoto-u.ac.jp/nenpo/no53/ronbunB/a53b0p37.pdf

Takemi T, Kusunoki K, Araki K, Imai T, Bessho K, Hoshino S, Hayashi S (2010) Representation and localization of gusty winds induced by misocyclones with a high-resolution meteorological modeling. Theor Appl Mech Jpn 58:121–130

Takemura T, Nakamura H, Takigawa M, Kondo H, Satomura T, Miyasaka T, Nakajima T (2011) A numerical simulation of global transport of atmospheric particles emitted from the Fukushima Daiichi nuclear power plant. SOLA 7:101–104

Yasunari T, Stohl A, Hayano RS, Burkhart JF, Eckhardt S, Yasunari T (2011) Cesium-137 deposition and contamination of Japanese soils due to the Fukushima nuclear accident. Proc Natl Acad Sci 108:19530–19534

Chapter 13
Uncertainty in Simulation of Global Transport of Radioactive Tracer Emitted from Fukushima Daiichi Nuclear Power Plant

Takao Iguchi, Hitoshi Mukougawa, and Takeshi Enomoto

Abstract Global transport of radioactive tracers emitted from Fukushima Daiichi Nuclear Power Plant was simulated by using an atmospheric transport model, and the levels of uncertainties in the results were investigated. These uncertainties are attributed to the reanalysis atmospheric data used as the input of the transport model and imprecision of the details of the radiation flux time series. Simulation results were found using the National Centers for Environmental Prediction/National Center for Atmospheric Research (NCEP/NCAR) reanalysis data, the atmospheric general circulation model for the Earth Simulator—local ensemble transform Kalman filter experimental ensemble reanalysis 2 (ALERA2) data, the European Centre for Medium-Range Weather Forecasts (ECMWF) ERA Interim data, and the Japan Meteorological Agency Climate Data Assimilation System (JCIDAS) data. The standard deviation of the simulation results using these data sets was larger than the standard deviations (which were within 10 % of the mean values) of the results using the data of the ALERA2 ensemble members. Simulation results of 1-day emissions showed a clear difference in the transport of the emitted tracer and suggest the availability of an inverse method to estimate a detailed flux time series.

Keywords Atmospheric transport • Flux time series • Reanalysis data • Simulation • Uncertainty

T. Iguchi (✉) • H. Mukougawa • T. Enomoto
Disaster Prevention Research Institute (DPRI), Kyoto University, Kyoto, Japan
e-mail: iguchi@dpac.dpri.kyoto-u.ac.jp

H. Kawase (ed.), *Studies on the 2011 Off the Pacific Coast of Tohoku Earthquake*,
Natural Disaster Science and Mitigation Engineering: DPRI reports,
DOI 10.1007/978-4-431-54418-0_13, © Springer Japan 2014

13.1 Introduction

The Fukushima Daiichi Nuclear Power Plant accident, which occurred after the 2011 Off of the Pacific Coast of Tohoku Earthquake and its accompanying massive tsunami, received attention from all over the world. In particular, transport of the radioactive materials emitted as a result of the accident has been predicted and simulated by many institutions. In these studies, high-resolution regional models have been employed to simulate the domestic distribution in Japan (Takemi and Ishikawa 2011; Kondo et al. 2011; Takigawa et al. 2011; Kajino et al. 2011; Kato et al. 2011), and global atmospheric transport models have been employed to simulate the long-distance transport (Takemura et al. 2011; Tanaka et al. 2011).

However, to precisely estimate the radiation levels both in the atmosphere and on the ground, the effects of dry and wet deposition, radioactive decay, and other factors must be added to transport and diffusion models of the atmosphere. The factors associated with deposition and decay differ for each type of radionuclide; therefore, the estimation of radiation levels needs a detailed understanding of the emitted radioactive material. In addition, Tanaka et al. (2011) stated that the resolution and accuracy of topography in a model affect the simulation results.

Since simulations are implemented by using reanalysis atmospheric data or data calculated by a general circulation model, the uncertainty attributed to this data should be also considered. Moreover, accurate simulation requires a time series of the radiation flux; however, few researchers have estimated the temporal variation of this flux (Chino et al. 2011). Therefore, inversion of the flux time series using an accurate transport model is expected to offset the limited research (Maki et al. 2011).

In this study, the long-distance atmospheric transport of emitted radioactive tracer was simulated by using a global model, and the levels of uncertainties in the model attributed to reanalysis atmospheric data and emission date were investigated.

13.2 Model and Data

13.2.1 Global Atmospheric Transport Model

A three-dimensional global transport model (Iguchi and Kida 1999) was employed for the simulations in this study. The atmosphere is divided into grid boxes in this model and the tracer fluxes between boxes are calculated. Then tracer mass at the next time step of each grid box is calculated by adding fluxes to current tracer mass. Thus, this scheme accumulates and conserves the total tracer mass.

The horizontal resolution of the model is $1.25° \times 1.25°$. The vertical domain is divided into 14 sigma layers, with the top layer having a pressure of 10 hPa. The time step in the simulations is 5 min.

Table 13.1 Horizontal resolution and vertical levels of reanalysis data sets

Data set name	Horizontal resolution (degree)	Vertical levels
NCEP/NCAR	2.5	17 levels (1,000, 925, 850, 700, 600, 500, 400, 300, 250, 200, 150, 100, 70, 50, 30, 20, 10 hPa)
JCIDAS	1.25	
ERA interim	1.5	18 levels (1,000, 925, 850, 775, 700, 600, 500, 400, 300, 250, 200, 150, 100, 70, 50, 30, 20, 10 hPa)
ALERA2	1.25	

13.2.2 Reanalysis Atmospheric Data

The input data for the atmospheric transport model described in Sect. 13.2.1 were taken from the National Centers for Environmental Prediction, National Oceanic and Atmospheric Administration/National Center for Atmospheric Research, University Corporation for Atmospheric Research (NCEP/NCAR) reanalysis data (Kalnay et al. 1996), the atmospheric general circulation model for the Earth Simulator—local ensemble transform Kalman filter experimental ensemble reanalysis 2 (ALERA2) atmospheric data (Enomoto et al. 2012), the European Centre for Medium-Range Weather Forecasts (ECMWF) ERA Interim data (Dee et al 2011), and the Japan Meteorological Agency Climate Data Assimilation System (JCIDAS) data (Onogi et al. 2007). The ALERA2 ensemble consists of 63 members, which represent the uncertainties of the atmospheric state.

The horizontal resolutions and vertical levels of NCEP/NCAR, ALERA2, JCDAS, and ERA Interim data set are shown in Table 13.1. As to ERA Interim data set, pressure levels are selected so that they correspond to those of ALERA2 data set.

13.3 Simulation Method

First, transport of the emitted radioactive tracer from the accident was simulated. We assumed a constant radiation flux from 00:00 Z on March 12 to 00:00 Z on March 19, 2011, after which emissions were halted. The total amount of the tracer was set at 7.7×10^{17} Bq, which was adopted from the figure stated in a press release by the Nuclear and Industry Safety Agency (2011). Because Fukushima Daiichi Nuclear Power Plant was located near the central point of four grid areas in the model, the flux was equally divided between these areas. Transport of the emitted tracer continued to be simulated until 00:00 Z on May 1 for NCEP/NCAR reanalysis data, ERA Interim data, and JCIDAS data, but was discontinued at 00:00 Z on April 30 for ALERA2 data, owing to a lack of available data. For ALERA2 data, the simulation was run 64 times using all 63 members and the mean data of the members.

Next, simulations of the 1-day emissions on different dates were implemented to investigate the difference between the transports. The start dates of the simulations were March 12–18, and the start time of all simulations was 00:00 Z. In each

simulation, a constant flux was applied in the model on only the first day and was then halted. The total amount of the emitted tracer was set at 1.1×10^{17} Bq. After stopping the emission, transport of the tracer was simulated until 00:00 Z on April 1 by using NCEP/NCAR reanalysis data.

To focus on the effect of atmospheric transport in this study, other processes such as dry deposition, wet deposition, and radioactive decay were disregarded in all simulations.

13.4 Results

13.4.1 Simulation Using NCEP/NCAR Reanalysis Data

Figure 13.1 shows the distributions of radioactive tracer in the lowest layer of the transport model simulated using NCEP/NCAR reanalysis data. Emitted tracer was transported northward and eastward over the Pacific Ocean (Fig. 13.1a) and partly toward Southeast Asia (Fig. 13.1b). The tracer covered North America and passed over the Arctic Ocean to reach Europe (Fig. 13.1c). Finally, the tracer spread over the entire Northern Hemisphere (Fig. 13.1d).

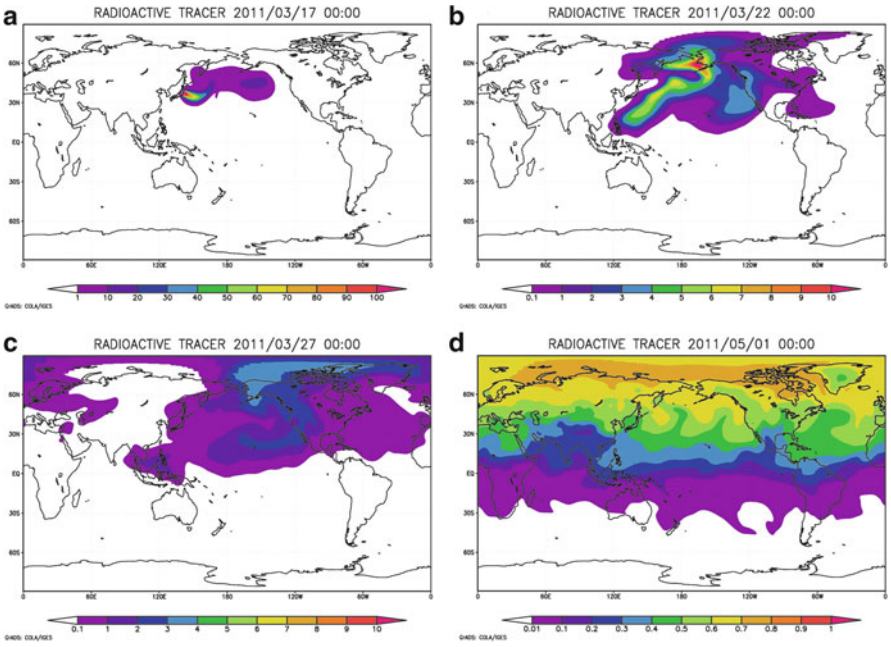

Fig. 13.1 Simulated concentrations of radioactive tracer in the lowest layer of the transport model using NCEP/NCAR reanalysis data at 00:00 Z on (**a**) March 17, (**b**) March 22, (**c**) March 27, and (**d**) May 1, 2011. The emission period was from 00:00 Z on March 12 to 00:00 Z on March 19

13.4.2 Simulation Using ALERA2 Ensemble Data

As shown in Fig. 13.1, the emitted radioactive tracer spread over the Northern Hemisphere during a period of about 1 month, and at this point the concentrations were low. Thus, in this subsection, only concentrations exceeding a threshold value are followed and discussed. To determine this threshold concentration, we referred to the "air concentration limit":

$$\rho_{\mathrm{AL}} = \frac{D_{\mathrm{EL}}}{C_{\mathrm{D}} \times V_{\mathrm{R}}},$$

where ρ_{AL} is air concentration limit (Bq/m^3), D_{EL} is effective dose limit (mSv/year), C_{D} is dose coefficient (mSv/Bq), V_{R} is respiratory volume (m^3/year).

Here, we set $D_{\mathrm{EL}} = 1$. Moreover, the International Commission on Radiological Protection (1995) estimated that the breathing rate of a man is 22.2 m^3/day, and so we set $V_{\mathrm{R}} = 8103$. For C_{D}, the total emissions 7.7×10^{17} Bq can be equated to those of an amount of ^{131}I, and so we used the dose coefficient of ^{131}I, 1.5×10^{-5} mSv/Bq. Hence, the calculated value of ρ_{AL} was 8.22, and we determined a threshold concentration of 1 Bq/m^3, which is the unit value of the same order as ρ_{AL}.

Figure 13.2 shows the distributions of mean tracer concentrations in the model's lowest layer simulated using the data of ALERA2's 63 members (left) and the distributions simulated using the mean data of the members (right). Both sets of distributions are highly similar. In the distributions on the left-hand side, grid areas in which at least one member exceeds 1 Bq/m^3 are colored gray even if the mean concentration is below 1 Bq/m^3. These gray areas are tiny compared with the areas having concentrations of 1 Bq/m^3, and this shows that the spread of values is small between the members. Figure 13.3 shows the ratios between the standard deviations and average concentrations of the simulation results using ALERA2 members' data. In the majority of the area with concentrations greater than 1 Bq/m^3, the standard deviations are within 10 % of the mean values. Here, standard deviations are regarded as uncertainties of the transport due to analysis error of the atmospheric state. However, note that ALERA2 data assimilated observation data at each time interval. If the future distribution of emissions was predicted immediately after the accident, uncertainty in the results would grow large without such assimilation.

13.4.3 Comparison of the Simulations Using Different Reanalysis Data Sets

Figure 13.4 shows the distributions of radioactive tracer in the model's lowest layer at 00:00 Z on March 24 simulated using (a) NCEP/NCAR data, (b) the mean data of ALERA2's 63 members, (c) ERA Interim data, and (d) JCIDAS data. After emissions were halted at 00:00 Z on March 19, the air mass of high concentration splits

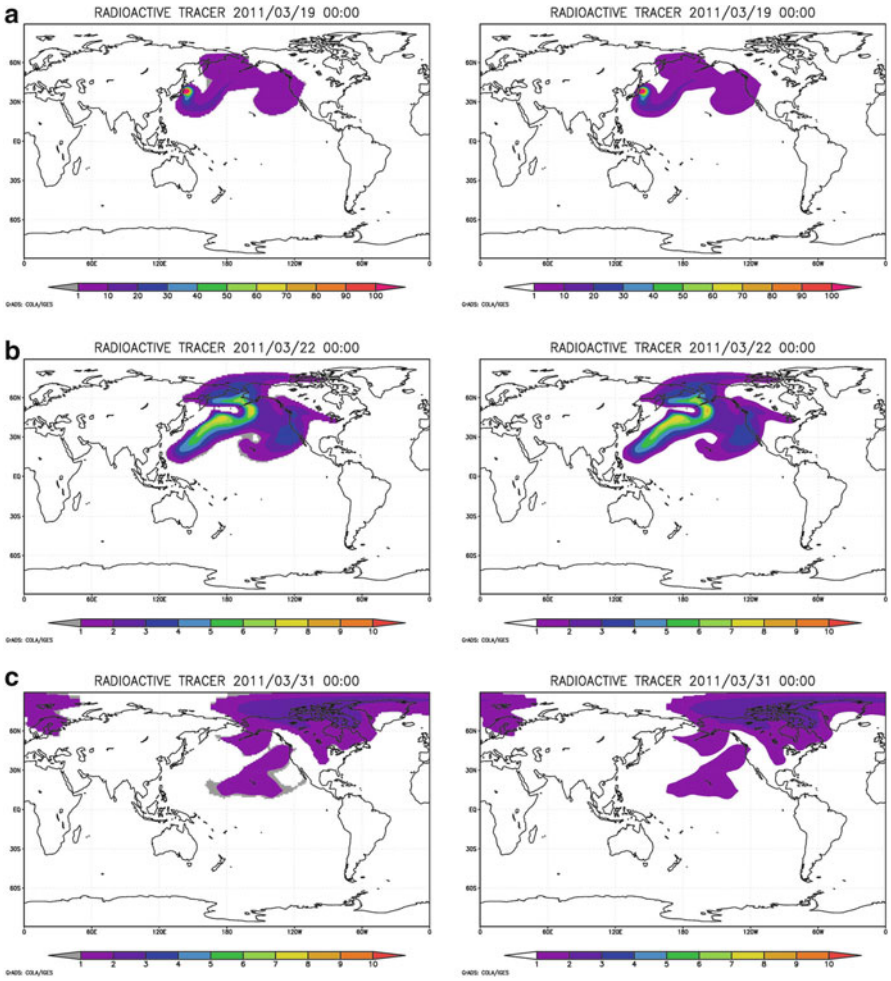

Fig. 13.2 Mean concentrations simulated using the data of the 63 members of ALERA2 ensemble reanalysis atmospheric data (*left-hand side*) and concentrations simulated using the mean data of the members (*right-hand side*). Figures are of the lowest layer of the transport model at 00:00 Z on (**a**) March 19, (**b**) March 22, and (**c**) March 31. Only grid areas with concentrations greater than 1 Bq/m^3 are colored. In the distributions on *left-hand side*, grid areas in which at least one member exceeds 1 Bq/m^3 are colored *gray* even if the mean concentration is below 1 Bq/m^3

into two, with one part moving toward the Arctic Ocean and the other moving toward the west coast of North America (see also Fig. 13.2a, b). In the distribution using NCEP/NCAR data and JCIDAS data, the concentration in the area that includes the Bering Strait and north coast of North America is higher than that in the area off the west coast of North America (Fig. 13.4a, d). However, this trend is reversed using ALERA2 data and ERA Interim data (Fig. 13.4b, c). Figure 13.5 shows ratios between standard deviations and mean concentrations of simulated results using the above four reanalysis data sets. These uncertainties are large

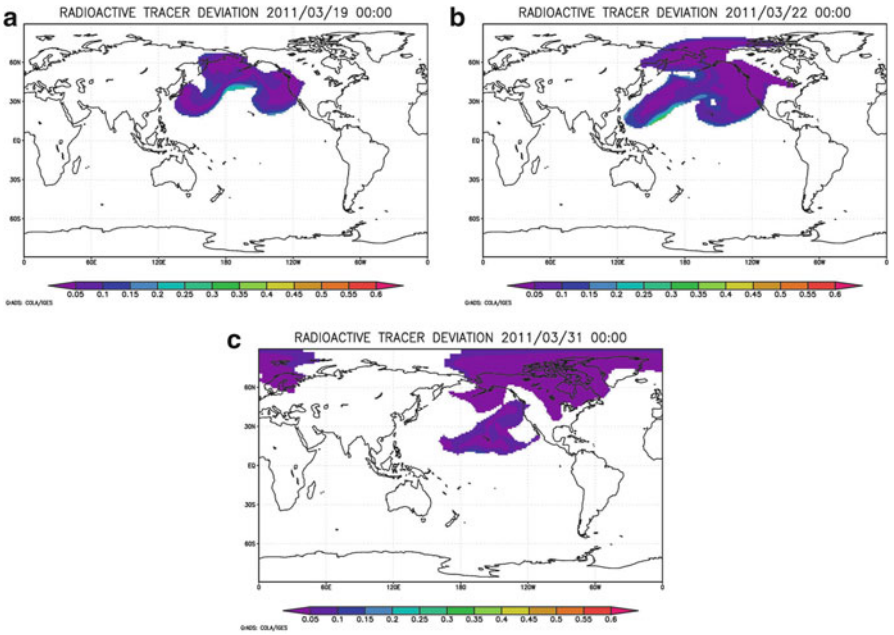

Fig. 13.3 Ratios between standard deviations and mean concentrations of simulated results using all members of ALERA2 data. Figures are of the lowest layer at 00:00 Z on (**a**) March 19, (**b**) March 22, and (**c**) March 31. The ratios are calculated for the grid areas in which at least one member exceeds 1 Bq/m^3

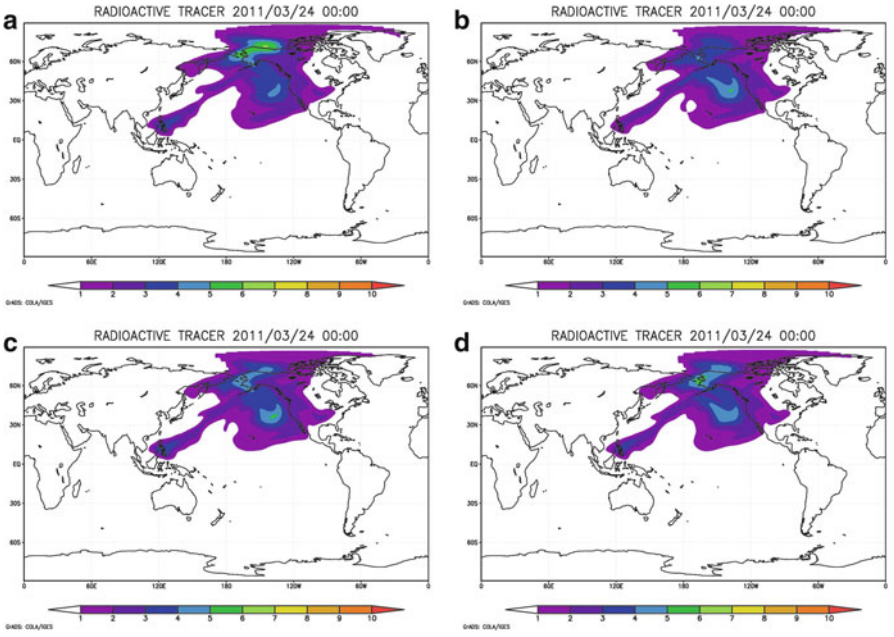

Fig. 13.4 Concentrations simulated using (**a**) NCEP/NCAR data, (**b**) the mean data of ALERA2 63 members, (**c**) ERA Interim data, and (**d**) JCIDAS data. Figures are of the lowest layer of the transport model at 00:00 Z on March 24. Only grid areas with concentrations greater than 1 Bq/m^3 are colored

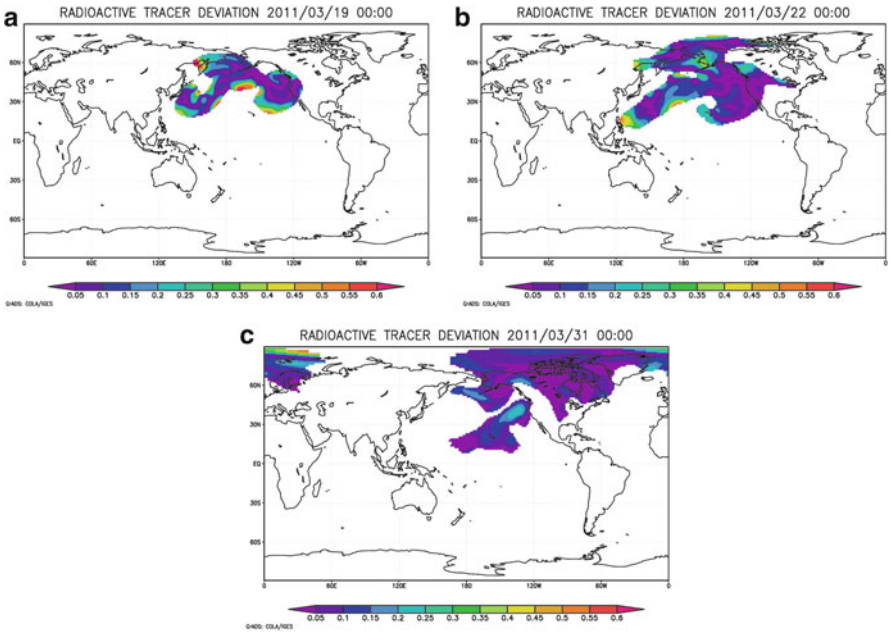

Fig. 13.5 Ratios between standard deviations and mean concentrations of simulated results using NCEP/NCAR data, the mean data of ALERA2 members, ERA Interim data, and JCIDAS data. Figures are of the lowest layer of the transport model at 00:00 Z on (**a**) March 19, (**b**) March 22, and (**c**) March 31. The ratios are calculated for the grid areas in which at least one result exceeds 1 Bq/m^3

compared with the uncertainties in the simulations using the data of ALERA2's 63 members (Fig. 13.3). The simulated values are within 30 % of each other in a large part of the area with concentrations of ≥1 Bq/m^3, but are separated by over 50 % in some edge parts of this area. The difference between the data sets is mainly due to the reanalysis methods and general circulation models used to generate the data.

13.4.4 Simulation of 1-Day Emissions

Tracer distributions in the lowest layer of the model at 00:00 Z on March 22 after 1 day emissions are shown in Fig. 13.6. These results were from simulations using NCEP/NCAR reanalysis data. For simulations of emissions on March 12 and 13, the highest concentration is seen on the west coast of North America, and the second highest is above east Siberia (Fig. 13.6a). For emissions on March 14 and 15, the concentration above east Siberia is higher than that on the west coast of North America (Fig. 13.6b). For emissions on March 16 and 17, the air mass transported to Southeast Asia has the highest concentration (Fig. 13.6c). Finally, for emissions on March 17 and 18, the air mass with the highest concentration was also transported

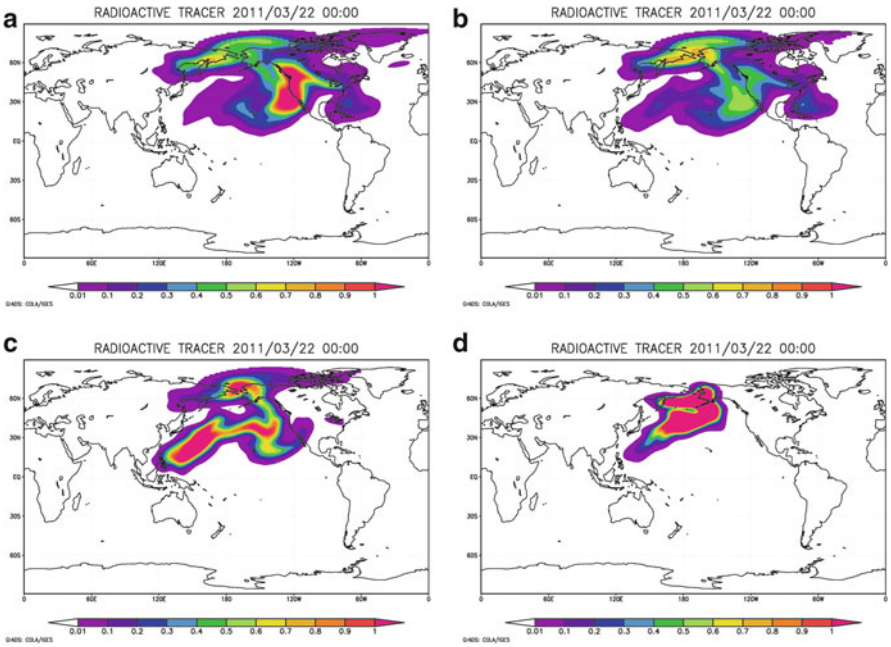

Fig. 13.6 Simulated concentrations of radioactive tracer in the lowest layer of the transport model using NCEP/NCAR reanalysis data at 00:00 Z on March 22, 2011, when the emission day was (**a**) March 12, (**b**) March 14, (**c**) March 16, and (**d**) March 18

northward (Fig. 13.6d). Hence, the distribution of the radioactive tracer differs largely according to the emission date. By utilizing these simulation results alongside sufficient observation data collected around the North Pacific Ocean, a detailed time series of the radiation flux could be estimated through the method of inversion (Enting et al. 1995; Bousquet et al. 1999). To achieve this, however, other processes such as dry and wet deposition and radioactive decay must also be included.

13.5 Summary

By employing a global atmospheric transport model, uncertainties in the transport of radioactive tracers emitted from the accident at Fukushima Daiichi Nuclear Power Plant were investigated. These uncertainties are attributed to the reanalysis data used in the simulations and imprecision of the details of the radiation flux time series. Comparison of simulations using different reanalysis data showed that the uncertainties resulting from the reanalysis method were considerably larger than the uncertainties resulting from analysis error of the atmospheric state. Simulation results of 1-day emissions differed according to the date of emission. These results suggest the availability of an inversion method to estimate a detailed time series of the radiation flux.

Acknowledgments The NCEP/NCAR reanalysis data set was downloaded from the homepage of the National Oceanic and Atmospheric Administration, Earth System Research Laboratory. The ALERA2 data were provided by the Japan Agency for Marine-Earth Science and Technology. The ERA Interim data was downloaded from the homepage of European Centre for Medium-Range Weather Forecasts Data Server. The JCIDAS data was downloaded from the home page of Japan Meteorological Agency. The figures in this paper were drawn using the Grid Analysis and Display System (GrADS) of the Institute of Global Environment and Society, Center for Ocean-Land-Atmosphere Studies.

References

Bousquet P et al (1999) Inverse modeling of annual atmospheric CO_2 sources and sinks: 1. method and control inversion. J Geophys Res 104(D21):26161–26178

Chino M et al (2011) Preliminary estimation of release amounts of ^{131}I and ^{137}Cs accidentally discharged from the Fukushima Daiichi Nuclear Power Plant into the atmosphere. J Nuclear Sci Technol 48(7):1129–1134

Dee DP et al (2011) The ERA-interim reanalysis: configuration and performance of the data assimilation system. Q J Royal Meteorol Soc 137(656):553–597. doi:10.1002/qj.828

Enomoto T et al (2013) Observing-system research and ensemble data assimilation at JAMSTEC. In: Park SK, Xu L (eds) Data Assimilation for Atmospheric, Oceanic and Hydrologic Applications (Vol. II). Springer Berlin Heidelberg: 509–526. doi: 10.1007/978-3-642-35088-7

Enting I et al (1995) A synthesis inversion of the concentration and $\delta^{13}C$ of atmospheric CO_2. Tellus B 47:35–52

Iguchi T, Kida H (1999) A study of budget of atmospheric CO_2 using a global 3-D transport model. Ann Disaster Prev Res Inst Kyoto Univ 42(B-1):385–395

International Commission on Radiological Protection (1995) Age-dependent doses to members of the public from intake of radionuclides – part 4 inhalation dose coefficients. ICRP Publication 71

Kajino M et al (2011) 2011 Fall meeting of the Meteorological Society of Japan, A209

Kalnay E et al (1996) The NCEP/NCAR 40-year reanalysis project. Bull Am Meteorological Soc 77:437–470

Kato M et al (2011) 2011 Fall meeting of the Meteorological Society of Japan, A210

Kondo H et al (2011) 2011 Fall meeting of the Meteorological Society of Japan, A207

Maki T et al (2011) 2011 Fall meeting of the Meteorological Society of Japan, A204

Nuclear and Industry Safety Agency (2011) Press release 6 June 2011

Onogi K et al (2007) The JRA-25 reanalysis. J Meteorological Soc Jpn 85:369–432

Takemi T, Ishikawa H (2011) 2011 Fall meeting of the Meteorological Society of Japan, A206

Takemura T et al (2011) A numerical simulation of global transport of atmospheric particles emitted from the Fukushima Daiichi Nuclear Power Plant. SOLA 7:101–104. doi:10.2151/sola.2011-026

Takigawa M et al (2011) 2011 Fall meeting of the Meteorological Society of Japan, A208

Tanaka T et al (2011) 2011 Fall meeting of the Meteorological Society of Japan, A211